INTERNATIONAL ATOMIC ENERGY AGENCY

INDC(NDS)-0473
Distr. SD/EL

I N D C INTERNATIONAL NUCLEAR DATA COMMITTEE

WORKSHOP

ON NUCLEAR STRUCTURE AND DECAY DATA:

THEORY AND EVALUATION

ADDENDUM - 2005

Editors: A.L.Nichols and P.K.McLaughlin
IAEA Nuclear Data Section
Vienna, Austria

July 2005

IAEA NUCLEAR DATA SECTION, WAGRAMER STRASSE 5, A-1400 VIENNA

INDC documents may be downloaded in electronic form from http://www-nds.iaea.org/indc_sel.html or sent as an e-mail attachment. Requests for hardcopy or e-mail transmittal should be directed to services@iaeand.iaea.org or to:

Nuclear Data Section
International Atomic Energy Agency
PO Box 100
Wagramer Strasse 5
A-1400 Vienna
Austria

Produced by the IAEA in Austria
June 2005

INDC(NDS)-0473
Distr. SD/EL

WORKSHOP ON NUCLEAR STRUCTURE AND DECAY DATA: THEORY AND EVALUATION

ADDENDUM - 2005

ICTP Trieste, Italy

4 – 15 April 2005

Edited by

A.L. Nichols and P.K. McLaughlin

IAEA Nuclear Data Section

Vienna, Austria

Abstract

A two-week Workshop on Nuclear Structure and Decay Data under the auspices of the IAEA Nuclear Data Section was organised and administrated at the Abdus Salam International Centre for Theoretical Physics (ICTP) in Trieste, Italy from 4 to 15 April 2005. This workshop constituted a further development of previous Nuclear Structure and Decay Data Workshops held in 2002 and 2003. The aims and contents of this workshop are summarized, along with the agenda, list of participants, comments and recommendations. Most of the workshop material can be found in the INDC report of the equivalent workshop of 17 to 28 November 2003 (INDC(NDS)-452). However, some new material was prepared for 4 to 15 April 2005, and these new and modified lectures are brought together in this addendum report. All of this material is freely available on CD-ROM (all relevant PowerPoint presentations and manuals along with appropriate computer codes):

e-mail: services@iaeand.iaea.org
fax: (+43-1)26007
post to: International Atomic Energy Agency
Nuclear Data Section
P.O. Box 100
Wagramer Strasse 5
A-1400 Vienna
Austria

July 2005

TABLE OF CONTENTS

WORKSHOP
ON NUCLEAR STRUCTURE AND DECAY DATA: THEORY AND EVALUATION – ADDENDUM, 2005

Summary

ICTP Trieste, Italy

4 – 15 April 2005

Prepared by

A.L. Nichols

IAEA Nuclear Data Section

Vienna, Austria

Abstract

Basic aspects of a two-week Workshop on Nuclear Structure and Decay Data: Theory and Evaluation are outlined in this short summary note for the record. The aims and contents of this workshop are summarized, along with the agenda, list of participants, comments and recommendations. Much was achieved and one aim will be to hold this specific workshop at various time intervals for training purposes (with agreed changes and regular modifications) on the advice of the International Nuclear Data Committee (INDC) and the International Network of Nuclear Structure and Decay Data Evaluators.

July 2005

1.1 OBJECTIVES

The International Atomic Energy Agency sponsored a two-week Workshop on "Nuclear Structure and Decay Data: Theory and Evaluation" at the Abdus Salam International Centre for Theoretical Physics (ICTP) in Trieste from 4 to 15 April 2005. This workshop was organised and directed by A.L. Nichols (IAEA Nuclear Data Section), J. Tuli (NNDC, Brookhaven National Laboratory, USA) and A. Ventura (ENEA, Bologna, Italy).

As with earlier workshops [1,2], the primary objective was to familiarize nuclear physicists and engineers from both developed and developing countries with

(i) modern nuclear models;
(ii) relevant experimental techniques;
(iii) statistical analyses procedures to derive recommended data sets;
(iv) evaluation methodologies for nuclear structure and decay data;
(v) international efforts to produce the Evaluated Nuclear Structure Data File (ENSDF).

Reliable nuclear structure and decay data are important in a wide range of nuclear applications and basic research. Participants were introduced to both the theory and measurement of nuclear structure data, and the use of computer codes to evaluate decay data.

Detailed presentations were given by invited lecturers, along with computer exercises and workshop tasks. Participants were also invited to contribute their own thoughts and papers of direct relevance to the workshop.

1.2 PROGRAMME

The workshop programme is listed in Section 1.2.1 of this brief summary.

1.2.1 Agenda

Monday, 4 April 2005

08:30 - 10:30	Registration and coffee
10:30 - 12:30	Opening Session Welcome (Alan Nichols (IAEA) and Jag Tuli (BNL)) Aims (Jag Tuli) NSDD – general features (Jag Tuli) IAEA-NDS – NSDD network and recent relevant CRPs (Alan Nichols)
12:30 - 14:00	Lunch break
14:00 – 15:30	Introduction ICTP computer facilities (Johannes Grassberger/Kevin McLaughlin)
15:30 – 16:00	Coffee break
16:00 – 17:30	Introduction (cont.) Web capabilities (Tom Burrows and Alan Nichols) Bibliographic databases (Tom Burrows)

Tuesday, 5 April 2005

09:00 – 10:30	Nuclear theory (Piet Van Isacker)
10:30 – 11:00	Coffee break
11:00 – 12:30	ENSDF format + model exercises (Jag Tuli)
12:30 - 14:00	Lunch break
14:00 – 15:30	ENSDF programs (Tom Burrows)
15:30 – 16:00	Coffee break
16:00 – 17:30	Workshop activities (JagdishTuli; Thomas Burrows; Coral Baglin; Eddie Browne; Kevin McLaughlin)

Wednesday, 6 April 2005

09:00 – 10:30	Nuclear theory (Piet Van Isacker)
10:30 – 11:00	Coffee break
11:00 – 12:30	Experimental techniques (Peter von Brentano)
12:30 - 14:00	Lunch break
14:00 – 15:30	ENSDF programs+model exercise (Tom Burrows)
15:30 – 16:00	Coffee break
16:00 – 17:30	Students' presentations

Thursday, 7 April 2005

09:00 – 10:30	Experimental techniques (Peter von Brentano)
10:30 – 11:00	Coffee break
11:00 – 12:30	ENSDF – decay (Eddie Browne)
12:30 - 14:00	Lunch break
14:00 – 15:30	Model exercise – decay (lead by Eddie Browne)
15:30 – 16:00	Coffee break
16:00 – 17:30	Workshop activities (JagdishTuli; Thomas Burrows; Coral Baglin; Eddie Browne; Kevin McLaughlin)

Friday, 8 April 2005

09:00 – 10:30	ENSDF - evaluation (Jag Tuli)
10:30 – 11:00	Coffee break
11:00 – 12:30	ENSDF- reaction (Coral Baglin)
12:30 - 14:00	Lunch break
14:00 – 15:30	Model exercise- reaction (lead by Coral Baglin)
15:30 – 16:00	Coffee break
16:00 – 17:30	Students' presentations

Monday, 11 April 2005

09:00 – 10:30	ENSDF – Theory (Slobodan Brant)
10:30 – 11:00	Coffee break
11:00 – 12:30	ENSDF- adopted (Coral Baglin)
12:30 - 14:00	Lunch break
14:00 – 15:30	Workshop activities (JagdishTuli; Thomas Burrows; Coral Baglin; Eddie Browne; Kevin McLaughlin)

15:30 – 16:00	Coffee break
16:00 – 17:30	Students' presentations

Tuesday, 12 April 2005

09:00 – 10:30	ENSDF – Theory (Slobodan Brant)
10:30 – 11:00	Coffee break
11:00 – 12:30	Model exercises- adopted (Coral Baglin)
12:30 - 14:00	Lunch break
14:00 – 15:30	Workshop activities (JagdishTuli; Thomas Burrows; Coral Baglin; Eddie Browne; Kevin McLaughlin)
15:30 – 16:00	Coffee break
16:00 – 17:30	Workshop activities (JagdishTuli; Thomas Burrows; Coral Baglin; Eddie Browne; Kevin McLaughlin)

Wednesday, 13April 2005

09:00 – 10:30	ENSDF – Experimental techniques (Filip Kondev)
10:30 – 11:00	Coffee break
11:00 – 12:30	Data analyses (Desmond MacMahon)
12:30 - 14:00	Lunch break
14:00 – 15:30	Workshop activities (JagdishTuli; Thomas Burrows; Coral Baglin; Eddie Browne; Kevin McLaughlin)
15:30 – 16:00	Coffee break
16:00 – 17:30	Workshop activities (JagdishTuli; Thomas Burrows; Coral Baglin; Eddie Browne; Kevin McLaughlin)

Thursday, 14April 2005

09:00 – 10:30	ENSDF – Experimental techniques (Filip Kondev)
10:30 – 11:00	Coffee break
11:00 – 12:30	Data analyses (Desmond MacMahon)
12:30 - 14:00	Lunch break
14:00 – 15:30	Workshop activities (JagdishTuli; Thomas Burrows; Coral Baglin; Eddie Browne; Kevin McLaughlin)
15:30 – 16:00	Coffee break
16:00 – 17:30	Workshop activities (JagdishTuli; Thomas Burrows; Coral Baglin; Eddie Browne; Kevin McLaughlin)

Friday, 15 April 2005

09:00 – 10:30	Workshop activities (JagdishTuli; Thomas Burrows; Coral Baglin; Eddie Browne; Kevin McLaughlin)
10:30 – 11:00	Coffee break
11:00 – 12:30	Review of workshop (JagdishTuli; Thomas Burrows; Eddie Browne; Alan Nichols)
12:30	Close of workshop

1.2.2 Participants

Twenty-seven participants (predominantly from developing countries) with full or partial support from the IAEA were selected to attend the workshop in April 2005. Selection was undertaken by Nuclear Data Section staff in association with the workshop directors and ICTP staff.

First row, standing from left to right:
Coral M. BAGLIN (USA), Elie SIMO (Cameroon), Elizabeth Brancaccio (Seated, ITALY), Ghania ISHAKI BOUSHAKI (Algeria), Caroline NESARAJA (USA), Mane MANE (Cameroon), Edgardo BROWNE-MORENO (USA), Mohamed KOUTHER (Sudan), Jagdish K. TULI (USA), Daniel ABRIOLA (Argentina),

Second row, standing from left to right:
Mirshod ERMAMATOV (Ubekistan), Stefan LALKOVSKI (Bulgaria), Adam GARNSWORTHY (UK), Nicholas THOMPSON (UK), Omidreza KAKUEE (Iran), Aurelian LUCA (Romania), Sami HADDAD (Syria), Marialena AVRIGEANU (Romania), Marie Martine BE (France), Thomas W. BURROWS (USA)

Third row, standing from left to right:
Kyoung LEE (Korea), Xiongiun CHEN (China), Nure ABDULLAH (Bangladesh), Alan NICHOLS (IAEA), Kevin MCLAUGHLIN (IAEA), Alexey CHEMEZOV (Russia), Alexander RODIONOV (Russia), Anwesa GHOSH (India)

Fourth row, standing from left to right:
Ruy CASTRO (Brazil), Ninel NICA (Romania), Peter VON BRETANO (Germany), Piet VAN ISACKER (France), Ameeya BHAGWAT (India), Sukhjeet DHINDSA (India)

LIST OF PARTICIPANTS

ABDULLAH Md. Nure Alam
Rajshahi University of Engineering & Technology (RUET)
Department of Physics
Rajshahi 6204
BANGLADESH
E-mail mnaa03l@yahoo.com

ABRIOLA Daniel Hugo
Comision Nacional de Energia Atomica (CNEA)
Centro Atomico Constituyentes Av. del Libertador 8250
1429 Buenos Aires
ARGENTINA

AVRIGEANU (BOATA) Marilena
National R & D Institute For Physics and Nuclear Engineering
'Horia Hulubei'
Str.. Atomistilor No.1
Magurele. Sector 5
79617 Bucharest
ROMANIA
E-mail MVRIGI@ IFIN.NIPNE.RO

BE Marie Martine
Lab. National Henri Bequerel
911911 Gif sur Yvette Cedex
FRANCE
E-mail mmbe@cea.fr

BHAGWAT Ameeya Ashok
Indian Institute of Technology
Dept. of Physics Powai
Maharashtra
400 076 Mumbai
INDIA
E-mail ameeya@phy.iitb.ac.in

CASTRO Ruy Morgado
Centro Tecnico Aerospacial (Cta)
Istituto de Estudos Avancados (leav)
D. Physica Teorica
Caixa Postal 6044
12231-970 Sao Jose Dos Campos
BRAZIL
E-mail rmcastro@ieav .cta.br

CHEMEZOV Alexey Victor
Petersburg Nuclear Physics Institute, PNPI
Gatchina
Orlova Rosha 1
188300 St Petersburg
RUSSIAN FEDERATION
E-mail chemezov2004@mail.ru

CHEN Xiongjun
China Institute of Atomic Energy (C.I.A.E.)
Chinese Nuclear Data Centre
P.O. Box 275- 41
102413 Beijing
PEOPLE'S REPUBLIC OF CHINA
E-mail chenxj@iris.ciae.ac.cn

DHINDSA Sukhjeet Singh
Guru Nanak Dev University
Department of Physics
143005 Amritsar
INDIA
E-mail dcse-gndu@yahoo.com

ElSA Mohamed Eltayeb
Sudan University of Science & Technology
College of Science
Department of Physics
P .O. Box 9024
11111 Khartoum
SUDAN
E-mail MEMEISA@YAHOO.COM

ERMAMATOV Mirshod
Uzbek Academy of Sciences
Institute of Nuclear Physics
Department Theoretical Physics
Ulugbek
702132 Tashkent
UZBEKISTAN
E-mail ermamat@inp.uz

GARNSWORTHY Adam Benjamin
University of Surrey
Department of Physics
GU2 7XH
Guildford
UNITED KINGDOM
E-mail a.garnsworthy@surrey.ac.uk

GHOSH Anwesha
Indian Institute of Technology Roorkee
{Former University of Roorkee}
Department of Physics
247 667 Roorkee
INDIA
E-mail anwesha-tua@yahoo.co.in

HADDAD Sami
Atomic Energy Commission
Department of Physics
P .0. Box 6091
Gazaoui Street,
13 Damascus
SYRIAN ARAB REPUBLIC
E-mail shaddad@aec.org.sy

ISHAKI BOUSHAKI {MEDKOUR} Ghania
University of Sciences and Technology
Houari Boumedienne
Institute of Physics
B.P. 32 El Alia Bab
Ezzouar
Algiers
ALGERIA
E-mail gmedkour@yahoo.com

KAKUEE Omidreza
Nuclear Research Center
Karegar Ave
P.O. Box 14155-1339
Tehran
ISLAMIC REPUBIC OF IRAN
E-mail okakuee@aeoi.org.ir

KOUTHER Mohamed Elhaj
Sudan University of Science & Technology
College of Science
Department of Physics
P.O. Box 9024
11111 Khartoum
SUDAN

LALKOVSKI Stefan Peshev
University of Sofia 'St. Kliment Ohridski'
Faculty of Physics
Dept. of Atomic Physics
5 James Bourchier Blvd.
1164 Sofia
BULGARIA
E-mail stl@phys.uni-sofia.bg

LEE Kyoung
Korea Research Institute of Standards and Science
Ionizing Radiation Group
P.O. Box 102
Yuseong
Daejeon 305-600
REPUBLIC OF KOREA
E-mail lee@kriss.re.kr

LUCA Aurelian
National R & D Institute For Physics and Nuclear Engineering
'Horia Hulubei'
Str.. Atomistilor No.1
Magurele. Sector 5 7
9617 Bucharest
ROMANIA
E-mail aluca@ifin.nipne.ro

MANE MANE
Ecole Nationale Superieure Polytechnique
University of Yaounde'l
Dept. of Maths and Physical Sc
Bp 8390
Yaounde
REPUBLIC OF CAMEROON

NESARAJA Caroline Delini
University of Tennessee
Departments of Materials Science! Physics and Astronomy
218 South College
Knoxville
37996-1508 TN
UNITED STATES OF AMERICA
E-mail nesaraja@mail.phy.ornl.gov

NICA Ninel
National R & D Institute For Physics and Nuclear Engineering
'Horia Hulubej'
Str.. Atomistilor No.1
Magurele. Sector 5
79617 Bucharest
ROMANIA
E-mail nica@comp.tamu.edu
Until when: 1 August 2006

RODIONOV Alexander
St. Petersburg Nuclear Physics Institute
Neutron Research Department
Pnpi Gatchina Leningrad Distrct.
188350 St Petersburg
RUSSIAN FEDERATION
E-mail Oz@rambler.ru

SIMO Elie
Universite' de Yaounde' I
Faculte' des Sciences
Departement de Physique
P.O. Box 6052
Yaounde
REPUBLIC OF CAMEROON
E-mail esimoch@yahoo.fr

THIODJIO SENDJA Bridinette
Universite' de Yaounde' I
Faculte' des Sciences
Departement de Physique
P.O. Box 6052
Yaounde
REPUBLIC OF CAMEROON
E-mail tsbridinette@yahoo.fr

THOMPSON Nicholas James
University of Surrey
Department of Physics
GU2 lXH
Guildford
UNITED KINGDOM
E-mail M.Thompson@surrey.ac.uk

LIST OF LECTURERS

Ms. Coral M. **BAGLIN**
Nuclear Science Division
Lawrence Berkeley National Laboratory
University of California
1 Cyclotron Road
MS 88R0192
Berkeley, CA 94720
USA
Tel: +1-510-486-6152
Fax: +1-510-486-5757
E-mail: cmbaglin@lbl.gov

Mr. Slobodan **BRANT**
Permanent Institute:
University of Zagreb
Faculty of Science
Department of Physics
Bijenicka Cesta 32
P.O. Box 162
10000 Zagreb
CROATIA
E_mail Brant@phy.hr

Mr. Edgardo **BROWNE-MORENO**
Nuclear Science Division
Lawrence Berkeley National Laboratory
University of California
1 Cyclotron Road
MS 88R0192
Berkeley, CA 94720-8101
USA
Tel: +1-510-486-7647
Fax: +1-510-486-5757
E-mail: ebrowne@lbl.gov

Mr. Thomas W. **BURROWS**
National Nuclear Data Center
Building 197D
Brookhaven National Laboratory
P.O. Box 5000
Upton, NY 11973-5000
USA
Tel: +1 631 344 5084
Fax: +1 631 344 2806
E-mail: burrows@bnl.gov

Mr. Filip **G KONDEV**
Permanent Institute:
Argonne National Laboratory
Nuclear Data Program
Nuclear Engineering Division
9700 South Cass Avenue
IL 60439 Argonne
Argonne IL 60439
UNITED STATES OF AMERICA
E-mail: kondev@anl.gov

Mr. Desmond **MACMAHON**
Centre for Acoustics and Ionising Radiation
National Physical Laboratory
Queens Road
Teddington, Middlesex TW11 0LW
UNITED KINGDOM
Tel: +44-20-8943-8573
Fax: +44-20-8943-6161
E-mail: desmond.macmahon@npl.co.uk

Mr. Jagdish K. **TULI** (Director)
National Nuclear Data Center
Building 197D
Brookhaven National Laboratory
P.O. Box 5000
Upton, NY 11973-5000
USA
Tel: +1-631-344-5080
Fax: +1-631-344-2806
E-mail: tuli@bnl.gov

Mr. Piet **VAN ISACKER**
Groupe Physique
Grand Accelerateur National d'Ions Lourds (GANIL)
BP 55027
F-14076 Caen Cedex 5
FRANCE
Tel: +33-2-31 45 45 65
Fax: +33-2-31 45 44 21
E-mail: isacker@ganil.fr

Mr. Peter **VON BRENTANO**
Institut für Kernphysik der Universität Köln
Zülpicher Strasse 77
D-50937 Köln
GERMANY
Tel: +49-221-470-6960
Fax: +49-221-470-5168
E-mail: brentano@ikp.uni-koeln.de

IAEA STAFF

Mr. Alan L. **NICHOLS** (Director)
Nuclear Data Section
International Atomic Energy Agency
Wagramerstrasse 5
A-1400 Vienna
Austria
Tel: +43-1-2600-21709
Fax: +43-1-26007
E-mail: a.nichols@iaea.org

Mr. Kevin **MCLAUGHLIN** (Tutor)
Nuclear Data Section
International Atomic Energy Agency
Wagramerstrasse 5
A-1400 Vienna
Austria
Tel: +43-1-2600-21713
Fax: +43-1-26007
E-mail: p.mclaughlin@iaea.org

1.3 PRESENTATIONS AVAILABLE IN ELECTRONIC FORM ON CD-ROM

Presentations by Lecturers

Aims of the Workshop - General features of NSDD, J. Tuli

Nuclear Theory:
Nuclear Shell Model, P. Van Isacker (November 2003)
Interacting Boson Model, P. Van Isacker
Structure of the odd-even nuclei in the interacting boson model, S. Brant (April 2005)
High spin states in the interacting boson and boson-fermion model, S. Brant (April 2005)
Structure of odd-odd nuclei in the interacting boson-fermion-fermion model, S. Brant (April 2005)
β decay in the interacting boson-fermion model, S. Brant (April 2005)
Geometrical Symmetries in Nuclei – An Introduction, A. Jain ((November 2003)
Geometrical Symmetries in Nuclei, A. Jain (November 2003)
Lectures on Geometrical Symmetries in Nuclei, A. Jain (November 2003)
Hartree-Foch-Bogoliubov Method, D. Vretenar (November 2003)
Self-consistent Mean-field Models – Structure of Heavy Nuclei, D. Vretenar (November 2003)

Experimental Nuclear Spectroscopy:
Introduction, P. Von Brentano
Lecture I – Nuclear Shapes, P. Von Brentano
Lecture II – Measurement of Lifetimes, P. Von Brentano
Lecture I – Experimental Nuclear Structure Physics, F. Kondev (April 2005)
Lecture II – Experimental Nuclear Structure Physics at the extreme, F. Kondev (April 2005)

Statistical Analyses:
Evaluation of Discrepant Data I, D. MacMahon
Evaluation of Discrepant Data II, D. MacMahon
Convergence of Techniques for the Evaluation of Discrepant Data: D. MacMahon, A. Pearce, P. Harris
Techniques for Evaluating Discrepant Data, M.U. Rajput, D. MacMahon
Possible Advantages of a Robust Evaluation of Comparisons, J.W. Muller (presented by D. MacMahon)

ENSDF:
Evaluated Nuclear Structure Data Base, J.K. Tuli
Evaluations – A Very Informal History, J.K. Tuli
Evaluated Nuclear Structure Data File – A Manual for Preparation of Data Sets, J.K. Tuli
Guidelines for Evaluators, M.J. Martin, J.K. Tuli
Bibliographic Databases, T.W. Burrows

ENSDF Analysis and Utility Codes, T.W. Burrows:
- Their Descriptions and Uses, T.W. Burrows
- FMTCHK (Format and Syntax Checking), T.W. Burrows
- PowerPoint presentations, T.W. Burrows
- LOGFT (Calculates log *ft* for beta decay), T.W. Burrows
- GTOL (Gamma to Level), T.W. Burrows
- HSICC (Hager-Seltzer Internal Conversion Coefficients), T.W. Burrows

ENSDF – Decay Data, E. Browne
Model Exercises – Decay, E. Browne
ENSDF – Reaction Data, C. Baglin
ENSDF – Adopted Levels and Gammas, C. Baglin
ENSDF – Examples 1, 2, 3, 4 and 5, C. Baglin

Additional Material:
IAEA: NSDD Network, Recent Relevant CRPs and Other Activities (PowerPoint presentation), A.L. Nichols
IAEA: NSDD Network, Recent Relevant CRPs and Other Activities (draft paper), A.L. Nichols
Nuclear Structure and Decay Data: Introduction to Relevant Web Pages (draft paper), T.W. Burrows, P.K. McLaughlin, A.L. Nichols

Presentations by Participants

Compton Add-Back Protocols for use with the EXOGAM Array, A. Garnswothy
Experimental determination of photon emission probabilities, A. Luca
Nuclear data activities for Astrophysics at Oak Ridge National Laboratory, C. Nesaraja
Tandar Laboratory, CNEA. Argentina, D. Abriola
Experimental approach to the dynamics of fission, G. Ishak Boushaki
Laboratoire National Henri Becquerel, M.M. Be
Nuclear structure by gamma-ray spectroscopy, a completeness perspective, N. Nica
Radioactive beam spectroscopy of ^{212}Po and ^{213}At with the EXOGAM array, N. Thompson
Developing ^{152}Eu into a standard for detector efficiency calibration, R.M. Castro

1.4 OTHER WORKSHOP MATERIALS ON CD-ROM

Atomic Masses
Access to ENSDF Codes and Tools
Isotope Explorer
PCNuDat
Access to NSDD Resources

NNDC Online Data Service Manual and Data Citation Guidelines

Introduction to International Nuclear Structure and Decay Data Network
Contact names and addresses

Access to ENSDF Format Summary and Examples

Nuclear Structure Manuals

1.5 ADDENDUM MANUAL

Significant quantities of written material were prepared for the workshop. Their accumulation in various forms acted as an aid to the participants in their understanding of nuclear theory, measurement techniques, data analysis and ENSDF mass-chain evaluations, representing an important combination of technical information for future reference and other NSDD workshops. Therefore, a relatively large fraction of these presentations, background papers and manuals have been assembled for further use in the form of an earlier document [2] and this Addendum report.

Our intention is to use and develop this material in the years to come, particularly for other workshops of this type. Another aim is to ensure that such presentations are not lost, and can be readily at hand for new mass-chain and decay-data evaluators to assist them in their preparation of recommended data for the ENSDF files.

1.6 RECOMMENDATIONS AND CONCLUSIONS

A number of important points can be made concerning the workshop:

1. Twenty-seven participants were selected and attended a two-week workshop that covered nuclear theory and modeling, relevant experimental techniques, statistical analyses, and the philosophy and methodology for comprehensive mass chain evaluations. Support materials and information were also provided on the International Network of Nuclear Structure and Decay Data Evaluators and the most relevant CRPs organized by the IAEA Nuclear Data Section.

2. Workshop participants were introduced to mass chain evaluations through group and individual PC/computing activities (50% of the agenda of the second week) CD-ROM and hardcopy materials were provided by IAEA staff for all students/lecturers.

3. Administrative functions leading up to and during the course of the workshop worked smoothly, including visa arrangements, travel and subsistence payments to students and lecturers, additional banking transactions, and hotel/guest-house accommodation.

4. Specific participants were identified for future involvement in NSDD and mass chain evaluations.

5. Further lessons were learnt by the IAEA staff and lecturers involved in this ICTP workshop, and much experience was gained in ensuring future success in the organization of such events. This particular workshop ran extremely smoothly, and all participants were able to attend (i.e., 100% success with visas). Students were given the opportunity to review the workshop through a written questionnaire and direct discussions (on 15 April). Their major recommendations are as follows:

(a) 1½ hour lectures should be broken down further to 2 x 40 min plus 10 min break;

(b) provision of sample questions and answers prior to the workshops (answers also to be worked out during the course of individual lectures – ICTP to note);

(c) forewarn participants that they will be asked to give a short presentation on their own nuclear physics studies (ICTP to note);

(d) every participant/student to operate their own individual PC, rather than share (ICTP to note);

(e) outside activities during the middle weekend (ICTP to note);

(f) further development of nuclear theory lectures beyond just IBM;

(g) introduce ENSDF format to participants prior to the workshop (through IAEA-NDS web pages?);

(h) additional presentations of the details of XUNDL and NSR databases;

(i) allow an afternoon off from the intensive training (first Friday afternoon?).

As before, this combination of Wednesday/Thursday written questionnaire and Friday face-to-face review session produced constructive feedback. The overall opinion of all of the students was that they had thoroughly enjoyed the 2-week workshop, made useful new contacts with lecturers, IAEA-NDS staff and other students, and learnt much about nuclear structure and decay data; all of the primary objectives of the workshop were successfully achieved.

ACKNOWLEDGEMENTS

The authors wish to thank our fellow co-directors of the NSDD Workshop for their support leading up to April 2005, and particularly the lecturers (all experts in their fields) for their enthusiasm during the workshop and provision of the various technical input to this document. Administrative aspects of the workshop were considerable leading up to and during the course – as an ICTP-supported activity, all such features and problems were handled by Ms Elizabeth Brancaccio (ICTP), and her efforts were much appreciated. Finally, none of the lectures and associated

materials would have been delivered without the enthusiastic involvement of all participants at this workshop.

REFERENCE

1. PRONYAEV, V.G., NICHOLS, A.L., Summary Report on Workshop on Nuclear Structure and Decay Data Evaluation, 18-22 November 2002, INDC(NDS)-439, January 2003.

2. NICHOLS, A.L., MCLAUGHLIN, P.K., Workshop on Nuclear Structure and Decay Data: Theory and Evaluation, Manual, Parts 1 and 2, INDC(NDS)-452, November 2004.

Nuclear Theory:
Notes on IBM-1 programmes

P. Van Isacker

GANIL, France

E.mail: isaker@ganil.fr

Notes on IBM-1 programmes

These notes contain a short and practical introduction on how to do numerical calculations with an IBM-1 code. Only the simplest version of the model is explained which corresponds to N identical s and d bosons. Numerical codes are available for several extensions of this approach, such as IBM-2 and IBM-3 or IBFM, and they function along similar principles.

1. Getting started

To run the IBM-1 programmes (energies and transitions), you should have the following files:

- `cfp20.for`: Fortran source of the programme that constructs a data file with the coefficients of fractional parentage (cfp's). This programme is selfcontained: no library is required with which to link it and no input file is required to run it. It produces two output files:
  - `write(4)`: output file to be saved containing the cfp's (suggested name: `cfp20.dat`);
  - `write(6)`: large output file that can be consulted should problems arise but can be discarded otherwise.

  The programme is currently set for producing a data file so that a calculation up to 20 s and d bosons can be performed.
- `ibm1.for`: Fortran source of the programme that diagonalises an IBM-1 hamiltonian (*i.e.*, determines its eigenspectrum) with wave functions that are stored for subsequent use with `ibm1t`. The basis and the hamiltonian are described in section 2. It should be linked with `ibml` and `eig500`. Input and output files are:
  - `read(3)`: input data file containing cfp's, usually named `cfp20.dat`;
  - `read(5)`: input data file `ibm1a.inp` or `ibm1b.inp`;
  - `write(1)`: output file containing the wave functions in unformatted form to be used by `ibm1t`;
  - `write(6)`: output file summarising the results of the calculation.
- `ibml.for`: Fortran source of library routines to be linked with `ibm1` and `ibm1t`.
- `eig500.for`: Fortran source of the diagonalisation routine to be linked with `ibm1`. The maximum dimension the matrix that can be diagonalised is set to 500.

- `ibm1t.for`: Fortran source of the programme that calculates E0 and E2 transition matrix elements and probabilities. The transition operators are described in section 3. It should be linked with `ibm1`. Input and output files are:
  - `read(3)`: input data file containing cfp's, usually named `cfp20.dat`;
  - `read(5)`: input data file `ibm1t.inp`;
  - `write(6)`: output file summarising the results of the calculation.
- `ibm1a.inp`: Input file for `ibm1` with the two-body hamiltonian in multipole expansion.
- `ibm1b.inp`: Input file for `ibm1` with the two-body hamiltonian in "standard" representation.
- `ibm1t.inp`: Input file for `ibm1t`.

2. Running ibm1

The first 20 characters on each input line are for description purposes: they contain the name(s) of the variable(s) that is (are) read on that line. Integer variables (`NMIN`, `NMAX`, `LMIN`, `LMAX`, `MVMAX`, `I1`, `I2`, `I3`, `I4`) are in `I2`, logical variables (`MULT`, `CUB`, `DEF`) are in `L1` (*i.e.*, `T` for `.TRUE.` and `F` for `.FALSE.`) and real variables (all others) are in `F9.6`.

The integer and logical variables are defined as follows:

- `NMIN`, `NMAX`: minimum and maximum values of the number of bosons N;
- `LMIN`, `LMAX`: minimum and maximum values of the angular momentum L;
- `LVMAX`: number of levels calculated for each angular momentum;
- `I1`, `I2`, `I3`, `I4`: print control parameters with
  - all four zero: minimal output with relative energies;
  - `I1` $= 1$: absolute energies;
  - `I2` $= 1$: probability distribution in N;
  - `I2` $= 2$: probability distribution in N and in n_d;
  - `I3` $= 1$: wave functions in a vibrational basis;
  - `I4` $= 1$: hamiltonian matrix.
- `MULT`: whether the hamiltonian is in multipole or standard representation;
- `CUB`: whether three-body interactions are included or not;

- DEF: whether the deformation parameter γ is calculated or not.

The real variables are explained below as well as in the source code `ibm1.for`.

With the `ibm1` programme one can perform "normal" calculations; these are described in section 2.1. Some extensions that are possible with `ibm1` are summarised in section 2.2.

2.1. Standard IBM1 calculations

The following choice of parameters corresponds to a standard IBM-1 calculation:

- `NMIN` = `NMAX`: the total number of bosons N;
- `CUB` = .`FALSE`.: no three-body interactions;
- `DEF` = .`FALSE`.: no calculation of the deformation parameter γ.

It this case all lines after `O6` (in `ibm1a.inp`) or `U0` (in `ibm1b.inp`) are ignored.

The basis is the usual one in IBM-1, which consists of N s or d bosons. The hamiltonian can be specified in multipole form (if `MULT` = .`TRUE`.) or in terms of single-boson energies and two-body boson interaction matrix elements (in "standard" representation, if `MULT` = .`FALSE`.). The hamiltonian in multipole expansion is of the form

$$\hat{H} = \texttt{EPS}\,\hat{n}_d + \texttt{A(0)}\hat{P}^\dagger\hat{P} + \texttt{A(1)}\hat{L}\cdot\hat{L} + \texttt{A(2)}\hat{Q}_\chi\cdot\hat{Q}_\chi + \texttt{A(3)}\hat{T}_3\cdot\hat{T}_3 + \texttt{A(4)}\hat{T}_4\cdot\hat{T}_4,$$

where $\cdot$ denotes a scalar product, $\hat{T}_\lambda\cdot\hat{T}_\lambda \equiv \sum_\mu \hat{T}_{\lambda\mu}\hat{T}_{\lambda\mu}$, and where the following multipole operators appear:

- d-boson number operator $\hat{n}_d = d^\dagger\cdot\tilde{d} = \sqrt{5}[d^\dagger\times\tilde{d}]^{(0)}$;
- pairing operator $\hat{P}^\dagger = \frac{1}{2}(s^\dagger s^\dagger - \texttt{O6}\,d^\dagger\cdot d^\dagger)$;
- angular momentum operator $\hat{L} = \sqrt{10}[d^\dagger\times\tilde{d}]^{(1)}$;
- quadrupole operator $\hat{Q}_\chi = [s^\dagger\times\tilde{d} + d^\dagger\times\tilde{s}]^{(2)} + \texttt{CHI}[d^\dagger\times\tilde{d}]^{(2)}$;
- octupole operator $\hat{T}_3 = [d^\dagger\times\tilde{d}]^{(3)}$;
- hexadecapole operator $\hat{T}_4 = [d^\dagger\times\tilde{d}]^{(4)}$.

The hamiltonian in standard representation is of the form

$$\begin{aligned}\hat{H} \;=\; & \texttt{C(1)}\hat{N} + \texttt{C(2)}\hat{n}_d + \texttt{C(3)}\tfrac{1}{2}[[d^\dagger\times d^\dagger]^{(0)}\times[\tilde{d}\times\tilde{d}]^{(0)}]^{(0)} \\ & + \texttt{C(4)}\sqrt{5}\tfrac{1}{2}[[d^\dagger\times d^\dagger]^{(2)}\times[\tilde{d}\times\tilde{d}]^{(2)}]^{(0)} \\ & + \texttt{C(5)}\tfrac{3}{2}[[d^\dagger\times d^\dagger]^{(4)}\times[\tilde{d}\times\tilde{d}]^{(4)}]^{(0)}\end{aligned}$$

$$+\mathtt{C(6)}[[s^\dagger \times d^\dagger]^{(2)} \times [\tilde{d} \times \tilde{d}]^{(2)} + [d^\dagger \times d^\dagger]^{(2)} \times [\tilde{s} \times \tilde{d}]^{(2)}]^{(0)}$$
$$+\mathtt{C(7)}[[s^\dagger \times s^\dagger]^{(0)} \times [\tilde{d} \times \tilde{d}]^{(0)} + [[d^\dagger \times d^\dagger]^{(0)} \times [\tilde{s} \times \tilde{s}]^{(0)}]^{(0)}$$
$$+\mathtt{C(8)}\sqrt{5}[[s^\dagger \times d^\dagger]^{(2)} \times [\tilde{s} \times \tilde{d}]^{(2)}]^{(0)}$$
$$+\mathtt{C(9)}[[s^\dagger \times s^\dagger]^{(0)} \times [\tilde{s} \times \tilde{s}]^{(0)}]^{(0)}.$$

All parameters have units of energy, except `CHI` and `O6` which are dimensionless.

2.2. Extensions

There are a number of options which allow the definition of a more general IBM-1 hamiltonian.

- *Multi-particle–hole excitations.* If `NMIN` $\neq$ `NMAX`, the total boson number N is not a constant but can take the values $N =$ `NMIN`, `NMIN` $+ 2, \ldots,$ `NMAX`. The different N values correspond to 0p–0h, 2p–2h, $\ldots$, $2n$p–$2n$h excitations, and each configuration is specified by its IBM-1 hamiltonian. Configurations differing by two bosons (*e.g.*, N and $N + 2$) are mixed by the following hamiltonian

  $$\mathtt{ALPHA}(s^\dagger s^\dagger + \tilde{s}\tilde{s}) + \mathtt{BETA}(d^\dagger \cdot d^\dagger + \tilde{d} \cdot \tilde{d}),$$

  and, furthermore, configurations are separated by an offset `DELTA`.

- *Three-boson interactions.* The most general IBM-1 hamiltonian which contains all three-boson interactions can be considered if `CUB` = `.TRUE.`. The three-boson interactions can be defined through matrix elements between normalised three-boson states in a vibrational or in an SU(3) basis. Definitions of these interactions are given in the source code `ibm1.for`. [There are two possible definitions of SU(3) basis, corresponding to `SU3` $= -1$ (standard) or `SU3` $= +1$.] Finally, with `CUB` = `DEF` = `.TRUE.`, it is possible to add a Q^3 term

  $$\mathtt{VQQQ}[\hat{Q}_\chi \times \hat{Q}_\chi \times \hat{Q}_\chi]^{(0)},$$

  with a quadrupole operator of the form

  $$\hat{Q}_\chi = [s^\dagger \times \tilde{d} + d^\dagger \times \tilde{s}]^{(2)} + \mathtt{CHIQ}[d^\dagger \times \tilde{d}]^{(2)}.$$

  Note that all contributions to the hamiltonian are additive, which can thus be of one- + two- + three-body nature. However, if `CUB` = `.FALSE.`, the three-body interactions are ignored; if either `CUB` = `.FALSE.` or `DEF` = `.FALSE.`, the Q^3 term is ignored.

- *Deformation parameter γ.* For `DEF` = `.TRUE.` the programme calculates the deformation parameter γ in each eigenstate from the following expectation values in that state:

  $$\langle [\hat{Q} \times \hat{Q}]^{(0)}_0 \rangle = \sqrt{\frac{1}{5}}\beta^2, \qquad \langle [\hat{Q} \times \hat{Q} \times \hat{Q}]^{(0)}_0 \rangle = -\sqrt{\frac{2}{35}}\beta^3 \cos 3\gamma.$$

The programme `ibm1` also prints the classical limit (the potential in β and γ) of the one- and two-body part of the hamiltonian.

3. Running ibm1t

The first 20 characters on each input line are for description purposes: they contain the name(s) of the variable(s) that is (are) read on that line. The first line specifies `NMIN` and `NMAX`; their values should be consistent with those used in `ibm1`. The next two lines specify the boson E0 transition operator

$$\hat{T}(\mathrm{E0}) = \texttt{E0(1)}\hat{n}_s + \texttt{E0(2)}\hat{n}_d,$$

where `E0(1)` and `E0(2)` are in units of $e$fm. This operator can also be used for the calculation of nuclear radii. The next two lines specify the boson E2 transition operator

$$\hat{T}(\mathrm{E2}) = \texttt{E2(1)}\left([s^\dagger \times \tilde{d} + d^\dagger \times \tilde{s}]^{(2)} + \texttt{E2(2)}[d^\dagger \times \tilde{d}]^{(2)}\right),$$

where `E2(1)` is a boson effective charge which has the units of $e\mathrm{fm}^2$ and `E2(2)` is dimensionless. For `E2(2)` = `CHI` we obtain the so-called consistent-Q formalism. All subsequent input lines contain 7 integers (in `I3`) $L_1\ n_{11}\ n_{12}\ L_2\ n_{21}\ n_{22}\ \lambda$ with the following meaning:

- L_1 and L_2: angular momenta of initial and final states;
- n_{i1} and n_{i2}: for angular momentum L_i, consider states from n_{i1} to n_{i2};
- λ: multipolarity of the transition (only $\lambda = 0, 2$ is implemented). If λ is negative, reduced matrix elements are computed, otherwise B(E2) values are given.

Nuclear Theory:
Structure of the odd-even nuclei in the interacting boson model

S. Brant

University of Zagreb, Croatia

E.mail: Brant@phy.hr

Fermion degrees of freedom in the interacting boson model

Slobodan Brant

Department of Physics, Faculty of Science
University of Zagreb
Zagreb
Croatia

1. Structure of odd-even nuclei in the interacting boson-fermion model
2. High spin states in the interacting boson and interacting boson-fermion model
3. Structure of odd-odd nuclei in the interacting boson-fermion-fermion model
4. β decay in the interacting boson-fermion model

1.

Structure of odd-even nuclei in the interacting boson fermion model

Shell model $\longrightarrow$ matrix elements of the effective interaction between identical nucleons are strongly attractive when the two nucleons are in a $J = 0$ state and remain attractive when the two nucleons are in a $J = 2$ state. They become repulsive for $J \geq 4$.

Nucleons tend to form pairs with angular momentum $J = 0$ or $J = 2$

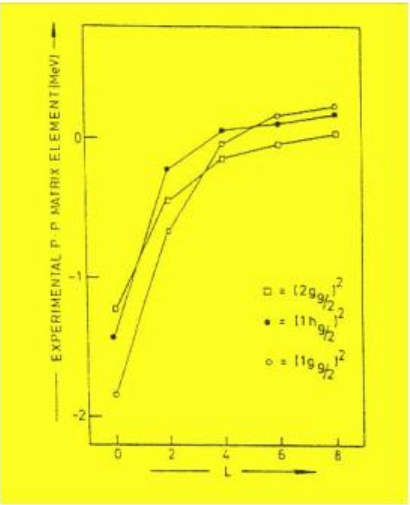

Generalized seniority scheme: generalization of the seniority scheme to several non-degenerate orbits. The number of active nucleons is counted in respect to the nearest closed shell (valence nucleons). Contributions from orbitals outside the valence shell can be neglected since they lie at a too high energy.

A collective $J = 0$ pair is generated by the operator

$$S^\dagger = \sum_j \alpha_j S_j^\dagger$$
$$S_j^\dagger = \frac{1}{2}\sqrt{2j+1}\ (c_j^\dagger \tilde{c}_j)^{(0)}$$

State with generalized seniority $w = 0$ and $n = 2N$ particles

$$|n,\ J = 0,\ w = 0\rangle = (S^\dagger)^N\ |0\rangle$$

An excited 2^+ state is generated by the operator that creates a collective state with $J = 2$ and $w = 2$

$$D^\dagger = \sum_{jj'} \frac{1}{2}\beta_{jj'}\sqrt{1+\delta_{jj'}}\ (c_j^\dagger \tilde{c}_{j'})^{(2)}$$

State with generalized seniority $w = 2$, $J = 2$ and $n = 2N$ particles

$$|n,\ J = 2,\ w = 2\rangle = D^\dagger (S^\dagger)^{N-1}\ |0\rangle$$

The structure coefficients α_j and $\beta_{jj'}$ can be obtained by diagonalizing the shell model interaction in the space of all $w = 0, 2$ states.

Instead of having to use the full shell model space, it is sufficient to consider the much smaller (S, D) subspace.

- Low-lying collective states can be described very well
- Non collective states can not be described
- The matrix elements of the fermion operators in the (S, D) subspace can be cumbersome
- The space built on S and D fermion pairs is mapped onto a corresponding space built on s and d boson degrees of freedom

- For states containing more than one D fermion pair, we have to map the components of the state which is orthogonal to all the states containing fewer D fermion pairs.

$$
\begin{aligned}
|S^N,\ L=0\rangle &\longrightarrow |s^N,\ L=0\rangle \\
|D\ S^{N-1},\ L=2\rangle &\longrightarrow |d\ s^{N-1},\ L=2\rangle \\
|D^m\ S^{N-m},\ L\rangle_{\ orth} &\longrightarrow |d^m\ s^{N-m},\ L\rangle
\end{aligned}
$$

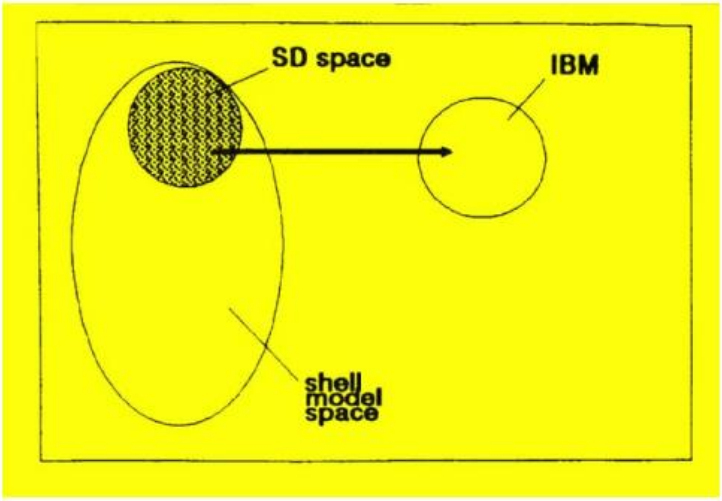

- By equating matrix elements in (S, D) and (s, d) spaces, the operators in the (s, d) space are obtained.
- Since the S and D fermion pairs are always pairs of like nucleons (two protons or two neutrons), one has proton (s_π, d_π) and neutron (s_ν, d_ν) bosons. The model is called IBM-2.

$$H_B = \epsilon_d \left(\hat{n}_{d_\nu} + \hat{n}_{d_\pi}\right) + \kappa \left(Q^B_\nu \cdot Q^B_\pi\right) + M_{\nu\pi} + V_{\nu\nu} + V_{\pi\pi}$$

$$\begin{aligned} Q^B_\nu &= d^\dagger_\nu s_\nu + s^\dagger_\nu \tilde{d}_\nu + \chi_\nu \left[d^\dagger_\nu \tilde{d}_\nu\right]^{(2)} \\ Q^B_\pi &= d^\dagger_\pi s_\pi + s^\dagger_\pi \tilde{d}_\pi + \chi_\pi \left[d^\dagger_\pi \tilde{d}_\pi\right]^{(2)} \end{aligned}$$

$$\begin{aligned} M_{\nu\pi} = & \frac{1}{2}\xi_2 \left(\left(d^\dagger_\nu s^\dagger_\pi - d^\dagger_\pi s^\dagger_\nu\right) \cdot \left(\tilde{d}_\nu s_\pi - \tilde{d}_\pi s_\nu\right)\right) \\ & - \sum_{K=1,3} \xi_K \left(\left[d^\dagger_\nu d^\dagger_\pi\right]^{(K)} \cdot \left[\tilde{d}_\nu \tilde{d}_\pi\right]^{(K)}\right) \end{aligned}$$

$$V_{\nu\nu} = \frac{1}{2} \sum_{L=0,2,4} c^\nu_L \left(\left[d^\dagger_\nu d^\dagger_\nu\right]^{(L)} \cdot \left[\tilde{d}_\nu \tilde{d}_\nu\right]^{(L)}\right)$$

$$V_{\pi\pi} = \frac{1}{2} \sum_{L=0,2,4} c^\pi_L \left(\left[d^\dagger_\pi d^\dagger_\pi\right]^{(L)} \cdot \left[\tilde{d}_\pi \tilde{d}_\pi\right]^{(L)}\right)$$

- The major part of the interaction between like particles is contained in the boson energies and a smaller in the $V_{\nu\nu}$ and $V_{\pi\pi}$ terms.
- The $Q^B_\nu \cdot Q^B_\pi$ interaction is the boson image of the neutron-proton quadrupole-quadrupole interaction.
- $M_{\nu\pi}$ (Majorana term) shifts up all states that are not totally symmetric in the neutron-proton degree of freedom. It is a consequence of the truncation of the basis to s and d bosons only.

Introducing the concept of F spin, the IBM-1 Hamiltonian can be obtained by projecting out the part that acts only on the maximal F spin subspace (on states that are totally symmetric in the neutron-proton degree of freedom).

$$\begin{aligned} H_B = & \varepsilon\, \hat{N} + \frac{1}{2}\, v_0 \, \left(\left[d^\dagger d^\dagger\right]_{(0)} \left[\tilde{s}\tilde{s}\right]_{(0)} + h.c.\right)_{(0)} \\ & + \frac{1}{\sqrt{2}}\, v_2 \, \left(\left[d^\dagger d^\dagger\right]_{(2)} \left[\tilde{d}\tilde{s}\right]_{(2)} + h.c.\right)_{(0)} \\ & + \sum_{L=0,2,4} \frac{1}{2}\, C_L \, \sqrt{2L+1} \, \left(\left[d^\dagger d^\dagger\right]_{(L)} \left[\tilde{d}\tilde{d}\right]_{(L)}\right)_{(0)} \end{aligned}$$

LIMITS

$$
\begin{array}{lcll}
U(6) & \supset & U(5) \supset O(5) \supset O(3) \supset O(2) & \textit{vibrational limit} \\
U(6) & \supset & SU(3) \supset O(3) \supset O(2) & \textit{rotational limit} \\
U(6) & \supset & O(6) \supset O(5) \supset O(3) \supset O(2) & \gamma - \textit{soft limit}
\end{array}
$$

The Lie algebra U(6) admits:

- Schwinger boson realization in terms of 6 bosons s, d_μ
- Holstein-Primakoff boson realization in terms of 5 bosons b_μ

$$
\begin{aligned}
d^\dagger_{2\mu} &\longleftrightarrow b^\dagger_{2\mu} \\
s^\dagger &\longleftrightarrow \sqrt{N - \sum_\mu b^\dagger_{2\mu} b_{2\mu}}
\end{aligned}
$$

- In the IBFM, an odd-nucleon operator a^{i}_{j} is introduced in addition to the *s* and *d* boson operators
- The states in the IBFM model space can be related to the shell model basis by using the generalized seniority scheme.
- The odd-nucleon operator $a^\dagger_j$ should not be regarded as a nucleon creation operator (in the shell model sense) but as a generalized seniority raising operator.

$$
\begin{aligned}
a^\dagger_j \, |s^N\rangle = \quad |js^N\rangle \quad &\longleftrightarrow \quad |n = 2N+1, J = j, w = 1\rangle \\
(a^\dagger_j d^\dagger)^{(J)} \, |s^{N-1}\rangle = |(jd)^{(J)} s^{N-1}\rangle \quad &\longleftrightarrow \quad |n = 2N+1, J, w = 3\rangle
\end{aligned}
$$

- The operator $a^\dagger_j$ operating on an N boson state with n_d d -bosons creates a state which corresponds to a shell model state with $n = 2N + 1$ and $w = 2n_d + 1$.
- For the shell model single-nucleon operator $c^\dagger_j$
  $c^\dagger_j \, |w = 2\rangle = \alpha |w = 1\rangle + \beta |w = 3\rangle$
- For the odd-nucleon operator $a^\dagger_j$
  $a^\dagger_j \, |w = 2\rangle = |w = 3\rangle$

A microscopic theory for a system that includes both fermionic and bosonic degrees of freedom is complicated.

The dominant interaction in the coupling of the odd-particle to the bosons is the proton-neutron quadrupole interaction → construction of the IBFM image of the shell model quadrupole operator.

There are several methods for obtaining the IBFM image of the shell model quadrupole operator. One of them is to introduce the pseudo particle operator $\check{c}_j^\dagger$ (Scholten).

Condition:

The matrix elements of $\check{c}_j^\dagger$ in the IBFM space are equal to the matrix elements of $c_j^\dagger$ in the shel model space.

For $w \leq 1$ (α_j are the coefficients which enter in the definition of the S pair operator):

$$\hat{n} = \sum_j \alpha_j^2 \sum_m c_{jm}^\dagger c_{jm} = \sum_j \alpha_j^2 \hat{n}_j$$

$$\langle S^N | \hat{n} | S^N \rangle = 2N$$

Effective degeneracy

$$\Omega_e = \sum_j \alpha_j^2 \Omega_j$$

Here the spherical shell model OCCUPATION PROBABILITIES v_j^2 are introduced
($u_j^2 + v_j^2 = 1$).

$$v_j^2 = n_j/(2j+1)$$
$$n_j = \langle S^N | \hat{n}_j | S^N \rangle \approx 2N\alpha_j^2 \frac{\Omega_j}{\Omega_e}$$
$$v_j^2 = \alpha_j^2 N/\Omega_e$$

$$\langle S^N j' \parallel c_j^\dagger \parallel S^N \rangle = -\hat{j} u_j \delta_{jj'} = u_j \langle s^N j' \parallel a_j^\dagger \parallel s^N \rangle$$
$$\langle S^N \parallel c_j^\dagger \parallel S^{N-1} j' \rangle = \hat{j} v_j \delta_{jj'} = v_j \langle s^N \parallel (s^\dagger \tilde{a}_j)^{(j)} \parallel s^{N-1} j' \rangle / \sqrt{N}$$

For T ≤ 3, similar expressions can be obtained. Finally, the IBFM image of the shell model single-nucleon creation operator is

$$\begin{aligned} \check{c}_j^\dagger &= u_j a_j^\dagger - \sum_{j'} \frac{v_j}{\sqrt{N}} \sqrt{\frac{10}{2j+1}} \beta_{j'j} (K_\beta)^{-1} s^\dagger (\tilde{d}\, a_{j'}^\dagger)^{(j)} \\ &+ \frac{v_j}{\sqrt{N}} (s^\dagger \tilde{a}_j)^{(j)} + \sum_{j'} u_j \sqrt{\frac{10}{2j+1}} \beta_{j'j} (K_\beta)^{-1} (d^\dagger \tilde{a}_{j'})^{(j)} \end{aligned}$$

$$K_\beta^2 = \sum_{jj'} \beta_{j'j}^2$$

The coefficients $\beta_{j'j}$ define the microscopic structure of the *d*-boson.

The matrix elements of the quadrupole operator $\sum_{jj'} Q_{jj'} \ (c_j^\dagger \tilde{c}_{j'})^{(2)}$ in the fermion space are replaced by the matrix elements of the pseudo particle operator $\check{c}_j^\dagger$ acting in the boson space giving the quadrupole operator expressed in terms of boson and odd-particle operators.

$$\begin{aligned} Q^{(2)} &= Q_B^{(2)} + Q_F^{(2)} \\ Q_B^{(2)} &= [s^\dagger \tilde{d} + d^\dagger \tilde{s}]^{(2)} + \chi [d^\dagger \tilde{d}]^{(2)} \\ Q_F^{(2)} &= \sum_{jj'} Q_{jj'} \ (u_j u_{j'} - v_j v_{j'}) \ (a_j^\dagger \tilde{a}_{j'})^{(2)} \\ &- \sqrt{\frac{10}{N}} \sum_{jj'j''} Q_{jj'} (u_j v_{j'} + v_j u_{j'}) \beta_{j''j} [(d^\dagger \tilde{a}_{j''})^{(j)} (\tilde{s} a_{j'}^\dagger)^{(j')}]^{(2)} (\hat{j} K_\beta)^{-1} \end{aligned}$$

The boson-fermion interaction can be generated by the interaction between like particles or by the proton-neutron quadrupole interaction. The structure of the interactions is identical. The product of $Q_B^{(2)}$ and $Q_F^{(2)}$ contributes to the boson-fermion interaction. By mapping the basis from IBM-2 onto IBM-1 and taking terms up to second order in *d*-boson operators, the standard form of the boson-fermion interaction is obtained.

The IBFM-1 Hamiltonian for an odd-even nucleus

$$H = H_B + H_F + V_{BF}$$

H_B is the boson Hamiltonian of IBM-1 describing a system of N interacting bosons (correlated S and D pairs) that approximate the valence nucleon pairs:

$$\begin{aligned} H_B &= \varepsilon\, \hat{N} + \frac{1}{2}\, v_0\, \left([d^\dagger \times d^\dagger]_{(0)} \times [\tilde{s} \times \tilde{s}]_{(0)} + h.c.\right)_{(0)} \\ &+ \frac{1}{\sqrt{2}}\, v_2\, \left([d^\dagger \times d^\dagger]_{(2)} \times [\tilde{d} \times \tilde{s}]_{(2)} + h.c.\right)_{(0)} \\ &+ \sum_{L=0,2,4} \frac{1}{2}\, C_L\, \sqrt{2L+1}\, \left([d^\dagger \times d^\dagger]_{(L)} \times [\tilde{d} \times \tilde{d}]_{(L)}\right)_{(0)} \end{aligned}$$

$$n_s = N - n_d$$

H_F is the fermion Hamiltonian containing quasiparticle energies of odd protons or neutrons. The quasiparticle energies and occupation probabilities contained in the fermion Hamiltonian, and other terms, are obtained in a BCS calculation with some standard set of single fermion energies.

$$H_F = \sum_i \varepsilon_i\, a_i^\dagger \tilde{a}_i$$

V_{BF} is the IBFM-1 boson-fermion interaction containing the dynamical, exchange and monopole term.

- The dynamical interaction V_{DYN} represents the direct component of the quadrupole interaction between the odd particle and the bosons.
- The exchange interaction V_{EXC} is due to the two-particle nature of the bosons, bringing the Pauli exclusion principle into play.
- The monopole interaction V_{MON} can result from a variety of causes, in particular from the blocking of certain degrees of freedom by the odd particle.

$$V_{BF} = V_{DYN} + V_{EXC} + V_{MON}$$

$$V_{DYN} = \Gamma_0 \sum_{j_1 j_2} \sqrt{5}\,(u_{j_1}u_{j_2} - v_{j_1}v_{j_2})\,\langle j_1 \parallel Y_2 \parallel j_2\rangle\,\left([a^\dagger_{j_1} \times \tilde{a}_{j_2}]^{(2)} \times Q_B^{(2)}\right)^{(0)}$$

$Q_B^{(2)}$ is the standard boson quadrupole operator

$$Q_B^{(2)} = [s^\dagger \times \tilde{d} + d^\dagger \times \tilde{s}]^{(2)} + \chi [d^\dagger \times \tilde{d}]^{(2)}$$

$$V_{EXC} = \Lambda_0 \sum_{j_1 j_2 j_3} (-2)\sqrt{\frac{5}{2j_3+1}}\,(u_{j_1}v_{j_3} + v_{j_1}u_{j_3})\;(u_{j_2}v_{j_3} + v_{j_2}u_{j_3})$$
$$\langle j_3 \parallel Y_2 \parallel j_1\rangle\,\langle j_3 \parallel Y_2 \parallel j_2\rangle\;:\left([a^\dagger_{j_1} \times \tilde{d}\,]_{j_3} \times [\tilde{a}_{j_2} \times d^\dagger\,]_{j_3}\right)^{(0)}:$$

$$V_{MON} = A_0 \sum_j \sqrt{5}\,(2j+1)\,\left([a^\dagger_j \times \tilde{a}_j]^{(0)} \times [d^\dagger \times \tilde{d}]^{(0)}\right)^{(0)}$$

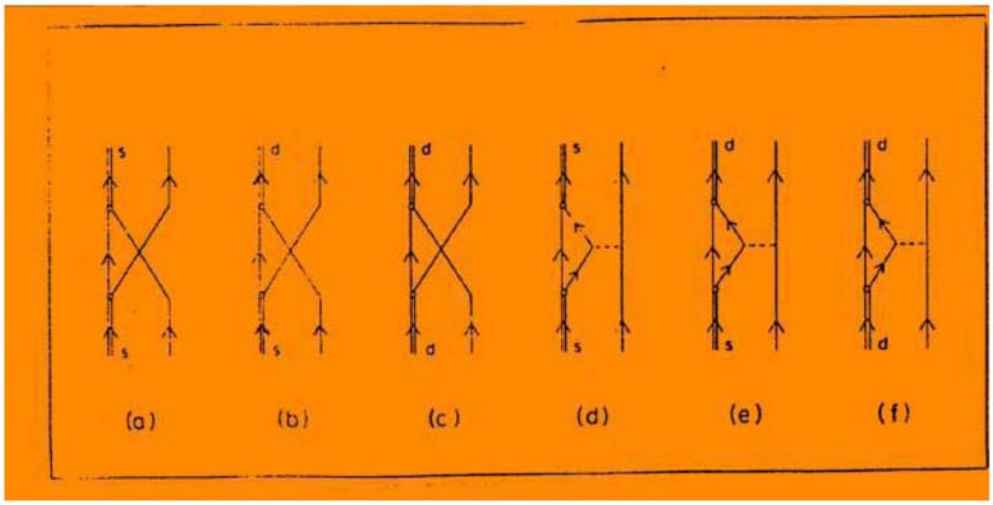

(a), (b), (c) exchange terms
(d), (e), (f) direct terms

The structure coefficients:

- The coefficients v_j are related to the structure coefficients of the fermion S-pair state, which is the microscopic equivalent of the s boson. In practice, they are the occupation probabilities of the single-particle orbits, as follows from a spherical BCS calculation.

- The coefficients $\beta_{j_a j_b} = (u_{j_a} v_{j_b} + v_{j_a} u_{j_b}) \ \langle j_a \parallel Y_2 \parallel j_b \rangle$ are the structure coefficients of the d boson.

The electromagnetic operators have the form:

$$M(E2) \quad = \quad M_B(E2) + M_F(E2)$$

$$M_B(E2) \quad = \quad \frac{3}{4\pi} \, R_0^2 \, e^{VIB} \, \left([s^\dagger \times \tilde{d} + d^\dagger \times \tilde{s}]^{(2)} + \chi [d^\dagger \times \tilde{d}]^{(2)} \right)$$

$$R_0^2 = 0.0144 \ A^{\frac{2}{3}} \qquad barn$$

$$M_F(E2) \quad = \quad \frac{3}{5} \, R_0^2 \, e_F \, Y_2$$

Common notation:

$$\frac{3}{4\pi} \, R_0^2 \, e^{VIB} \quad = \quad e_B$$

$$\vec{M}(M1) = \vec{M}_B(M1) + \vec{M}_F(M1)$$

$$\vec{M}_B(M1) = \sqrt{\frac{3}{4\pi}}\,\sqrt{10}\,g_R\,[d^\dagger \times \tilde{d}]^{(1)}$$

$$\vec{M}_F(M1) = \sqrt{\frac{3}{4\pi}}\,[\,g_l\,\vec{l} + g_s\,\vec{s} + g_T\,(Y_2 \times \vec{s}\,)_1\,]$$

Common notations:

$$\sqrt{\frac{3}{4\pi}}\,g_R = g_B$$

IBFM (and its extensions) provide a consistent description of nuclear structure phenomena in:

- spherical nuclei
- deformed nuclei
- transitional nuclei

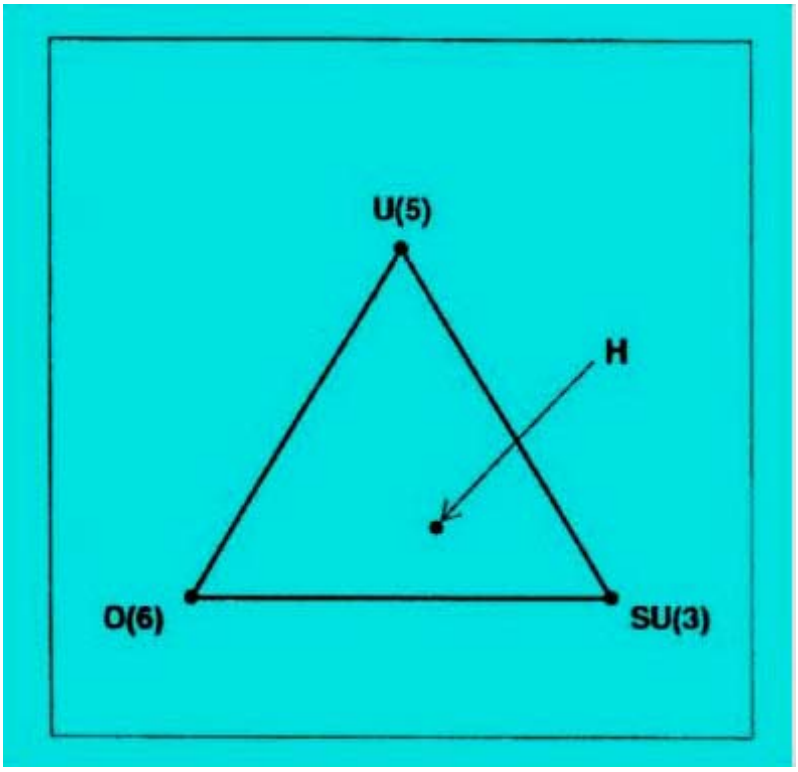

Spherical nuclei

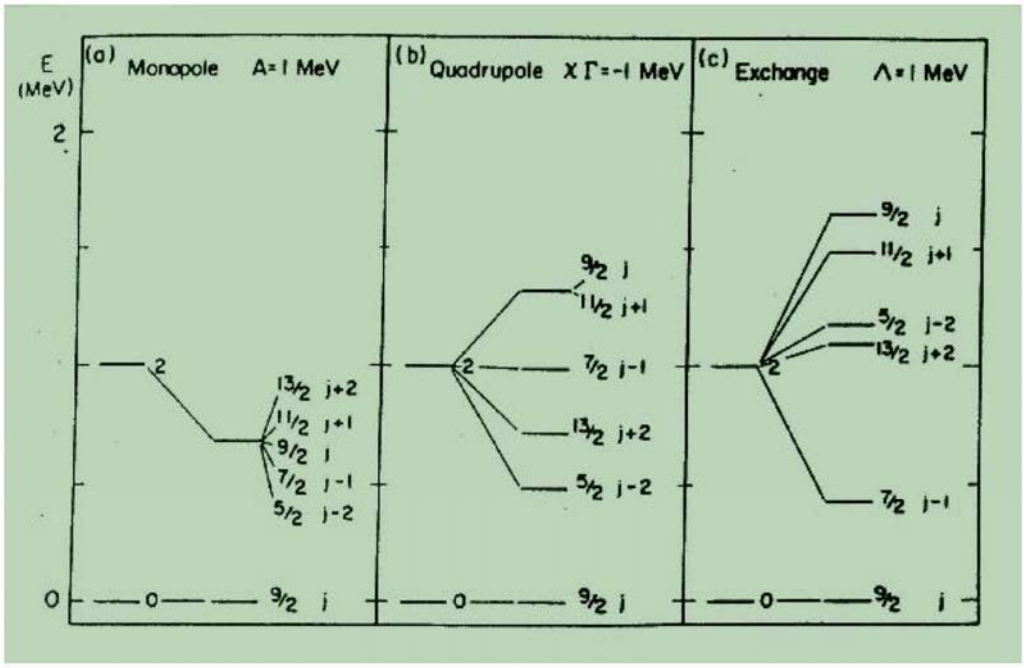

Scholten

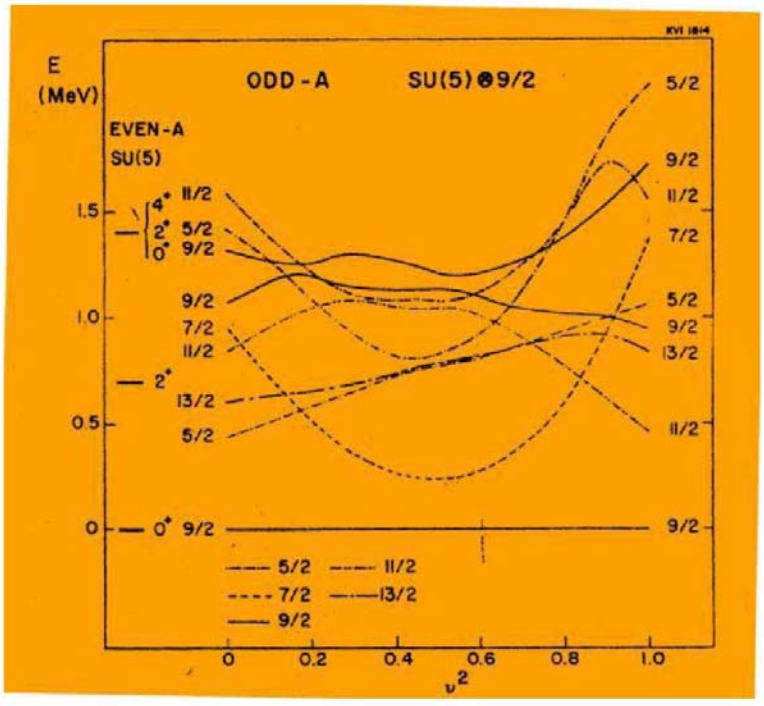

Scholten

Deformed nuclei

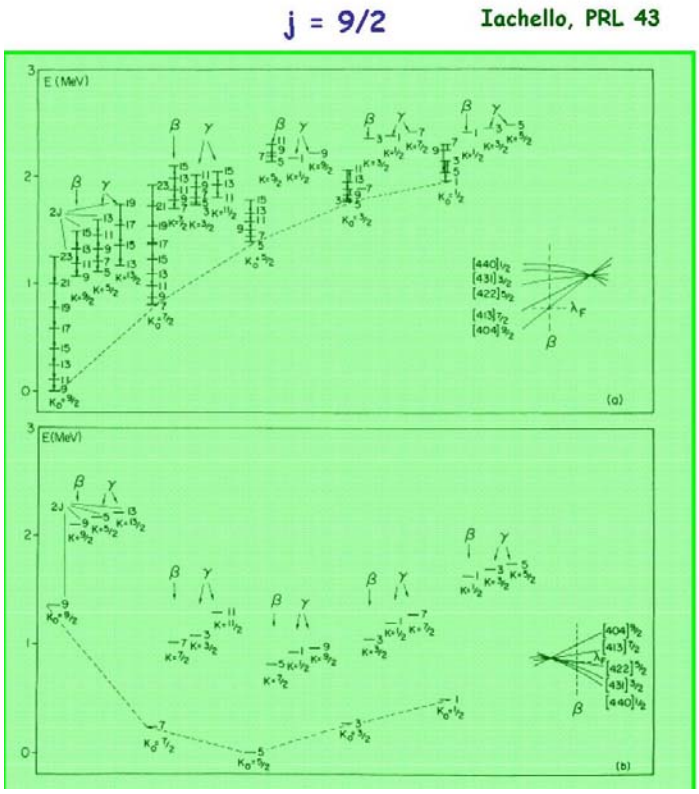

Λ = 0

The levels are arranged into bands denoted by the lowest value of the angular momentum K contained in the band.

This quantum number is only approximately equivalent to the quantum number K in the Nilsson model.

In the inset, the corresponding situation in the Nilsson model is shown.

Λ ≠ 0

The IBFM generates bands that are analogous to the bands which can be constructed in the Nilsson model. In addition it generates bands that could be called β and γ bands. While they arise automatically here, in the Nilsson model they must be either placed ad hoc or calculated by use of other methods.

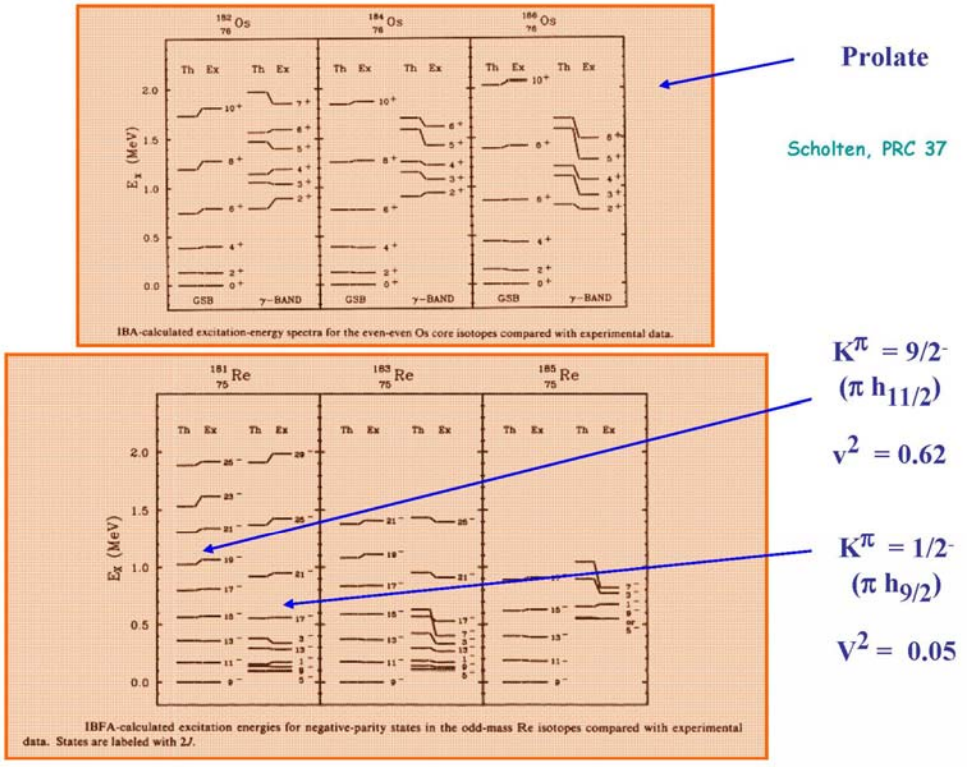

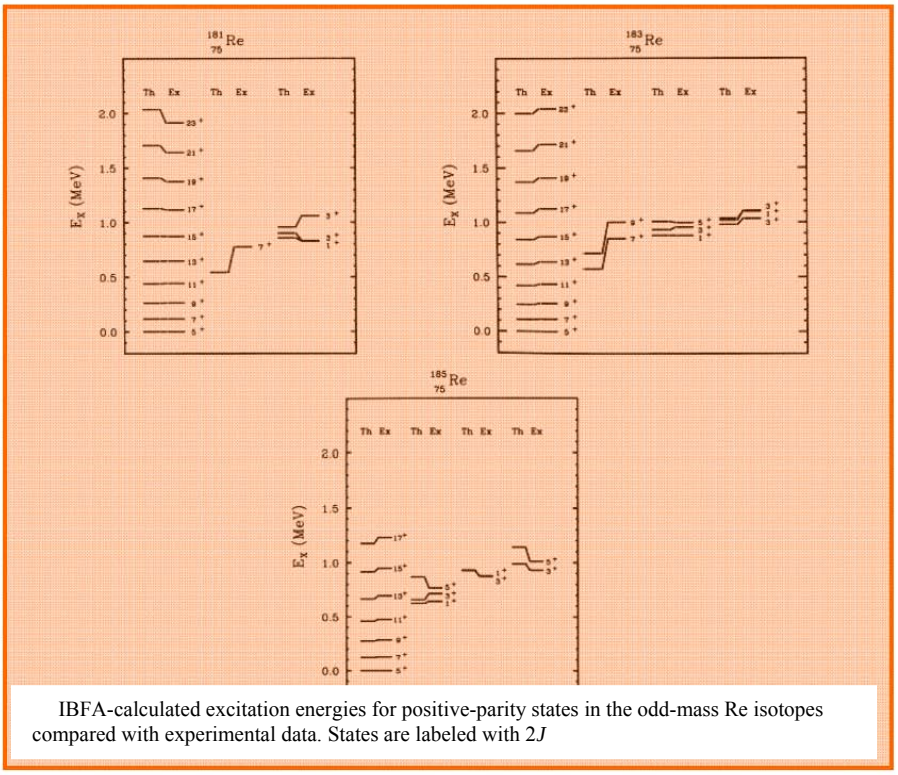

IBFA-calculated excitation energies for positive-parity states in the odd-mass Re isotopes compared with experimental data. States are labeled with 2*J*

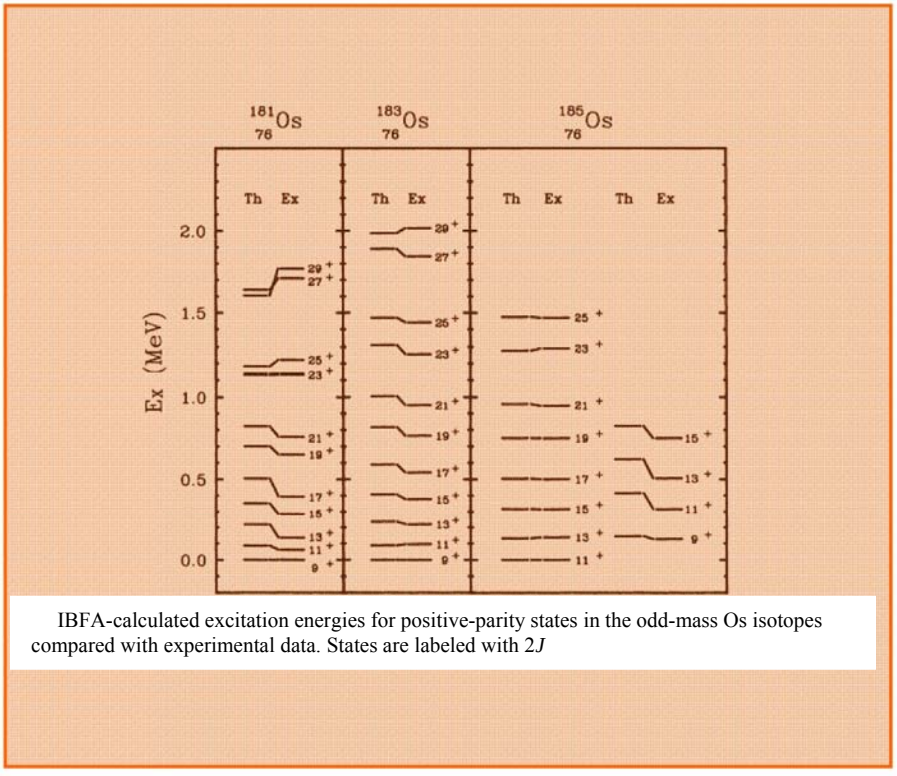

IBFA-calculated excitation energies for positive-parity states in the odd-mass Os isotopes compared with experimental data. States are labeled with 2*J*

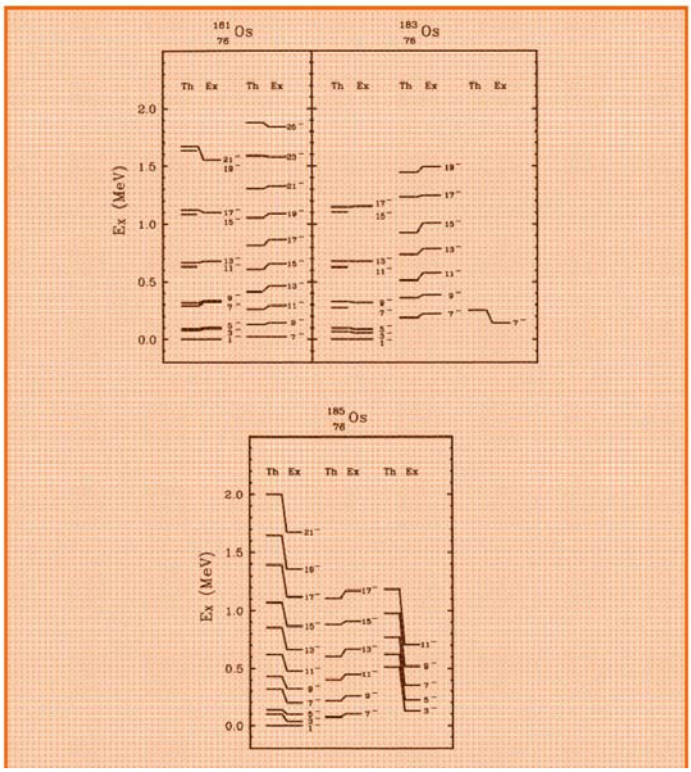

IBFA-calculated excitation energies for negative-parity states in the odd-mass Os isotopes compared with experimental data. States are labeled with $2J$

The IBFM states for odd-A Re and Os nuclei are obtained in multi-j calculations.

The choice of the model space has a strong influence on the model parameters. Even if there is a large separation between shells, the mixing due to the strong core-particle quadrupole interaction does not allow for restricting the model space to a single j shell. For example: Levels based on the $g_{9/2}$ particle. Here the $d_{5/2}$ particle from the next major shell has to be included due to the large non-spinflip matrix element $\langle d_{5/2} \parallel Y_2 \parallel g_{9/2} \rangle$. The same situation appears in the case of $h_{11/2}$ ($f_{7/2}$ has to be included in the model space). Restricting the model space requires a renormalization of the interactions. For unique-parity states:

- Strengths of boson-fermion interactions obtained in a single j calculation are effective strengths
- Strengths of boson-fermion interactions obtained in a multi j calculation are real strengths

Intruder deformed bands in odd Ag isotopes

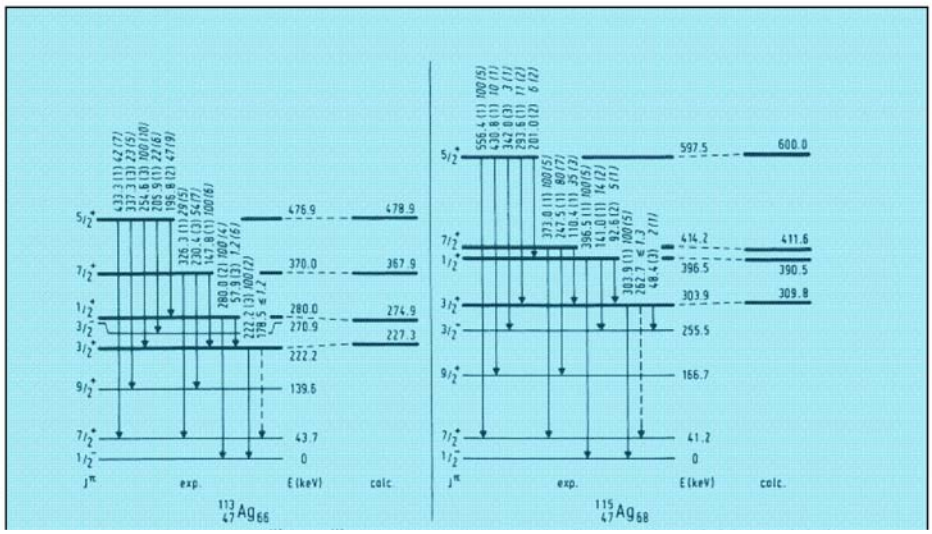

Fig.2 Partial level scheme of ^{113}Ag and ^{115}Ag. Energies and relative intensities of γ rays are given with their uncertainties in parentheses. The energies of the intruder band members are compared to the values calculated with the rotational formula K = ½.

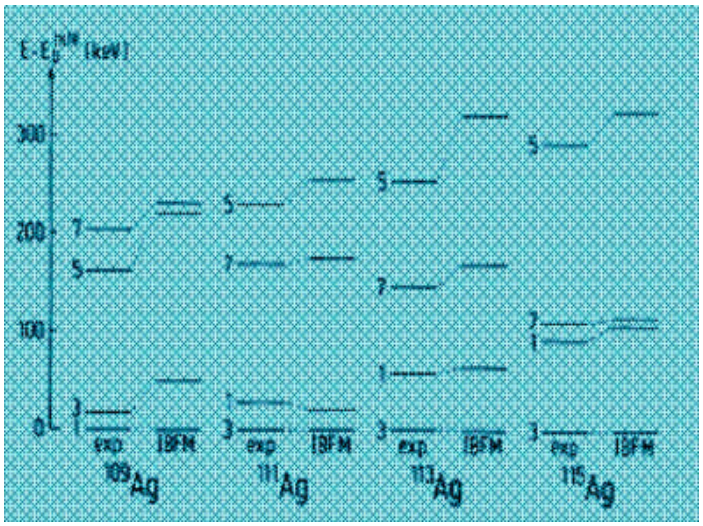

Fig. 3. Intruder positive-parity states of ^{109,111,113,115}Ag in comparison to IBFM calculations. Indicated spin values are twice the actual value.

Only the monopole fermion-boson interaction strength is slightly changed from isotope to isotope. All other interaction strengths and occupation probabilities are the same for all isotopes.

O(6) nuclei

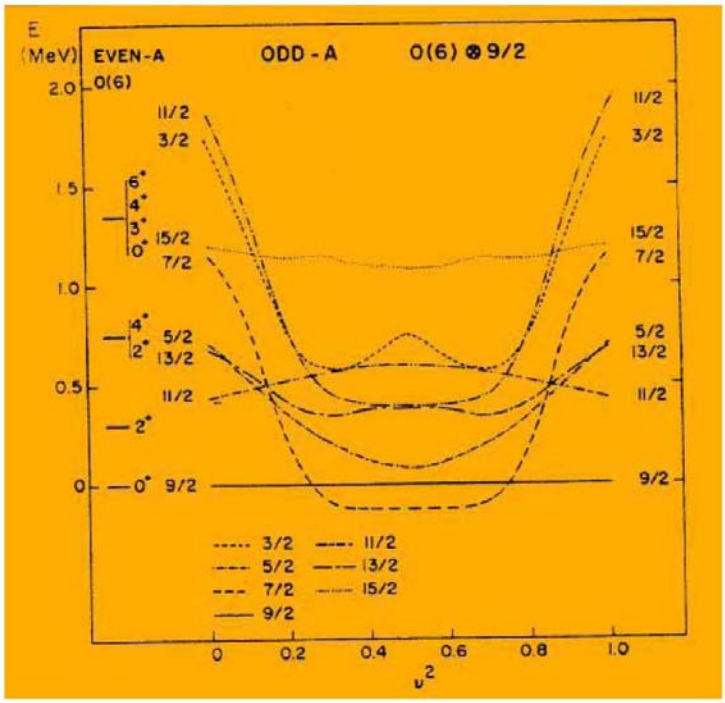

Scholten

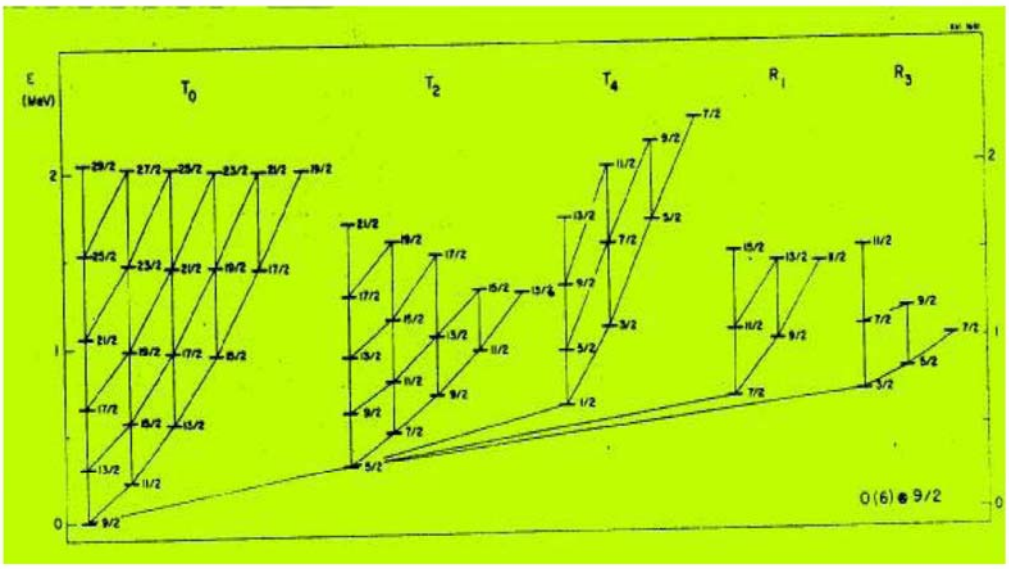

Scholten

Transitional nuclei

^{71}Ge

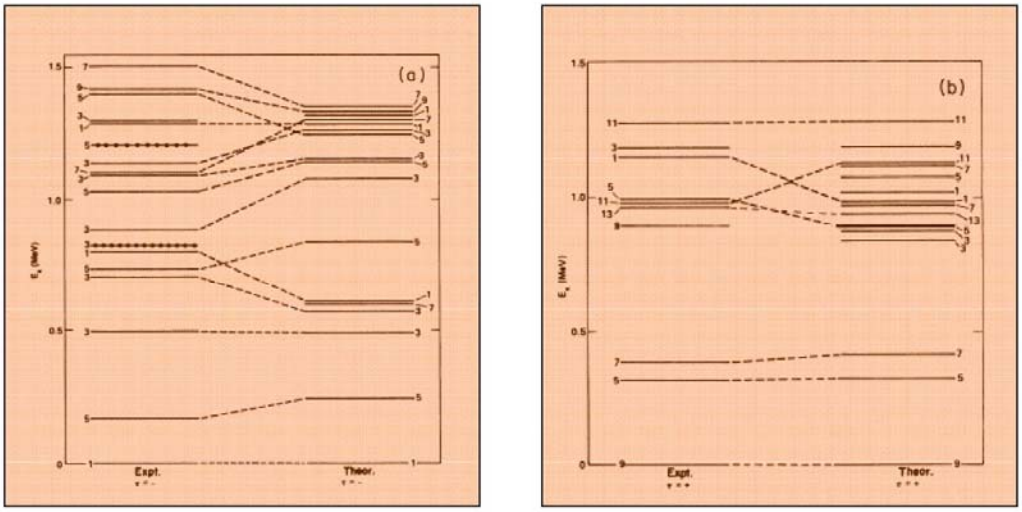

Negative parity levels **Positive parity levels**

Angular momentum x 2

^{105}Pd

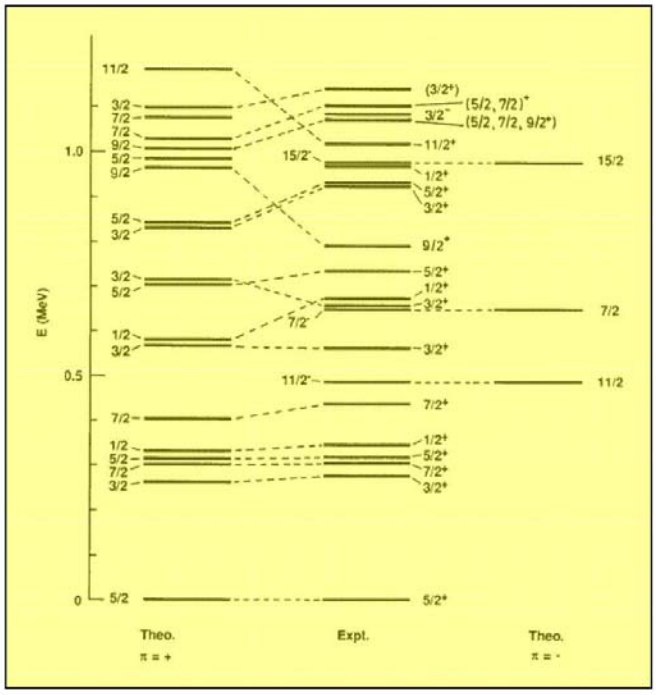

J of Level		I_γ	
From	To	Expt.	Theor.
$3/2_1^+$	$5/2_1^+$	100	100
$7/2_1^+$	$3/2_1^+$		0.0005
	$5/2_1^+$	100	100
$5/2_2^+$	$7/2_1^+$		0.0002
	$3/2_1^+$	0.12	0.7
	$5/2_1^+$	100	100
$1/2_1^+$	$5/2_2^+$		0
	$3/2_1^+$	27	93
	$5/2_1^+$	100	100
$7/2_2^+$	$5/2_2^+$		2
	$7/2_1^+$		0.0006
	$3/2_1^+$		0.03
	$5/2_1^+$	100	100
$3/2_2^+$	$7/2_2^+$		0.0005
	$1/2_1^+$	2.4	1
	$5/2_2^+$		2
	$7/2_1^+$		0.005
	$3/2_1^+$		0.4
	$5/2_1^+$	100	100
$3/2_4^+$	$3/2_2^+$	0.8	0.4
	$7/2_2^+$		0.08

Halflives

J	Expt. [a]	Theor.
$3/2_1^+$	0.067 ns	0.03 ns
$5/2_2^+$	0.04 ns	0.1 ns
$7/2_2^+$	3.8 ps	7.7 ps
$1/2_1^+$	0.88 ns	0.22 ns
$3/2_2^+$	1.9 ps	6.3 ps
$1/2_2^+$	>2 ps	1.6 ps

BOSON-FERMION SYMMETRIES
SUPERSYMMETRIES

If the Hamiltonian can be expressed in terms of Casimir invariants of the chain of subgroups, the energy spectrum can be obtained ANALYTICALLY. Other observables (B(E2), B(M1), static moments, spectroscopic factors, ...) can be expressed in analytical form, too.

The symmetry group related to IBM-1 is $U(6)$. The six dimensions are formed by the s boson and five components of d_μ boson. Since the number of bosons is invariant, the group is unitary. There are three chains of subgroups:

$$\begin{array}{lcll} U(6) & \supset & U(5) \supset O(5) \supset O(3) \supset O(2) & \textit{vibrational limit} \\ U(6) & \supset & SU(3) \supset O(3) \supset O(2) & \textit{rotational limit} \\ U(6) & \supset & O(6) \supset O(5) \supset O(3) \supset O(2) & \gamma - \textit{soft limit} \end{array}$$

For boson-fermion systems, many group chains have been investigated. Example: A j = 3/2 particle coupled to an $O(6)$ core (j = 3/2 has four different m-states, and therefore forms a representation of the $U(4)$ group).

$$U^B(6) \otimes U^F(4) \supset O^B(6) \otimes U^F(4) \supset Spin(6) \supset Spin(5) \supset Spin(3) \supset Spin(2)$$

$$E = -\frac{A}{4}[\sigma_1(\sigma_1+4) + \sigma_2(\sigma_2+2) + \sigma_3^2] + \frac{B}{6}[\tau_1(\tau_1+3) + \tau_2(\tau_2+1)] + CJ(J+1) + D\Sigma(\Sigma+4)$$

$$\begin{array}{rll} U^B(6) & \textit{quantum numbers} & [N] \\ U^F(4) & \textit{quantum numbers} & \{M\} \\ O^B(6) & \textit{quantum numbers} & \Sigma \\ Spin(6) & \textit{quantum numbers} & (\sigma_1, \sigma_2, \sigma_3) \\ Spin(5) & \textit{quantum numbers} & (\tau_1, \tau_2) \\ Spin(3) & \textit{quantum numbers} & J \\ Spin(2) & \textit{quantum numbers} & M_J \end{array}$$

$O^B(6) \otimes U^F(4) \supset Spin(6) \longrightarrow$ Parameters describing the boson system are in a unique relation to the parameters describing the boson-fermion system.

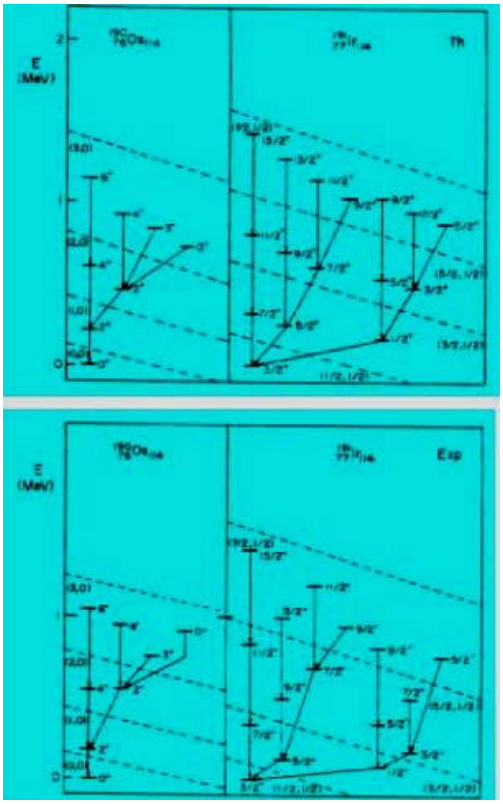

Problems:

- The symmetry approach to boson-fermion systems is more phenomenological in nature
- It can be applyed only in special cases when one or few fermion configurations are coupled to boson cores in one of the symmetry limits of IBM

Advantages:

- This approach was extended to boson-fermion-fermion systems (odd-odd nuclei)
- The spectra of neighboring even-even, odd-even and odd-odd nuclei can be described with the same set of parameters
- Analytical expressions are available
- Evidence that collective and single-particle degrees of freedom are closely related

Nuclear Theory:
High spin states in the interacting boson and interacting boson-fermion model

S. Brant

University of Zagreb, Croatia

E.mail: Brant@phy.hr

2.

High spin states in the interacting boson and interacting boson-fermion model

Interacting Boson Model (IBM-1) based models constructed to describe the physics of high-spin states in nuclei ($10\ \hbar \leq J \leq 30\ \hbar$):

- **Interacting boson plus broken pairs model (IBBPM) for even-even nuclei**
- **Interacting boson fermion plus broken pairs model (IBFBPM) for odd-even nuclei**

In the formulation of these models, one has to go beyond the boson approximation and include selected non-collective fermion degrees of freedom. By including part of the original shell-model fermion space through successive breaking of correlated S and D pairs, IBM can describe the structure of high-spin states.

The models are based on the IBM-1; the boson space consists of *s* and *d* bosons, with no distinction between protons and neutrons. To generate high-spin states, the models allow one or two bosons to be destroyed and to form non-collective fermion pairs, represented by two- and four-quasiparticle states which recouple to the boson core. High-spin states are described in terms of broken pairs.

Advantages of using models based on the IBM over more traditional approaches based on the cranking approximations:

- No assumption has to be made about the geometrical picture of high-spin bands
- The bands result from a consistent calculation of the complete excitation spectrum, which includes also the ground state band
- Polarization effects directly result from the model fermion-boson interactions
- All calculations are performed in the laboratory frame, and therefore the results can be directly compared with experimental data
- This extension of the model is especially relevant for transitional regions, where single-particle excitations and vibrational collectivity are dominant modes, and the traditional cranking approach to high-spin physics is not adequate

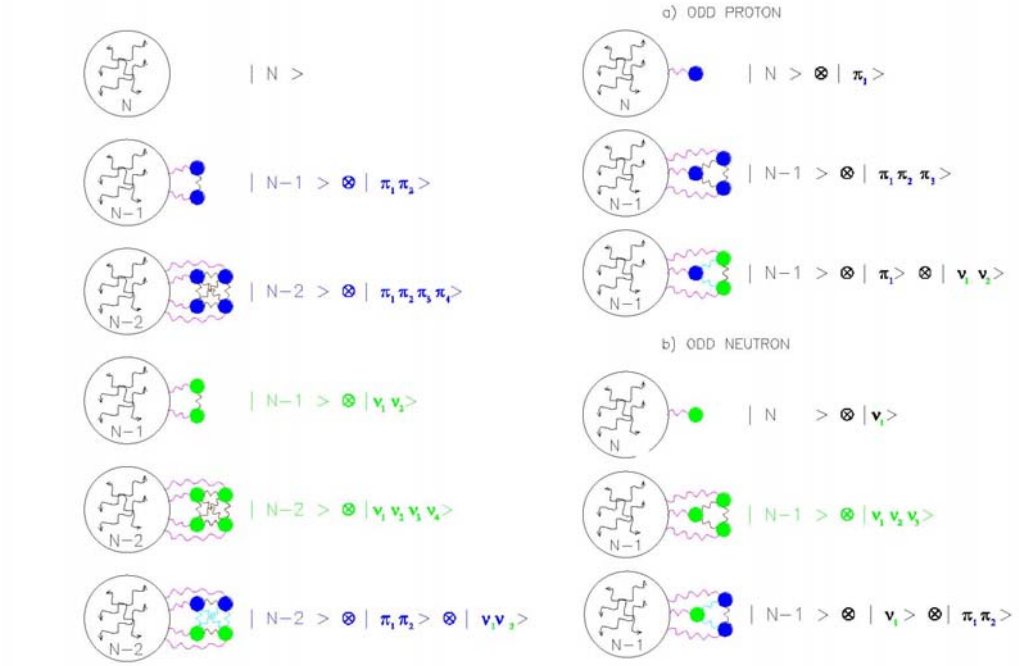

The model space for an even-even nucleus with $2N$ valence nucleons is

$$| N \; bosons \; > \oplus | \; (N-1) \; bosons \otimes 1 \; broken \; pair > \oplus | \; (N-2) \; bosons \otimes 2 \; broken \; pairs >$$

This means that the fermion basis can contain two-proton, two-neutron, four-proton, four-neutron and two-proton-two-neutron configurations.

For odd-A nuclei, two-broken pair configurations are not included in the model space. They would generate five-quasiparticle configurations resulting in exhaustive numerical calculations. The IBFBPM can describe one- and three-fermion structures. The two fermions in a broken pair can be of the same type as the unpaired fermion, resulting in a space with three identical fermions. If the fermions in the broken pair are different from the unpaired fermion, the fermion basis contains two protons and one neutron or vice versa.

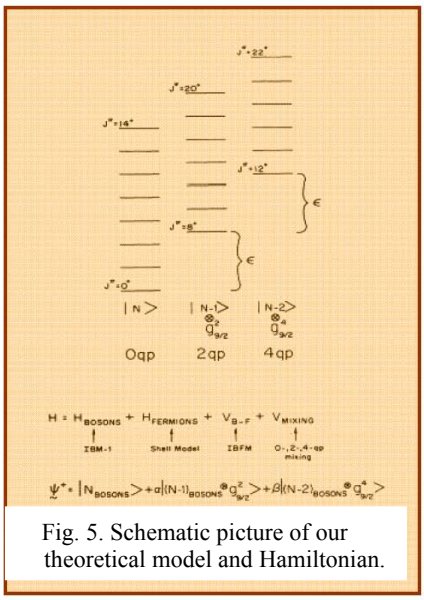

Fig. 5. Schematic picture of our theoretical model and Hamiltonian.

The Interacting boson plus broken pairs model (IBBPM) Hamiltonian for an even-even nucleus:

$$H = H_B + H_{\nu F} + H_{\pi F} + V_{\nu BF} + V_{\pi BF} + V_{\nu}^{mix} + V_{\pi}^{mix} + V_{\nu\pi}$$

The label π stands for protons and ν for neutrons. If broken pairs contain both protons and neutrons, the full model Hamiltonian is used. Otherwise, when broken pairs contain only protons ($\alpha = \pi$) or neutrons ($\alpha = \nu$), the model Hamiltonian is reduced to:

$$H = H_B + H_{\alpha F} + V_{\alpha BF} + V_{\alpha}^{mix}$$

In description of high-spin states in odd-even nuclei we employ the Interacting boson fermion plus broken pairs model (IBFBPM).

- When the two fermions in a broken pair are of the same type as the unpaired fermion, the reduced Hamiltonian is used, where α labels the type of fermion (proton or neutron).
- If the fermions in the broken pair are different from the unpaired fermion, the full Hamiltonian is used, without the pair breaking interaction of the unpaired fermion and with the fermion Hamiltonian of the unpaired fermion containing only single-fermion energies.

H_B is the boson Hamiltonian of IBM-1 describing a system of N interacting bosons (correlated S and D pairs) that approximate the valence nucleon pairs:

$$\begin{aligned} H_B &= \varepsilon \hat{N} + \frac{1}{2} v_0 \left([d^\dagger \times d^\dagger]_{(0)} \times [\tilde{s} \times \tilde{s}]_{(0)} + h.c. \right)_{(0)} \\ &+ \frac{1}{\sqrt{2}} v_2 \left([d^\dagger \times d^\dagger]_{(2)} \times [\tilde{d} \times \tilde{s}]_{(2)} + h.c. \right)_{(0)} \\ &+ \sum_{L=0,2,4} \frac{1}{2} C_L \sqrt{2L+1} \left([d^\dagger \times d^\dagger]_{(L)} \times [\tilde{d} \times \tilde{d}]_{(L)} \right)_{(0)} \end{aligned}$$

$$n_s = N - n_d$$

$H_{\alpha F}$ is the fermion Hamiltonian which contains single-fermion (quasiparticle) energies and fermion-fermion interactions. The quasiparticle energies and occupation probabilities contained in the fermion Hamiltonian and other terms, are obtained in a BCS calculation with some standard set of single fermion energies.

$$H_{\alpha F} = \sum_i \varepsilon_{\alpha_i} a^\dagger_{\alpha_i} \tilde{a}_{\alpha_i} + \frac{1}{4} \sum_{abcd} \sum_{JM} V^J_{\alpha abcd} A^\dagger_{JM}(\alpha_a \alpha_b) A_{JM}(\alpha_c \alpha_d)$$

$$A^\dagger_{JM}(\alpha_a \alpha_b) = \frac{1}{\sqrt{1+\delta_{ab}}} [a^\dagger_{\alpha_a} a^\dagger_{\alpha_b}]^M_J$$

$$V^J_{\alpha abcd} = (u_{\alpha_a} u_{\alpha_b} u_{\alpha_c} u_{\alpha_d} + v_{\alpha_a} v_{\alpha_b} v_{\alpha_c} v_{\alpha_d}) G(\alpha_a \alpha_b \alpha_c \alpha_d J) + 4 v_{\alpha_a} u_{\alpha_b} v_{\alpha_c} u_{\alpha_d} F(\alpha_a \alpha_b \alpha_c \alpha_d J)$$

$V_{\alpha BF}$ is the interaction between the unpaired fermions and the boson core containing the dynamical, exchange and monopole interactions of the IBFM-1:

$$V_{\alpha BF} = V_{\alpha DYN} + V_{\alpha EXC} + V_{\alpha MON}$$

$$V_{\alpha DYN} = \Gamma_0 \sum_{\alpha j_1 \alpha j_2} \sqrt{5}\,(u_{\alpha j_1} u_{\alpha j_2} - v_{\alpha j_1} v_{\alpha j_2})\,\langle \alpha j_1 \parallel Y_2 \parallel \alpha j_2 \rangle \left([a^\dagger_{\alpha j_1} \times \tilde{a}_{\alpha j_2}]^{(2)} \times Q_B^{(2)} \right)^{(0)}$$

$Q_B^{(2)}$ is the standard boson quadrupole operator

$$Q_B^{(2)} = [s^\dagger \times \tilde{d} + d^\dagger \times \tilde{s}]^{(2)} + \chi [d^\dagger \times \tilde{d}]^{(2)}$$

$$V_{\alpha EXC} = A_0 \sum_{\alpha j_1 \alpha j_2 \alpha j_3} (-2) \sqrt{\frac{5}{2\,\alpha j_3 + 1}}\,(u_{\alpha j_1} v_{\alpha j_3} + v_{\alpha j_1} u_{\alpha j_3})\;\; (u_{\alpha j_2} v_{\alpha j_3} + v_{\alpha j_2} u_{\alpha j_3})$$
$$\langle \alpha j_3 \parallel Y_2 \parallel \alpha j_1 \rangle\, \langle \alpha j_3 \parallel Y_2 \parallel \alpha j_2 \rangle\; : \left([a^\dagger_{\alpha j_1} \times \tilde{d}\,]_{\alpha j_3} \times [\tilde{a}_{\alpha j_2} \times d^\dagger\,]_{\alpha j_3} \right)^{(0)} :$$

$$V_{\alpha MON} = A_0 \sum_{\alpha j} \sqrt{5}\,(2\alpha j + 1)\,\left([a^\dagger_{\alpha j} \times \tilde{a}_{\alpha j}]^{(0)} \times [d^\dagger \times \tilde{d}]^{(0)} \right)^{(0)}$$

The pair breaking interaction V_α^{mix} which mixes states with different numbers of fermions, conserving the total nucleon number only:

$$V_\alpha^{mix} = -U_0 \left\{ \sum_{\alpha j_1 \alpha j_2} u_{\alpha j_1} u_{\alpha j_2} (u_{\alpha j_1} v_{\alpha j_2} + u_{\alpha j_2} v_{\alpha j_1}) \langle \alpha j_1 \parallel Y_2 \parallel \alpha j_2 \rangle^2 \frac{1}{\sqrt{2\,\alpha j_2 + 1}} \left([a^\dagger_{\alpha j_2} \times a^\dagger_{\alpha j_2}]^{(0)} \cdot \tilde{s} \right) + hc \right\}$$
$$-U_2 \left\{ \sum_{\alpha j_1 \alpha j_2} (u_{\alpha j_1} v_{\alpha j_2} + u_{\alpha j_2} v_{\alpha j_1}) \langle \alpha j_1 \parallel Y_2 \parallel \alpha j_2 \rangle \left([a^\dagger_{\alpha j_1} \times a^\dagger_{\alpha j_2}]^{(2)} \cdot \tilde{d} \right) + hc \right\}$$

The proton-neutron interaction is:

$$V_{\nu\pi} = \sum_{\nu\nu'\pi\pi'} \sum_J h_J(\nu\nu'\pi\pi')(u_\nu u_{\nu'} - v_\nu v_{\nu'})(u_\pi u_{\pi'} - v_\pi v_{\pi'}) \left(\left[a^\dagger_\nu \times \tilde{a}_{\nu'} \right]^{(J)} \cdot \left[a^\dagger_\pi \times \tilde{a}_{\pi'} \right]^{(J)} \right)$$

The coefficients $h_J(\nu\nu'\pi\pi')$ are connected to the two-body matrix elements of the residual proton-neutron interaction by:

$$h_J(\nu\nu'\pi'\pi) = (-)^{j_\nu + j_\pi} \sum_{J'} (-)^{J'} \sqrt{2J'+1}\,\langle (j_\nu j_\pi) J' \parallel V(1,2) \parallel (j_{\nu'} j_{\pi'}) J' \rangle\, W(j_\nu j_\pi j_{\nu'} j_{\pi'}; J' J)$$

The residual proton-neutron interaction is usually taken in the form:

$$H_\delta = 4\pi\, V_\delta\, \delta(\vec{r}_\pi - \vec{r}_\nu)\, \delta(r_\pi - R_0)\, \delta(r_\nu - R_0)$$

The strength parameters of the boson-fermion interactions should be those obtained in the analysis of the neighboring nuclei. For example, the boson-fermion strength parameters for the couplings of two and four-proton configurations to the boson core in an even-even nucleus, have to be the same as for coupling of one-proton configurations to the boson core in the neighboring odd-even nucleus. This is the case for spherical, transitional and γ-soft nuclei. However, approaching the rotational SU(3) limit of IBM, the boson-fermion interaction strengths are not identical for an even-even nucleus and its odd-even neighbor. The effective core for configurations based on broken pairs in a deformed nucleus can be somewhat different from the one obtained by a simple decrease of the boson number by one.

$$T(E2)=\frac{3}{4\pi}e^{\text{vib}}R_0^2[(d^\dagger\times\tilde{s}+s^\dagger\times\tilde{d})^{(2)}+\chi(d^\dagger\times\tilde{d})^{(2)}]$$

$$-e\frac{1}{\sqrt{5}}\sum_{j_1j_2}q_{j_1j_2}[(u_{j_1}u_{j_2}-v_{j_1}v_{j_2})(a_{j_1}^\dagger\times\tilde{a}_{j_2})^{(2)}-\frac{u_{j_1}v_{j_2}}{\sqrt{N}}[(a_{j_1}^+\times a_{j_2}^+)^{(2)}\times\tilde{s}]^{(2)}+\frac{u_{j_2}v_{j_1}}{\sqrt{N}}[(\tilde{a}_{j_1}\times\tilde{a}_{j_2})^{(2)}\times s^\dagger]^{(2)}]$$

where

$q_{j_1j_2}=\langle j_1\|r^2Y_2\|j_2\rangle$.

We take $\langle r^2\rangle=\frac{1}{5}R_0^2$, and $R_0=0.12A^{1/3}\times10^{-12}$ cm. N is the number of bosons.

$$T(M1)=\sqrt{30/4\pi}g_R(d^\dagger\times\tilde{d})^{(1)}$$

$$-\frac{1}{\sqrt{4\pi}}\sum_{j_1j_2}[g_1\langle j_1\|\vec{j}\|j_2\rangle+(g_s-g_1)\langle j_1\|\vec{s}\|j_2\rangle]$$

$$\times\{(u_{j_1}u_{j_2}+v_{j_1}v_{j_2})(a_{j_1}^\dagger\times\tilde{a}_{j_2})^{(1)}-\frac{u_{j_1}v_{j_2}}{\sqrt{N}}[(a_{j_1}^\dagger\times a_{j_2}^\dagger)^{(1)}\times\tilde{s}]^{(1)}+\frac{u_{j_2}v_{j_1}}{\sqrt{N}}[(\tilde{a}_{j_1}\times\tilde{a}_{j_2})^{(1)}\times s^\dagger]^{(1)}\}$$

Spherical nuclei

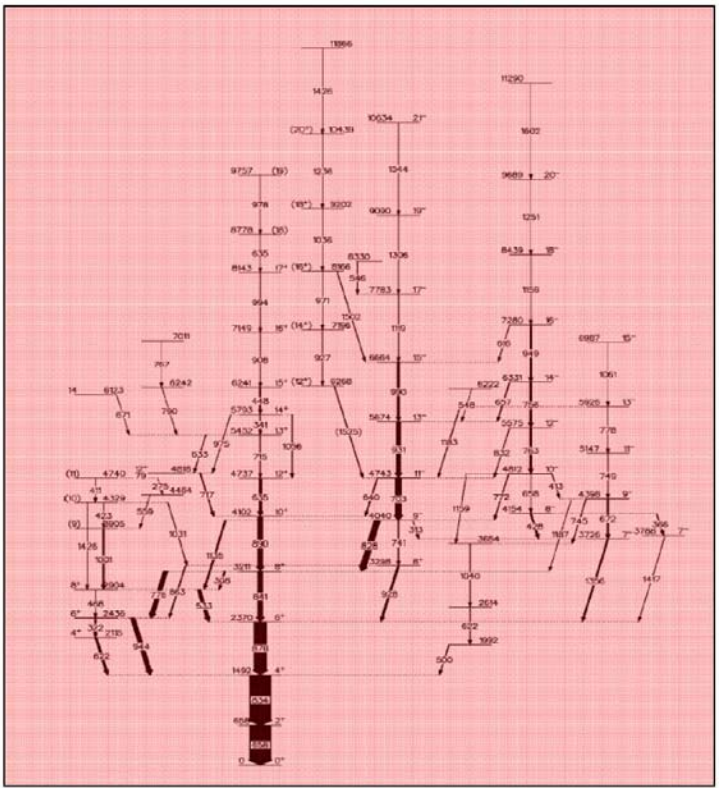

^{104}Cd

Parameterization for neutrons from even-odd Cd nuclei

Parameterization for protons in accordance with odd-even In and Ag nuclei

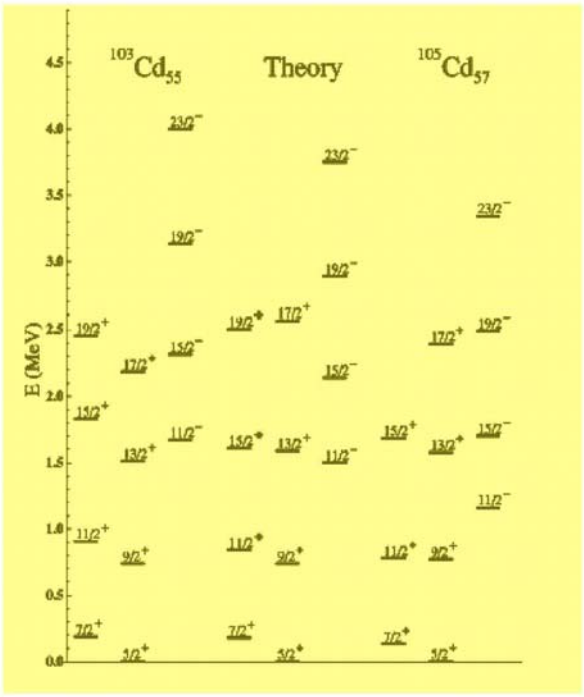

^{104}Cd

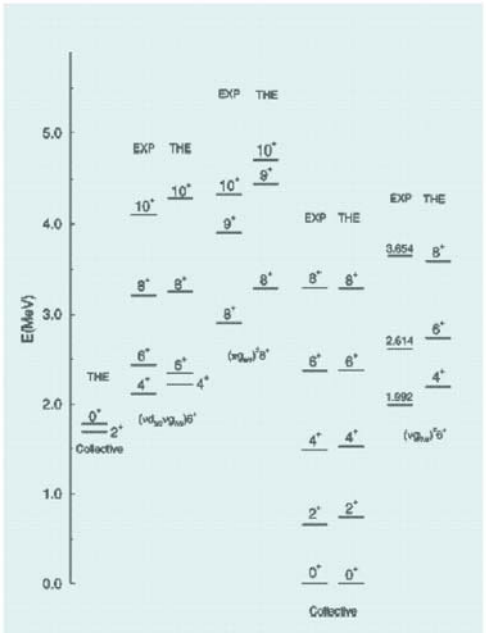

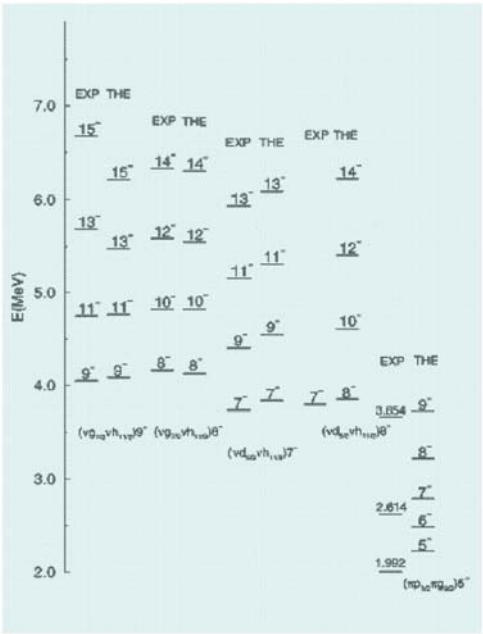

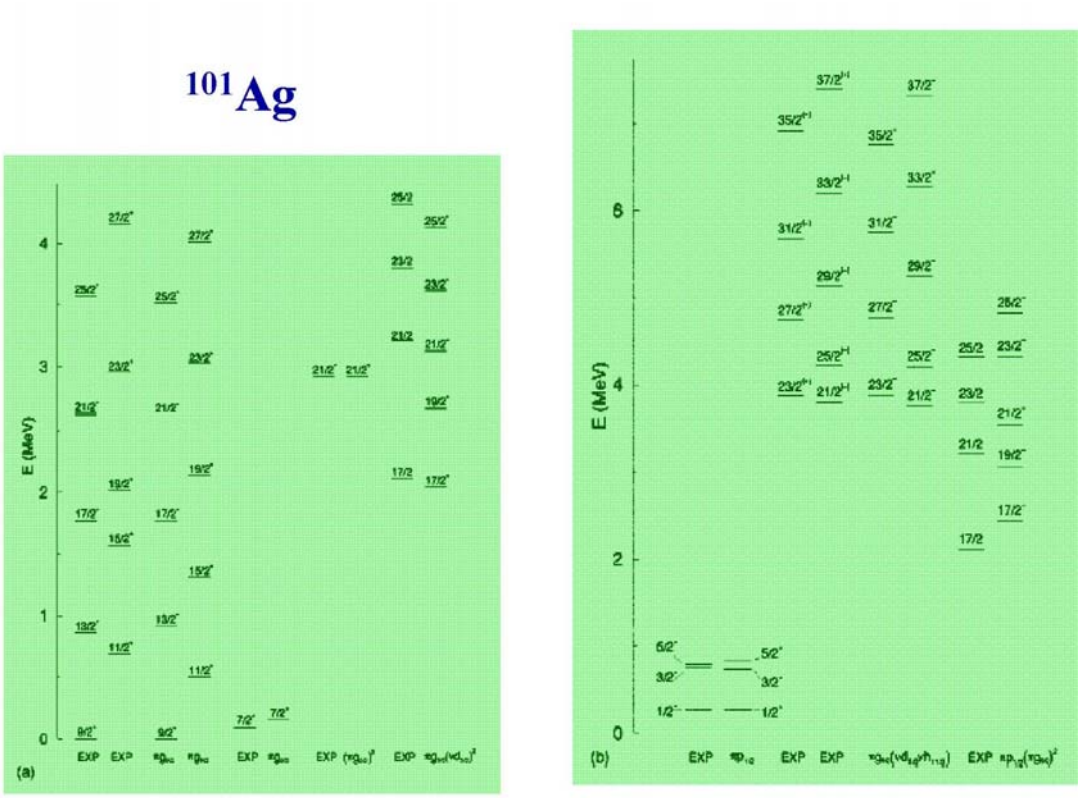

^{101}Ag

State E_x (keV)	I^π	Lifetime (ps) DDCM	RDDS	DSA/NGTB	Adopted	Theory	
Positive parity							
98	$7/2^+$					425	
687	$11/2^+$	2.7(3)			2.7(3)	2.0	
861	$13/2^+$	11.7(10)			11.7(10)	3.4	
1573	$15/2^+$	2.1(5)			2.1(5)	0.4	
1769	$17/2^+$	1.9(2)			1.9(2)	1.9	
2017	$19/2^+$	9(1)			9(1)	5.0	
2621	$21/2^+$	0.6(1)			0.6(1)	0.4	
2922	$21/2_2^+$					1700[a]	
						2.8[b]	
2956	$23/2^+$	1.8(3)			1.8(3)	0.9	
3578	$25/2^+$		<2.0		<2.0	0.4	
4159	$27/2^+$		<2.5		<2.5	0.3	
4572	$(29/2^+)$		14(1)		14(1)		
5300	$(31/2^+)$			≤1.7	≤1.7		
Negative parity							
750	$3/2^{(-)}$					10.2	
797	$5/2^{(-)}$					30.5	
3870	$23/2^{(-)}$	11.4(11)			11.4(11)	8.4	
4217	$25/2^{(-)}$	1.1(2)			1.1(2)	1.2	
4749	$27/2^{(-)}$		1.1(1)		1.1(1)	1.1	
5134	$29/2^{(-)}$			0.83(8)	0.83(8)	0.81	
5678	$31/2^{(-)}$			0.41(5)	0.41(5)	0.45	
6197	$33/2^{(-)}$			0.30(4)	0.30(4)	0.34	
6917	$35/2^{(-)}$			0.18(5)	0.18(5)	0.13	
7393	$37/2^{(-)}$			≤1.3	≤1.3	0.39	
No parity assigned						$\pi=+$	$\pi=-$
2115	17/2		199(7)		199(7)	120	
3210	21/2	1.2(1)			1.2(1)	1.0	2.9
3801	23/2					0.5	0.9
4315	25/2					0.5	0.4

[*]If wave function predominantly $\pi^3(g_{9/2})$
[h]If wave function predominantly $\pi(g_{9/2})$

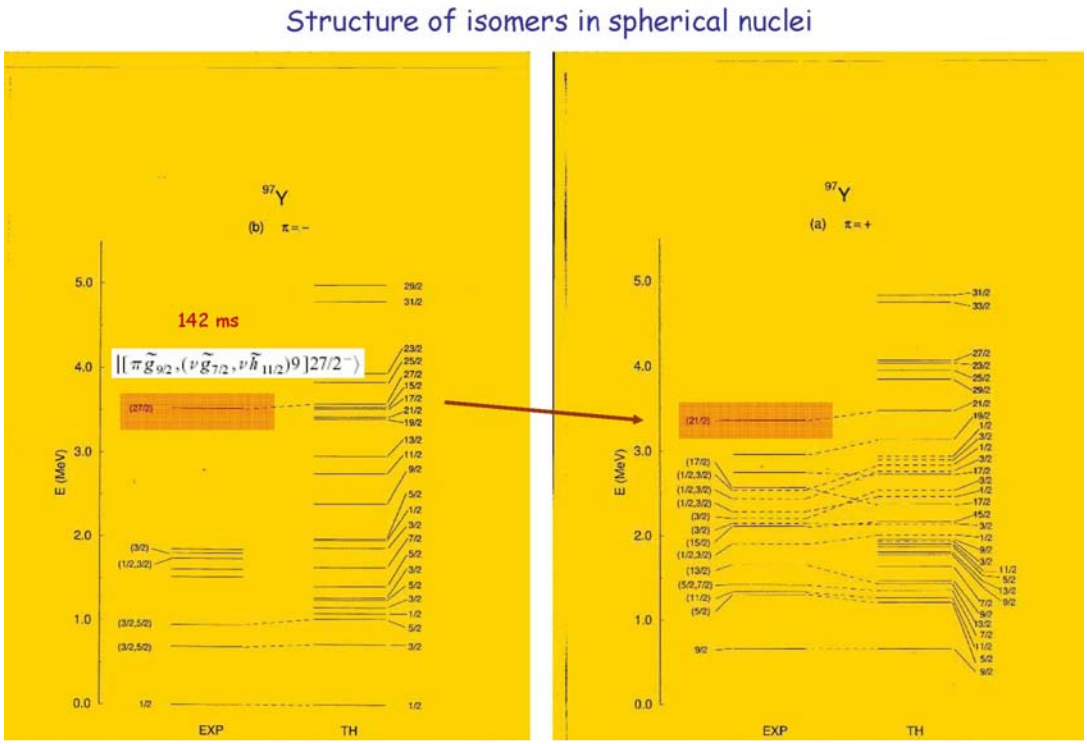

Fig. 1. Calculated states in ^{97}Y of (a) positive parity and (b) negative parity in comparison to the available data. Above 2 MeV of excitation energy only the calculated yrast states are shown and, in the energy interval between 2 and 3 MeV the calculated $½^-$ and $½^+$ states (dashed lines).

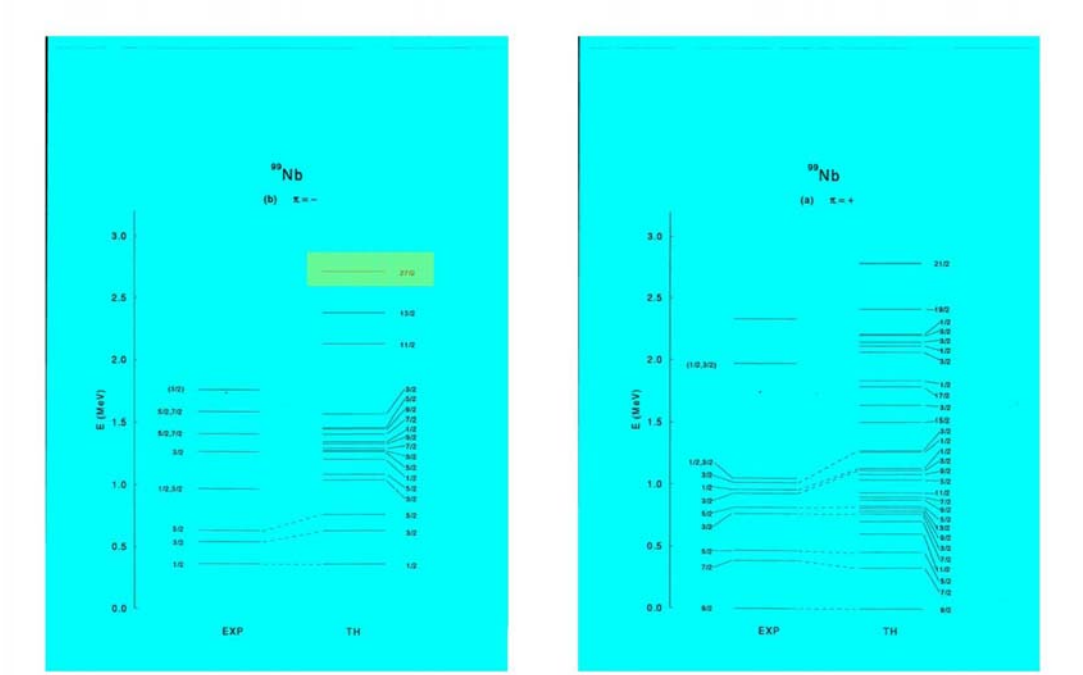

Deformed nuclei

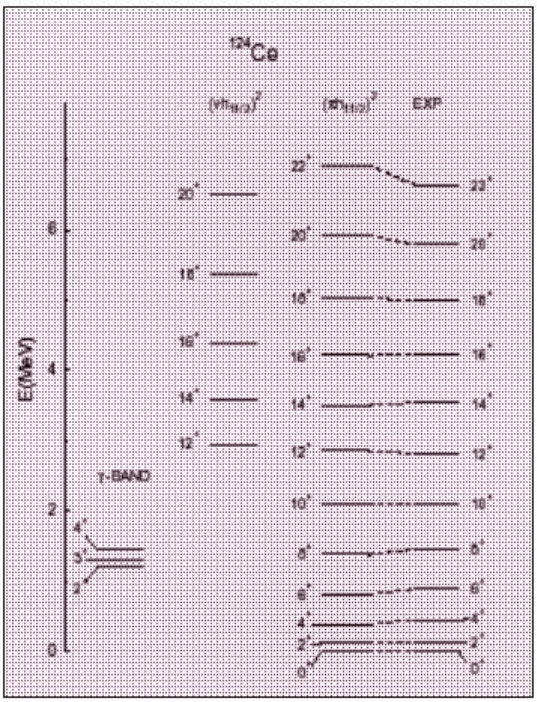

This nucleus displays a transitional structure between deformed nuclei (lighter Ce isotopes) described by the SU(3) limit of the IBM, and γ-soft nuclei (heavier Ce isotopes) which correspond to the O(6) limit of the of the IBM. The SU(3)-O(6) transition can be described by the boson Hamiltonian

$$H_{IBM} = -\frac{\alpha}{10}\, Q\cdot Q \;+\; \frac{\beta}{10}\, L\cdot L$$

and is determined by the value of the parameter χ in the quadrupole boson operator. The limiting cases are: $\chi = 0$ corresponds to the O(6) limit of the IBM-1, and $\chi = -\frac{\sqrt{7}}{2}$ describes a prolate shape in the SU(3) dynamical symmetry limit.

Here: $\alpha = 0.19$ MeV, $\beta = 0.13$ MeV, $\chi = -1.0$ and the boson number $N = 12$.

$v^2(\pi h_{11/2}) = 0.06$
$\varepsilon(\pi h_{11/2}) = 1.70$ MeV
$v^2(\nu h_{11/2}) = 0.40$
$\varepsilon(\nu h_{11/2}) = 1.32$ MeV

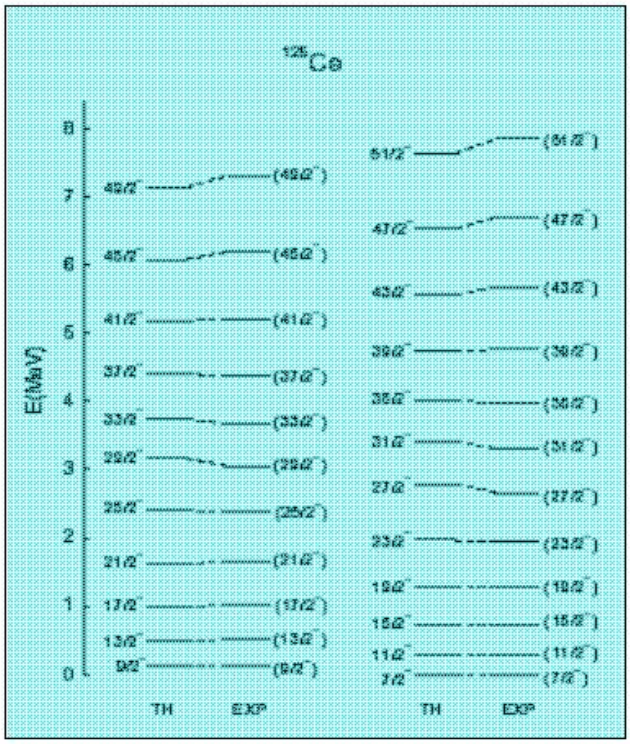

This band is based on the $\nu h_{11/2}$ orbital for the states with $I \leq 27/2^-$, and on the three-fermion configuration $\nu h_{11/2}\,(\pi h_{11/2})^2$ for $I \geq 29/2^-$. The structure of this band is very simple. The neutron $\nu h_{11/2}$ orbital couples to the yrast sequence of states in the core nucleus ^{124}Ce.

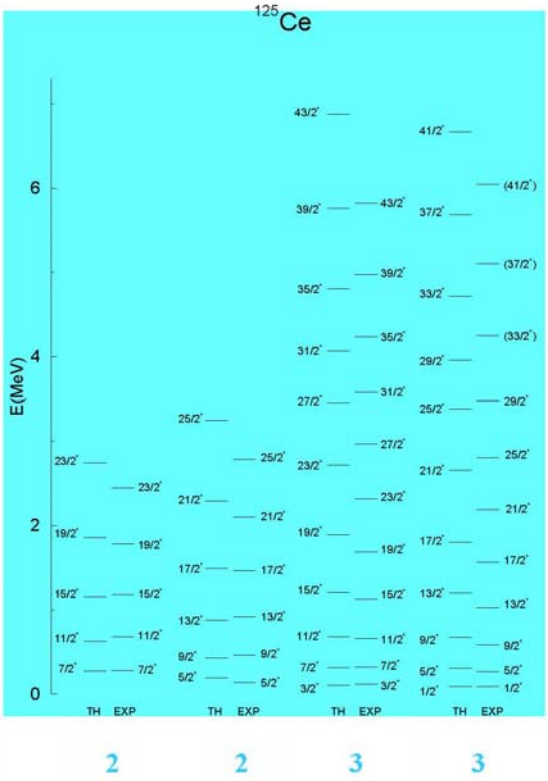

The band 2 is based on the $\nu d_{5/2}$ and $\nu g_{7/2}$ neutron orbitals. The band 3, in addition, contains sizeable components based on the $\nu d_{3/2}$ and $\nu s_{1/2}$ states. While the alignment of a proton pair is not observed in band 2, the states with $I \geq 25/2^+$ of band 3 are based on the one-neutron plus $(\pi h_{11/2})^2$ configuration.

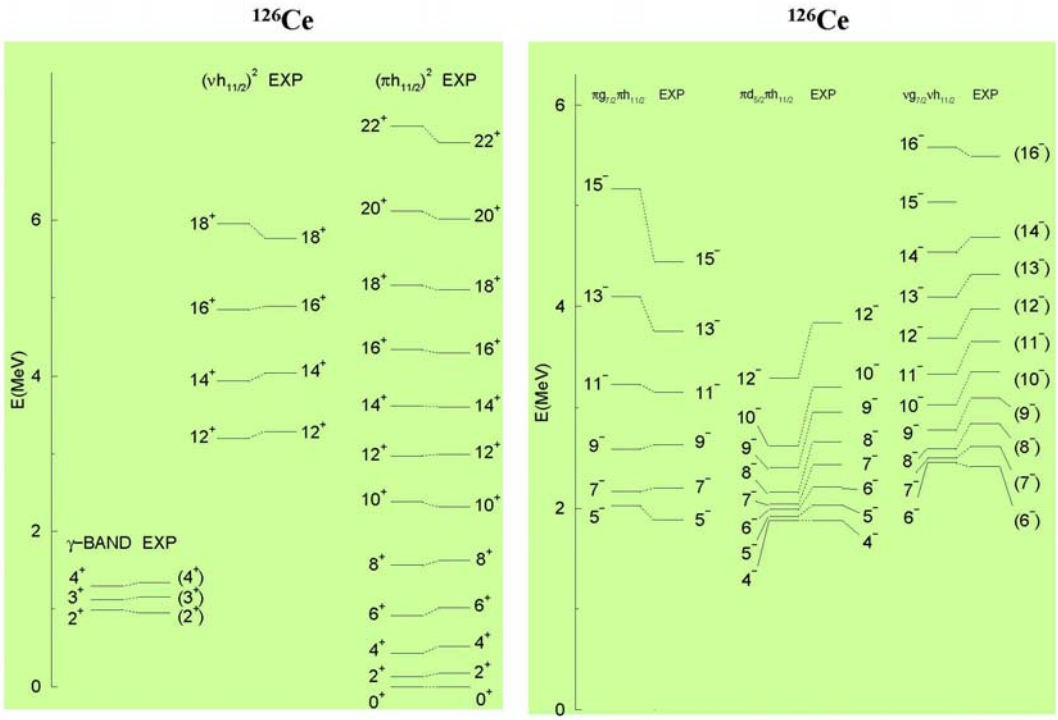

Transitional nuclei

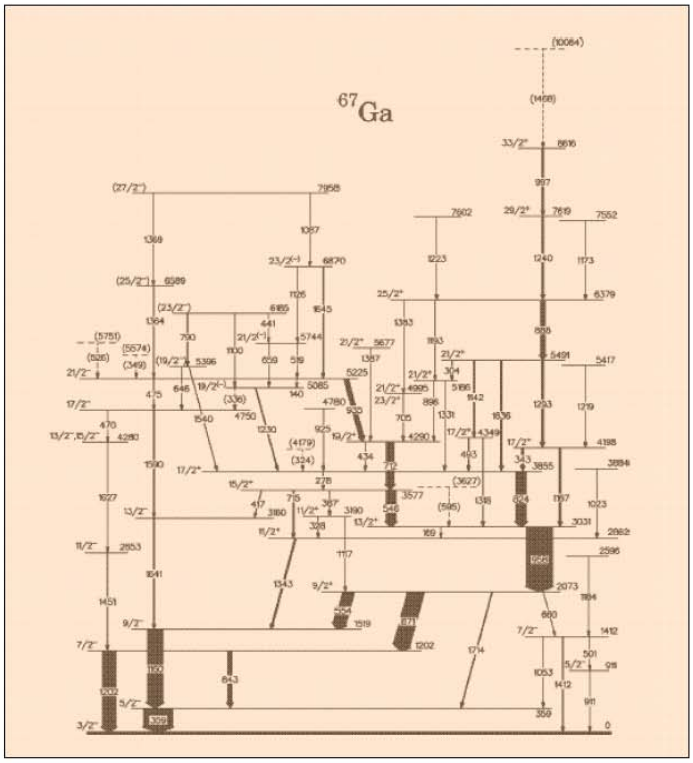

Wave functions

$$|I_k^{\pi}\rangle = \sum_{j n_d \upsilon R} \xi_{j,n_d \upsilon R;I} \; |\pi\tilde{j}, n_d \upsilon R; I\rangle$$

$$+ \sum_{jj'j''I_{\alpha\alpha}I_{\pi\alpha\alpha}n_d\upsilon R} \eta_{jj'j''I_{\alpha\alpha}I_{\pi\alpha\alpha},n_d\upsilon R;I}$$

$$\times |[\pi\tilde{j}, (\alpha\tilde{j}', \alpha\tilde{j}'')I_{\alpha\alpha}]I_{\pi\alpha\alpha}, n_d \upsilon R; I\rangle$$

Here $\pi\tilde{j}$ stands for a proton quasiparticle, and $\alpha\tilde{j}', \alpha\tilde{j}''$ for neutron quasiparticles ($\alpha = \nu$), or proton quasiparticles ($\alpha = \pi$), which are coupled to the angular momentum $I_{\alpha\alpha}$. Angular momenta j and $I_{\alpha\alpha}$ are coupled to the three-quasiparticle angular momentum denoted by $I_{\pi\alpha\alpha}$. In the boson part of the wave function, the $n_d d$ bosons are coupled to the total boson angular momentum R. The additional quantum number υ is used to distinguish between the n_d-boson states having the same angular momentum R. We note that the number of s bosons associated with the boson state $|n_d \upsilon R\rangle$ is $n_s = N - n_d$, where N is the total number of bosons.

To make it easier to follow the origin of states, for the indexing of the theoretical states we use I_{qp_i} for the quasiparticle+phonon states, I_{bp_i} for proton broken pair states and I_{bn_i} for neutron broken pair states. Here the index i denotes the ith state of the denoted type. In the standard notation I_k, the index k is used as total label obtained from the IBFBPM calculation. The indexing I_k is pointed out only for states where $i \neq k$. Otherwise, the indexes i and k are equal.

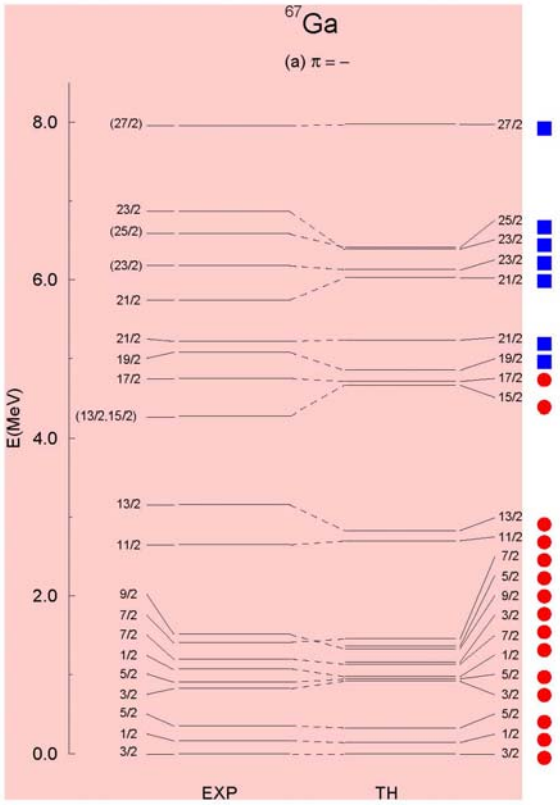

one proton two neutron state

one proton state

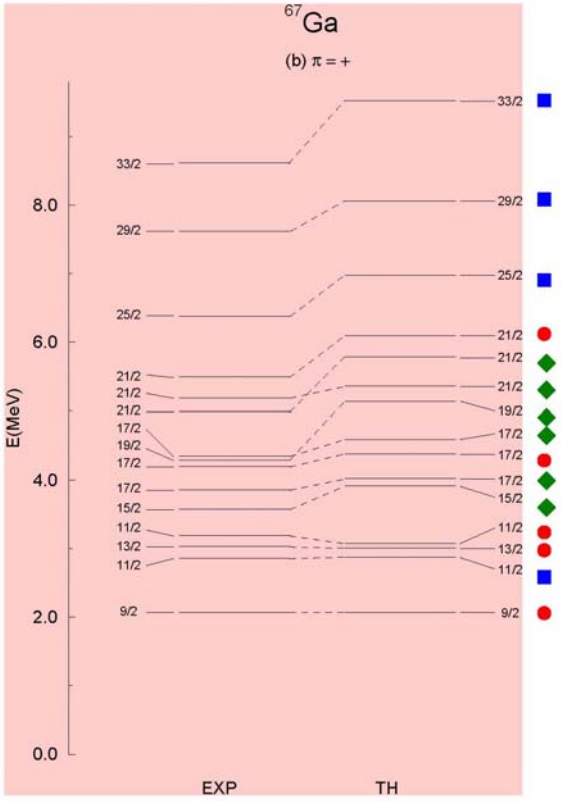

three proton state

one proton two neutron state

one proton state

$I_i^\pi \rightarrow I_f^\pi$ ($\hbar$) ($\hbar$)	$E_i \rightarrow E_f$ Expt. Expt.	$B(E2)(e^2b^2)$ IBFBPM	$B(M1)(\mu_N^2)$ IBFBPM	I_γ Expt.	I_γ IBFBPM
$1/2^-_{\phi_1} \rightarrow 3/2^-_{\phi_1}$	167→0	0.013	0.058	100	100
$5/2^-_{\phi_1} \rightarrow 1/2^-_{\phi_1}$	359→167	0.027			1.8
$\rightarrow 3/2^-_{\phi_1}$	→0	0.003	0.006	100	100
$3/2^-_{\phi_2} \rightarrow 5/2^-_{\phi_1}$	828→359	1×10^{-5}	0.013	4	6
$\rightarrow 1/2^-_{\phi_1}$	→167	2×10^{-5}	0.022	10	27
$\rightarrow 3/2^-_{\phi_1}$	→0	0.027	0.028	100	100
$5/2^-_{\phi_2} \rightarrow 3/2^-_{\phi_2}$	911→828	0.002	0.306		0.9
$\rightarrow 5/2^-_{\phi_1}$	→359	9×10^{-5}	0.0005	2.2	0.5
$\rightarrow 1/2^-_{\phi_1}$	→167	0.003		2.2	2.0
$\rightarrow 3/2^-_{\phi_1}$	→0	0.029	0.010	100	100
$1/2^-_{\phi_2} \rightarrow 5/2^-_{\phi_1}$	1082→911	0.0004			0.0002
$\rightarrow 3/2^-_{\phi_2}$	→828	0.0003	0.533	12	37
$\rightarrow 5/2^-_{\phi_1}$	→359	0.003			1.7
$\rightarrow 1/2^-_{\phi_1}$	→167		0.030	100	100
$\rightarrow 3/2^-_{\phi_1}$	→0	0.021	0.005	33	122
$7/2^-_{\phi_1} \rightarrow 5/2^-_{\phi_1}$	1202→911	0.002	0.131		6
$\rightarrow 3/2^-_{\phi_2}$	→828	0.0004			0.0004
$\rightarrow 5/2^-_{\phi_1}$	→359	0.002	0.012	31	14
$\rightarrow 3/2^-_{\phi_1}$	→0	0.033		100	100
$7/2^-_{\phi_2} \rightarrow 7/2^-_{\phi_1}$	1412→1202	0.002	0.002		0.06
$\rightarrow 5/2^-_{\phi_2}$	→911	0.002	0.011	20	5
$\rightarrow 3/2^-_{\phi_2}$	→828	0.001			0.2
$\rightarrow 5/2^-_{\phi_1}$	→359	0.024	0.008	100	100
$\rightarrow 3/2^-_{\phi_1}$	→0	3×10^{-5}		20	0.3
$9/2^-_{\phi_1} \rightarrow 7/2^-_{\phi_1}$	1519→1412	0.003	0.018		0.03
$\rightarrow 7/2^-_{\phi_1}$	→1202	0.0007	0.005		0.2
$\rightarrow 5/2^-_{\phi_2}$	→911	0.0003			0.02
$\rightarrow 5/2^-_{\phi_1}$	→359	0.049		100	100
$11/2^-_{\phi_1} \rightarrow 9/2^-_{\phi_1}$	2653→1519	0.001	0.007		5
$\rightarrow 7/2^-_{\phi_2}$	→1412	0.0004			0.4
$\rightarrow 7/2^-_{\phi_1}$	→1202	0.051		100	100
$13/2^-_{\phi_1} \rightarrow 11/2^-_{\phi_1}$	3160→2653	0.0003	0.004		0.1
$\rightarrow 9/2^-_{\phi_1}$	→1519	0.065		100	100
$15/2^-_{\phi_1} \rightarrow 13/2^-_{\phi_1}$	4280→3160	0.0009	0.004		1.5
$\rightarrow 11/2^-_{\phi_1}$	→2653	0.056		100	100
$17/2^-_{\phi_1} \rightarrow 15/2^-_{\phi_1}$	4750→4280	8×10^{-5}	0.002	12	0.04
$\rightarrow 13/2^-_{\phi_1}$	→3160	0.067		100	100
$21/2^-_{\pi_1} \rightarrow 21/2^-_{\pi_1}$	5744→5225	2×10^{-6}	0.003	100	100
$\rightarrow 19/2^-_{\pi_1}$	→5085	0.0003	0.002	24	161
$23/2^-_{\pi_1} \rightarrow 21/2^-_{\pi_2}$	6185→5744	0.0004	0.718	30	89
$\rightarrow 21/2^-_{\pi_1}$	→5225	0.0007	0.007		10
$\rightarrow 19/2^-_{\pi_1}$	→5085	0.025		40	40
$25/2^-_{\pi_1} \rightarrow 23/2^-_{\pi_1}$	6589→6185	0.0006	0.006		0.4
$\rightarrow 21/2^-_{\pi_2}$	→5744	8×10^{-6}			0.002
$\rightarrow 21/2^-_{\pi_1}$	→5225	0.036		100	100
$23/2^-_{\pi_2} \rightarrow 25/2^-_{\pi_1}$	6870→6589	0.007	0.598		20
$\rightarrow 23/2^-_{\pi_1}$	→6185	0.0002	0.0004		0.2
$\rightarrow 21/2^-_{\pi_2}$	→5744	4×10^{-5}	0.003	36	6
$\rightarrow 21/2^-_{\pi_1}$	→5225	0.008	0.0003	100	100
$\rightarrow 19/2^-_{\pi_1}$	→5085	3×10^{-7}			0.005

^{67}Ga

$I_i^\pi \rightarrow I_f^\pi$ ($\hbar$) ($\hbar$)	$E_i \rightarrow E_f$ Expt. Expt.	$B(E2)(e^2b^2)$ IBFBPM	$B(M1)(\mu_N^2)$ IBFBPM	I_γ Expt.	I_γ IBFBPM
$27/2^-_{\pi_2} \rightarrow 23/2^-_{\pi_2}$	7958→6870	0.041		50	259
$\rightarrow 25/2^-_{\pi_1}$	→6589	0.005	0.0001	100	100
$\rightarrow 23/2^-_{\pi_1}$	→6185	9×10^{-6}			0.6
$13/2^+_{\phi_1} \rightarrow 9/2^+_{\phi_1}$	3031→2073	0.037		100	100
$11/2^+_{\phi_1} \rightarrow 13/2^+_{\phi_1}$	3190→3031	0.001	0.119		0.4
$\rightarrow 9/2^+_{\phi_1}$	→2073	0.041	0.058	100	100
$15/2^+_{\pi_1} \rightarrow 11/2^+_{\phi_1}$	3577→3190	0.002		3.4	33
$\rightarrow 13/2^+_{\phi_1}$	→3031	0.0009	4×10^{-5}	100	100
$17/2^+_{\pi_1} \rightarrow 15/2^+_{\pi_1}$	3855→3577	0.006	0.039	1.2	22
$\rightarrow 13/2^+_{\phi_1}$	→3031	0.015		100	100
$17/2^+_{\phi_1} \rightarrow 17/2^+_{\pi_1}$	4198→3855	6×10^{-5}	0.095	90	6
$\rightarrow 15/2^+_{\pi_1}$	→3577	0.001	0.028		11
$\rightarrow 13/2^+_{\phi_1}$	→3031	0.043		100	100
$19/2^+_{\pi_1} \rightarrow 17/2^+_{\phi_1}$	4290→4198	0.002	0.001		0.02
$\rightarrow 17/2^+_{\pi_1}$	→3855	0.004	9×10^{-5}	1.6	1.2
$\rightarrow 15/2^+_{\pi_1}$	→3577	0.029		100	100
$17/2^+_{\phi_2} \rightarrow 19/2^+_{\pi_1}$	4349→4290	6×10^{-5}	0.004		0.02
$\rightarrow 17/2^+_{\phi_1}$	→4198	3×10^{-5}	0.008		0.8
$\rightarrow 17/2^+_{\pi_1}$	→3855	0.0004	0.001	52	5
$\rightarrow 15/2^+_{\pi_1}$	→3577	0.0001	0.012	<10	146
$\rightarrow 13/2^+_{\phi_1}$	→3031	0.0014		100	100
$21/2^+_{\pi_2} \rightarrow 17/2^+_{\pi_2}$	4995→4349	0.035			24
$\rightarrow 19/2^+_{\pi_1}$	→4290	2×10^{-5}	0.033	100	100
$\rightarrow 17/2^+_{\phi_1}$	→4198	0.009			17
$\rightarrow 17/2^+_{\pi_1}$	→3855	0.0002			2.7
$21/2^+_{\pi_1} \rightarrow 21/2^+_{\pi_2}$	5186→4995	0.0002	0.005		0.03
$\rightarrow 17/2^+_{\pi_2}$	→4349	0.0002			0.04
$\rightarrow 19/2^+_{\pi_1}$	→4290	0.003	0.106	31	67
$\rightarrow 17/2^+_{\phi_1}$	→4198	0.0003			0.2
$\rightarrow 17/2^+_{\pi_1}$	→3855	0.040		100	100
$21/2^+_{\phi_1} \rightarrow 21/2^+_{\pi_1}$	5491→5186	0.0002	0.029	2.1	0.7
$\rightarrow 21/2^+_{\pi_2}$	→4995	1×10^{-5}	0.001		0.1
$\rightarrow 17/2^+_{\pi_2}$	→4349	0.008		27	9
$\rightarrow 19/2^+_{\pi_1}$	→4290	0.0004	0.004		7
$\rightarrow 17/2^+_{\phi_1}$	→4198	0.048		100	100
$\rightarrow 17/2^+_{\pi_1}$	→3855	0.002		67	14

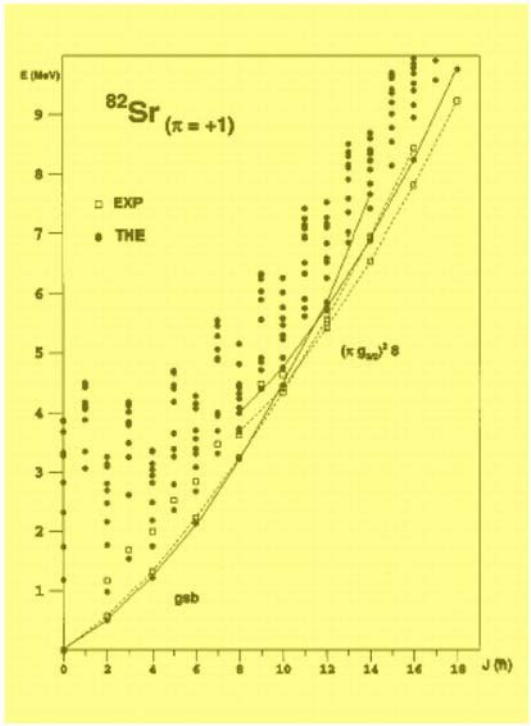

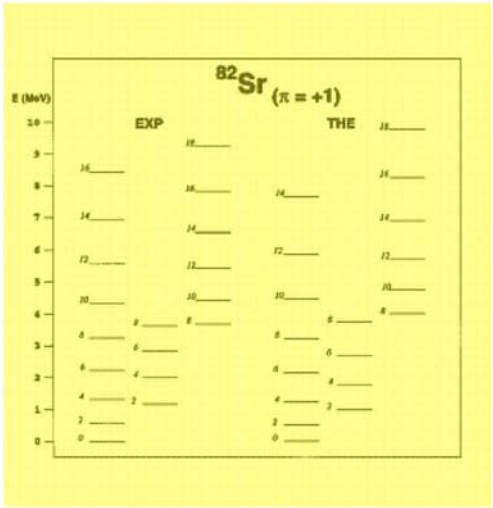

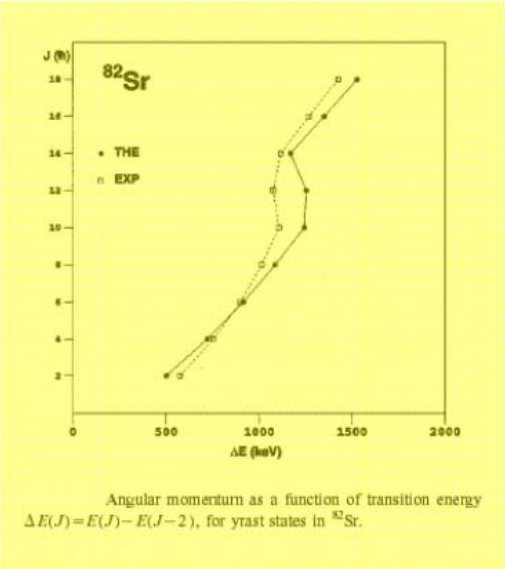

Angular momentum as a function of transition energy $\Delta E(J)=E(J)-E(J-2)$, for yrast states in ^{82}Sr.

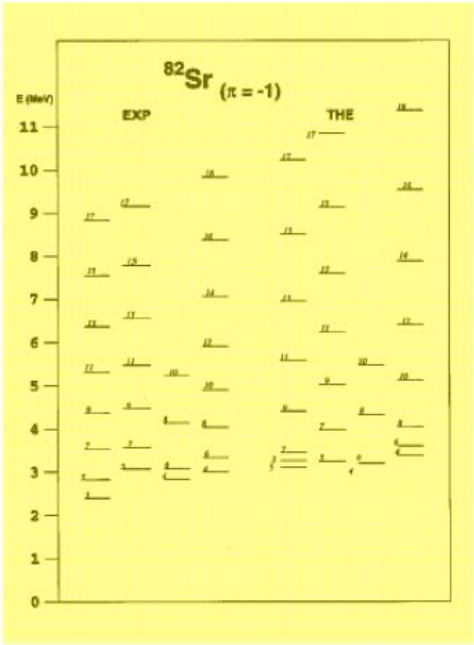

Interactions ?

The strength of the exchange interaction is adjusted to reproduce the energy spacings of negative-parity states in ^{82}Sr. It differs considerably from that used for odd-even isotopes In order to understand the origin of this anomaly, one may consider the coupling of unpaired protons to proton bosons in the ^{82}Sr. To create multiproton states in the even-even nucleus we destroy proton bosons and the effective coupling of the exchange interaction is reduced. In the IBM-2 framework this reduction would be implicit and no adjustment of strength parameters should be needed. However, in our model based on IBM-1, we couple to all the core bosons, irrespective of their nature and the suppression of coupling is greatly diminished. Thus, the need to empirically reduce the strength of coupling parameter. This effect should be especially pronounced near closed shells, and in our case the reduction of the exchange interaction might be due to the subshell closure at $Z=40$.

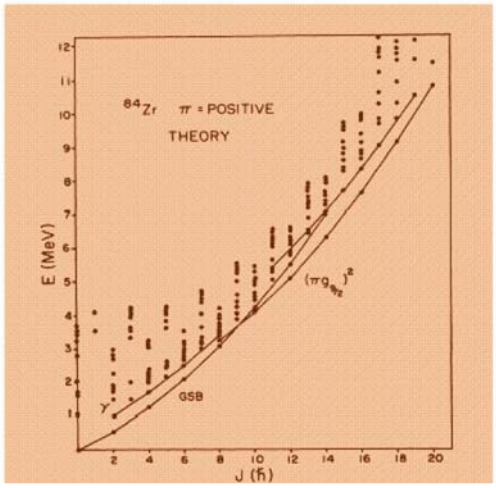

Some of the positive-parity states calculated for ^{84}Zr. The first ten states of each spin are shown for configurations involving core vibrations coupled to quasiproton states.

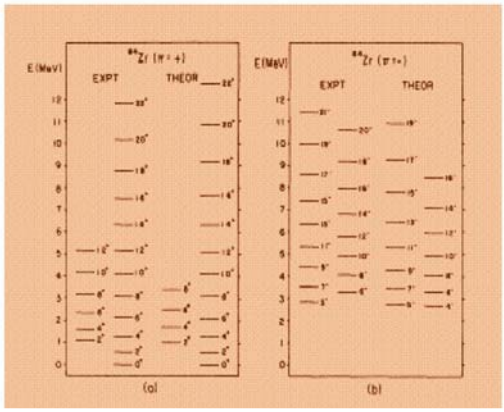

A detailed comparison of states calculated for ^{84}Zr (a) in the positive-parity sequence (b) in the negative-parity sequence

A comparison of experimental B(E2) for ^{86}Zr along the ground-state sequence compared with geometrical models (-.-.-.), our calculations in the full 28-50 shell model space (----), and our calculations in a space truncated by the Z = 38 subshell closure (. . . .).

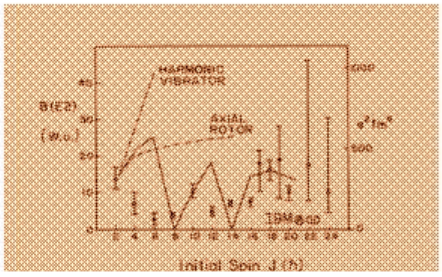

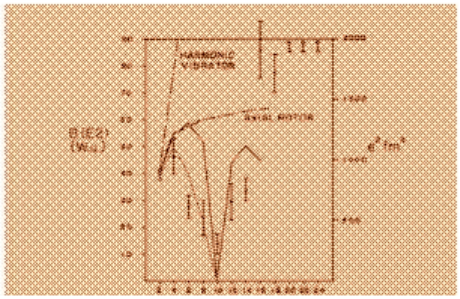

B(E2) strengths measured for the yrast sequence in ^{86}Zr compared with geometrical models and the present calculation.

The pair breaking interaction V^{mix}, which mixes states with different number of fermions, and conservs only the total number of valence nucleons, in general does not induce sufficient mixing as can be deduced, for example, from observed transition strengths. It is the lowest order contribution to a pair-breaking interaction. Since the interaction contains only fermion operators of rank 0 and 2, it cannot connect in first order the ground state band with two-fermion states of higher fermion angular momenta. In order to enhance the mixing, interactions that contain fermion operators of higher rank could be included in the model Hamiltonian. However, such an interaction would also require higher order boson operators, with parameters that cannot be determined from available experimental data, or from the intrinsic structure of the model.

^{138}Nd

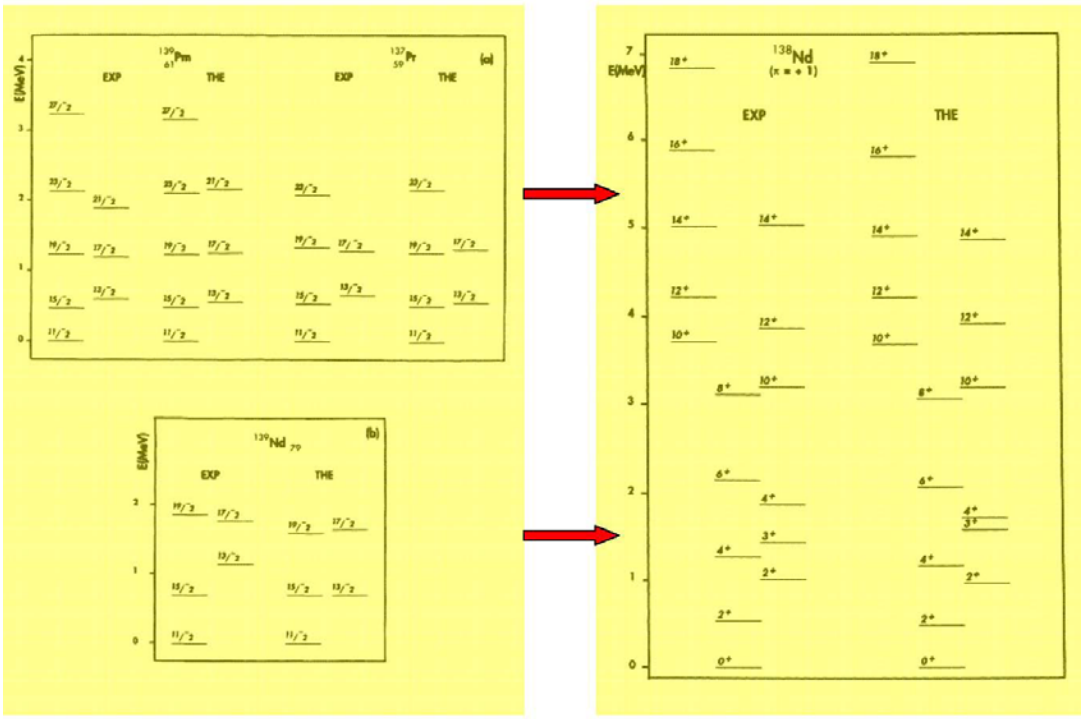

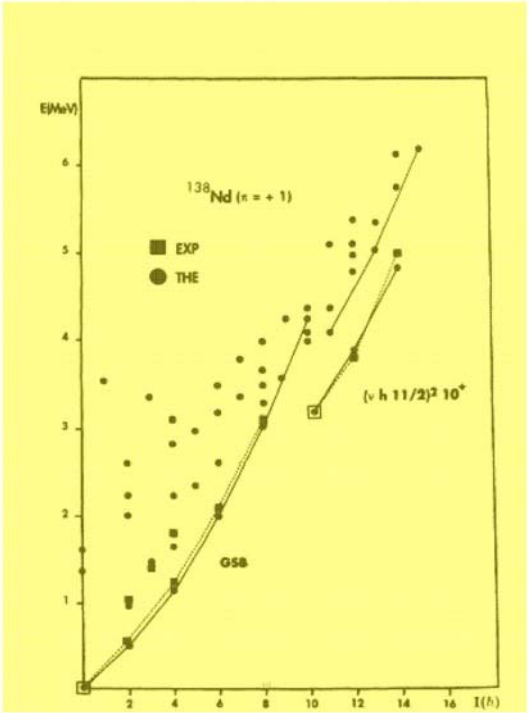

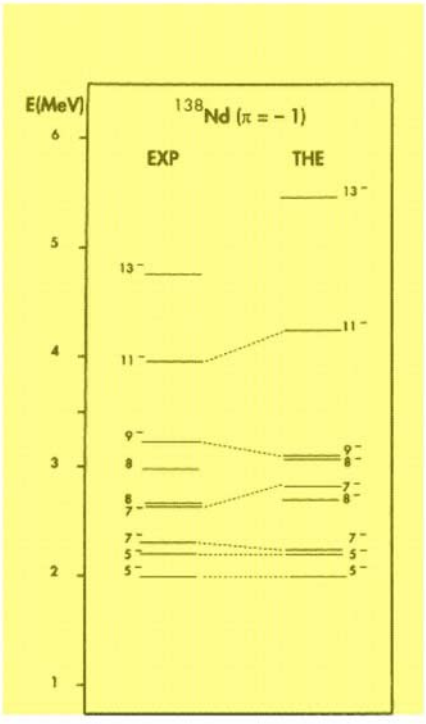

h11/2 d3/2 neutron pair

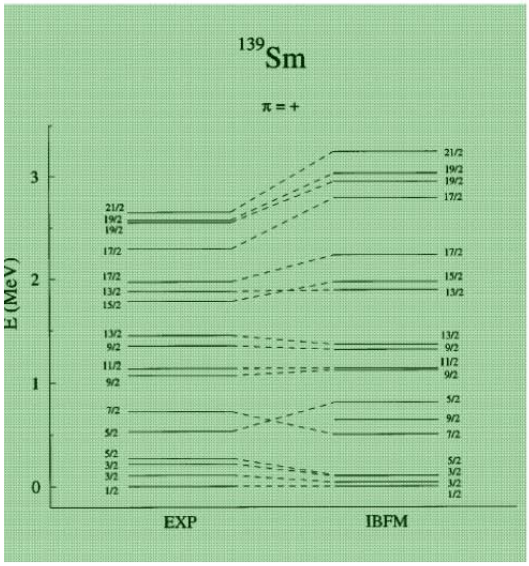

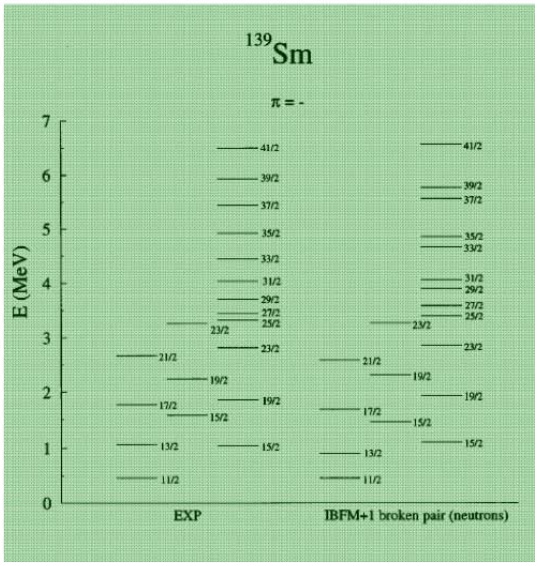

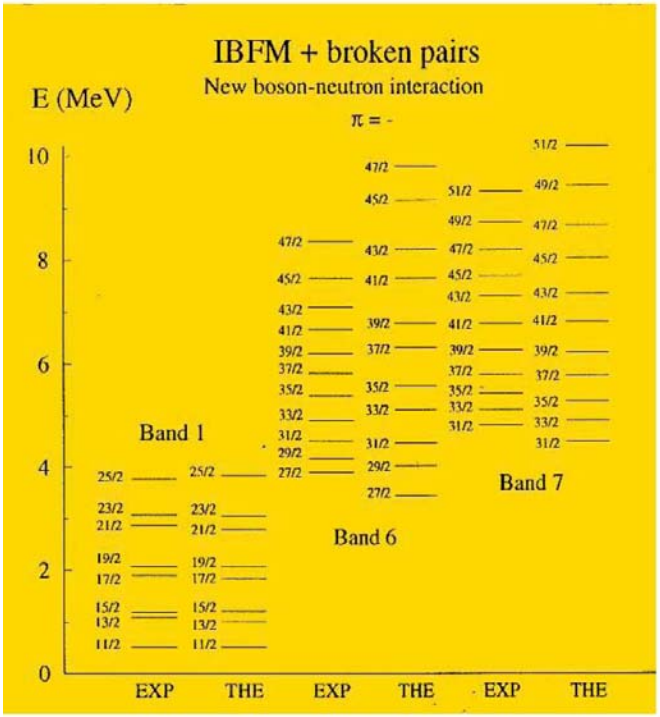

$^{137}Nd_{77}$

Band 1 (ν h11/2)

Band 6 (ν h11/2)^3

Band 7 (ν h11/2) (π h11/2)^3

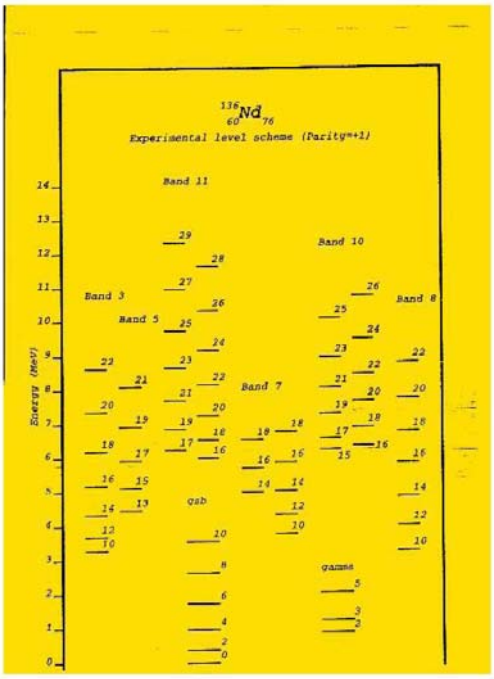

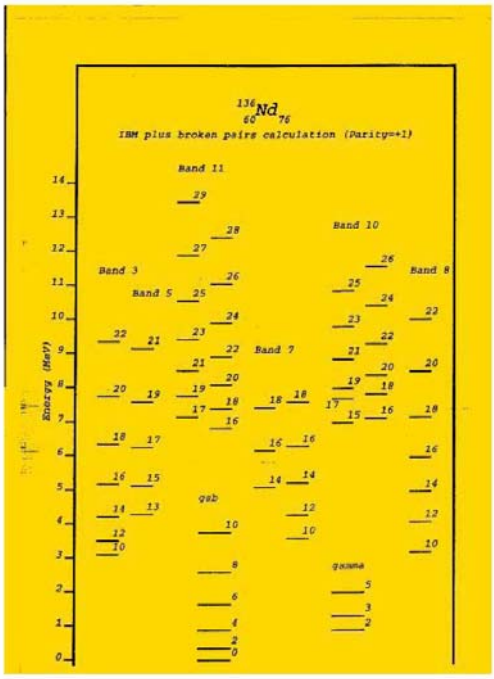

Bands 3, 5, 7 $(\pi\ h11/2)^2$

Band 8 $(\nu\ h11/2)^2$

Bands 10, 11 $(\pi\ h11/2)^2\ (\nu\ h11/2)^2$!!!

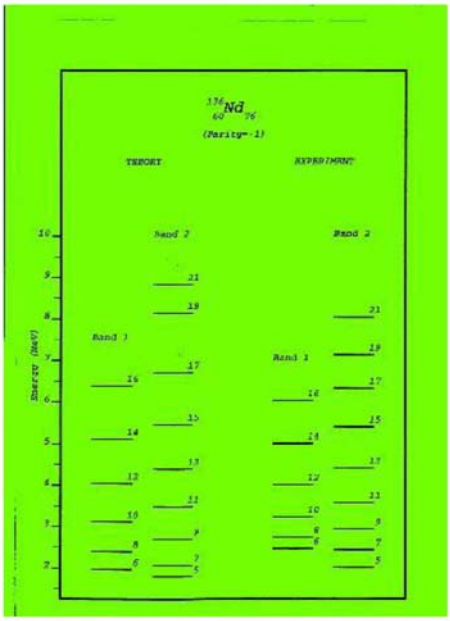

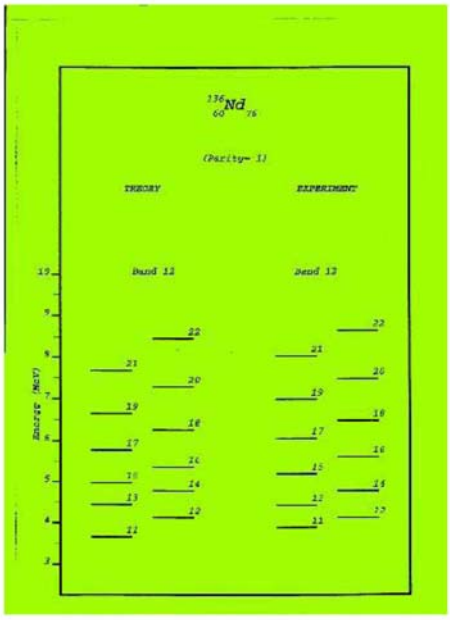

Bands 1, 2 $(\nu\ d3/2\ \ \nu\ h11/2)$

Band 12 $(\nu\ d3/2\ \ (\nu\ h11/2)^3)$

^{101}Rh

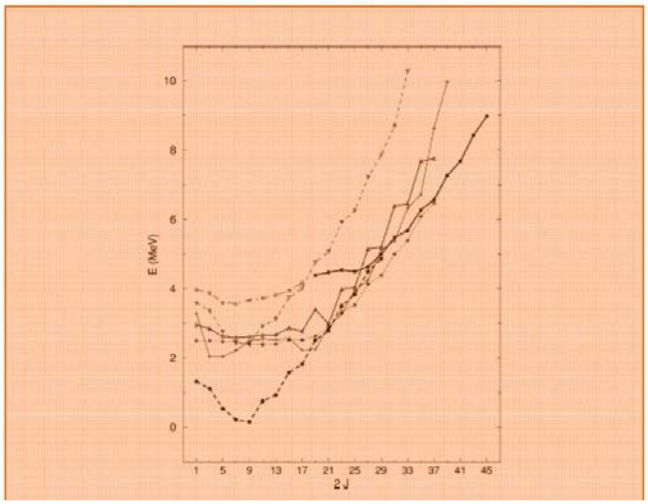

FIG. 4. Positive-parity levels calculated with the IBFBPM model for the following configuration: ●: πg9/2, □: πg9/2ν(h$^{2}_{1}$ $_{1/2}$)small *I*, ■: πg9/2 ν(h$^{2}_{1}$ 1/2)I=10, *: πg9/2ν(d5/2 and/or g7/2), +: (πp1/2 and/or π*p*3/2 and/or π ∫ 5/2) νh11/2ν(d5/2 or g7/2), Δ: πg$^{3}_{9/2}$, ∇: πg9/2 (πp1/2 and/or πp3/2 and/or π ∫ 5/2).

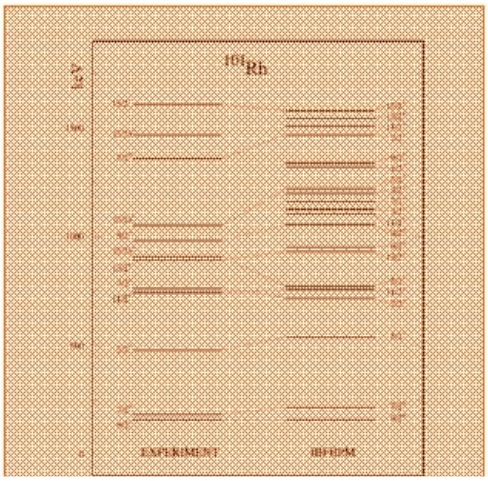

Fig. 5. Comparison of positive parity levels in the 0 – 1.6 MeV range observed in experiments and calculated using the IBFBPM model. All the calculated levels are shown for a given spin.

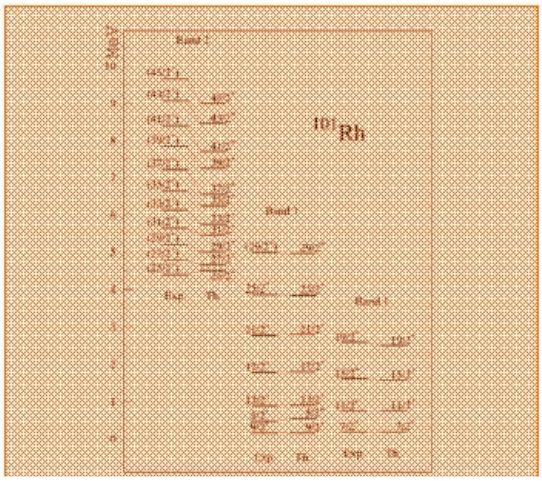

Fig.6. Comparison of positive parity levels in bands 1 and 2 observed in the present experiment (Exp.) and calculated using the IBFBPM model (Th.) up to spin *I* = 45/2.

Band 1 π g9/2

Band 2 π g9/2 (ν h11/2)²

^{101}Rh

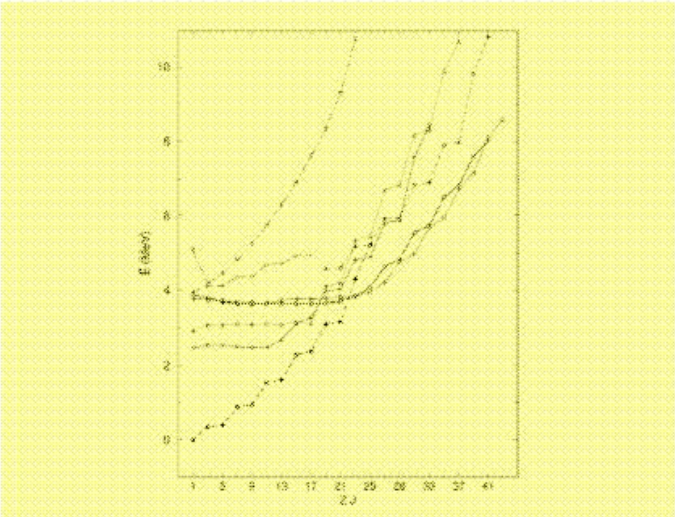

Fig. 7. Negative-parity levels calculated with the IBFBPM model for the following configurations: •: $\pi p_{1/2}$ from $1/2^-$ to $21/2^-$ and $\pi f_{5/2}$ for $23/2^-$ and $25/2^-$, □: $\pi g_{9/2}\nu(d_{5/2}h_{11/2})$, ○: $\pi g_{9/2}\nu(g_{7/2}h_{11/2})$, ∗: $\pi p_{1/2}\nu(h^2_{11/2})_{10}$ from $I = 19/2^-$ to $37/2^-$ and $\pi f_{5/2}\nu(h^2_{11/2})_{10}$ from $I = 39/2^-$ to $41/2^-$, +: $\pi(p_{1/2}$ and/or $p_{3/2}$ and/or $f_{5/2})\nu(h^2_{11/2})_{\text{small }I}$, ▽: $\pi(p_{1/2}$ and/or $p_{3/2}$ and/or $f_{5/2})^3$, △: $\pi(p_{1/2}$ and/or $p_{3/2}$ and/or $f_{5/2})\pi g^3_{9/2}$, ⋄: $\pi(p_{1/2}$ and/or $p_{3/2}$ and/or $f_{5/2})\nu(d_{5/2}$ and/or $g_{7/2})$.

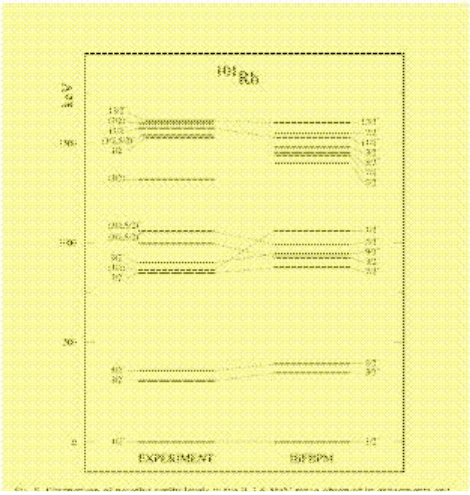

Fig 8. Comparison of negative–parity levels in the 0 – 1.5 Mev range observed in experiments and calculated using IBFBPM model. For a given spin, all the calculated levels are shown.

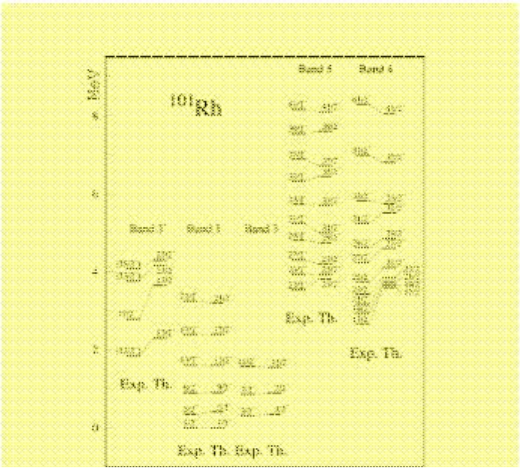

Fig 9. Comparison of negative–parity levels in Bands 3, 4, 5 observed in the present experiment (EXP.) and calculated using IBFBPM model (Th) up to spin I = 41/2.

Band 3 π p1/2

Bands 4, 5 (π g9/2) (ν d5/2 ν h11/2) or
(π g9/2) (ν g7/2 ν h11/2)

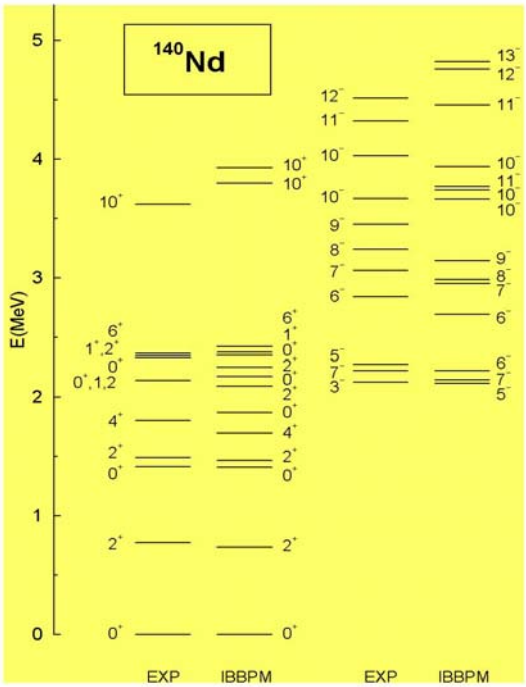
140Nd
E(MeV)
EXP
IBBPM
EXP
IBBPM

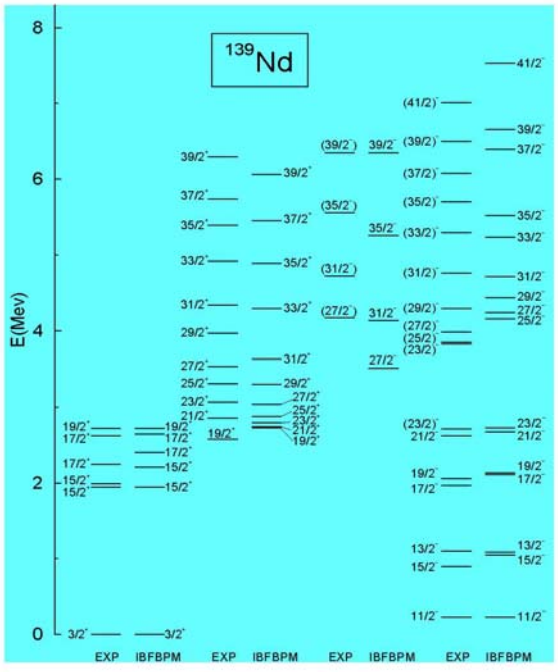
139Nd
E(Mev)
EXP
IBFBPM
EXP
IBFBPM
EXP
IBFBPM
EXP
IBFBPM

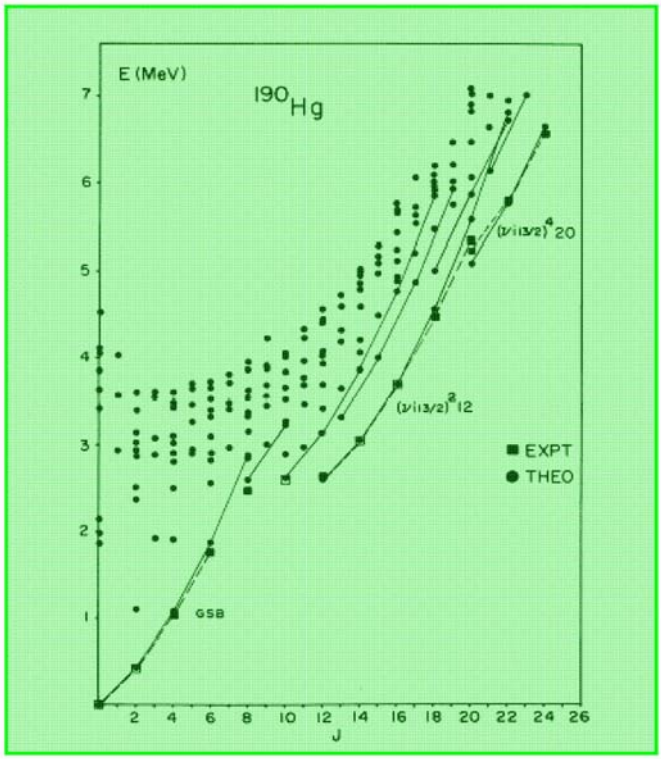

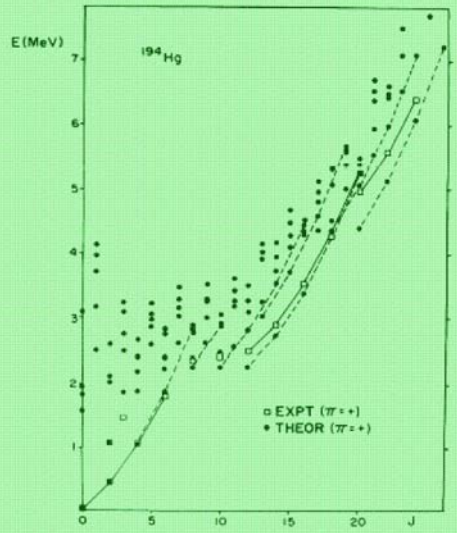

Comparison between calculated (0, 2, and 4qp) (circles) and experimental (squares) positive-parity states in ^{194}Hg. Only the first five calculated levels of each angular momentum J are shown. Sets of states with similar structure (bands) are joined together: dashed lines (calculated bands), solid lines (experimental bands).

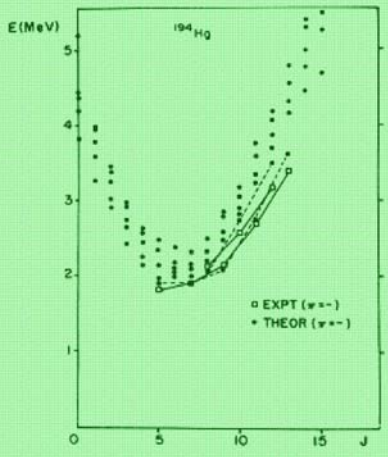

Comparison between calculated (0 and 2qp) (circles) and experimental (squares) negative-parity states in ^{194}Hg. Only the first five calculated levels of each angular momentum J are shown. Sets of states with similar structure (bands) are joined together a

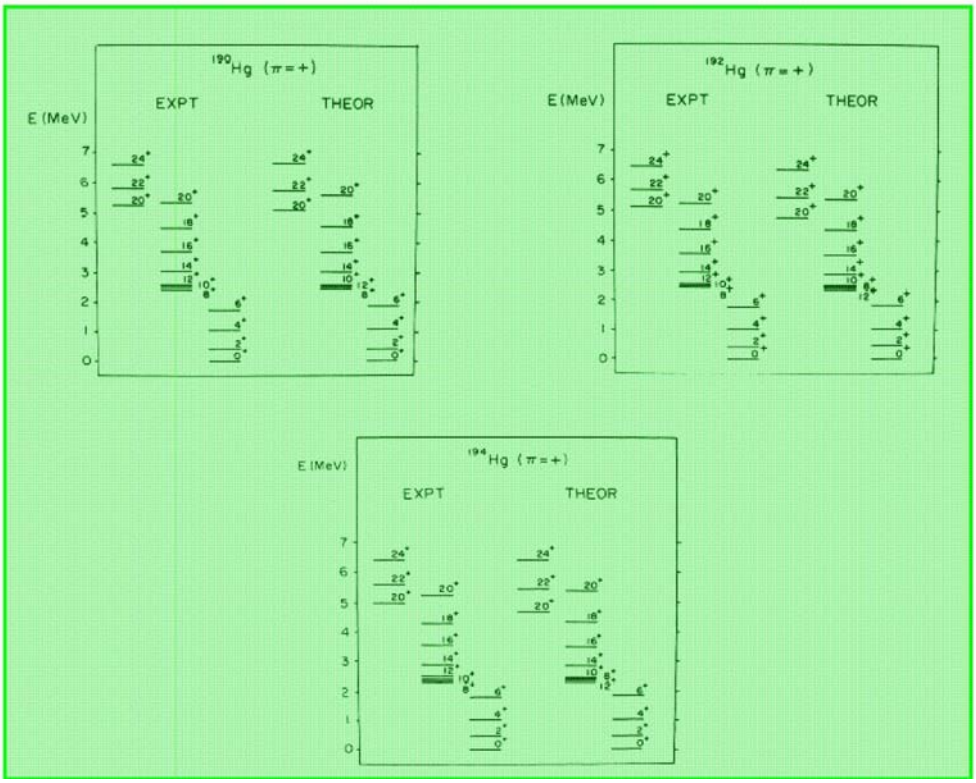

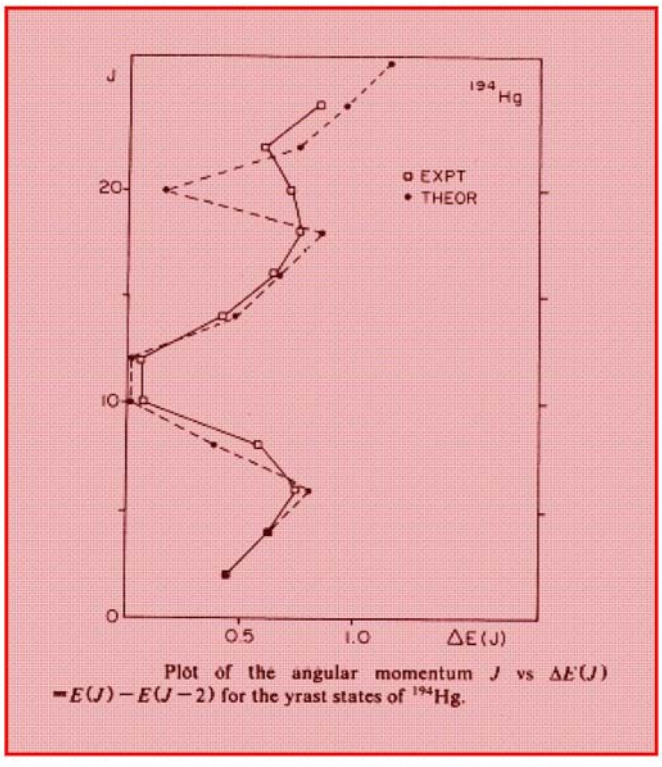

Plot of the angular momentum J vs $\Delta E(J) = E(J) - E(J-2)$ for the yrast states of ^{194}Hg.

Nuclear Theory:
Structure of the odd-odd nuclei in the interacting boson-fermion-fermion model

S. Brant

University of Zagreb, Croatia

E.mail: Brant@phy.hr

3.

Structure of odd-odd nuclei in the interacting boson fermion-fermion model

The IBFFM is able to give an accurate description of the structure of odd-odd nuclei. Odd-odd nuclei constitute a very stringent test of the model:

- A detailed knowledge of even-even cores and odd-mass neighbours is required
- Odd-odd nuclei do not provide the same sort of smoothly varying systematics as do other types of nuclei

IBFFM is successful in describing and predicting

- Level energies
- Electromagnetic properties
- Transfer properties
- Isomers

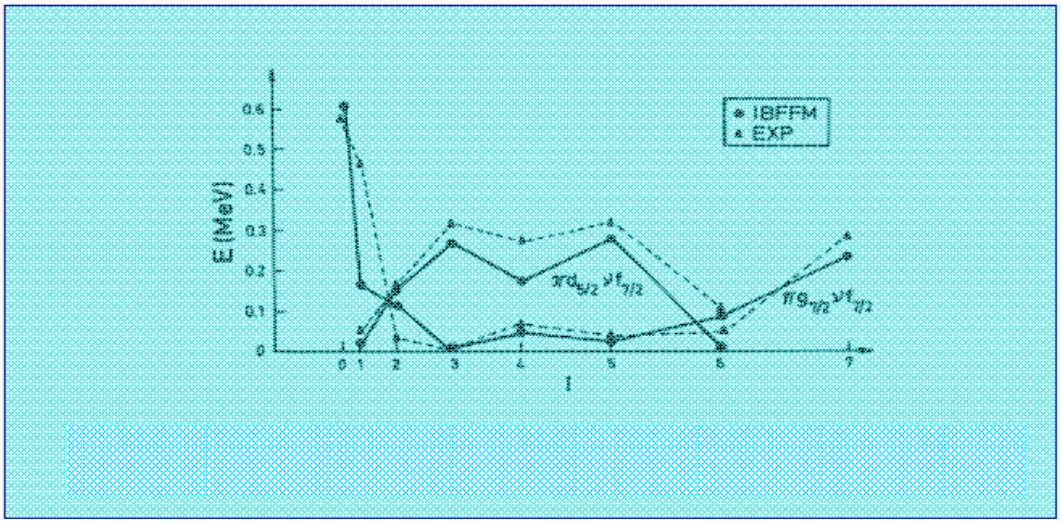

Fig. 8 Classification of the IBFFM levels into multiplets on the basis of largest components in the wave functions. The experimental levels of ^{140}La are compared with the theoretical spectra on the basis of level energies, electromagnetic de-excitation, and transfer properties. IBFFM and experimental levels are presented by solid circles and triangles respectively.

The IBFFM Hamiltonian for an odd-odd nucleus is:

$$H = H_B + H_{\nu F} + H_{\pi F} + V_{\nu BF} + V_{\pi BF} + V_{\pi\nu}$$

H_B is the boson Hamiltonian of IBM-1 describing a system of N interacting bosons (correlated S and D pairs) that approximate the valence nucleon pairs:

$$\begin{aligned} H_B &= \varepsilon\,\hat{N} + \frac{1}{2}\,v_0\,\left([d^\dagger \times d^\dagger]_{(0)} \times [\tilde{s} \times \tilde{s}]_{(0)} + h.c.\right)_{(0)} \\ &+ \frac{1}{\sqrt{2}}\,v_2\,\left([d^\dagger \times d^\dagger]_{(2)} \times [\tilde{d} \times \tilde{s}]_{(2)} + h.c.\right)_{(0)} \\ &+ \sum_{L=0,2,4} \frac{1}{2}\,C_L\,\sqrt{2L+1}\,\left([d^\dagger \times d^\dagger]_{(L)} \times [\tilde{d} \times \tilde{d}]_{(L)}\right)_{(0)} \end{aligned}$$

$$n_s = N - n_d$$

$H_{\pi F}$ and $H_{\nu F}$ are the fermion Hamiltonians containing quasiparticle energies of protons and neutrons, respectively. The quasiparticle energies and occupation probabilities contained in the fermion Hamiltonian, and other terms, are obtained in a BCS calculation with some standard set of single fermion energies. For protons ($\alpha = \pi$) and for neutrons ($\alpha = \nu$).

$$H_{\alpha F} = \sum_i \varepsilon_{\alpha_i} \, a^\dagger_{\alpha_i} \tilde{a}_{\alpha_i}$$

$V_{\nu BF}$ and $V_{\pi BF}$ are the IBFM-1 boson-fermion interactions containing the dynamical, exchange and monopole interactions. For protons ($\alpha = \pi$) and for neutrons ($\alpha = \nu$).

$$V_{\alpha BF} = V_{\alpha DYN} + V_{\alpha EXC} + V_{\alpha MON}$$

$$V_{\alpha DYN} = \Gamma_0 \sum_{\alpha j_1 \alpha j_2} \sqrt{5} \, (u_{\alpha j_1} u_{\alpha j_2} - v_{\alpha j_1} v_{\alpha j_2}) \, \langle \alpha j_1 \parallel Y_2 \parallel \alpha j_2 \rangle \, \left([a^\dagger_{\alpha j_1} \times \tilde{a}_{\alpha j_2}]^{(2)} \times Q^{(2)}_B \right)^{(0)}$$

$Q^{(2)}_B$ is the standard boson quadrupole operator

$$Q^{(2)}_B = [s^\dagger \times \tilde{d} + d^\dagger \times \tilde{s}]^{(2)} + \chi [d^\dagger \times \tilde{d}]^{(2)}$$

$$V_{\alpha EXC} = \Lambda_0 \sum_{\alpha j_1 \alpha j_2 \alpha j_3} (-2) \sqrt{\frac{5}{2\,\alpha j_3 + 1}} \, (u_{\alpha j_1} v_{\alpha j_3} + v_{\alpha j_1} u_{\alpha j_3}) \, (u_{\alpha j_2} v_{\alpha j_3} + v_{\alpha j_2} u_{\alpha j_3})$$
$$\langle \alpha j_3 \parallel Y_2 \parallel \alpha j_1 \rangle \, \langle \alpha j_3 \parallel Y_2 \parallel \alpha j_2 \rangle \, : \left([a^\dagger_{\alpha j_1} \times \tilde{d} \,]_{\alpha j_3} \times [\tilde{a}_{\alpha j_2} \times d^\dagger \,]_{\alpha j_3} \right)^{(0)} :$$

$$V_{\alpha MON} = A_0 \sum_{\alpha j} \sqrt{5} \, (2\alpha j + 1) \, \left([a^\dagger_{\alpha j} \times \tilde{a}_{\alpha j}]^{(0)} \times [d^\dagger \times \tilde{d}]^{(0)} \right)^{(0)}$$

$V_{\pi\nu}$ is the residual proton-neutron interaction taken in the form of spin-spin, surface-delta, spin-spin-delta, tensor or multipole-multipole interaction.

$$H_{\sigma\sigma} = -\sqrt{3}\, V_{\sigma\sigma}\, [\vec{\sigma}_\pi \cdot \vec{\sigma}_\nu]$$

$$H_\delta = 4\pi\, V_\delta\, \delta(\vec{r}_\pi - \vec{r}_\nu)\, \delta(r_\pi - R_0)\, \delta(r_\nu - R_0)$$

$$H_{\sigma\sigma\delta} = 4\pi\, V_{\sigma\sigma\delta}\, [\vec{\sigma}_\pi \cdot \vec{\sigma}_\nu]\, \delta(\vec{r}_\pi - \vec{r}_\nu)\, \delta(r_\pi - R_0)\, \delta(r_\nu - R_0)$$

$$H_T = V_T \left(3\, \frac{[\vec{\sigma}_\pi \cdot \vec{r}_{\pi\nu}]\, [\vec{\sigma}_\nu \cdot \vec{r}_{\pi\nu}]}{r_{\pi\nu}^2} - [\vec{\sigma}_\pi \cdot \vec{\sigma}_\nu] \right)$$

$$H_{MM} = 4\pi\, \frac{\delta(r_\pi - r_\nu)}{r_\pi r_\nu} \sum_{\kappa\mu} V_\kappa\, Y^*_{\kappa\mu}(\pi)\, Y_{\kappa\mu}(\nu)$$

$$\vec{r}_{\pi\nu} = \vec{r}_\pi - \vec{r}_\nu \qquad R_0 = 1.2\, A^{\frac{1}{3}}\ \ fm$$

The electromagnetic operators have the form (for protons ($\alpha = \pi$) and for neutrons ($\alpha = \nu$)):

$$M(E2) = M_B(E2) + M_\pi(E2) + M_\nu(E2)$$

$$M_B(E2) = \frac{3}{4\pi}\, R_0^2\, e^{VIB} \left([s^\dagger \times \tilde{d} + d^\dagger \times \tilde{s}]^{(2)} + \chi [d^\dagger \times \tilde{d}]^{(2)} \right)$$

$$R_0^2 = 0.0144\, A^{\frac{2}{3}} \qquad barn$$

$$M_\alpha(E2) = \frac{3}{5}\, R_0^2\, e_\alpha\, Y_2(\alpha)$$

$$\vec{M}(M1) = \vec{M}_B(M1) + \vec{M}_\pi(M1) + \vec{M}_\nu(M1)$$

$$\vec{M}_B(M1) = \sqrt{\frac{3}{4\pi}}\, \sqrt{10}\, g_R\, [d^\dagger \times \tilde{d}]^{(1)}$$

$$\vec{M}_\alpha(M1) = \sqrt{\frac{3}{4\pi}}\, [\, g_l(\alpha)\, \vec{l}(\alpha) + g_s(\alpha)\, \vec{s}(\alpha) + g_T(\alpha)\, (Y_2(\alpha) \times \vec{s}(\alpha))_1\,]$$

Spherical nuclei

Parabolic rule for proton-neutron multiplets in the particle-vibration model

Exchange of the quadrupole phonon

The particle-quadrupole vibration interaction is

$$H_2 = \sqrt{20\pi}a_2|Y_2(b_2^\dagger + b_2)|_0$$

$$a_2 = \tfrac{1}{3}(4\pi)^{\frac{1}{2}} \frac{1}{ZR_0^2} \langle k \rangle [B(\mathrm{E2}; 2_1^+ \rightarrow 0_1^+)_{\mathrm{vib}}]^{\frac{1}{2}}$$

For the quasiparticle, we also include the usual blocking factors U and V in the interaction strength a_2. The symbol $b_2^\dagger$ denotes the creation operator of the quadrupole phonon.

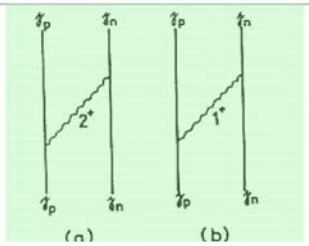

Second order diagrams for the exchange of the quadrupole (Fig. a) and spin-vibrational phonons (Fig. b).

The contribution to the splitting of the multiplet $|(j_p, j_n)I = |j_p - j_n|, \ldots, j_p + j_n\rangle$ coming from the exchange of quadrupole phonons (fig. a) is

$$\delta E_2 = -\alpha_2 \mathscr{V} \cdot \frac{[I(I+1) - j_n(j_n+1) - j_p(j_p+1)]^2 + [I(I+1) - j_n(j_n+1) - j_p(j_p+1)]}{2j_n(2j_n+2)2j_p(2j_p+2)}$$

$$+ \frac{\alpha_2 \mathscr{V}}{12},$$

$$\alpha_2 = 15a_2^2/\hbar\omega_2$$

Here $\hbar\omega_2$ is the energy of the quadrupole phonon. We assume the coupling strength a_2 to be equal both for protons and for neutrons.

We rewrite the I-dependent terms

$$\delta E_2(I) = A[I(I+1)]^2 + BI(I+1)$$

where A and B stand for the factors which multiply $[I(I+1)]^2$ and $I(I+1)$ respectively.

The quantity $\mathscr{V}$ is the occupation number defined as $\mathscr{V} = 1$ if $|j_p\rangle$ and $|j_n\rangle$ are both particle-like or both hole-like; $\mathscr{V} = -1$ if $|j_n\rangle$ is particle-like and $|j_n\rangle$ is hole-like, or vice versa.

Inclusion of the spin-vibrational 1^+ phonon

The particle-spin-vibration interaction reads

$$H_1 = \sqrt{3}a_1[\sigma_1 \times (b_1^\dagger + b_1)]_0$$

Here a_1 is the coupling strength defined as $a_1 = \kappa_1(\hbar\omega_1/2c_1)^{\frac{1}{2}}$, σ_1 is the spin operator and $b_1^\dagger$ the creation operator of the $\lambda = 1^+$ spin vibration

We derive the expression for the contribution to the energy shift of the $|(j_p j_n)I\rangle$ states due to the exchange of the 1^+ phonon

$$\delta E_1(I) = B_1 I(I+1) + \alpha_1 \frac{j_n(j_n+1) + j_p(j_p+1)}{(2j_n+2)(2j_p+2)}$$

$$B_1 = -\alpha_1 \frac{\xi}{(2j_p+2)(2j_n+2)} \qquad \alpha_1 = 4\frac{a_1^2}{\hbar\omega_1}$$

$$\xi = \begin{cases} 1 & \text{if } \mathscr{N} = -1, \ \dfrac{(2j_p+2)(2j_n+2)}{2j_p 2j_n} \quad \text{if } \mathscr{N} = 1, \\ -\dfrac{2j_p+2}{2j_p} & \text{if } \mathscr{N} = 0^-, \ -\dfrac{2j_n+2}{2j_n} \quad \text{if } \mathscr{N} = 0^+. \end{cases}$$

$\mathscr{N}$ is the Nordheim number defined as

$$\mathscr{N} = j_p - l_p + j_n - l_n$$

For $\mathscr{N} = 0$, we use the labels $-$ and $+$. The symbols $\mathscr{N} = 0^-$ and $\mathscr{N} = 0^+$ denote the situations $j_n - l_n = -\frac{1}{2}$, $j_p - l_p = \frac{1}{2}$ and $j_n - l_n = \frac{1}{2}$, $j_p - l_p = -\frac{1}{2}$, respectively.

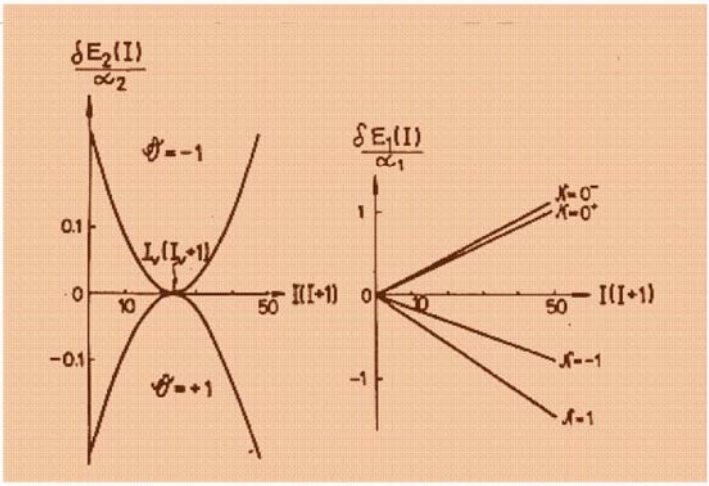

Illustration of energy contributions coming from the exchange of the quadrupole phonon (a) and the spin-vibrational phonon (b) for the multiplet ($j_p = \frac{5}{2}, j_n = \frac{7}{2}$), for four possible combinations of the pair (ϑ, K).

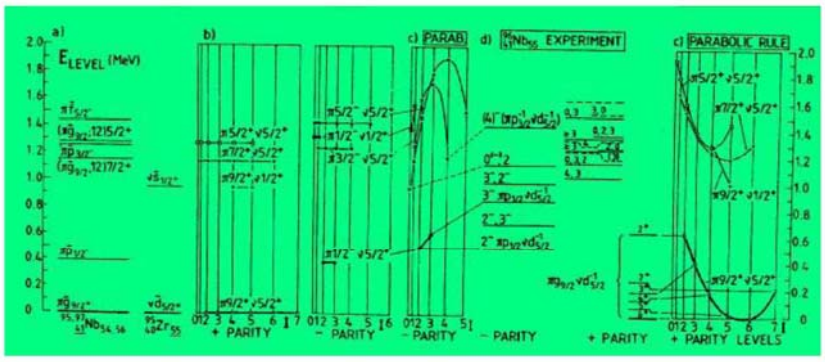

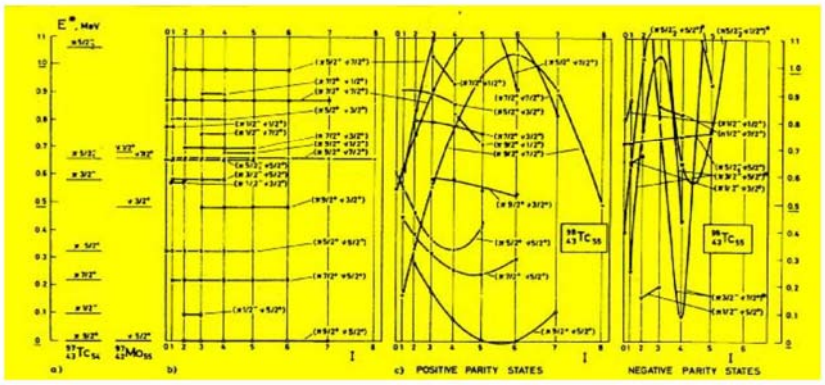

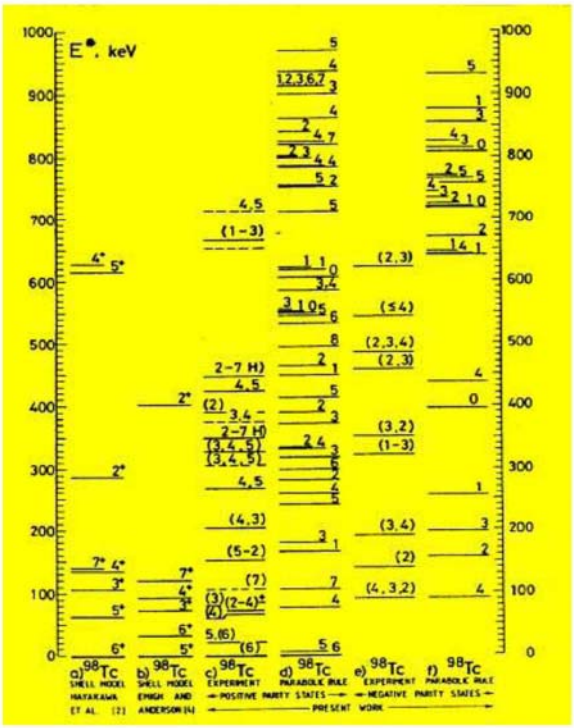

For spherical nuclei, with only the dynamical interaction and $\chi = 0$ → $\Gamma_0 = a\sqrt{\frac{4\pi}{5N}}$

^{96}Y

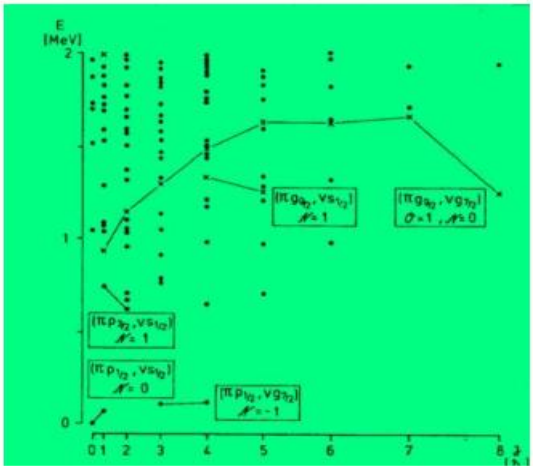

Fig. 4. Negative and positive parity levels of ^{96}Y calculated in IBFFM. Negative parity levels are denoted by full circles and positive parity by crosses. The states classified into the same multiplet on the basis of largest components in the wave function, are connected by full line.

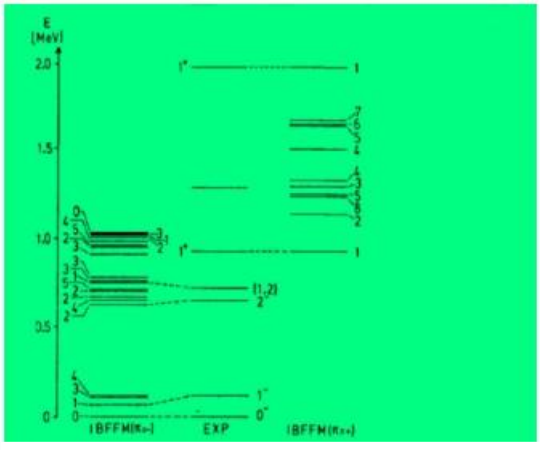

Fig. 5. IBFFM positive- and negative-parity energy spectrum of ^{96}Y in comparison to the available experimental data. The excitation energy of the 8* level is not known, but it should amount to ≥ 1 MeV, see text.

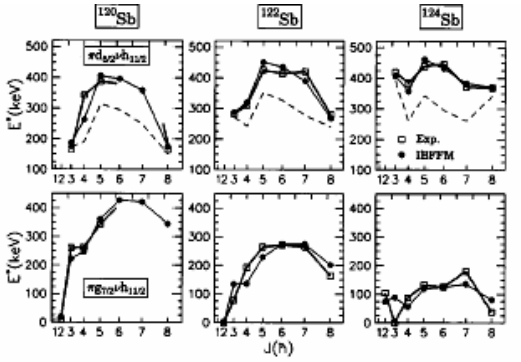

FIG. 1. Experimental (□) and calculated with the IBFFM (●) energy splittings of the $\pi d_{5/2}\nu\tilde{h}_{11/2}$ and $\pi g_{7/2}\nu\tilde{h}_{11/2}$ multiplets of ^{120,122,124}Sb. In the case of $\pi d_{5/2}\nu\tilde{h}_{11/2}$ multiplets also the theoretical splittings calculated with the assumption of best fits for the $\pi g_{7/2}\nu\tilde{h}_{11/2}$ multiplet V^2 values are shown as dashed lines. The abscissa is scaled according to $J(J+1)$, where J is the spin of the state.

In the whole sequence of nuclei it have been used the same:

Cores

Dynamical, exchange and monopole interactions for protons

Dynamical, exchange and monopole interactions for neutrons

Occupation probabilities for protons

Residual proton-neutron delta interaction

Occupation probabilities for neutrons depend on the isotope

Parabolic like structures are present in spherical nuclei, even in cases when other interactions (not the dynamical) dominate.

Sb isotopes

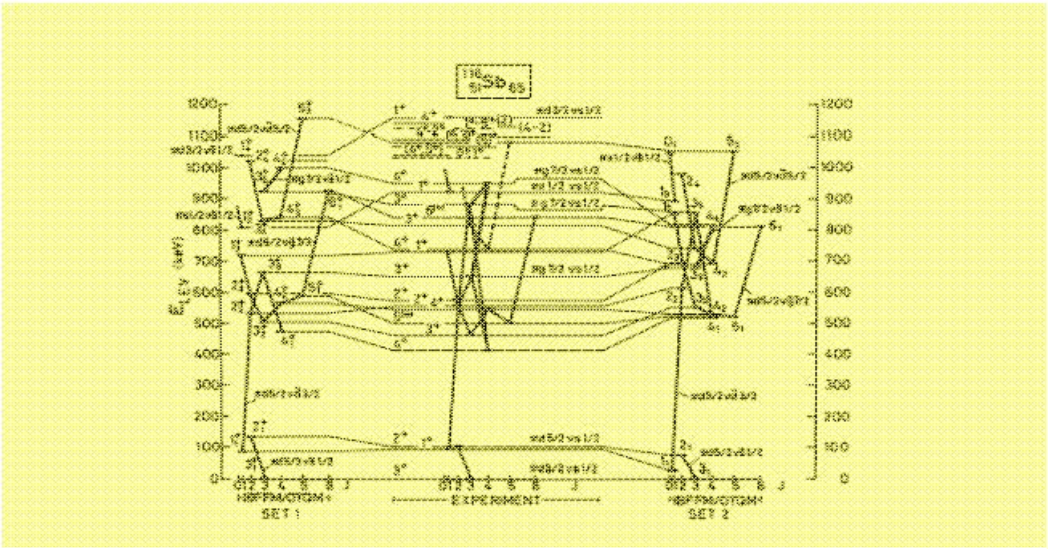

Fig. 6. IBFFM energy spectrum of ^{116}Sb in comparison with experimental data. The solid lines connect the members of the given multiplets. The leading proton-neutron configurations for several multiplets were identified on the basis of the (^{3}He, d) proton transfer results [4].

TABLE III. Comparison of measured and calculated in IBFFM spectroscopic factors for the ^{121}Sb(p, d)^{120}Sb one neutron transfer reaction. The first two columns contain the energy, spin and parity of the final states involved in the reaction taken from ref.[8].

Energy (keV)	J^π	L_n	$S_{(p,d)}$ [a]	S_{IBFFM} [b]
0	1^+	2	0.11	0.15
78	3^+	0	0.19	0.12
149	3^+	0	0.05	0.03
166	3^-	3	0.03	0.44
193	2^+	0	0.11	0.08
		2	0.07	0.05
253	2^-	3	0.06	0.03
		2	0.12	0.05
334	$4^{(+)}$	2	0.10	0.10
343	$4^{(-)}$	5	0.04	0.39
387	$(3-5)$	5	0.44	0.61
399	$(2,3)^+$	2	0.08	0.07
438	(2)	0	0.03	0.02
		2	0.02	0.13

a Reference [9]
b $S(2j_{target}+1)$

TABLE IV. Comparison of measured and calculated in IBFFM spectroscopic factors for the one neutron transfer reaction ^{122}Sb. The first two columns contain the energy, spin and parity of the final states involved in the reaction taken from ref [13].

Energy (keV)	J^π	L_n	$S_{(p,d)}$ [a]	L_n	$S_{(d,p)}$ [b]	S_{IBFFM} [d]	L_n	$S_{(d,p)}$ [c]	S_{IBFFM}
0	2^-	3	0.25		0.68	0.65			
61	3^+	0	0.23	(0)	0.45	0.13	(2)	0.05	0.00
79	3^-	3	0.60			0.52			
121	1^+						(2)	0.35	0.47
137	5^+	2	0.38	(2)	0.37	0.20			
164	5^-	5	0.50			0.53			
167	2^+	2	0.10			0.14	(2)	0.09	0.09
183	4^-	5	0.61			0.58			
219	6^+	0	0.50	(0)	0.34	0.11			
255	3^+						0	0.34	0.44
266	5^-					0.66			
285	7^-	5	0.62			0.57			
272	6^-					0.66			
282	3^-						(0)	2.40	0.60
313	4^-						(5)	0.80	0.63
323	2^+						0	0.30	0.60
334	3^+	2	0.07		0.09	0.22	2	0.15	0.01
384	4^+						2	0.45	0.46
397	2^+	2	0.03		0.10		2	0.45	0.56
414	5^-								0.55
420	7^-	5	0.03			0.16	(5)	1.70	0.43
425	5^-								0.49
461	4^+	2	0.19	(2)	0.50	0.22			
484	5^+						2	0.51	0.80

a Reference [9]
b Reference [7]
c Reference [13]
d $S(2j_{target}+1)$

TABLE VI. Magnetic dipole (μ in μ_N) and electric quadrupole (Q in e b) moments of some $^{120-124}$Sb states.

Nucleus	E^*	J^π	μ_{expt} [a]	μ_{IBFFM}	Q_{expt} [a]	Q_{IBFFM}
^{120}Sb	0 keV	1^+	±2.34(22)	+2.25		−0.10
	78 keV	3^+	+2.584(6)	+2.67	±0.41(4)	−0.47
		8^-	±2.34(4)	+2.45		−0.51
^{122}Sb	0 keV	2^-	−1.905(30)	−2.33	+0.85(11)	−0.08
	61 keV	3^+	+2.983(12)	+3.07	±0.41(4)	−0.48
	137 keV	5^+	+3.05(10)	+3.07		−0.62
^{124}Sb	0 keV	3^-	±1.20(2)	−1.23	+1.87(38)	+0.35
	41 keV	3^+	+2.970(33)	+3.01		−0.46
	125 keV	8^-	+0.384(12)	+0.36		+0.16

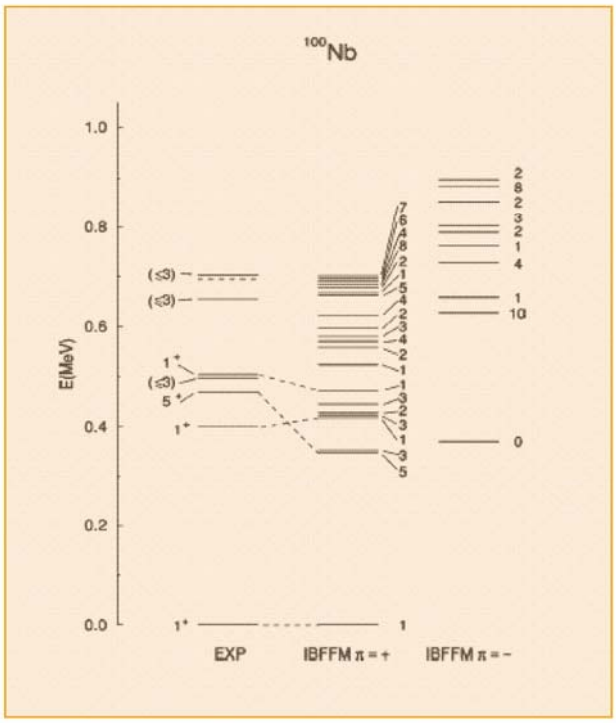

1^+ π g9/2 ν g7/2

5^+ π g9/2 ν s1/2

8^+ π g9/2 ν g7/2

10^- π g9/2 ν h11/2

5^+ 1.5 s isomer

10^- possibly 100 – 150 keV higher

10^- or 8^+ candidates for the 12 μs isomer

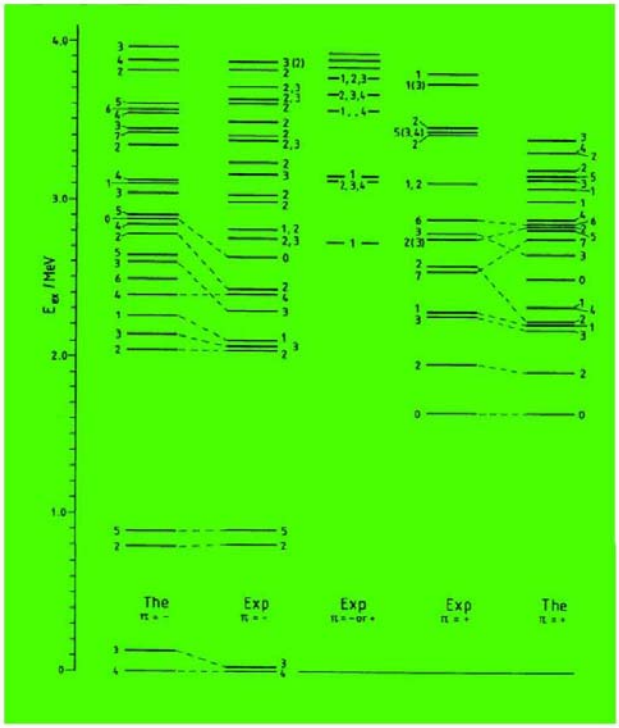

^{40}K

State (keV)	$T_{1/2}$	
	Exp	The
3_1^- (30)	4.24(8) ns	5.2 ns
2_1^- (800)	0.28(4) ps	0.23 ps
5_1^- (891)	0.87(14) ps	0.6 ps
2_2^- (2047)	0.34(4) ps	0.3 ps
3_2^- (2070)	0.47(10) ps	0.1 ps
1_1^- (2104)	0.52(10) ps	0.14 ps
4_2^- (2397)	0.035(14) ps	0.03 ps
0_1^- (2626)	0.21(4) ps	0.2 ps
1_1^+ (2290)	0.083(14) ps	0.25 ps
3_2^+ (2787)	<0.04 ps	0.07 ps
6_1^+ (2879)	0.27(10) ps	0.6 ps

^{40}K

Transition[a]	E_{tr}/keV	Gamma-branching	
		Exp[b]	The[c]
2_1^- (800) $\rightarrow 4_1^-$ (0)	800	0.15	0.17
$\rightarrow 3_1^-$ (30)	770	100	100
5_1^- (891) $\rightarrow 4_1^-$ (0)	891	99	99
$\rightarrow 3_1^-$ (30)	862	1	0.1
2_2^- (2047) $\rightarrow 4_1^-$ (0)	2047	29	128
$\rightarrow 3_1^-$ (30)	2018	29	100
$\rightarrow 2_1^-$ (800)	1247	41	41
3_2^- (2070) $\rightarrow 4_1^-$ (0)	2070	36	56
$\rightarrow 3_1^-$ (30)	2040	49	49
$\rightarrow 2_1^-$ (800)	1270	9	6
$\rightarrow 5_1^-$ (891)	1178	7	3
1_1^- (2104) $\rightarrow 3_1^-$ (30)	2074	70	70
$\rightarrow 2_1^-$ (800)	1304	29	96
$\rightarrow 2_2^-$ (2047)	57	–	0.1
$\rightarrow 3_2^-$ (2070)	34	–	0.0
4_2^- (2397) $\rightarrow 4_1^-$ (0)	2397	26	7
$\rightarrow 3_1^-$ (30)	2367	67	67
$\rightarrow 2_1^-$ (800)	1597	–	0.4
$\rightarrow 5_1^-$ (891)	1506	–	0.1
$\rightarrow 2_2^-$ (2047)	350	–	0.0
$\rightarrow 3_2^-$ (2070)	327	7	1
$\rightarrow 3_3^-$ (2291)	106	–	0.01
0_1^- (2626) $\rightarrow 2_1^-$ (800)	1826	30	41
$\rightarrow 2_2^-$ (2047)	579	–	0.001
$\rightarrow 1_1^-$ (2104)	522	70	70
$\rightarrow 2_3^-$ (2419)	207	–	0.0
1_1^+ (2290) $\rightarrow 0_1^+$ (1644)	646	56	56
$\rightarrow 2_1^+$ (1959)	331	9	10
$\rightarrow 3_1^+$ (2260)	30	–	0.0
3_2^+ (2787) $\rightarrow 2_1^+$ (1959)	828	17.4	17.4
$\rightarrow 3_1^+$ (2260)	527	–	0.5
$\rightarrow 1_1^+$ (2290)	497	–	0.0
$\rightarrow 2_2^+$ (2576)	211	–	0.0
$\rightarrow 2_3^+$ (2757)	30	–	0.0

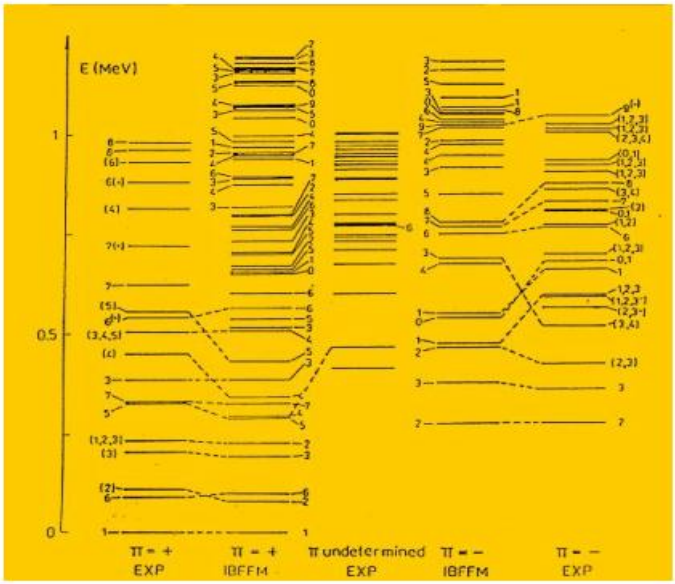

The structure of ^{106}Ag is very complex. The ground states of odd-mass Ag nuclei are $7/2^+$ states based on the proton g9/2 configuration. The IBFFM is even successful in the description of such nuclei.

Deformed nuclei

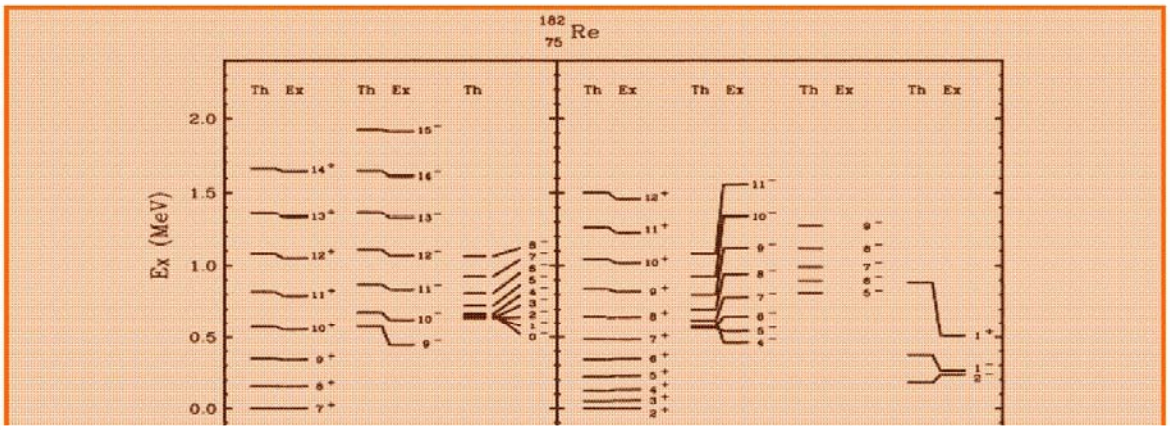

IBFFA-calculated excitation energies for states in odd-odd ^{182}Re compared with experimental data. Because the experimental separation between the 7^+ triplet and the 2^- singlet couplings is not known, the figure is divided into two parts, using each coupling as the reference point. Otherwise the triplet coupling is shown on the left of a pair of bands, the singlet coupling on the right. For example; 9^- triplet, 0^- singlet.

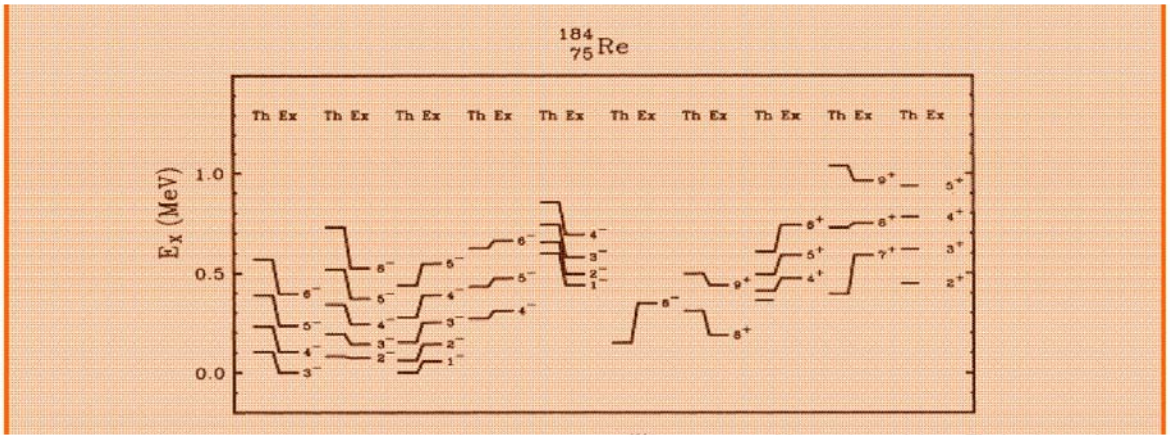

Scholten PRC 37

IBFFA-calculated excitation energies for states in odd-odd ^{184}Re compared with experimental data. The bands are plotted in pairs, with the triplet coupling on the left, the singlet coupling on the right of each pair.

Quadrupole moments for odd-odd Re isotopes.

Isotope	J^π	Q_{IBA} (e b)	Q_{exp} (e b)
^{180}Re	6^-	6.50	
	1^-	6.45	
^{182}Re	7^+	5.66	<6.4
	2^+	5.40	>6.6
^{184}Re	3^-	5.06	7.9 ± 0.7
	8^+	4.83	

Magnetic moments for odd-odd Re isotopes.

Isotope	J^π	μ_{IBA} (μ_N)	μ_{exp} (μ_N)
^{180}Re	6^-	2.41	
	1^-	2.35	
^{182}Re	7^+	2.33	2.76 ± 0.07
	2^+	3.28	3.07 ± 0.24
^{184}Re	3^-	3.19	2.50 ± 0.19
	8^+	2.09	2.89 ± 0.13

The investigations of odd-A nuclei have revealed the following decoupled–strongly coupled rule:

(i) The strongly coupled band pattern arises if the odd fermion is a particle coupled to an oblate core, or a hole coupled to a prolate core.

(ii) The decoupled band pattern arises if the odd particle is coupled to a prolate core or a hole to the oblate core.

This rule was extended to odd-odd nuclei in the case of coupling two quasiparticles to the asymmetric rotor.

Rules (i) and (ii) can be expressed in terms of quadrupole moments of the odd particle and the core Taking into account the signs of quadrupole moments $Q(j)<0$, $Q(j^{-1})>0$, $Q(2_1^{\mathrm{prolate}})<0$, and $Q(2_1^{\mathrm{oblate}})>0$, the rule reads

$$\text{if } Q(\bar{j})\cdot Q(2_1^{\mathrm{core}}) \begin{cases} <0, & \text{the band is strongly coupled} \\ >0, & \text{the band is decoupled} , \end{cases}$$

where $\bar{j}$ denotes the odd quasiparticle coupled to the core.

This rule is of more general character, independent of the particular nature of the core. It applies as well to the IBFM and IBFFM.

We note that the case of two particles or holes coupled to the core, referred to as the "peaceful" case in the particle–plus–asymmetric rotor model, corresponds to the inverted parabola of the parabolic rule for odd-odd nuclei;[2] this yields the bandheads with angular momenta $J=j_p+j_n$ and $J=|j_p-j_n|$ as the lowest states on two branches of the parabola.

By coupling the proton particle j_1 and the neutron particle j_2 to the SU(3) boson core, there arise $2(j_1+\frac{1}{2})(j_2+\frac{1}{2})$ bands, based on the states of angular momenta $J=J_1\pm J_2$, with $J_1=j_1, j_1-1, \ldots, \frac{1}{2}$ and $J_2=j_2, j_2-1, \ldots, \frac{1}{2}$. For the particular interaction strengths Γ_1^{SUSY} and Γ_2^{SUSY} the band based on the lowest $J=j_1+j_2$ state exhibits an exact $J(J+1)$ energy rule, with the same moment of inertia as for the ground-state band of the boson core. Furthermore, the states of this band are characterized by the exact quantum numbers $(K_1=j_1, K_2=j_2)K=j_1+j_2$, defined according to the IBFFM relation The other IBFFM bands in the odd-odd system deviate from the $J(J+1)$ energy rule; in general, more so with increasing energy (decrease of K_1, K_2). Simultaneously, the IBFFM wave functions expressed in the KR basis are a mixture of different K values. However, in each state a particular KR basis state dominates. In this way we can attribute approximate quantum numbers $(K_1, K_2)K$ to each state.

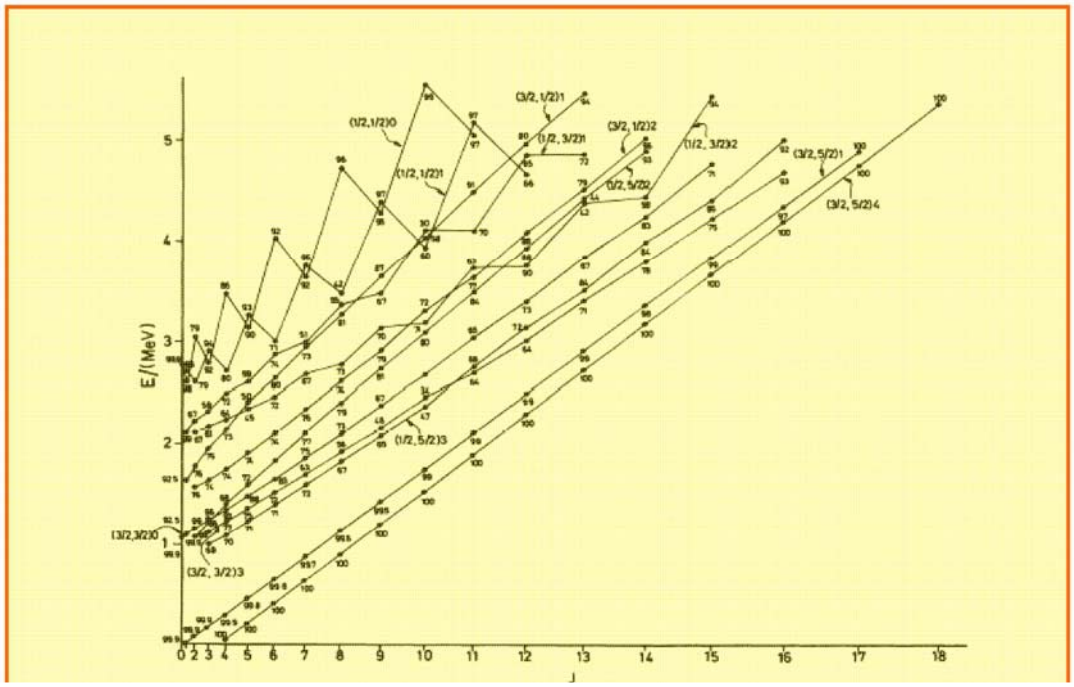

Twelve ground state bands calculated in the IBFFM for the odd-odd system with $j_1 = \frac{1}{2}$ proton hole and $j_2 = \frac{5}{2}$ neutron hole coupled to the SU(3) prolate boson core. The $J(J+1)$ scale is employed for the angular momentum axis.

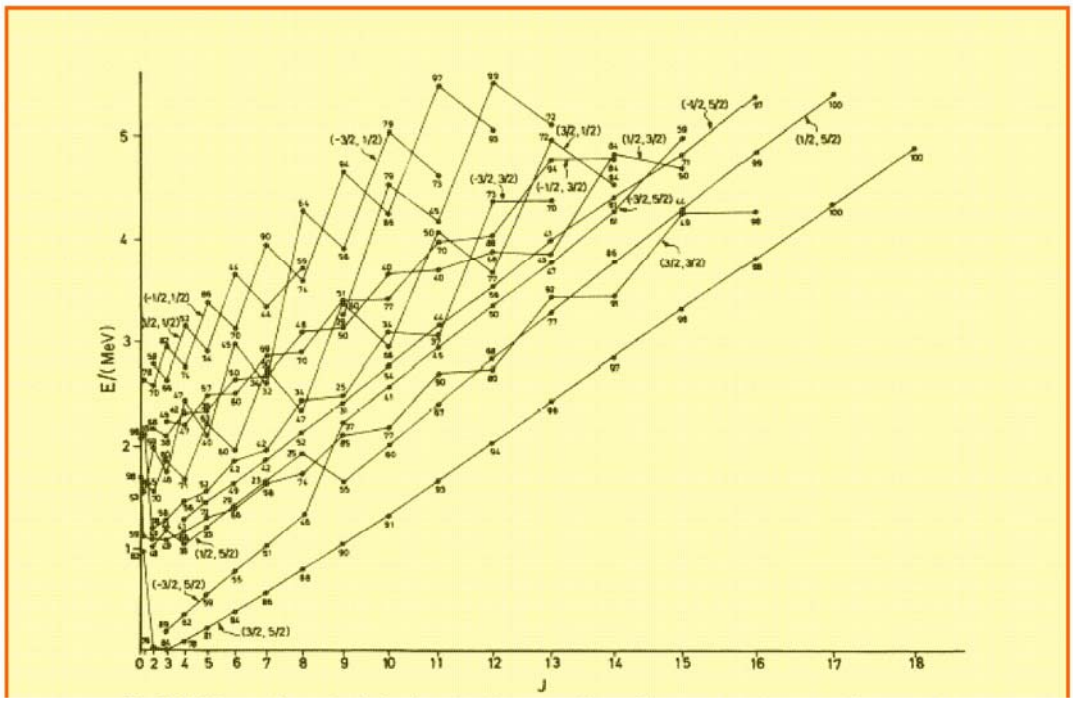

The IBFFM ground state bands for the odd-odd system with $j_1 = \frac{1}{2}$ proton particle and $j_2 = \frac{5}{2}$ neutron hole coupled to the SU(3) prolate boson core.

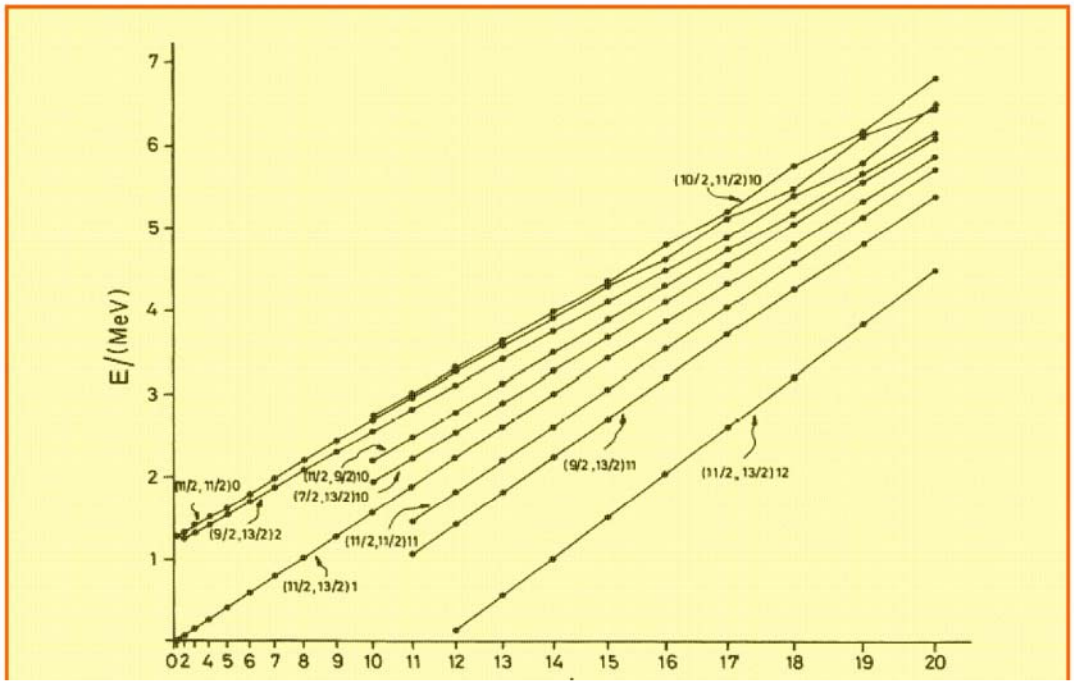

Lowest bands in the odd-odd system with $j_1 = \frac{11}{2}$ proton hole and $j_2 = \frac{11}{2}$ neutron hole coupled to the SU(3) prolate boson core.

Realistic case: Dynamical and exchange interactions different from zero and not limited by supersymmetry constraints

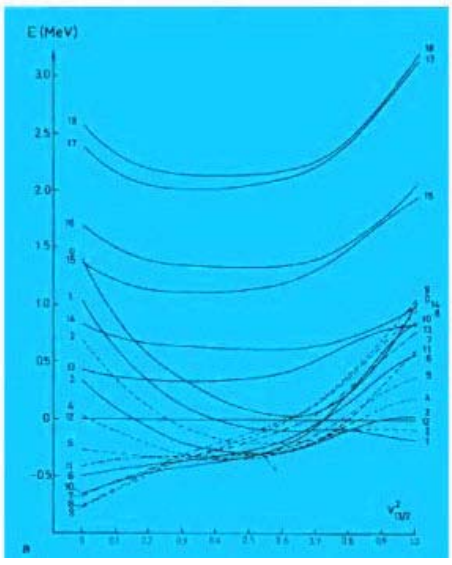

Calculated IBFFM yrast states (0_1, 1_1, …, 20_1) for $\bar{j}_\pi = h^{-1}_{11/2}$, $\bar{j}\ \nu = \bar{i}_{13/2}$ coupled to an O(6) core, as a function of $\nu^2_{i\ 3/2}$.

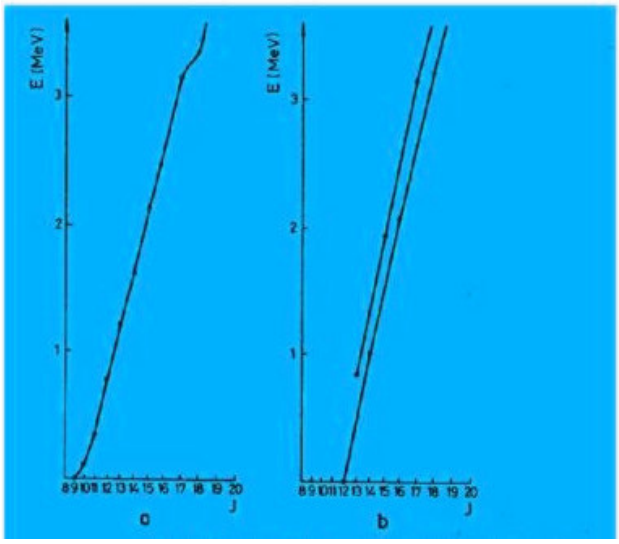

E/J plots for the lowest-lying high-spin bands for $\nu^2_{i\ 3/2} = 0$ a, and $\nu^2_{i\ 3/2} = 1$ b.

E/J plots for the levels 1, 2, …., 12, for $\nu^2_{1\ 3/2}$=0 a, $\nu^2_{1\ 3/2}$=0.5 b and $\nu^2_{1\ 3/2}$=1 c. The scale on the abscissa is given by $J(J+1)$. The points for levels are connected by curves to guide the eye.

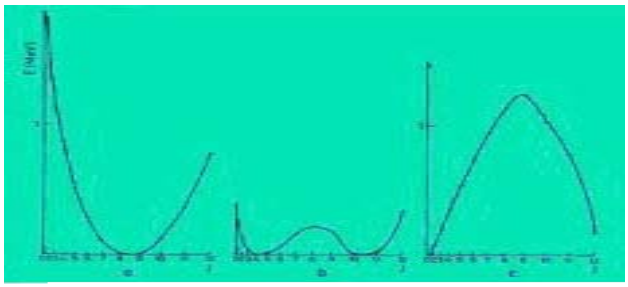

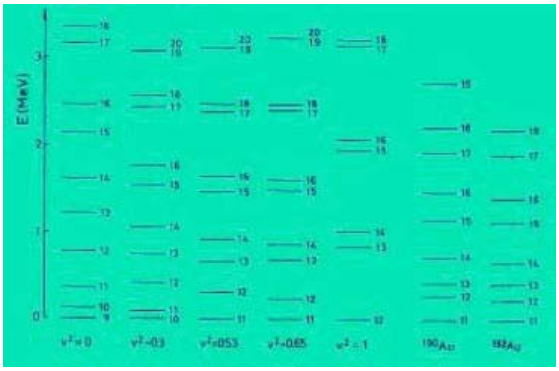

The head of the lowest high-spin band is

$J = j_\pi + j_\nu - 3 = 9$ for $\nu^2_{1\ 3/2}$. 0.2,

$J = j_\pi + j_\nu - 2 = 10$ for . $0.2\nu^2_{1\ 3/2}$. 0.2,

$J = j_\pi + j_\nu - 1 = 11$ for . $0.5\nu^2_{1\ 3/2}$. 0.8

and

$J = j_\pi + j_\nu = 12$ for . $0.8\nu^2_{1\ 3/2}$.

A pronounced feature is rather broad region with $J = J_\pi + J_\nu - 1 = 11$ level as the lowest high-spin state. This resembles the J = j – 1 anomaly for rather broad region around $\nu^2 = 0.5$ in odd-even nuclei.

Characteristic lowest high-spin band patterns associated with O(6) limit for several values of $\nu^2_{1\ 3/2}$ in the illustrative IBFFM calculation. Examples with all possible high-spin band heads are presented. For comparison the experimental bands $^{190,\ 192}$Au are presented to the right. We note that the Au-region is approximately associated with an O(6) symmetry, but the present calculation is not fitted to Au isotopes

Calculated IBFFM yrast states (0_1, 1_1, …., 20_1) for $\bar{j}_\pi = h^{-1}_{11/2}, \bar{j}_\gamma = \bar{i}_{13/2}$ coupled to an SU(3) core, as a function of $\nu^2_{1\ 3/2}$

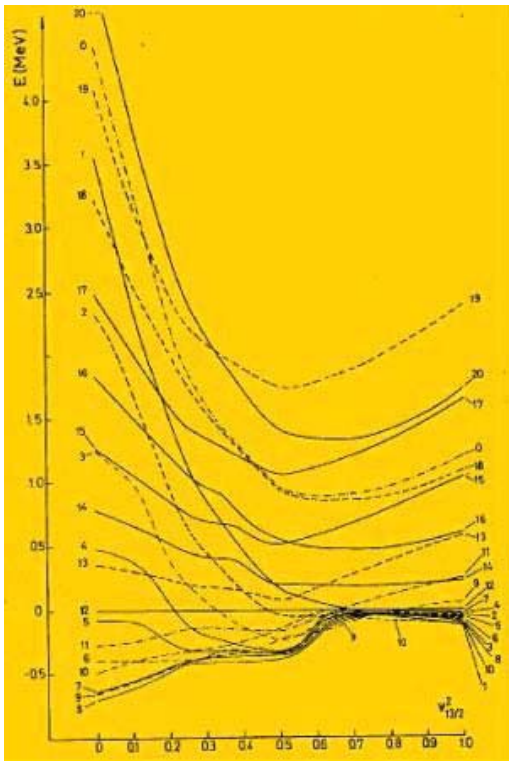

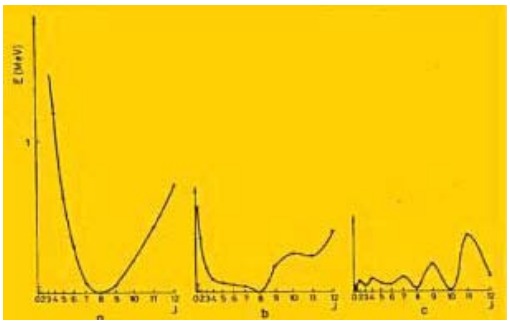

E/J plots for the levels 1_1, 2_1, …., 12_1, $\nu^2_{1\ 3/2}$=0 a, $\nu^2_{1\ 3/2}$ = 0.5 b and $\nu^2_{1\ 3/2}$ = 1 c.

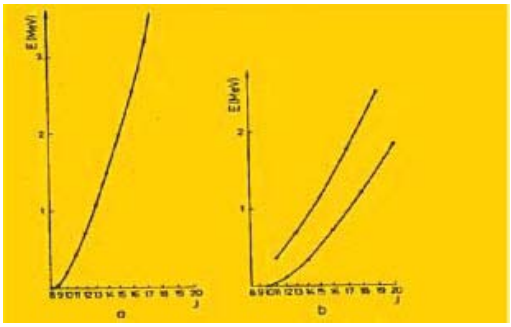

E/J plots for the lowest-lying high-spin bands for $\nu^2_{1\ 3/2}$ = 0 a, and $\nu^2_{1\ 3/2}$ = 0.5 b

Transitional nuclei

^{68}As

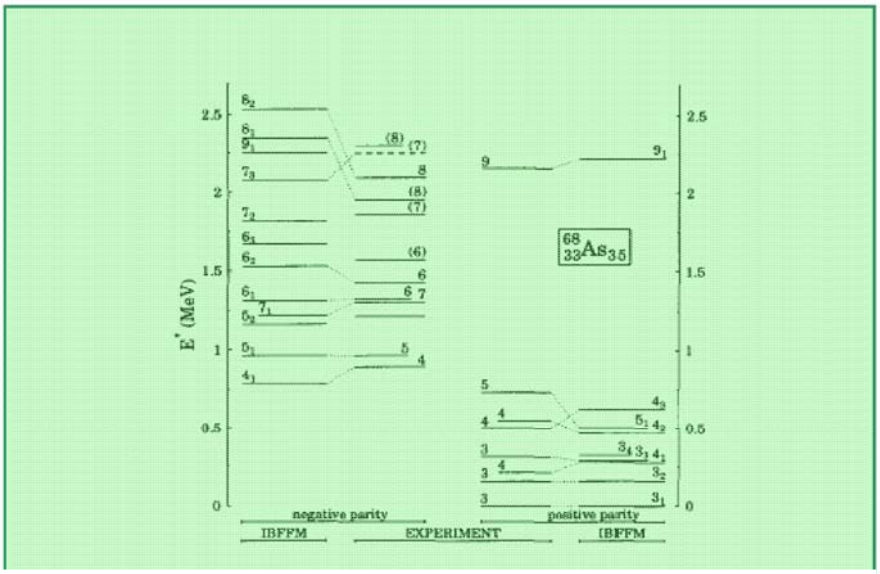

Experimental and theoretical IBFFM energy spectra of the low lying states in ^{68}As. Up to 0.6 MeV, the positive parity levels 3^+, 4^+, 5^+ are shown. In addition the high spin isomer 9^*_1 is shown. For negative parity the calculated states with $J^\pi = 4^-_1$, 5^-_1, 5^-_2, 6^-_1, 6^-_2, 6^-_3, 7^-_1, 7^-_2, 7^-_3, 8^-_1, 8^-_2, 9^-_1 are shown.

Calculated in IBFFM branching ratio for ^{68}As compared with the experimental data

E^{*}_{exp} (MeV)	J^{π}_{exp} ($\hbar$)	$J^{\pi}_{i} \rightarrow J^{\pi}_{f}$ (theor.)	I_{γ} Exp.	I_{γ} Theor.
0.158	3^+	$3^+_2 \rightarrow 3^+_1$	100(6)	100
0.214	4^+	$4^+_1 \rightarrow 3^+_2$	6(2)	5
		$\rightarrow 3^+_1$	100(14)	100
0.313	3^+	$3^+_3 \rightarrow 4^+_1$	<2	4
		$\rightarrow 3^+_2$	16(2)	86
		$\rightarrow 3^+_1$	100(2)	100
0.500	4^+	$4^+_3 \rightarrow 3^+_3$	5(1)	12
		$\rightarrow 4^+_1$	5(1)	5
		$\rightarrow 3^+_1$	100(2)	100
0.550	4^+	$4^+_2 \rightarrow 3^+_3$	9(1)	100
		$\rightarrow 4^+_1$	36(2)	16
		$\rightarrow 3^+_2$	100(4)	9
		$\rightarrow 3^+_1$	48(2)	10
0.733	5^+	$5^+_1 \rightarrow 4^+_2$	17(2)	3
		$\rightarrow 4^+_3$	<6	26
		$\rightarrow 4^+_1$	100(5)	100
3.183	$11^{(+)}$	$11^+_1 \rightarrow 9^+_1$	100(3)	100
0.965	$5^{(-)}$	$5^-_1 \rightarrow 4^-_1$	100(3)	100
1.304	$7^{(-)}$	$7^-_1 \rightarrow 5^-_1$	100(3)	100
1.323	$6^{(-)}$	$6^-_1 \rightarrow 5^-_1$	100(4)	100
		$\rightarrow 4^-_1$	<3	4
1.427	$6^{(-)}$	$6^-_2 \rightarrow 5^-_2$	8(2)	2
		$\rightarrow 5^-_1$	100(5)	100
1.956	(8^-)	$8^-_1 \rightarrow 6^-_1$	100(8)	100
		$\rightarrow 7^-_1$	23(6)	16
2.094	$8^{(-)}$	$8^-_2 \rightarrow 7^-_1$	100(3)	100
2.251	(7^-)	$7^-_3 \rightarrow 6^-_2$	<55	75
		$\rightarrow 6^-_1$	100(15)	100
		$\rightarrow 5^-_2$	<40	45

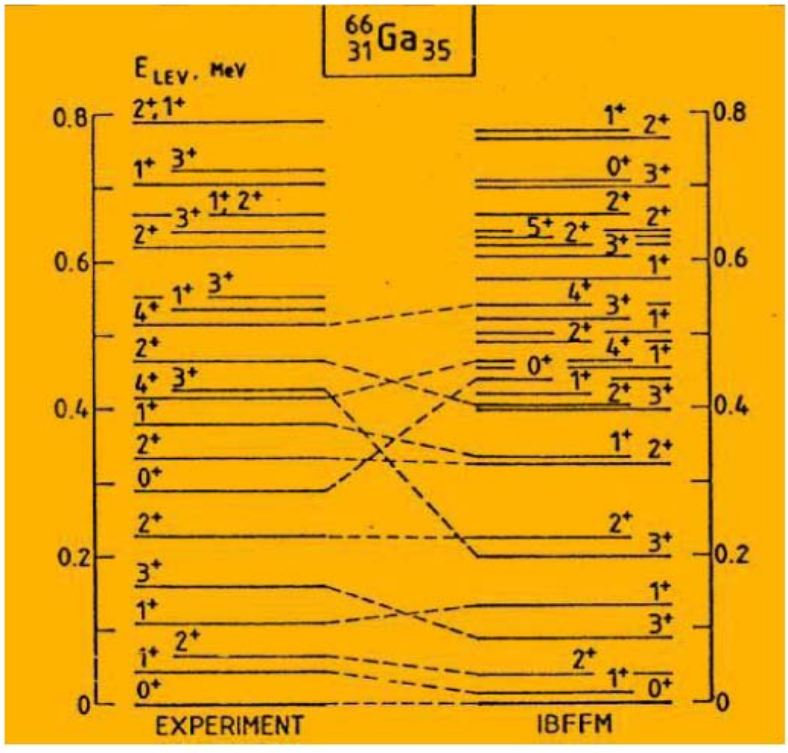

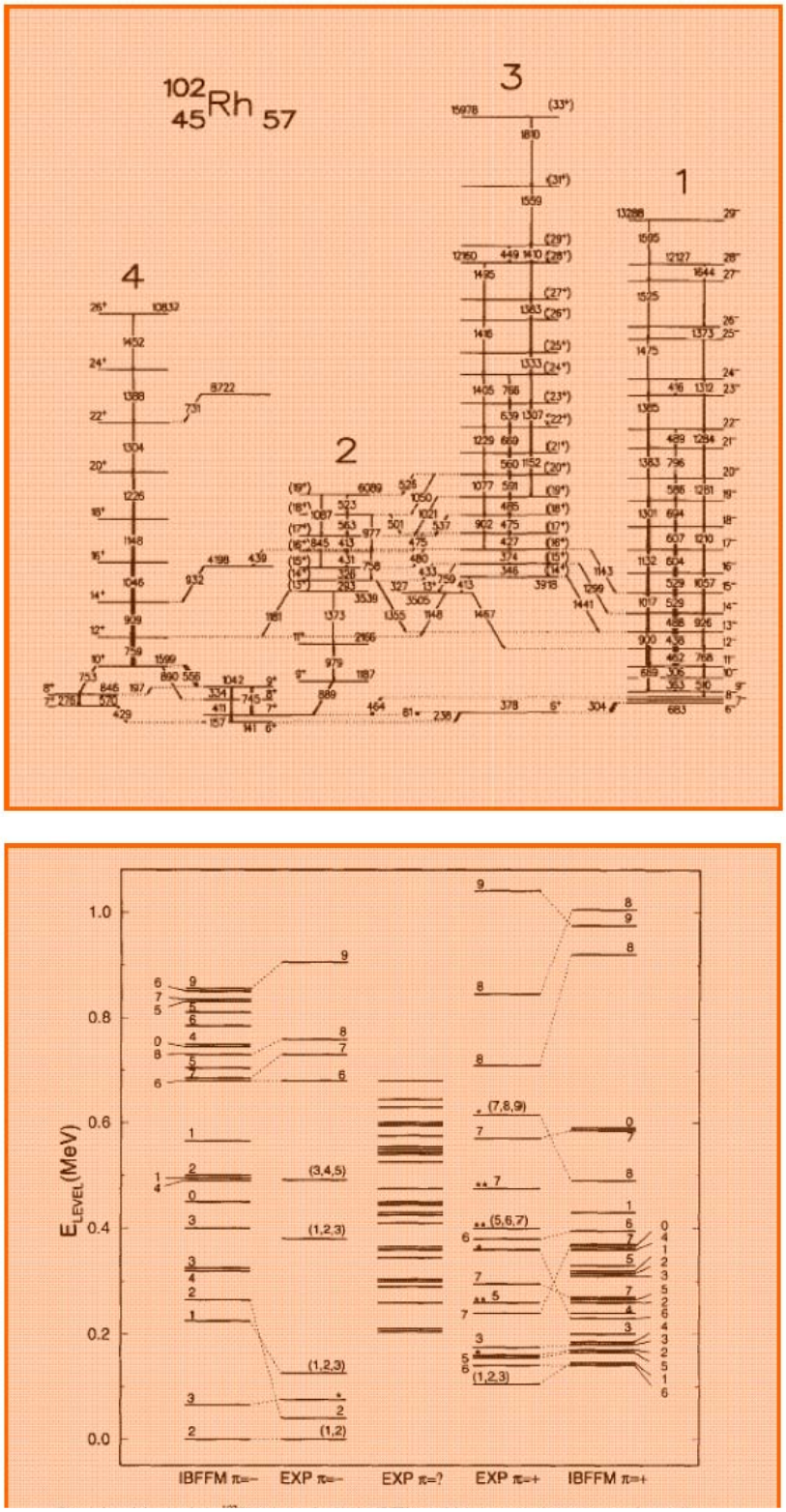

Fig. 4. Low-lying yields in ^{102}Rh calculated with the IBFFM model and compared to experimental ones. For the clarity of the figures, only the three lowest calculated levels for a given spin are shown. The left- hand and right-hand sides of the figure are for the negative- and positive-parity states, respectively. Levels with unidentified parity are shown in the central column. Experimental states of uncertain parity are denoted by *, states interpreted as intruders are denoted by **.

^{102}Rh

Transition $I_i^\pi \to I_f^\pi$	$E_i \to E_f$	$B(E2)(e^2b^2)$ Exp.	$B(E2)(e^2b^2)$ IBFFM	$B(M1)(\mu_N^2)$ Exp.	$B(M1)(\mu_N^2)$ IBFFM	I_γ Exp.	I_γ IBFFM
$2_2^- \to 2_1^-$	42 → 0		0.0089	0.0054(18)	0.0033	100	100
$3_1^- \to 2_2^-$	76 → 42		0.0206		0.0731		68
$\to 2_1^-$	→ 0		0.0065		0.0097		100
$1_1^- \to 3_1^-$	124 → 76		0.0092				0.0
$\to 2_2^-$	→ 42		0.0068	0.0072(54)	0.0169	12.9	3.4
$\to 2_1^-$	→ 0		0.0307	0.034(18)	0.1436	100	100
$5_1^+ \to 6_1^+$	155 → 141		0.0003		0.0515	100	100
$2_2^+ \to 1_1^+$	157 → 105		0.0246		1.1948	100	100
$3_1^+ \to 2_1^+$	179 → 157		0.0109		1.2919	82[a]	43[a]
$\to 1_1^+$	→ 105		0.0232				0.1[a]
$7_2^+ \to 5_1^+$	242 → 155		0.0033				0.0
$\to 6_1^+$	→ 141		0.0342		0.1286	100	100
$7_1^+ \to 7_2^+$	297 → 242		0.0057		0.0019		8
$\to 5_1^+$	→ 155		0.0178				20
$\to 6_1^+$	→ 141	≥0.039[b]	0.0164	≥ 0.093[b]	0.0007	100	100
$6_2^+ \to 7_1^+$	360 → 297		0.0322		0.2138		100
$\to 7_2^+$	→ 242		0.0181		0.0287		90
$6_1^+ \to 6_2^+$	378 → 360		0.0099		0.0002		0.0
$\to 7_1^+$	→ 297		0.0009	0.045[b]	0.5392	92	69
$\to 7_2^+$	→ 242		0.0023	0.016[b]	0.0046	58	3
$\to 5_1^+$	→ 155	0.0063[b]	0.0006		0.0375	83	100
$\to 6_1^+$	→ 141	0.0044[b]	0.0038	0.0018[b]	0.0309	100	100
$7_3^+ \to 6_2^+$	570 → 378		0.0343		0.1572		19
$\to 6_2^+$	→ 360		0.0000		0.0088		1.4
$\to 7_1^+$	→ 297		0.0018		0.0000	5	0.1
$\to 7_2^+$	→ 242		0.0000		0.0035		2.1
$\to 5_1^+$	→ 155		0.0076		0.0000		1.1
$\to 6_1^+$	→ 141		0.0016		0.0728	100	100
$8_1^+ \to 7_3^+$	616 → 570		0.0080		0.2705		0.3
$\to 6_2^+$	→ 378		0.0009				0.0
$\to 6_2^+$	→ 360		0.0228				0.2
$\to 7_1^+$	→ 297		0.0374		0.2572	100	100
$\to 7_2^+$	→ 242		0.0022		0.0006		0.5
$\to 6_1^+$	→ 141		0.0020				0.4

^{102}Rh

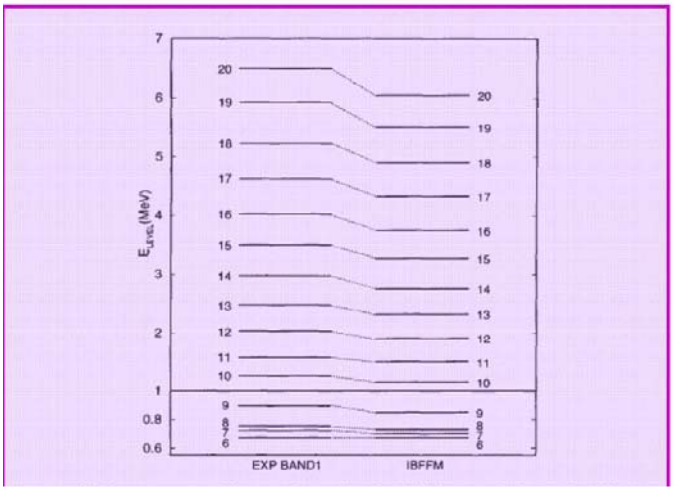

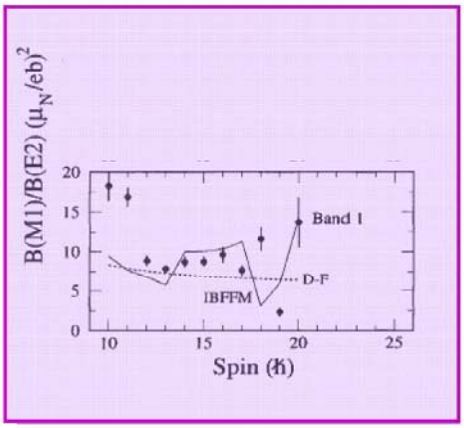

IBFFM energy spectrum of the $\pi g_{9/2} \nu h_{11/2}$ configuration in ^{102}Rh compared to experimental band 1. Because of the concentration of the lowest states, the bottom of the band is shown with a different scale.

π g9/2 ν h11/2 Full line IBFFM

Dashed line Donau-Frauendorf model

The ΔI=2 positive-parity band 4

In the present IBFFM calculation we obtain two positive-parity high-spin bands, based on $\pi p_{1/2}\nu h_{11/2}$ and $\pi g_{9/2}\nu g_{7/2}$ two-quasiparticle configurations, respectively These bands are clearly formed above the 10^+ state, while for lower spins there is a stronger configuration mixing. The two lowest 10^+ states are based on the $(\pi p_{1/2}\nu h_{11/2})$6, 2 4; 10 (50%) and $(\pi g_{9/2}\nu g_{7/2})$8, 1 2; 10 (59%) configurations

These two calculated bands appear close lying and they cross at angular momentum $I \approx 15\hbar$. Contrary to the experimental band 4 which is of $\Delta I = 2$ type with signature $\alpha = 0$, the calculated bands show doublet-type structures. The $\pi p_{1/2}\nu h_{11/2}$ configuration is associated with a much larger signature splitting than the $\pi g_{9/2}\nu g_{7/2}$ configuration and exhibit a pronounced tendency towards decoupled band On this basis we attribute the $\pi p_{1/2}\nu h_{11/2}$ configuration to band 4.

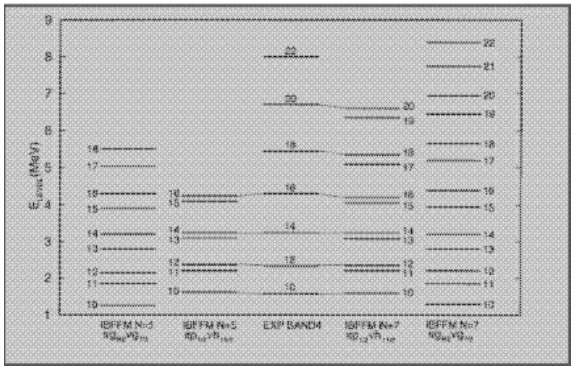

B(E2) and B(M1) reduced transition probabilities calculated between states of the $\pi p_{1/2}\nu h_{11/2}$ configuration with $N = 7$ in ^{102}Rh and comparison of the intensities of γ-rays observed in band 4 with those calculated for the above configuration

Transition	B(E2)(e^2b^2)	B(M1)(μ_N^2)	I_γ	
	IBFFM	IBFFM	Exp.	IBFFM
$12^+ \rightarrow 11^+$	0.0016	0.0073		0.0
$12^+ \rightarrow 10^+$	0.4295		100	100
$14^+ \rightarrow 13^+$	0.0021	0.0001		0.0
$14^+ \rightarrow 12^+$	0.1003		100	100
$16^+ \rightarrow 15^+$	0.0005	0.0049		0.1
$16^+ \rightarrow 14^+$	0.0418		100	100
$18^+ \rightarrow 17^+$	0.0010	0.0019		0.0
$18^+ \rightarrow 16^+$	0.1076		100	100
$20^+ \rightarrow 19^+$	0.0011	0.0061		0.1
$20^+ \rightarrow 18^+$	0.0634		100	100

The two remaining experimental bands, bands 2 and 3, are expected to be based on four-quasiparticle states involving broken neutron pairs, in particular the $\nu h_{1}^{2}{}_{1/2}$ broken pair, so that four-quasiparticle states should be coupled to the boson core. The model including boson pairs of fermions has not been applied yet to odd-odd nuclei and therefore the corresponding theoretical states are missing in the present IBFFM calculations.

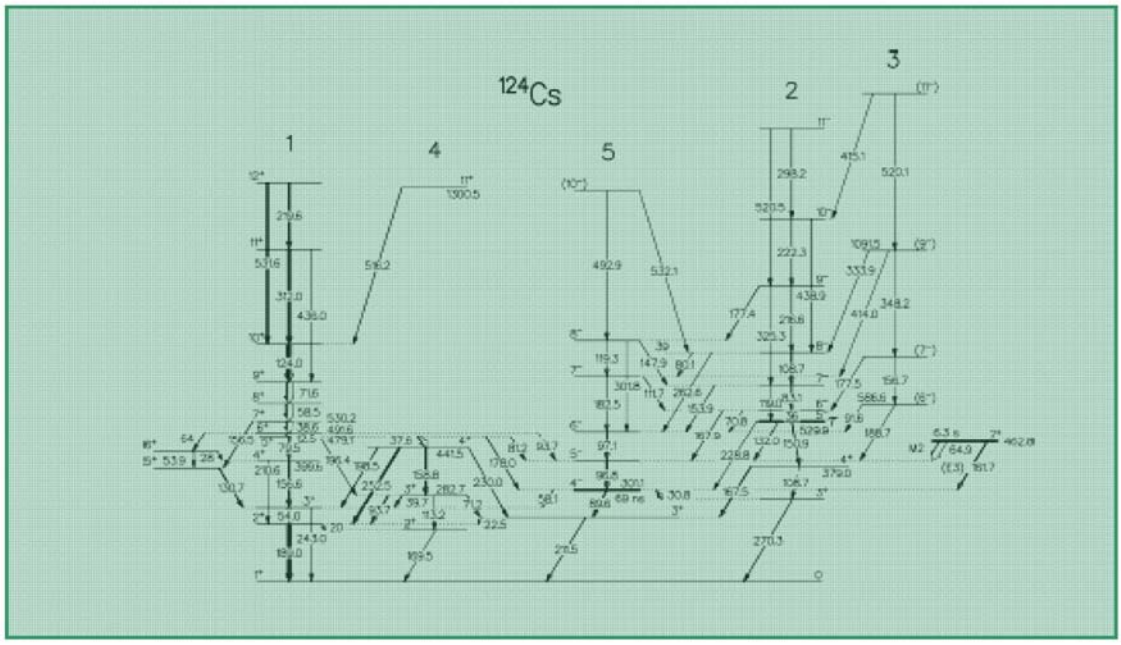
124Cs
1
2
3
4
5

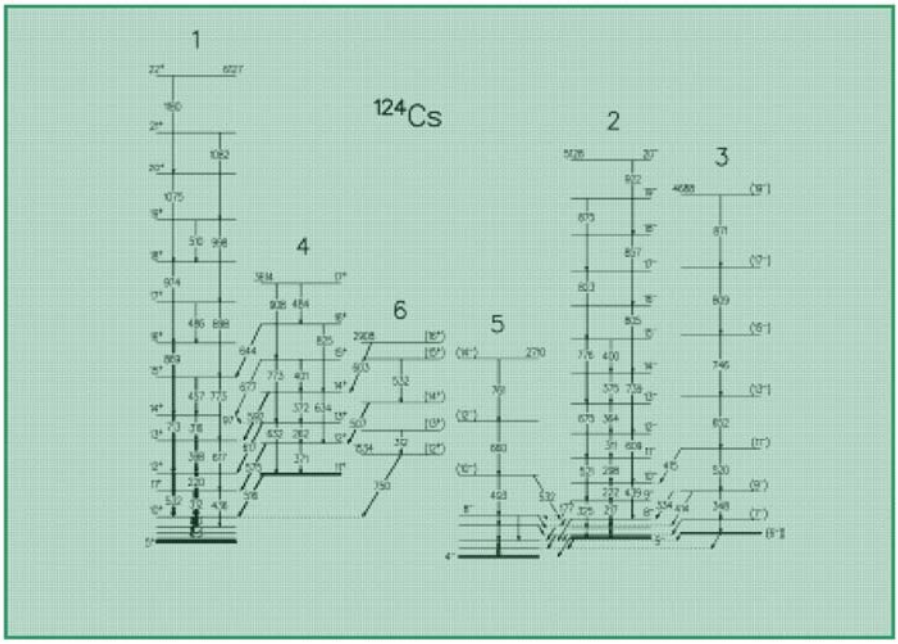
124Cs
1
2
3
4
5
6

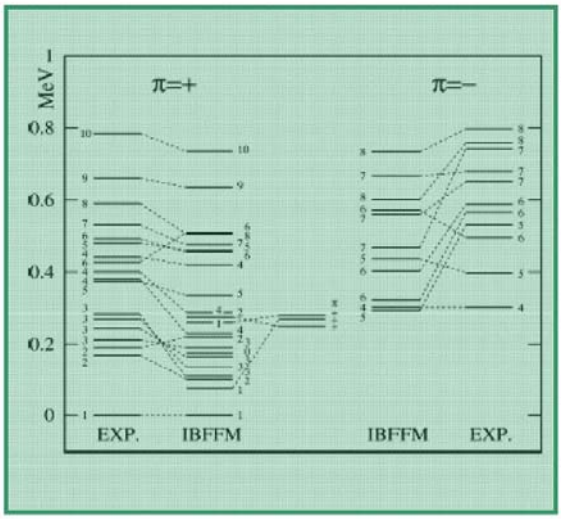

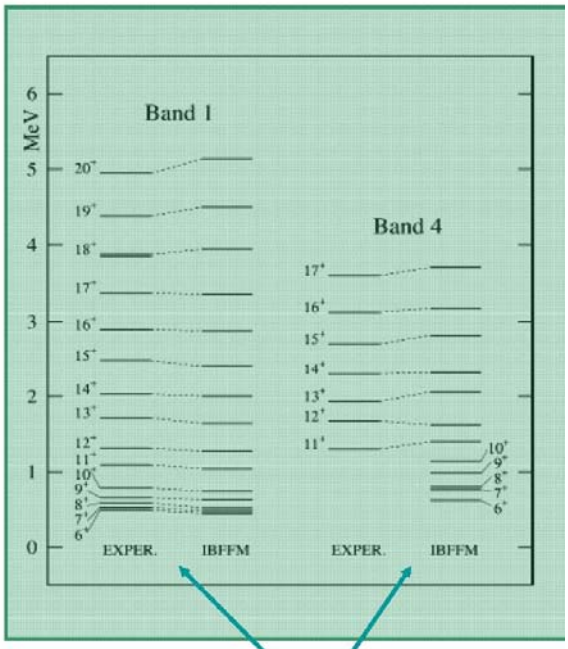

^{124}Cs

π h11/2 ν h11/2

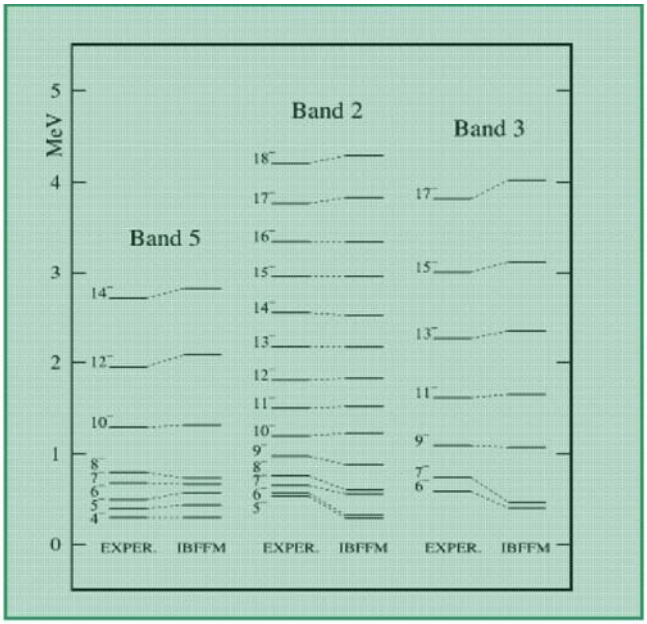

^{124}Cs

Wave functions are very complex !!!!

There is a strong configuration mixing

IBFFM is able to properly predict the structure of high spin states in a multy-j case

On the basis of the IBFFM analysis, we propose that the negative-parity bands presented have a $\pi(d_{5/2g7/2})\nu h_{11/2}$ configuration in their low-spin part and, starting from $I \approx 12$, are almost pure $\pi h_{11/2\nu g7/2}$, with band 2 being the yrast structure and bands 3 and 5 the yrare structures. Thus the collective band structures start at spin $I \approx 12$.

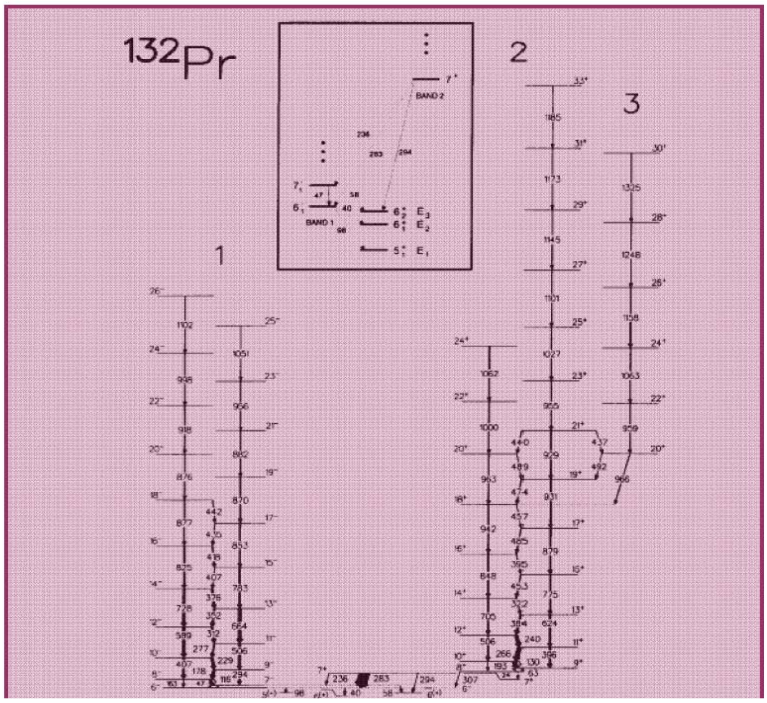

Level scheme of ^{132}Pr deduced from the present work. The transition intensities are proportional to the width of the arrows. The inset shows the IBFFM identification of levels populated in the decays of bands 1 and 2.

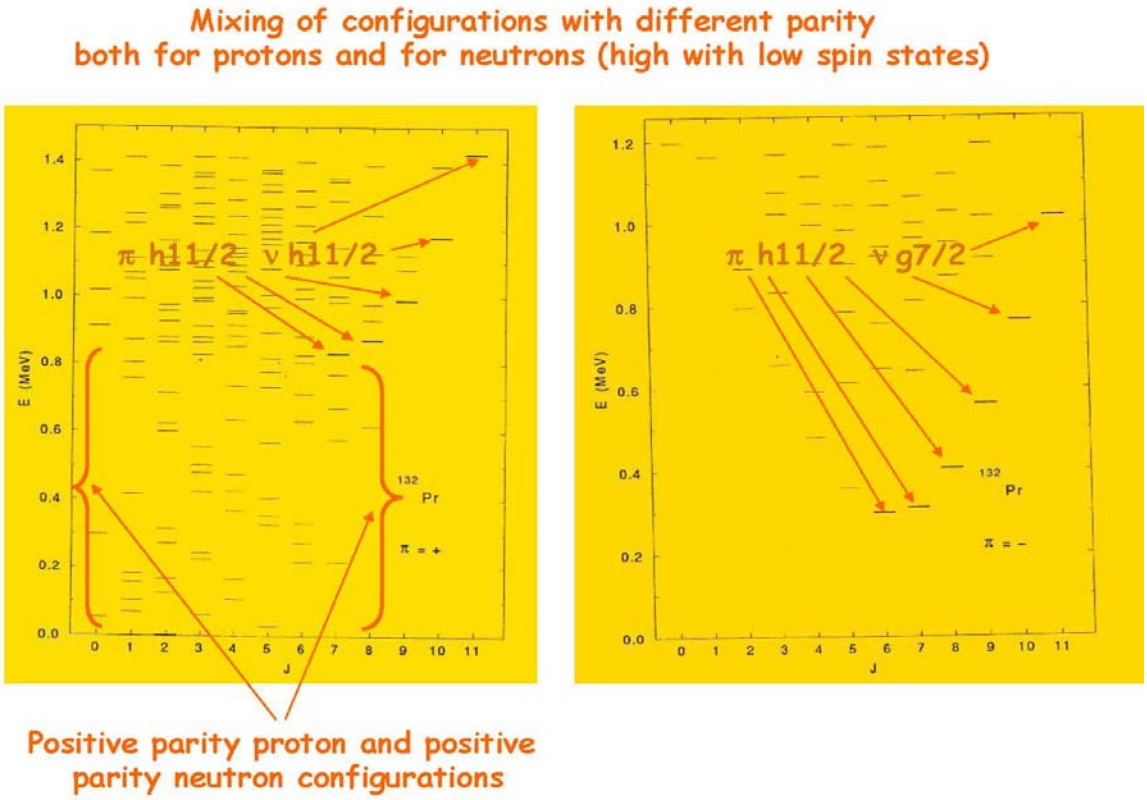

The formation of regular $\Delta I = 1$ high-spin band pattern in odd-even and odd-odd nuclei with O(6) boson core presents a challenging problem for the IBFM and IBFFM models, respectively. Namely, both models predict normal or decoupled band patterns with close-lying unfavored and favored bands, resulting in characteristic "doublet structures" and $\Delta I = 2$ transitions. This is because the standard IBFM interactions can not induce a sufficiently strong effective interaction which would establish a regular $\Delta I = 1$ band pattern, without sizeably altering the low-energy part of the spectrum.

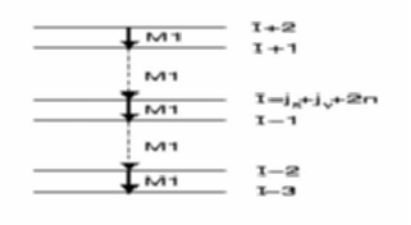

Schematic presentation of the conflicting pattern in odd-odd nuclei associated with unique-parity proton and neutron quasiparticles of opposite occupancy coupled to the O(6) boson core (n is an integer).

In order to account for this problem, we introduce a new term in the quadrupole operator of the dynamical boson-fermion interaction.

$$H_{dyn} = \Gamma_0\sqrt{5}\sum_{j_1 j_2}(u_{j_1}u_{j_2} - v_{j_1}v_{j_2})\times < j_1 \parallel Y_2 \parallel j_2 > \{Q_2^B(c_{j_1}^\dagger \tilde{c}_{j_2})_2\}_0$$

$$Q_{2\mu}^B = d_{2\mu}^\dagger s + s^\dagger \tilde{d}_{2\mu} + \chi(d^\dagger \tilde{d})_{2\mu} + \eta\sum_{L_1 L_2}[(d^\dagger \tilde{d})_{L_1}(d^\dagger \tilde{d})_{L_2}]_{2\mu}$$

The effect of the last term is to induce an effective deformation of a soft O(6) core due to polarization caused by odd fermions. In this way a regular $\Delta I = 1$ yrast band is established in odd-odd nuclei with O(6) boson core. Without the η - term a familiar "doublet structure" is obtained in IBFFM, while taking $\eta \neq 0$ leads to a regular $\Delta I = 1$ pattern, both in energies and M1 transitions on the yrast.

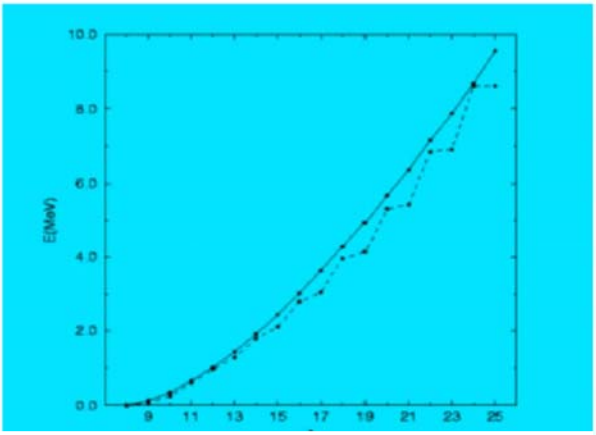

IBFFM calculation for yrast states in odd-odd system with inclusion of $h_{11/2}$ proton ($\nu^2 = 0.1$) and $h_{11/2}$ neutron ($\nu^2 = 0.8$) quasiparticles coupled to the O(6) boson core. The non vanishing parameters are: core parameters from R. F. Casten and P. von Bretano, *Phys. Lett.* **B152** (1985) 22, N=7, $\Gamma_0^{\pi} = \Gamma_0^{\nu} = 0.4$ MeV. These values are used in other illustrative figures as well as: $g_{\pi} = 1$, $g_{\nu} = 0$, $g_{\pi} = 0.7\, g_{\pi}$, $g_{\nu} = 0.7\, g_{\nu}$, $g_R = 0.43$. The energies of 8_1^+ states are taken as zero. In this figure χ = 0 (full and dashed lines corresponds to η = -0.4 and 0, respectively).

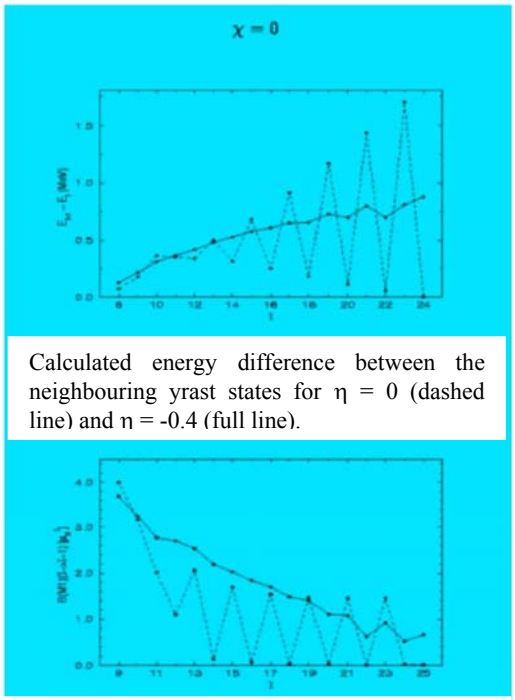

Calculated energy difference between the neighbouring yrast states for η = 0 (dashed line) and η = -0.4 (full line).

Calculated B(M1) values from transitions between the yrast states for η = 0 (dashed line) and η = -0.4 (full line).

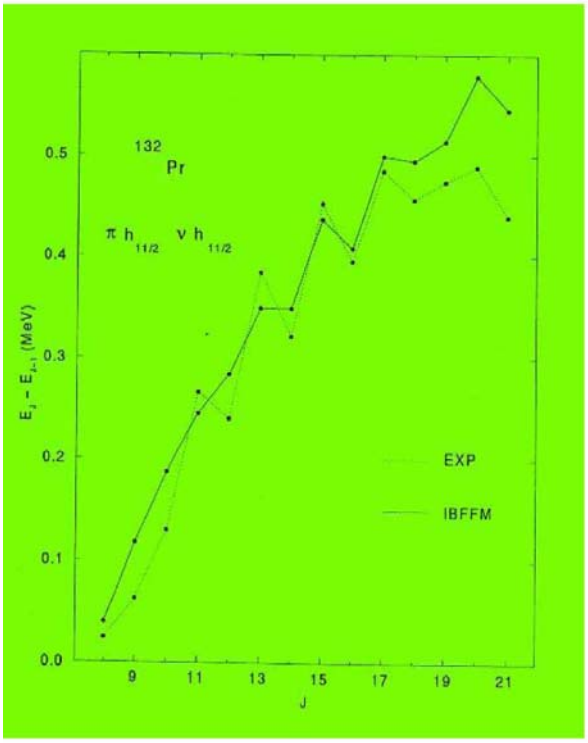

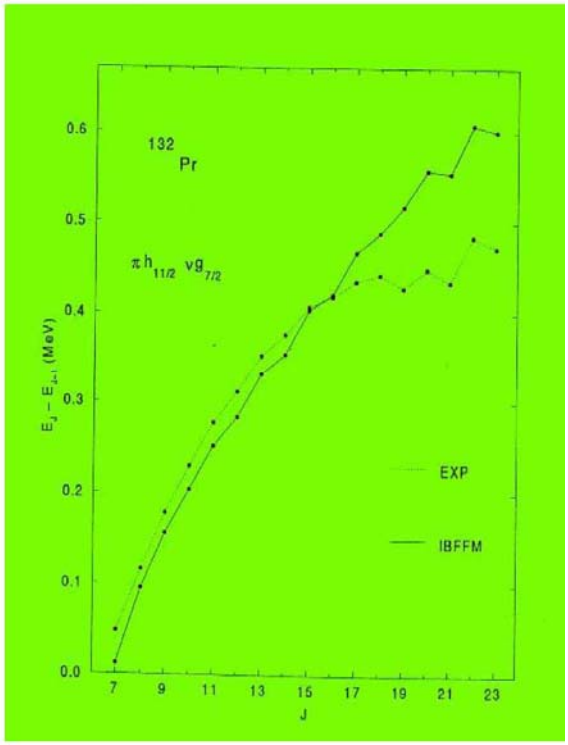

Signature inversion has been investigated in various models. Taking a very strong (!!??) boson-fermion exchange interaction, a change of signature pattern from inverted to the normal with increasing spin can be achieved within the unique-parity two-quasiparticle band. However, the strength of the exchange interaction is not a free parameter. A sizable increase of the strength of exchange interaction would destroy the agreement of the calculation with the low-spin data.

$J_i^\pi \to J_f^\pi$	$B(E2)$ (e^2b^2)	$B(M1)$ (μ_N^2)	I_γ		$B(M1)/B(E2)$	
	IBFFM	IBFFM	EXP.	IBFFM	EXP.	IBFFM
$7_1^- \to 6_1^-$	0.698	0.949	100	100	-	-
$8_1^- \to 7_1^-$	0.668	0.727	100	100	0.97(2)	1.62
$\to 6_1^-$	0.448	-	5	3		
$9_1^- \to 8_1^-$	0.585	0.538	100	100	0.75(10)	0.95
$\to 7_1^-$	0.567	-	36	28		
$10_1^- \to 9_1^-$	0.490	0.459	95	110	0.61(5)	0.71
$\to 8_1^-$	0.648	-	100	100		
$11_1^- \to 10_1^-$	0.406	0.375	61	48	0.66(5)	0.52
$\to 9_1^-$	0.716	-	100	100		
$12_1^- \to 11_1^-$	0.330	0.337	29	27	0.47(6)	0.45
$\to 10_1^-$	0.751	-	100	100		
$13_1^- \to 12_1^-$	0.273	0.294	30	18	0.62(5)	0.38
$\to 11_1^-$	0.763	-	100	100		
$14_1^- \to 13_1^-$	0.219	0.261	20	13	0.52(5)	0.34
$\to 12_1^-$	0.760	-	100	100		
$15_1^- \to 14_1^-$	0.179	0.246	-	11	-	0.34
$\to 13_1^-$	0.727	-	-	100		
$16_1^- \to 15_1^-$	0.142	0.201	14	8	0.5(1)	0.29
$\to 14_1^-$	0.697	-	100	100		
$17_1^- \to 16_1^-$	0.113	0.215	9	9	0.35(5)	0.34
$\to 15_1^-$	0.635	-	100	100		
$18_1^- \to 17_1^-$	0.087	0.146	-	6	-	0.25
$\to 16_1^-$	0.581	-	-	100		
$19_1^- \to 18_1^-$	0.066	0.192	-	9	-	0.38
$\to 17_1^-$	0.508	-	-	100		
$8_2^+ \to 7_5^+$	0.721	2.103	100	100	-	-
$9_1^+ \to 8_2^+$	0.714	1.365	-	100	-	2.69
$\to 7_5^+$	0.507	-	-	0.5		
$10_1^+ \to 9_1^+$	0.727	1.684	100	100	3.3(5)	2.87
$\to 8_2^+$	0.587	-	3	3		
$11_1^+ \to 10_1^+$	0.629	1.408	100	100	2.3(3)	1.86
$\to 9_1^+$	0.758	-	16	19		
$12_1^+ \to 11_1^+$	0.530	1.457	100	100	2.5(3)	1.83
$\to 10_1^+$	0.798	-	66	91		
$13_1^+ \to 12_1^+$	0.430	1.236	100	100	2.6(3)	1.47
$\to 11_1^+$	0.837	-	45	79		
$14_1^+ \to 13_1^+$	0.347	1.194	47	40	1.7(2)	1.44
$\to 12_1^+$	0.828	-	100	100		
$15_1^+ \to 14_1^+$	0.263	1.152	100	100	2.4(1)	1.48
$\to 13_1^+$	0.778	-	87	141		
$16_1^+ \to 15_1^+$	0.203	0.856	32	23	1.6(5)	1.15
$\to 14_1^+$	0.748	-	100	100		
$17_1^+ \to 16_1^+$	0.132	1.128	61	57	1.95(10)	1.83
$\to 15_1^+$	0.615	-	100	100		
$18_1^+ \to 17_1^+$	0.092	0.351	24	11	1.3(3)	0.61
$\to 16_1^+$	0.580	-	100	100		
$19_1^+ \to 18_1^+$	0.051	1.103	35	51	1.6(5)	2.32
$\to 17_1^+$	0.476	-	100	100		
$20_1^+ \to 19_1^+$	0.031	0.233	26	14	1.3(3)	0.71
$\to 18_1^+$	0.328	-	100	100		
$21_1^+ \to 20_1^+$	0.018	0.980	-	63	-	3.52
$\to 19_1^+$	0.279	-	-	100		

^{132}Pr

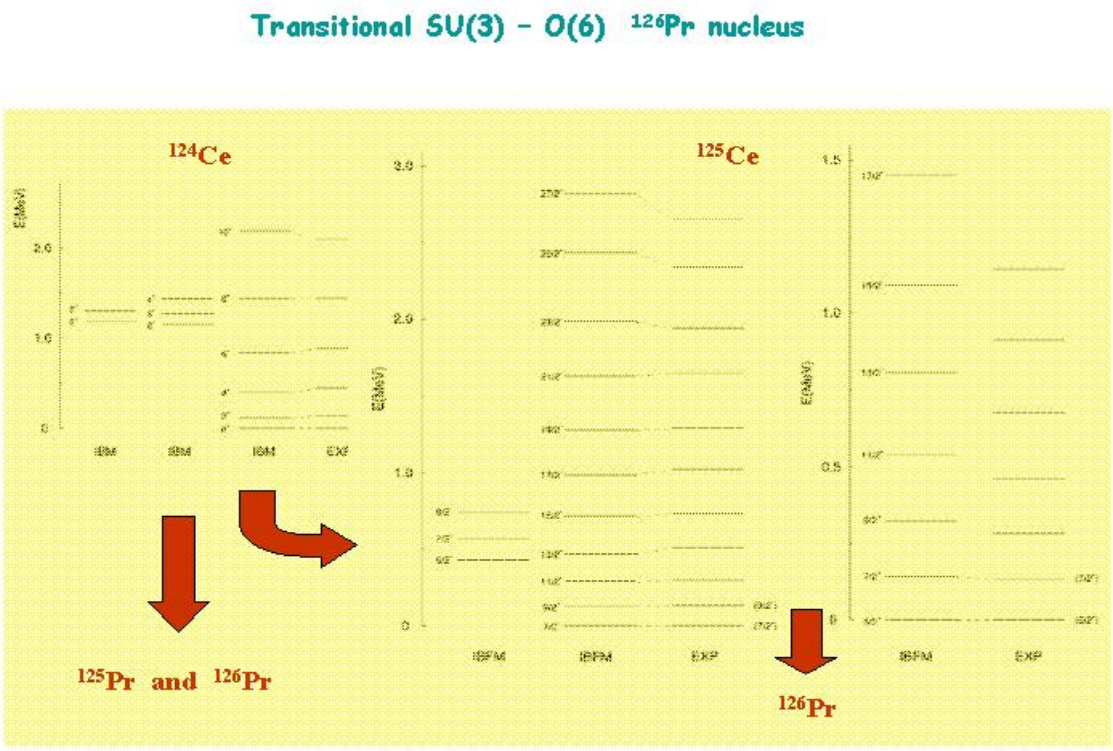

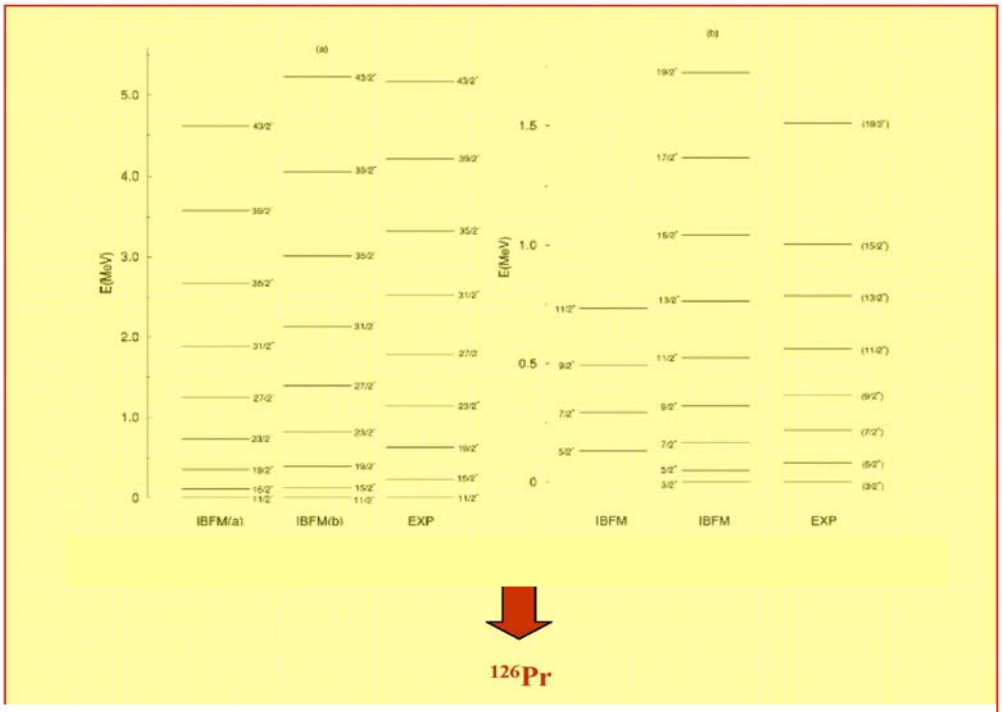

Fig. 12. The negative parity (a) and positive parity (b) yrast states in the Z-nucleus ^{125}Pr are compared with the experimental states of ^{127}Pr.

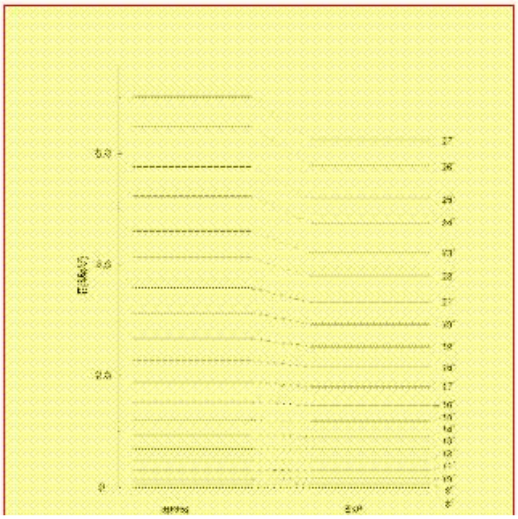

Fig. 13. The yrast sequence of high angular momentum positive parity states based on the $\pi h_{11/2} \otimes \nu h_{11/2}$ configuration is compared with experimental counterpart in ^{126}Pr. The assignment for the band head (i.e., the lowest observed state) is 8^+.

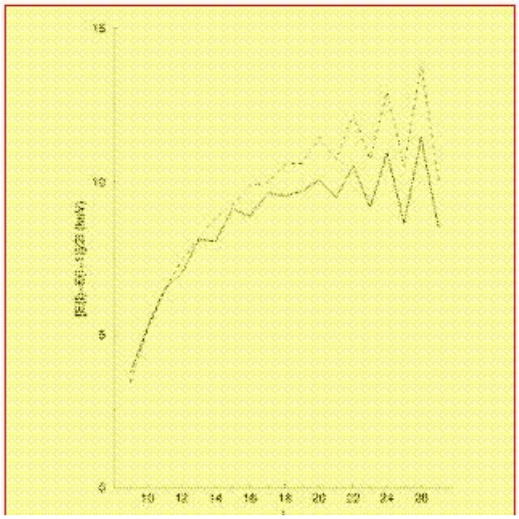

Fig. 14. IBFFM (dashed line) and experimental (solid line) [E(*I*) – (E(*I* – 1)]/2*I* vs *I* plots for the $\pi h_{11/2} \otimes \nu h_{11/2}$ yrast band in ^{126}Pr. The state 8+ is assigned to the band head.

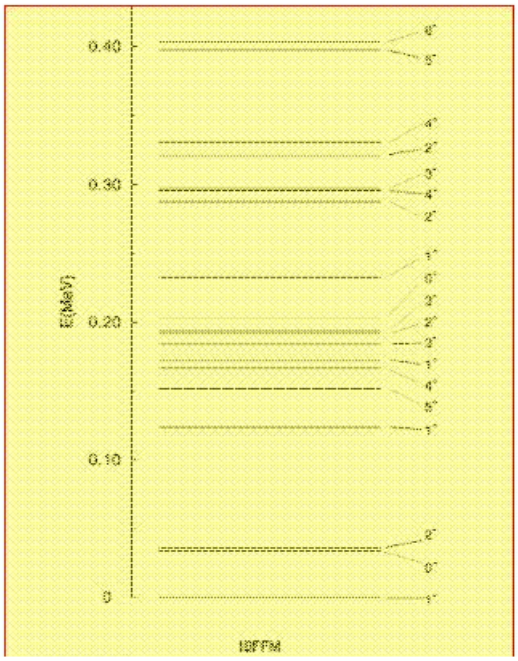

The IBM prediction for low angular momentum states in ^{126}Pr. These states are based on positive parity proton and neutron configurations.

The IBFFM analysis predicts the existence of another isomer in ^{126}Pr 5^+ at ≈ 150 keV excitation energy - isomeric character depends strongly on the choice of the proton-neutron interaction. In the present calculation 5^+_1 is below 4^+_1 and therefore it is an isomer with a possible γ decay to 2^+_1. This transition is slow enough to allow for a β decay that has been reported

^{198}Au

The first odd-odd nucleus calculated in IBFFM

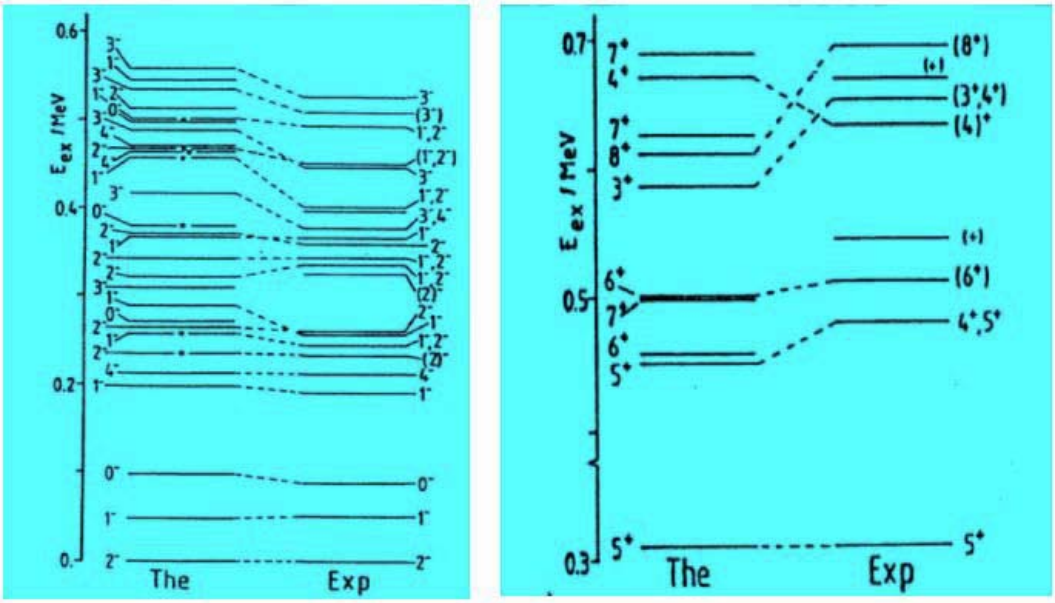

Chiral bands in IBFFM

The rotation of triaxial nuclei may give rise to pairs of identical $\Delta I = 1$ bands with the same parity in odd-odd nuclei – chiral doublet bands. These structures arise from configurations in which the angular momenta of the valence proton, the valence neutron and the core are mutually perpendicular, and can be arranged to form two systems that differ by intrinsic chirality, a left- and a right-handed system. When chiral symmetry is thus broken in the body-fixed frame, the restoration of the symmetry in the laboratory frame results in the occurrence of degenerate doublet $\Delta I = 1$ bands. It has been suggested that such nearly degenerate rotational bands might be observed in the region of transitional nuclei with $A \approx 130$. A number of nuclei in this region are susceptible to triaxial deformation and the yrast bands of odd-odd nuclei are built on the $\pi h_{11/2}$ particle-like $- \nu h_{11/2}$ hole-like configuration. The existence of self-consistent rotating mean field solutions with chiral character has been demonstrated for ^{134}Pr and ^{188}Ir. The theoretical prediction of chiral doublet structures has prompted quite a number of experimental studies of odd-odd $N = 75$ and $N = 73$ isotones in the $A \approx 130$ region, and nearly degenerate $\Delta I = 1$ bands built on the $\pi h_{11/2} \otimes \nu h_{11/2}$ configuration have been identified in many of these nuclei. Sideband partners of the $\pi h_{11/2} \otimes \nu h_{11/2}$ yrast band have been identified in $_{55}$Cs, $_{57}$La and $_{61}$Pm $N = 75$ isotones of ^{134}Pr. For ^{134}Pr the energy spacing between the doublet rotational bands gradually decreases from ≈ 0.19 MeV at low spin to the point where the two bands cross between $I = 14$ and $I = 15$. For the other $N = 75$ isotones the two lowest $\pi h_{11/2} \otimes \nu h_{11/2}$ bands are almost parallel in the E *vs* I plot, and the energy spacing between the corresponding states with the same spin is ≈ 0.3 MeV.

In ^{134}Pr the two lowest, yrast and yrare $\pi h_{11/2} \otimes \nu h_{11/2}$ bands have been interpreted as chiral restored doublet bands. In order to explain similar doublet bands in the other $N = 75$ odd-odd nuclei, it has been suggested that in these cases the triaxial core deformation is not stable, but perhaps more γ-soft, resulting in collective chiral vibration of the core angular momentum between the left- and right-handed chiral systems. It has to be emphasized that in all studies of chiral doublet bands it has been argued that the empirical separation of ≤ 300 keV is too small for the sideband to be interpreted as a band built either on the unfavored signature of the proton orbital, or on the γ-vibrational excitation. A γ-vibration coupled to the yrast band has been ruled out because in this region the γ-vibration energies are ≥ 600 keV.

IBM/IBFM calculations are performed in the laboratory frame, and the results can be directly compared with experimental data. All states within the model space and their electromagnetic properties are compared with experiment, rather than just band-head energies. In the particular case of ^{134}Pr, it will be assumed that the nucleus is triaxial but, unlike in a geometric description based on the tilted axis cranking model, the occurrence of nearly degenerate doublet ΔI = I bands is not related to a definite alignment of the angular momenta of the odd proton and odd neutron along the body-fixed axes of the core nucleus.

The spectrum of the core nucleus $^{134}_{58}\mathrm{Ce}_{76}$ is described by the Hamiltonian

$$H_{IBM} = \epsilon_d\, \hat{n}_d + p\; P \cdot P + k'\; L \cdot L + k\; Q \cdot Q + \Theta_3 \left[(d^\dagger\; d^\dagger)_2\; d^\dagger \right]_3 \cdot \left[(\tilde{d}\; \tilde{d})_2\; \tilde{d} \right]_3$$

The first four terms represent the standard Hamiltonian of the Interacting Boson Model (IBM-1). The cubic interaction in the last term, with the strength parameter Θ_3, introduces a degree of triaxiality. The best agreement with the experimental spectrum is obtained for the following choice of parameters:

$\epsilon_d = 0.75$, $p = 0.25$, $k' = 0.014$, $k = -0.003$, $\Theta_3 = 0.025$ (all in MeV), and $\chi = -0.3$ in the quadrupole operator Q_2. This value of χ is also used in the boson quadrupole operator appearing in the boson-fermion dynamical interaction, as well as in the E2 operator.

With the inclusion of the three-body term in the boson Hamiltonian, the boson quadrupole operator appearing in the dynamical boson-fermion interaction and in the E2 operator should also be extended to higher order. The standard boson quadrupole operator is modified by including the additional term

$$\eta \left[(d^\dagger\; \tilde{d})_3\; (d^\dagger\; \tilde{d})_3 \right]_2$$

This term is included in the dynamical boson-fermion interaction and in the E2 operator, with the strength parameter $\eta = -0.46$ MeV.

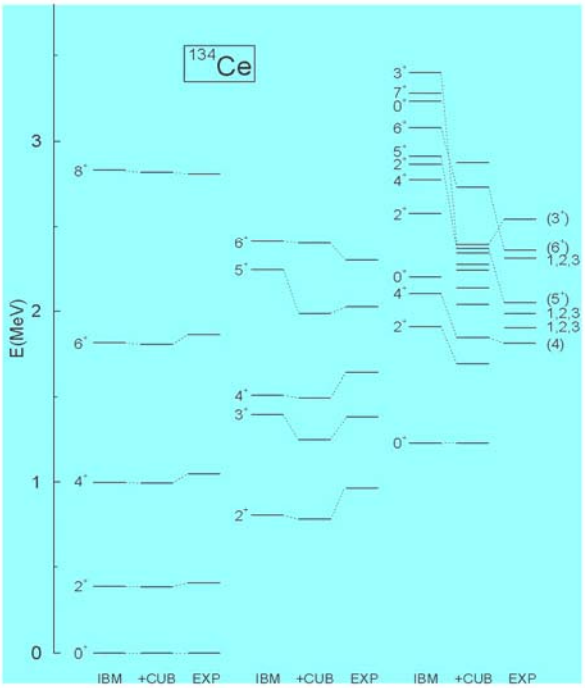

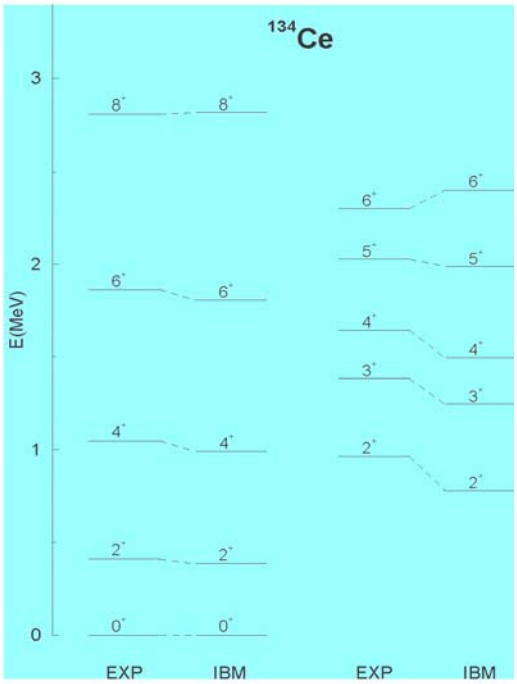

The spectrum of positive-parity states in ^{134}Pr, based on negative-parity orbitals of the odd proton and odd neutron, is calculated by using the quasi-particle energies, occupation probabilities and boson-fermion interaction strengths obtained in the IBFM calculations of negative-parity spectra in $^{135}_{59}Pr_{76}$ and $^{133}_{58}Ce_{75}$. Most of the model parameters, therefore, are determined by the structure of collective and single-nucleon states in the even-even and odd-even neighbors of ^{134}Pr and, in principle, only the residual interaction between the odd proton and odd neutron has to be adjusted to the experimental data in the odd-odd nucleus.

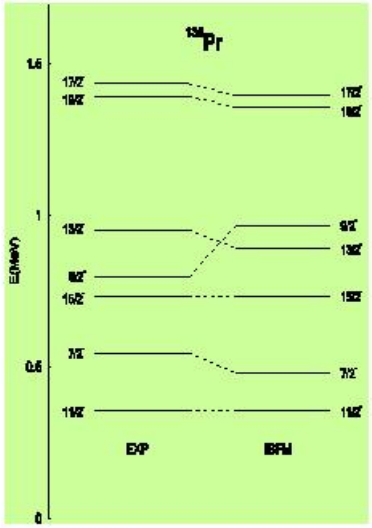

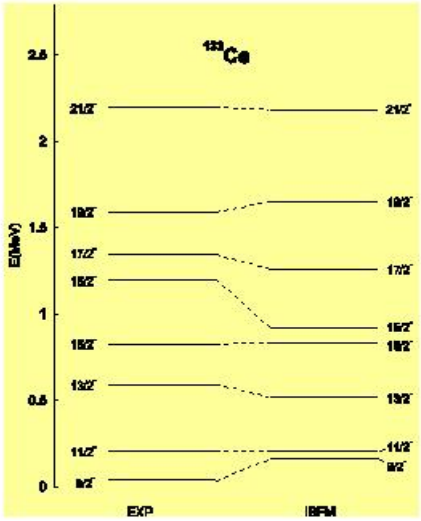

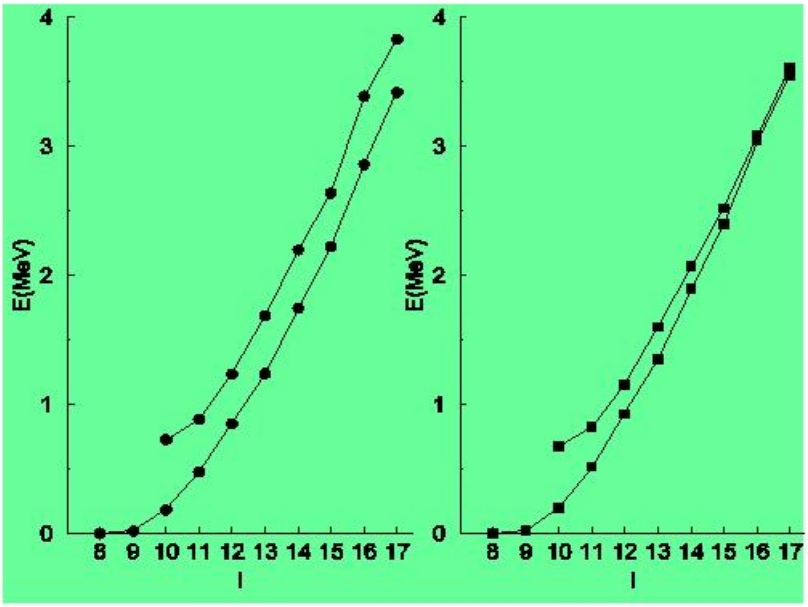

The yrast and yrare $\pi h_{11/2} \otimes \nu h_{11/2}$ bands in ^{134}Pr calculated in the IBFFM for the ^{134}Ce core without triaxiality (left panel, $\Theta_3 = 0$), and with stable triaxial deformation (right panel, $\Theta_3 = 0.03$ MeV).

For $\Theta_3 = 0$ the core is γ-soft and the two bands do not cross or become degenerate. Rather, an almost constant energy spacing ≈ 400 keV between the two bands is predicted. For a stable triaxial deformation ($\Theta_3 = 0.03$ MeV) the energy difference between the yrast and yrare bands gradually decreases, and between angular momenta 16^+ and 17^+ the two bands cross. Except for the exact position of the band crossing (which can be also affected by four-quasiparticle configurations not included in the model space), the "energy *vs* spin" diagram is in excellent agreement with the experimentally observed evolution of the two lowest positive-parity bands in ^{134}Pr. The results are also in agreement with the conclusions of calculations in the body-fixed frame, where it has been suggested that in the odd-odd $N = 75$ nuclei other than ^{134}Pr the triaxial core deformation is not stable, rather it is γ-soft, resulting in the two lowest $\pi h_{11/2} \otimes \nu h_{11/2}$ bands being almost parallel in the E *vs* I plot, with the energy spacing of ≈ 0.3 MeV. In ^{134}Pr, on the other hand, the stable triaxial deformation causes the two lowest positive-parity bands to become almost degenerate.

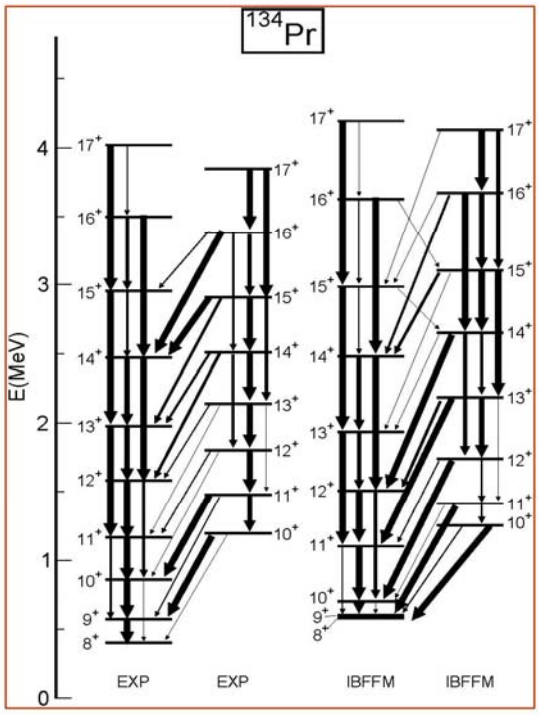

The yrast band is basically built on the ground-state band of the even-even core. With increasing angular momentum the admixture of the γ-band of the core becomes more pronounced. The structure of the second – yrare band, however, is that of the odd proton and odd neutron coupled to the γ-band of the core, especially in the lower part of the band. With increasing angular momentum both ground-state band and γ-band components contribute to the wave functions of the yrare band in ^{134}Pr. In the region of band crossing, in particular, the wave functions of the yrare band contain sizeable components of the higher-lying core structures. The IBFFM prediction, therefore, is that the two lowest $\pi h_{11/2} \otimes \nu h_{11/2}$ bands in ^{134}Pr are built, in leading order, on the ground-state band and the γ-band of the core nucleus, respectively. Their wave functions closely follow the triaxial structure of the core nucleus. This result is at variance with previous analyses of the doublet bands in ^{134}Pr, based on the tilted axis cranking approach, which have basically excluded the possibility that the second band might be built on the γ-band of the core. This was done only on the basis of the relatively high excitation energy of the γ-vibration.

As the IBFFM calculations are performed in the laboratory frame, they cannot determine the alignment of the odd particles along the body fixed axes. The IBFFM analysis indicates that the γ degree of freedom plays an important role in the formation of these bands.

Nuclear Theory:
β decay in the interacting boson-fermion model

S. Brant

University of Zagreb, Croatia

E.mail: Brant@phy.hr

4.

β decay in the interacting boson-fermion model

OBJECTIVES

- To test the nuclear model by analyzing experimental data

  Wave functions (two odd-even and one even-even nucleus are involved)

  Transition operators

- To provide reliable information for astrophysical applications

The process is very sensitive to configuration mixing both in the initial and final states. A detailed knowledge of the wavefunctions is required. Beta decay properties can be calculated by using:

- Shell model (in light nuclei and in medium-mass and heavy nuclei in the neighborhood of doubly magic nuclei)
- Other models for medium-mass and heavy nuclei.

Example: Simple pairing theory

⇩

Overestimates the Gamow-Teller strengths by a large factor (up to a factor 70 !!!!!)

How to account for the large hindrance:

Nuclear deformation
Mixing with 2p-2h states
Mesonic degrees of freedom

In the IBFM there is NO quenching factor (once the wave functions have been calculated, the calculation of beta decay properties is parameter free), or the quenching factor is SMALL.

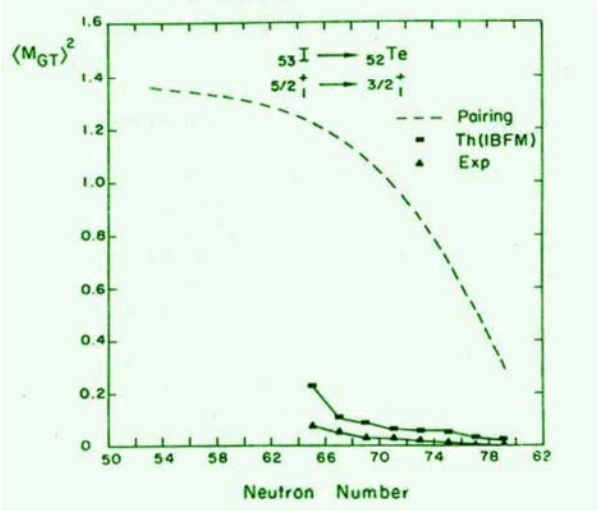

Comparison of experimental Gamow–Teller matrix elements with pairing theory and results of the calculation using the interacting boson–fermion model (IBFM).

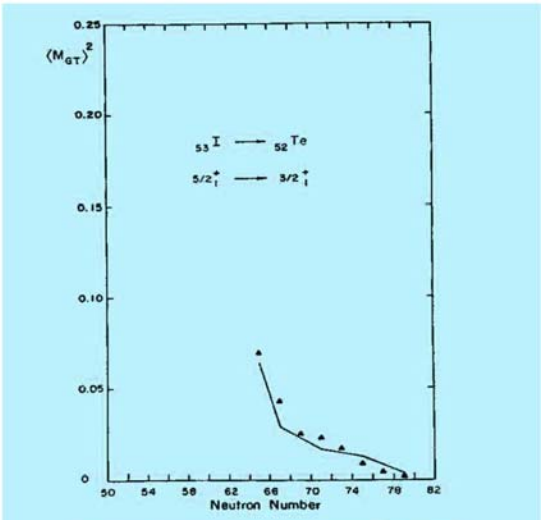

Comparison between experimental Gamow – Teller matrix elements (triangles) and those obtained using IBFM renormalized by a factor 3.5 (continuous line).

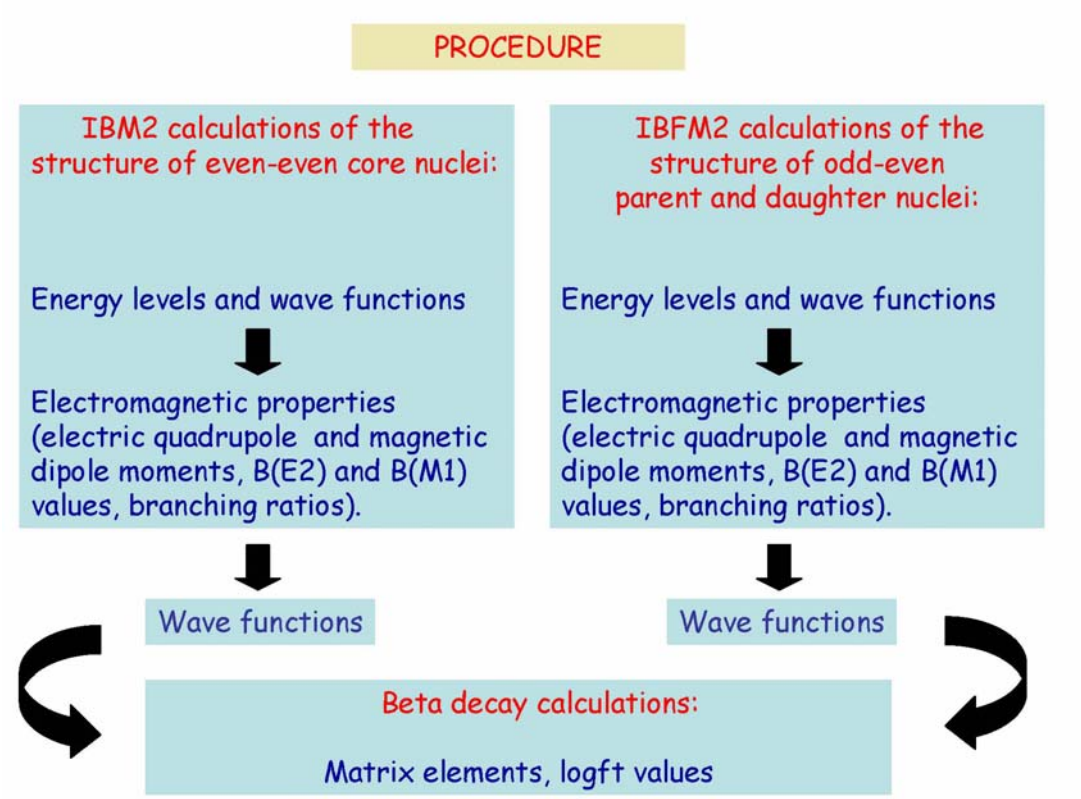

Cs → Xe

A = 125, 127, 129

Soft nuclei close to the O(6) limit → complex wave functions

→ Sensitive test of the model

IBFM2 Hamiltonian → $H = H^{\mathrm{B}} + H^{\mathrm{F}} + V^{\mathrm{BF}}$

IBM2 Hamiltonian (core nuclei) :

$$
\begin{aligned}
H^{\mathrm{B}} \;=\; & \epsilon_d\,(n_{d_\nu} + n_{d_\pi}) + \kappa\,(Q^{\mathrm{B}}_\nu \cdot Q^{\mathrm{B}}_\pi) \\
& + \frac{1}{2}\xi_2\,((d^\dagger_\nu s^\dagger_\pi - d^\dagger_\pi s^\dagger_\nu)\cdot(\tilde{d}_\nu s_\pi - \tilde{d}_\pi s_\nu)) + \sum_{K=1,3}\xi_K\,([d^\dagger_\nu d^\dagger_\pi]^{(K)}\cdot[\tilde{d}_\pi \tilde{d}_\nu]^{(K)}) \\
& + \frac{1}{2}\sum_{L=0,2,4} c^\nu_L\,([d^\dagger_\nu d^\dagger_\nu]^{(k)}\cdot[\tilde{d}_\nu \tilde{d}_\nu]^{(k)}) + \frac{1}{2}\sum_{L=0,2,4} c^\pi_L\,([d^\dagger_\pi d^\dagger_\pi]^{(k)}\cdot[\tilde{d}_\pi \tilde{d}_\pi]^{(k)})
\end{aligned}
$$

$$Q^{\rm B}_\nu = d^\dagger_\nu s_\nu + s^\dagger_\nu \tilde{d}_\nu + \chi_\nu [d^\dagger_\nu \tilde{d}_\nu]^{(2)}$$
$$Q^{\rm B}_\pi = d^\dagger_\pi s_\pi + s^\dagger_\pi \tilde{d}_\pi + \chi_\pi [d^\dagger_\pi \tilde{d}_\pi]^{(2)}$$

Boson quadrupole operators

IBM2 parameters. The unit is MeV except for the dimensionless χ_ν. The parameters $\chi_\pi = -0.80$ and $\xi_1 = \xi_2 = 0.24$ MeV, $\xi_3 = -0.18$ MeV are fixed.

odd nuclei	core nucleus	ϵ_d	κ	χ_ν	c^ν_0	c^ν_2
^{125}Cs	^{124}Xe	0.70	−0.145	0.00	0.05	−0.10
^{125}Xe, ^{127}Cs	^{126}Xe	0.70	−0.155	0.20	0.10	−0.10
^{127}Xe, ^{129}Cs	^{128}Xe	0.70	−0.170	0.33	0.30	0.00
^{129}Xe	^{130}Xe	0.76	−0.190	0.50	0.30	0.10

$$H^{\rm F} = \sum_i \epsilon_i n_i$$

Hamiltonian of the odd fermion

BCS ⟹ ϵ_i is the quasi-particle energy of the ith orbital
n_i is its number operator

Interaction between bosons and the odd fermion :

$$\begin{aligned} V^{\rm BF} = & \sum_{i,j} \Gamma_{ij} \left([a^\dagger_i \tilde{a}_j]^{(2)} \cdot Q^{\rm B}_\rho \right) \\ & + \sum_{i,j} \Gamma'_{ij} \left([a^\dagger_i \tilde{a}_j]^{(2)} \cdot Q^{\rm B}_{\rho'} \right) \\ & + \sum A_i \, n_i n_{d_\rho} + \sum A'_i \, n_i n_{d_{\rho'}} \\ & + \sum_{i,j} \Lambda^j_{ki} \left\{ : \left[\left[d^\dagger_\rho \tilde{a}_j \right]^{(k)} a^\dagger_i s_\rho \right]^{(2)} : \cdot \left[s^\dagger_{\rho'} \tilde{d}_{\rho'} \right]^{(2)} \right. \\ & \left. + H.c. \right\} \\ & + B \, J \cdot L_\rho + B' \, J \cdot L_{\rho'}. \end{aligned}$$

ρ and ρ' denote π (ν) and ν (π) if the odd fermion is a proton (a neutron).

Orbital dependence of the interaction strengths

$$\Gamma_{i,j} = (u_i u_j - v_i v_j)\, Q_{i,j}\, \Gamma$$

$$\Lambda^{j}_{k,i} = -\beta_{k,i}\beta_{j,k}\left(\frac{10}{N_\rho(2j_k+1)}\right)^{1/2}\Lambda$$

$$\beta_{i,j} = (u_i v_j + v_i u_j)\, Q_{i,j}$$

$$Q_{i,j} = < l_i, \frac{1}{2}, j_i || Y^{(2)} || l_j, \frac{1}{2}, j_j >$$

uj and vj from BCS

Electromagnetic transition operators

$$T^{(E2)} = e^B_\pi Q^B_\pi + e^B_\nu Q^B_\nu + \sum_{i,j} e'_{i,j}\,[a^\dagger_i \tilde{a}_j]^{(2)}$$

u_j and v_j from BCS

$$e'_{i,j} = -\frac{e^F_\rho}{\sqrt{5}}(u_i u_j - v_i v_j) < i || r^2 Y^{(2)} || j >$$

$$T^{(M1)} = \sqrt{\frac{3}{4\pi}}\left(g^B_\pi L^B_\pi + g^B_\nu L^B_\nu + \sum_{i,j} e^{(1)}_{i,j}\,[a^\dagger_i \tilde{a}_j]^{(1)}\right)$$

$$e^{(1)}_{i,j} = -\frac{1}{\sqrt{3}}(u_i u_j + v_i v_j) < i || g_l \mathbf{l} + g_s \mathbf{s} || j >$$

Cs isotopes (odd proton)

Single particle energies (MeV)

$d_{5/2}$	$g_{7/2}$	$s_{1/2}$	$d_{3/2}$	$h_{11/2}$	$h_{9/2}$	$f_{7/2}$
0.05	0.00	3.35	3.00	1.50	7.00	8.00

Boson-fermion interaction strengths

isotope	Γ	A	Λ
^{125}Cs	0.90	−0.60	1.65
^{127}Cs	0.76	−0.66	2.30
^{129}Cs	0.74	−0.80	2.90

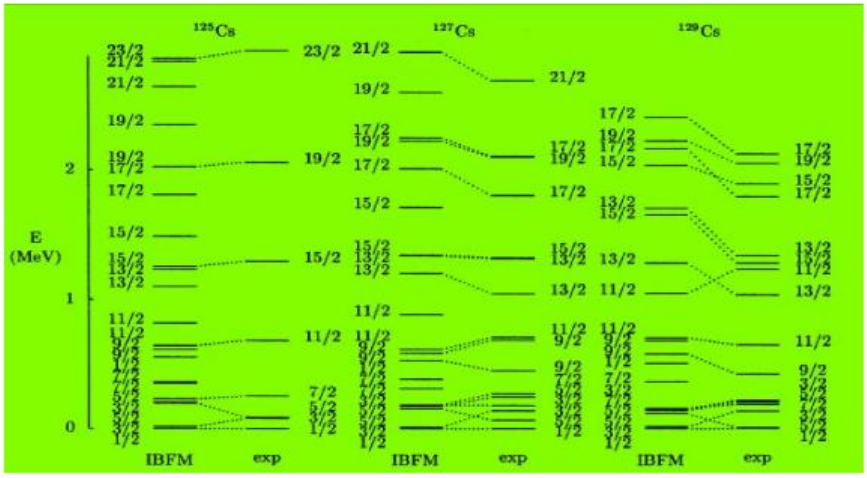

Positive parity levels

Xe isotopes (odd neutron)

Single particle energies (MeV)

Boson-fermion interaction strengths

	$d_{5/2}$	$g_{7/2}$	$s_{1/2}$	$d_{3/2}$	$h_{11/2}$
^{125}Xe	0.00	0.30	1.55	2.00	1.30
^{127}Xe	0.00	0.35	1.55	2.00	1.30
^{129}Xe	0.00	0.40	1.60	2.00	1.30

isotope	Γ	A	Λ
^{125}Xe	0.39	−0.42	0.40
^{127}Xe	0.44	−0.42	0.40
^{129}Xe	0.50	−0.42	0.40

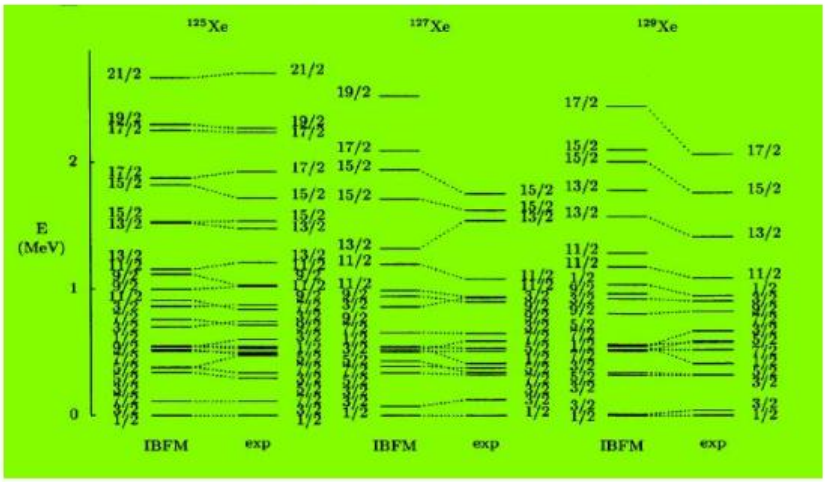

Positive parity levels

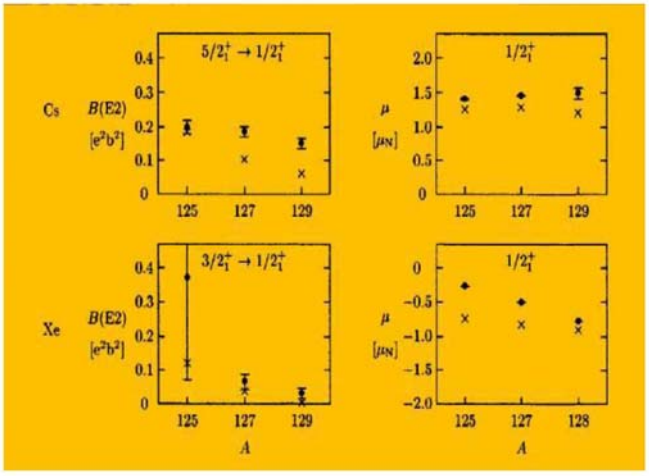

B(E2) and B(M1) values, static moments, branching ratios are calculated for the sequence of Cs and Xe nuclei

B(E2) values and magnetic moments. The symbol • with the error bar denotes the experimental data, while x shows the calculated values

Wave functions are realistic

The Fermi $\sum_k t^{\pm}(k)$ and the Gamow-Teller $\sum_k t^{\pm}(k)\sigma(k)$ transition operators can be expressed in the framework of IBFM2. They can be constructed from the transfer operators.

$$A^{\dagger(j)}_m = \zeta_j a^{\dagger}_{jm} + \sum_{j'} \zeta_{jj'} s^{\dagger} [\tilde{d} a^{\dagger}_{j'}]^{(j)}_m \qquad (\Delta n_j = 1,\ \Delta N = 0)$$

$$B^{\dagger(j)}_m = \theta_j s^{\dagger} \tilde{a}_{jm} + \sum_{j'} \theta_{jj'} [d^{\dagger} \tilde{a}_{j'}]^{(j)}_m \qquad (\Delta n_j = -1,\ \Delta N = 1)$$

The former creates a fermion, while the latter annihilates a fermion simultaneously creating a boson. Either operator increases the quantity $n_j + 2N$ by one unit. The conjugate operators are:

$$\tilde{A}^{(j)}_m = (-1)^{j-m} \left\{ A^{\dagger(j)}_{-m} \right\}^{\dagger} = \zeta^*_j \tilde{a}_{jm} + \sum_{j'} \zeta^*_{jj'} s [d^{\dagger} \tilde{a}_{j'}]^{(j)}_m \qquad (\Delta n_j = -1,\ \Delta N = 0)$$

$$\tilde{B}^{(j)}_m = (-1)^{j-m} \left\{ B^{\dagger(j)}_{-m} \right\}^{\dagger} = -\theta^*_j s a^{\dagger}_{jm} - \sum_{j'} \theta^*_{jj'} [\tilde{d} a^{\dagger}_{j'}]^{(j)}_m \qquad (\Delta n_j = 1,\ \Delta N = -1)$$

The asterisks mean complex conjugate. These operators decrease the quantity $n_j + 2N$ by one unit.

The IBFM image of the Fermi $\sum_k \mathbf{t}^{\pm}(k)$ and the Gamow-Teller transition operator $\sum_k t^{\pm}(k)\sigma(k)$

$$O^{\mathsf{F}} = \sum_j -\sqrt{2j+1} \left[P^{(j)}_{\nu} P^{(j)}_{\pi} \right]^{(0)}$$

$$O^{\mathsf{GT}} = \sum_{j'j} \eta_{j'j} \left[P^{(j')}_{\nu} P^{(j)}_{\pi} \right]^{(1)}$$

$$\eta_{j'j} = -\frac{1}{\sqrt{3}} < l' \tfrac{1}{2}; j' || \sigma || l \tfrac{1}{2}; j >$$

The transfer operators $P_\rho^{(j)}$ depend on nuclei. In the present case

$$\begin{aligned} P_\pi^{(j)} &= \tilde{A}_\pi^{(j)} \\ P_\nu^{(j)} &= \tilde{B}_\nu^{(j)} \end{aligned}$$

$$\begin{aligned} < M_{\mathsf{F}} >^2 &= \frac{1}{2I_i+1} | < I_f || O^{\mathsf{F}} || I_i > |^2 \\ < M_{\mathsf{GT}} >^2 &= \frac{1}{2I_i+1} | < I_f || O^{\mathsf{GT}} || I_i > |^2 \end{aligned}$$

$$ft = \frac{6163}{< M_{\mathsf{F}} >^2 + (G_{\mathsf{A}}/G_{\mathsf{V}})^2 < M_{\mathsf{GT}} >^2}$$

in units of second where $(G_{\mathsf{A}}/G_{\mathsf{V}})^2 = 1.59$

The coefficients η_j, $\eta_{jj'}$, θ_j, $\theta_{jj'}$ appearing in transfer operators

$$\begin{aligned} \zeta_j &= u_j \frac{1}{K'_j} \\ \zeta_{jj'} &= -v_j \beta_{j'j} \left(\frac{10}{N(2j+1)} \right)^{1/2} \frac{1}{KK'_j} \\ \theta_j &= \frac{v_j}{\sqrt{N}} \frac{1}{K''_j} \\ \theta_{jj'} &= u_j \beta_{j'j} \left(\frac{10}{2j+1} \right)^{1/2} \frac{1}{KK''_j} \end{aligned}$$

N is N_π or N_ν, depending on the transfer operator, and K, K'_j, K''_j are determined by

$$\begin{aligned} K &= \left(\sum_{jj'} \beta_{jj'}^2 \right)^{1/2} \\ \sum_{\alpha J} < \mathrm{odd};\alpha J || A^{\dagger j} || \mathrm{even};0_1^+ >^2 &= (2j+1) u_j^2 \\ \sum_{\alpha J} < \mathrm{even};0_1^+ || B^{\dagger j} || \mathrm{odd};\alpha J >^2 &= (2j+1) v_j^2 \end{aligned}$$

When the odd fermion is a hole in respect to the boson core, u_j and v_j have to be interchanged

Beta-decay rates from ^{A}Cs to ^{A}Xe shown in terms of $\log_{10} ft$ values. The symbol • with the error bar denotes experimental data, while × presents the calculated value.

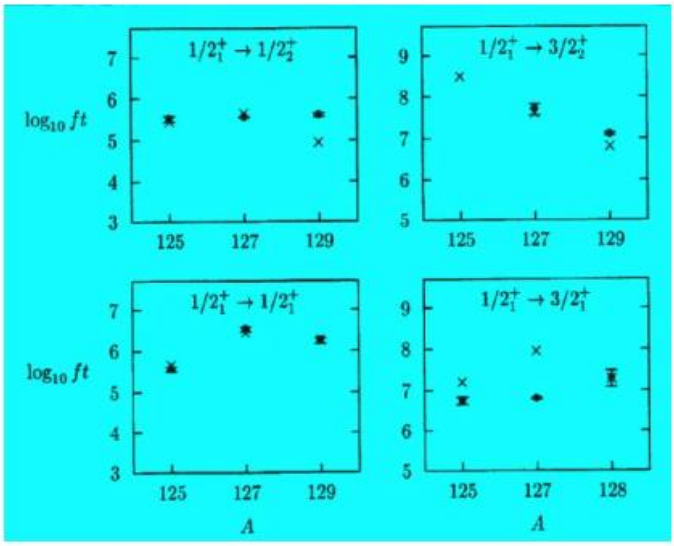

Rh ➡ Pd

A = 105, 107, 109

U(5) ⟷ O(6) nuclei

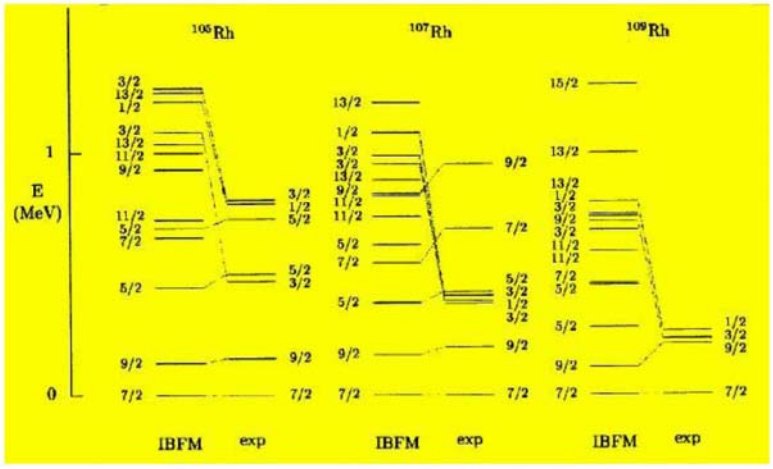

Positive parity levels

j – 1 anomaly !!!!

on $g_{9/2}$

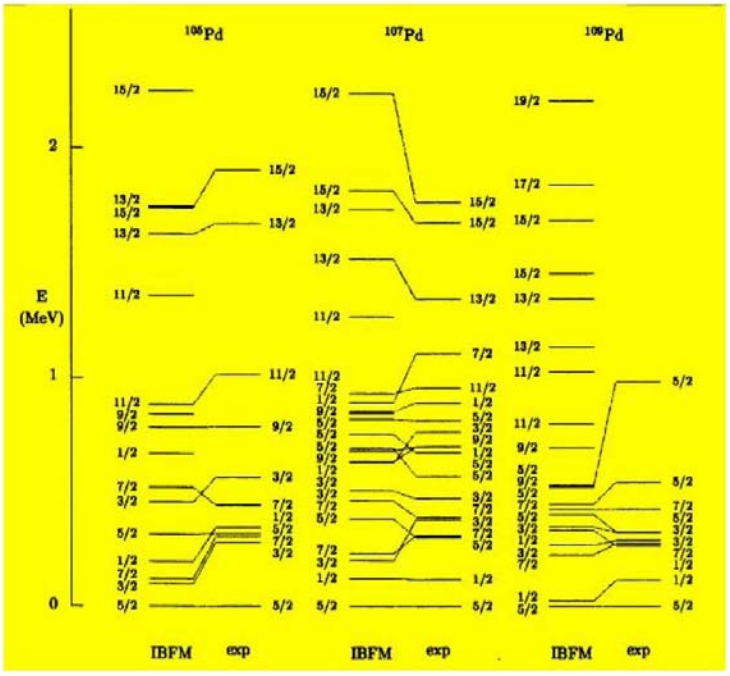

Positive parity levels

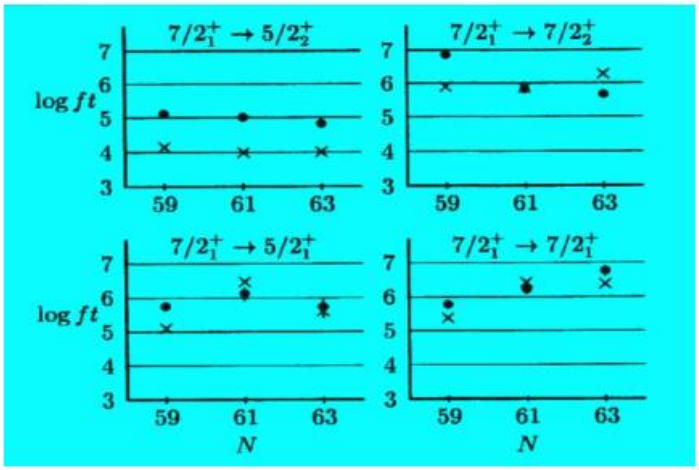

$\log_{10} ft$ values in the decays ${}_{45}\mathrm{Rh}_{N+1} \to {}_{46}\mathrm{Pd}_N$. The experimental data are presented by • while the calculated values are shown by $\times$.

As → Ge

A = 69, 71, 73

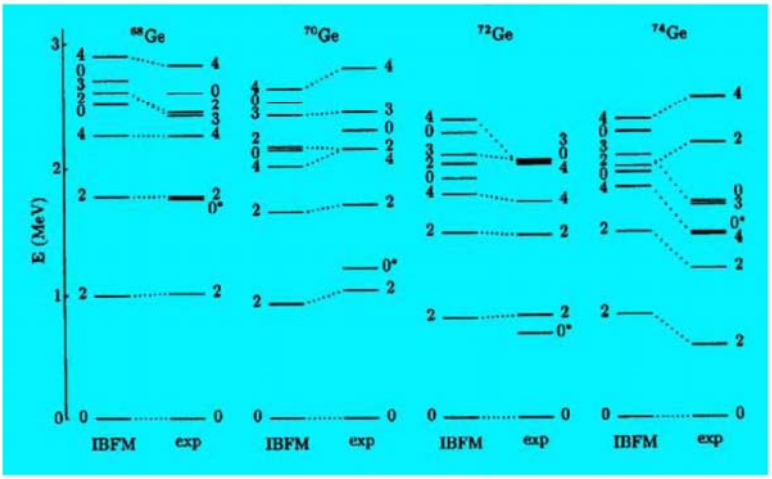

0_2^+ states are intruders !!!!

→ outside the boson space

Consequences ?????

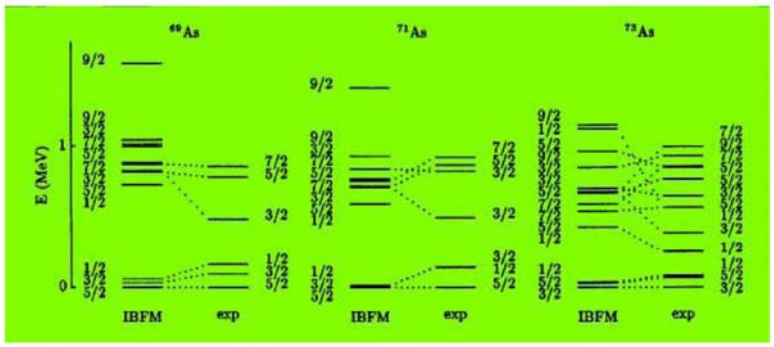

Negative parity levels

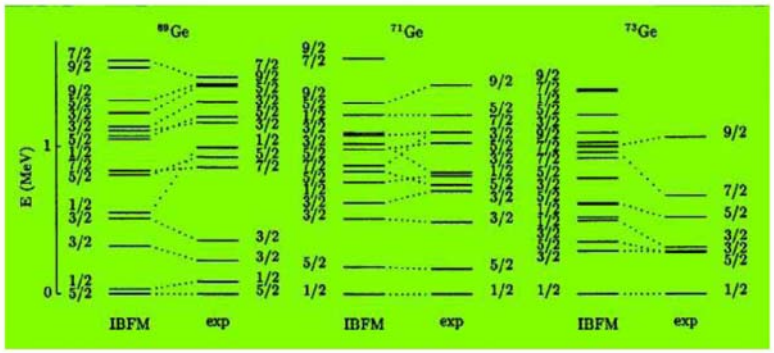

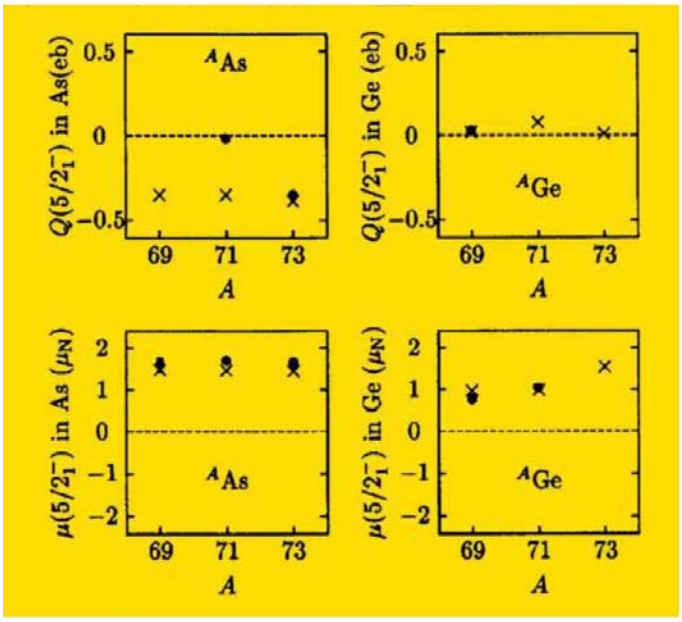

The exclusion of intruder components does not influence strongly the theoretical values of static moments

and branching ratios

Branching ratios in ^{71}As

level (MeV)	transition	$I_\gamma(IBFM2)$	$I_\gamma(EXP)$
0.143	$1/2_1^- \to 5/2_1^-$	100	100
0.147	$3/2_1^- \to 1/2_1^-$	0.0	
	$3/2_1^- \to 5/2_1^-$	100	100
0.506	$3/2_2^- \to 3/2_1^-$	100	100 (5)
	$3/2_2^- \to 1/2_1^-$	7.1	27 (14)
	$3/2_2^- \to 5/2_1^-$	8.2	
0.829	$3/2_3^- \to 3/2_2^-$	9.3	
	$3/2_3^- \to 3/2_1^-$	100	100 (14)
	$3/2_3^- \to 1/2_1^-$	30.3	9.3 (7)
	$3/2_3^- \to 5/2_1^-$	29.4	
0.870	$5/2_2^- \to 3/2_3^-$	0.0	
	$5/2_2^- \to 3/2_2^-$	28.8	
	$5/2_2^- \to 3/2_1^-$	36.4	40 (1)
	$5/2_2^- \to 1/2_1^-$	27.0	1.8 (7)
	$5/2_2^- \to 5/2_1^-$	100	100.0(7)
0.925	$7/2_1^- \to 5/2_2^-$	0.0	
	$7/2_1^- \to 3/2_3^-$	0.0	
	$7/2_1^- \to 3/2_2^-$	0.0	
	$7/2_1^- \to 3/2_1^-$	1.1	5.8 (16)
	$7/2_1^- \to 5/2_1^-$	100	100 (3)

Branching ratios in ^{69}Ge

level (MeV)	transition	$I_\gamma(IBFM2)$	$I_\gamma(EXP)$
0.087	$1/2_1^- \to 5/2_1^-$	100	100
0.233	$3/2_1^- \to 1/2_1^-$	43.2	48.3 (13)
	$3/2_1^- \to 5/2_1^-$	100	100 (3)
0.374	$3/2_2^- \to 3/2_1^-$	0.7	4.6 (8)
	$3/2_2^- \to 1/2_1^-$	100	100.0 (15)
	$3/2_2^- \to 5/2_1^-$	0.1	31.5 (8)
0.862	$7/2_1^- \to 3/2_2^-$	0.4	0.76 (13)
	$7/2_1^- \to 3/2_1^-$	0.1	8.4 (21)
	$7/2_1^- \to 5/2_1^-$	100	100 (3)
0.933	$5/2_2^- \to 7/2_1^-$	0.0	
	$5/2_2^- \to 3/2_2^-$	0.5	32 (7)
	$5/2_2^- \to 3/2_1^-$	16.7	8
	$5/2_2^- \to 1/2_1^-$	35.5	24 (7)
	$5/2_2^- \to 5/2_1^-$	100	100 (5)
0.995	$1/2_2^- \to 5/2_2^-$	0.0	
	$1/2_2^- \to 3/2_2^-$	7.9	9 (6)
	$1/2_2^- \to 3/2_1^-$	26.8	41 (9)
	$1/2_2^- \to 1/2_1^-$	0.7	
	$1/2_2^- \to 5/2_1^-$	100	100 (21)

$\log_{10} ft$ values for levels in ^{69}Ge.

level	$\log_{10} ft$ $(IBFM2)$	$\log_{10} ft$ (EXP)
$3/2_1^-$	5.88	6.05 (2)
$3/2_2^-$	7.90	7.21 (5)
$3/2_3^-$	5.07	6.79 (4)
$3/2_4^-$	6.46	6.71 (6)
$3/2_5^-$	6.73	7.02 (6)
$5/2_1^-$	4.26	5.49 (2)
$5/2_2^-$	6.65	6.94 (7)
$5/2_3^-$	5.33	6.65 (5)
$5/2_4^-$	5.49	6.80 (6)
$7/2_1^-$	7.54	6.98 (5)
$7/2_2^-$	6.54	6.81 (5)
$7/2_3^-$	5.96	6.20 (5)

$\log_{10} ft$ values for levels in ^{71}Ge.

level	$\log_{10} ft$ $(IBFM2)$	$\log_{10} ft$ (EXP)
$3/2_1^-$	6.52	7.19 (1)
$3/2_2^-$	7.79	
$3/2_3^-$	5.73	
$3/2_4^-$	5.21	6.33 (1)
$3/2_5^-$	7.34	6.94 (1)
$5/2_1^-$	4.60	5.85 (1)
$5/2_2^-$	6.08	
$5/2_3^-$	5.63	6.87 (2)
$5/2_4^-$	5.55	6.84 (2)
$7/2_1^-$	7.60	8.79 (25)

The ground states of parent ^{69}As and ^{71}As nuclei are $5/2_1^-$ levels. The hierarchy of values for transitions into different states of each angular momentum is reproduced for ^{69}Ge (except for the transition to the $3/2_3^-$ level that is predicted to have a rather small $\log_{10} ft$ value). The same is true for ^{71}Ge. The theory predicts that the smallest $\log_{10} ft$ value among all $3/2^-$ levels in ^{71}Ge has the $3/2_4^-$ level. This result is in agreement with the experimental data. The only available experimental $\log_{10} ft$ value in ^{73}Ge is for the $1/2_1^-$ level ($\log_{10} ft = 5.4$). The corresponding theoretical value (4.27) is the smallest calculated.

Systematic effect : For most decays the calculated values are smaller than the experimental values

a) Wave functions ?

If one takes the transition operators without normalization parameters, then the difference between the calculated and experimental values are caused by the transition matrix elements, that in this case have to be overestimated. This may indicate that other components are admixed in the wave functions (for example those involving intruder states), which would decrease the amplitudes of the present IBFM2 components, leading to an increase of the theoretical $\log_{10} ft$ values.

⬇

Accurate test of wave functions

b) Transfer operators ?

- **Normalization factors ?**
- **Additional terms ?**
- **Normalization factors + Additional terms ?**

$$A_m^{\dagger(j)} = [\ \zeta_j a_{jm}^\dagger + \sum_{j'} \zeta_{jj'}\ (\ s^\dagger [\tilde{d} a_{j'}^\dagger]_m^{(j)} + \ \ )\ ]$$

Overall normalization factor N ?

Normalization factor γ

a) Parameter
b) Microscopic

Additional term(s)

$\tilde{s}[d^\dagger a_{j'}^\dagger]_m^{(j)}$

or

$\sum_{j',J} \phi_{jj'}^J [(a_{j'}^\dagger \times d^\dagger)^{(J)} \times \tilde{d}]_m^{(j)}$

or

... ...

^{58}Ni (d, ^{3}He) ^{57}Co reaction

Normalization factor γ and the term $\tilde{s}[d^\dagger a_{j'}^\dagger]_m^{(j)}$

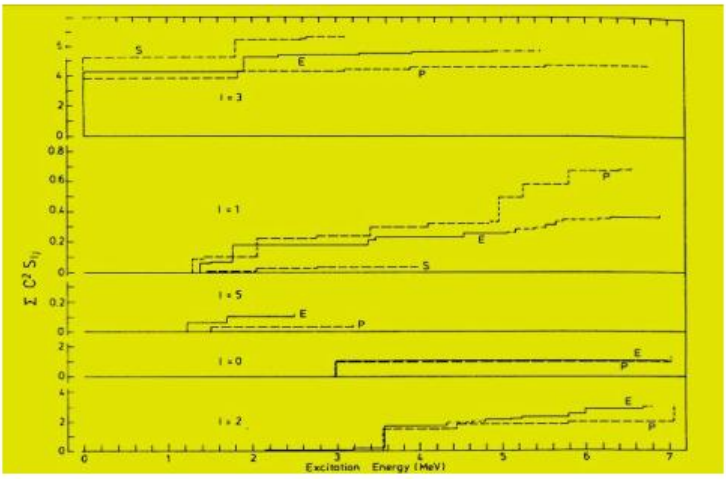

Sums of spectroscopic strengths

E experiment S shell model P IBFM1

^{62}Ni (d, ^{3}He) ^{61}Co reaction

Normalization factor γ and the term $\tilde{s}[d^{\dagger}a^{\dagger}_{j'}]^{(j)}_{m}$

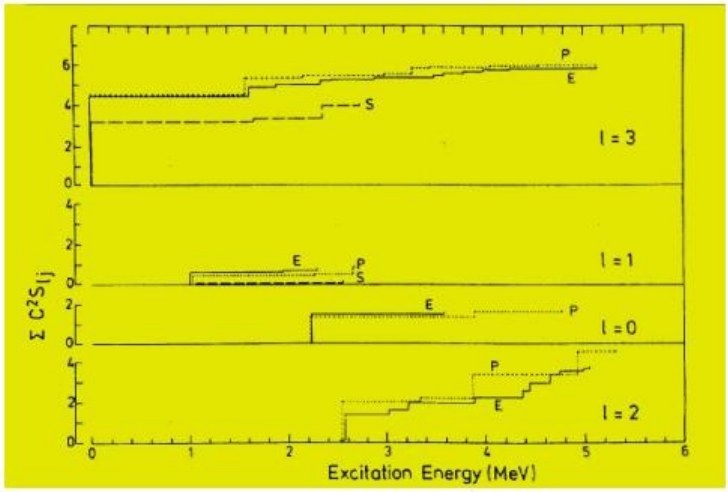

Sums of spectroscopic strengths

E experiment S shell model P IBFM1

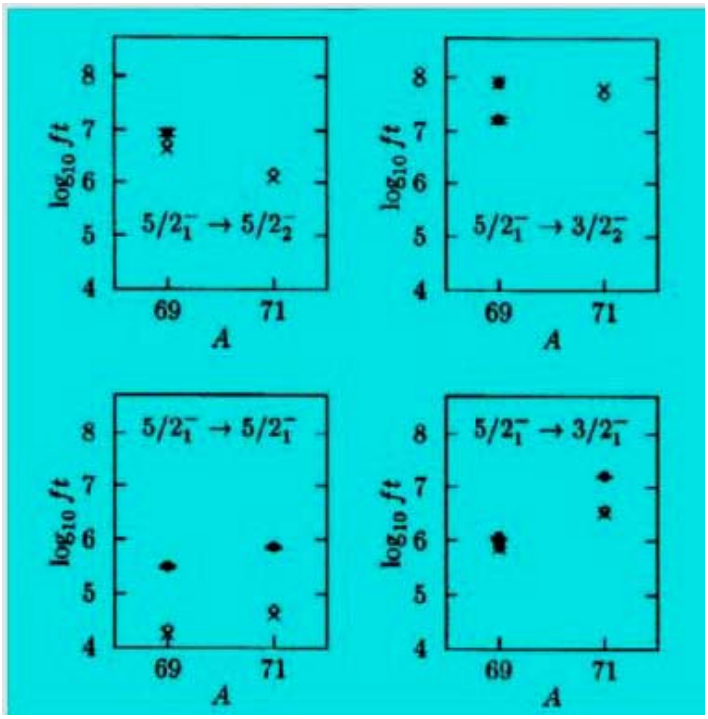

The effect of the additional term

$$\sum_{j',J} \phi^{J}_{jj'}[(a^{\dagger}_{j'} \times d^{\dagger})^{(J)} \times \tilde{d}]^{(j)}_{m}$$

is small

$\mathrm{Log_{10}}$ *ft* values of the β-decay from the As to the Ge isotopes. The symbol • shows the experimental values with their errors, while the symbol x shows the results of calculations with the conventional operators. The symbol ○ shows the results of calculations with the additional d boson number conserving terms.

CONCLUSIONS

The extensions of IBM with fermion degrees of freedom provide a consistent description of nuclear structure phenomena in:

- spherical nuclei
- deformed nuclei
- transitional nuclei

- The structure results from a consistent calculation that includes interaction strengths obtained in the analysis of neighboring nuclei
- All calculations are performed in the laboratory frame, and therefore the results can be directly compared with experimental data
- The models can be related to the shell model
- The symmetry approach can be applyed in special cases
- There is a strong evidence that collective and single-particle degrees of freedom are closely related

Experimental nuclear structure:

F. G. Kondev

Argonne National Laboratory, USA

E-mail: kondev@anl.gov

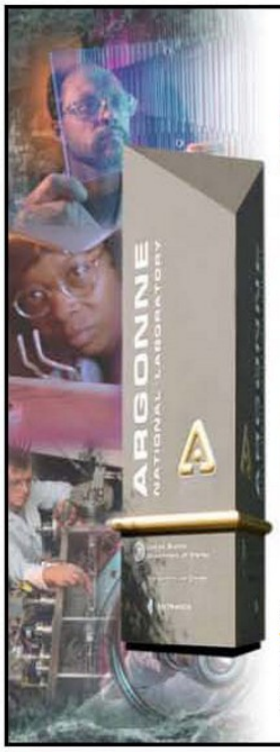

Experimental Nuclear Structure Part I

Filip G. Kondev
kondev@anl.gov

Workshop on "Nuclear Structure and Decay Data: Theory and Evaluation", Trieste, Italy

April 4-15th, 2005

Argonne National Laboratory

A U.S. Department of Energy
Office of Science Laboratory
Operated by The University of Chicago

Outline

I) **Lecture I: Experimental nuclear structure physics**

- **reactions used to populate excited nuclear states**
- **techniques used to measure the lifetime of a nuclear state**
  - ***Coulomb excitation, electronic, specific activity, indirect***
- **techniques used to deduce J^{π}**
  - ***ICC, angular distributions, DCO ratios etc.***

II) **Lecture II: Contemporary Nuclear Structure Physics at the Extreme**

- **spectroscopy of nuclear K-Isomers**
- **physics with large γ–ray arrays**
- **gamma-ray tracking – the future of the γ–ray spectroscopy**

Some Useful Books

"Handbook of nuclear spectroscopy", J. Kantele,1995

"Radiation detection and measurements", G.F. Knoll, 1989

"In-beam gamma-ray spectroscopy", H. Morinaga and T. Yamazaki, 1976

"Gamma-ray and electron spectroscopy in Nuclear Physics", H. Ejiri and M.J.A. de Voigt, 1989

"Techniques in Nuclear Structure Physics", J.B.A. England, 1964

"Techniques for Nuclear and Particle Physics Experiments", W.R. Leo, 1987

"Nuclear Spectroscopy and Reactions", Ed. J. Cerny, Vol. A-C

"Alpha-, Beta- and Gamma-ray Spectroscopy", Ed. K. Siegbahn, 1965

"The Electromagnetic Interaction in Nuclear Spectroscopy", Ed. W.D. Hamilton, 1975

Plenty of information on the Web

Input from many colleagues

C.J. Lister and I. Ahmad, Argonne National Laboratory, USA

M.A. Riley, Florida State University, USA

I.Y. Lee, Lawrence Berkeley National Laboratory, USA

D. Radford, Oak Ridge National Laboratory, USA

A. Heinz, Yale University, USA

C. Svensson, University of Guelph, Canada

G.D. Dracoulis and T. Kibedi, Australian National University, Australia

J. Simpson, Daresbury Laboratory, UK

E. Paul, University of Liverpool, UK

P. Reagan, University of Surrey, UK

and many others …

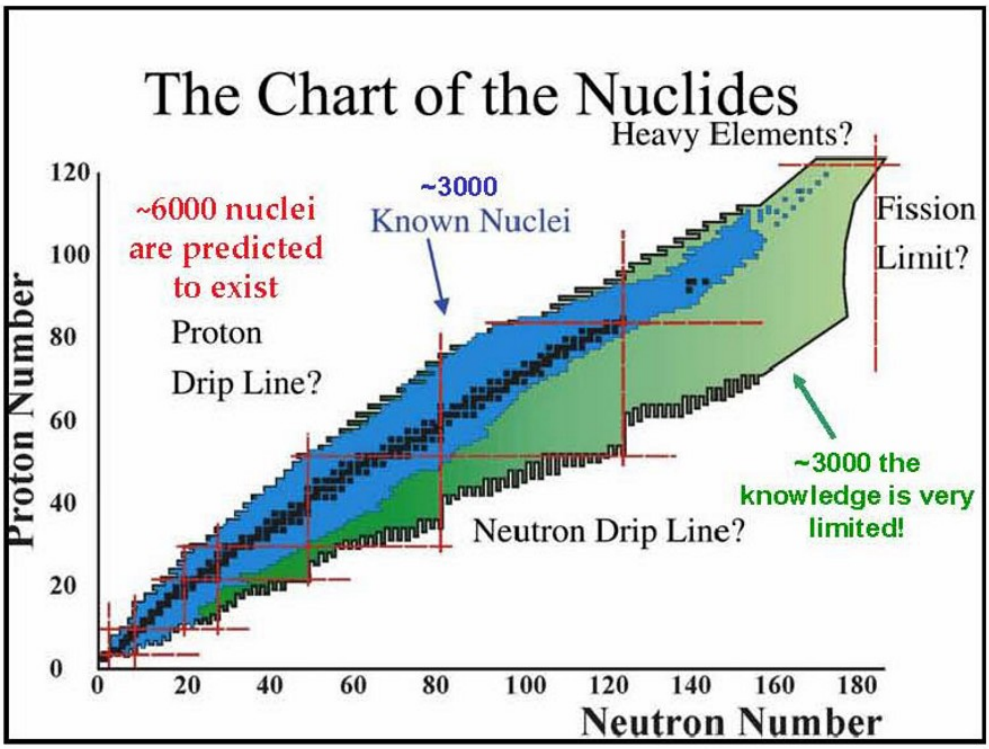

Introduction

- The nucleus is one of nature's most interesting quantal few-body systems
- It brings together many types of behaviour, almost all of which are found in other systems
- The major elementary excitations in nuclei can be associated with single-particle and collective modes.
- While these modes can exist in isolation, it is the interaction between them that gives nuclear spectroscopy its rich diversity

So to summarize …

NUCLEAR PHYSICS IS A BIG CHALLENGE

(because of complicated forces, energy scale, and sizes involved)

The challenge of understanding how nucleon-nucleon interactions build to create the mean field or how single-particle motions build collective effects like pairing, vibrations and shapes

NUCLEAR PHYSICS IS IMPORTANT

(intellectually, astrophysics, energy production, and security)

THIS IS A GREAT TIME IN NUCLEAR PHYSICS

(with new facilities just around the corner we have a chance to make major contributions to the knowledge - with advances in theory we have a great chance to understand it all - by compiling & evaluating data we have a chance to support various applications and to preserve the knowledge for future generations!)

7

Pioneering Science and Technology

Office of Science U.S. Department of Energy

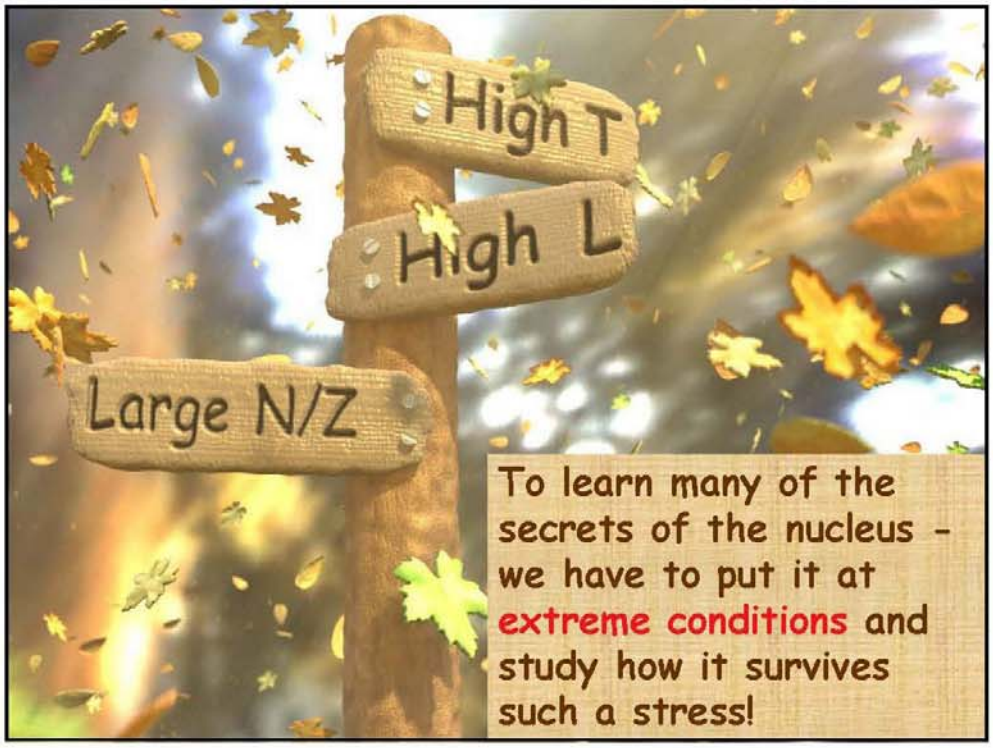

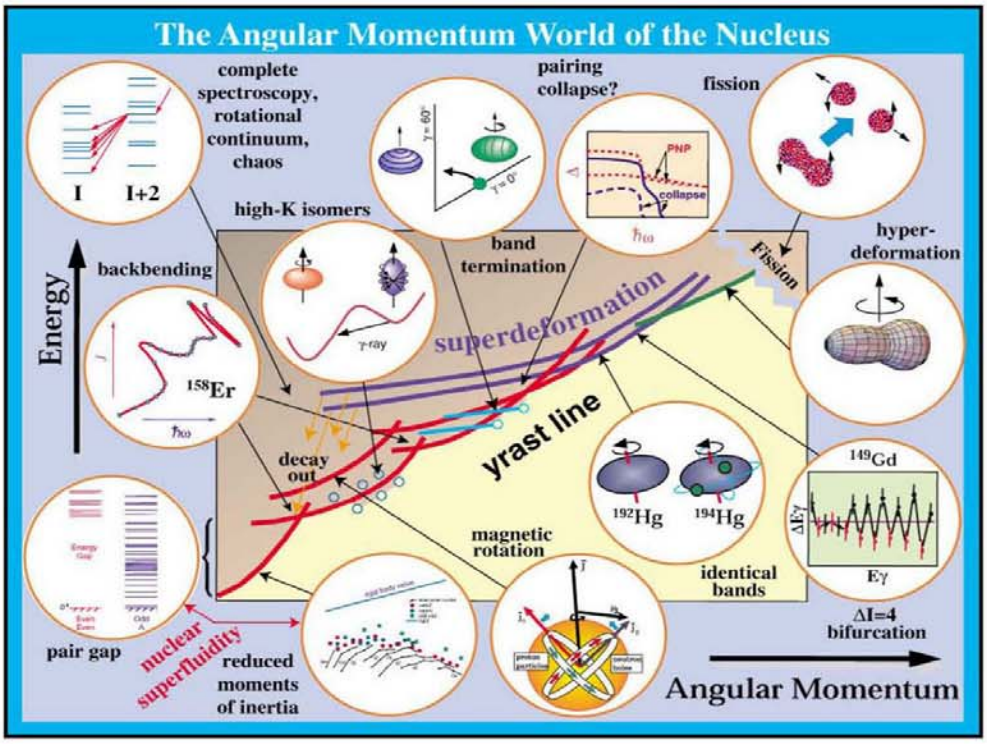

Nuclear Reactions – very schematic!

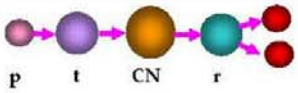

a multi-step process

- Gamma-ray induced
  - no Coulomb barrier
- Neutron induced
  - low-spin states
  - no Coulomb barrier
- Light charged particles, e.g. p, d, t, α
  - Coulomb barrier
  - low-spin states

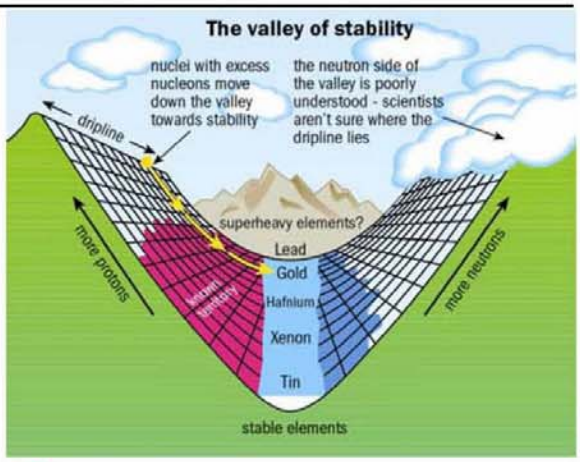

- Heavy Ions (1970 - ????)
  - high-spin phenomena
  - nuclei away from the line of stability

10

Pioneering Science and Technology

Office of Science U.S. Department of Energy

Reactions with Heavy Ions – Classical Picture

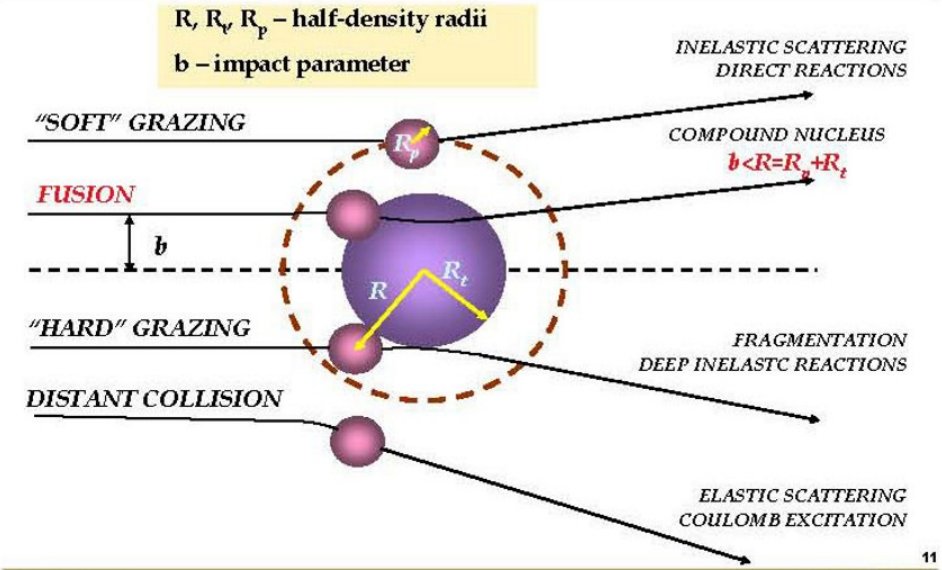

11

Pioneering Science and Technology

Office of Science U.S. Department of Energy

Heavy Ions at the Coulomb Barrier

Many properties of the collision can be quite well estimated by just using conservation of momentum and energy.

$$E_{cm} = M_t / (M_b + M_t)\, E_{lab}$$

Energy scale on which fusion starts is determined by Coulomb barrier, V_{cb}

$$V_{cb} = (4\pi\varepsilon)^{-1} Z_b Z_t e^2 / R = 1.44\, Z_b Z_t / 1.16\, [(A_b^{1/3} + A_t^{1/3}) + 2] \text{ MeV}$$

$$L_{max} = 0.22\, R\, [\, \mu\, (E_{cm} - V_{cb})\,]^{1/2} \qquad \hbar$$

Excitation energy is usually lowered by Q-value and K.E. of evaporated particles

$$E^*_{residue} = E_{cm} + Q - K.E.$$

Velocity of center-of-mass frame, which is ~ velocity of fused residues

$$\beta_r^2 = 2\, M_b c^2\, E_{lab} / [\, (M_b + M_t) c^2]^2$$

12

Pioneering Science and Technology

Office of Science U.S. Department of Energy

HI Fusion-Evaporation Reactions

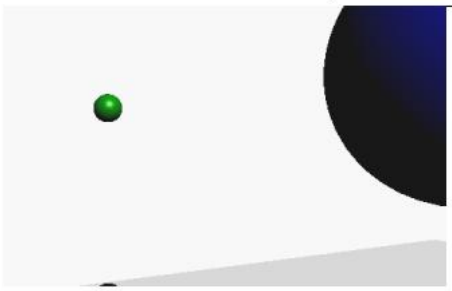

$$\sigma_R = \pi\lambda\!\!\!^{-2} \sum_{l=0}^{l\max} (2l+1)T_l = \pi\lambda\!\!\!^{-2} (l_{\max}+1)^2$$

$$\lambda\!\!\!^{-} = \hbar / \sqrt{2\mu E_{CM}}, \mu = \frac{A_1 A_2}{A_1 + A_2}$$

$$l_{\max}^2 = \left(\frac{2\mu R^2}{\hbar^2}\right)(E_{CM} - V_C)$$

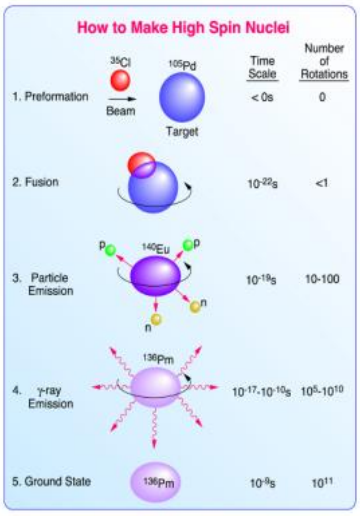

Pioneering Science and Technology

Office of Science U.S. Department of Energy

Decay of the Compound Nucleus

- In a typical HI fusion-evaporation reaction the final nucleus is often left with L~60-80 hbar and E_x~30-50 MeV

- The excited nucleus cools off by emitting γ–rays - their typical number is quite large, usually 30-40 and the average energy is ~1-2 MeV – it is not a trivial task to detect all of them - the big advantage came with the large γ–ray arrays

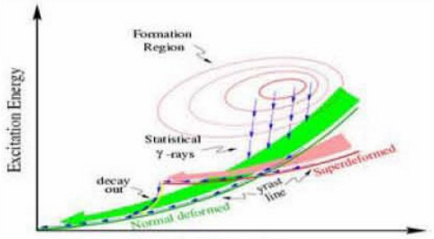

Pioneering Science and Technology

Office of Science U.S. Department of Energy

Channel Selection for γ-ray Spectroscopy

Detection of Light Charged Particles (α,p,n)

PLUS Efficient, flexible, powerful.....inexpensive.

MINUS Count-rate limited, Contaminant (Carbon etc, isotopic impurities) makes absolute identification of new nuclei difficult.

CROSS SECTION LOWER LIMIT ~100 μb that is, $\sim 10^{-4}$

Detection of Residues in Vacuum Mass Separator

PLUS True M/q, even true M measurement. With suitable focal plane detector can be ULTRA sensitive. Suppresses contaminants.

MINUS Low Efficiency

CROSS SECTION LOWER LIMIT ~100 nb that is $\sim 10^{-7}$

Detection of Residues in Gas Filled Separator

Improves efficiency of vacuum separators, at cost of mass information and clenliness. In some cases (heavy nuclei) focal plane counters clean up the data for good sensitivity.

15

Pioneering Science and Technology

Office of Science U.S. Department of Energy

Some Channel Selection Detectors

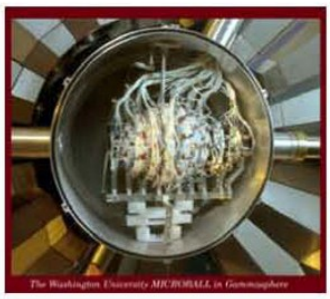

Argonne FMA

USA

Light charged-particle detector

Microball – 96 CsI with photo diodes

USA

Jyvaskyla

RITU

Europe

16

Pioneering Science and Technology

Office of Science U.S. Department of Energy

Calculate Reaction Rates

Reaction Yield/sec. $Y = N_b N_t \sigma$

$N_b = i_b/e\ q$
with i_b = electric current in amps, q = charge state, e = $1.6\ 10^{-19}$ c

$N_t = [N_a/A]\ \rho x$
with N_a = Avagadros #, A = Mass # of tgt, ρ = density in g/cc, x = thickness (cm).

σ= Cross Section in cm^2 .... note 1 barn is 10^{-24} cm

Accumulated data: $D = Y \times TIME \times Efficiency$

Typical "far from stability" near barrier experiment may have:
i_b = 100 nA, q=10, A=100, $\rho x = 10^{-3}$ & σ=1 barn - produces $3x10^5$ reactions/sec

BUT

If partial cross section is 100 nb and efficiency is 10%..... rate is 10 /hour, 10 pb gives ~ 1 every 10 weeks!!!.....the present situation for producing the heavies elements.

17

Pioneering Science and Technology

Office of Science U.S. Department of Energy

The basic knowledge

What we want to know

- Excitation energy
- Quantum numbers and their projections
- Lifetime
- Branching ratios

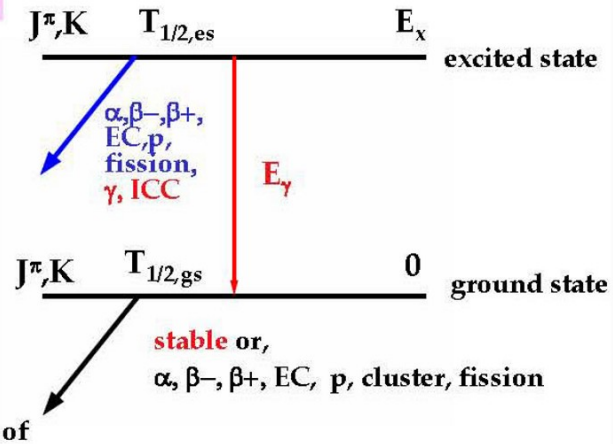

How

- By measuring properties of signature radiations

18

Pioneering Science and Technology

Office of Science U.S. Department of Energy

What is Stable?

A surprisingly difficult question with a somewhat arbitrary answer!
CAN'T Decay to something else, BUT

CAN'T Decay is a Philosophical Issue

- Violation of some quantity which **we believe** is conserved such as Energy, Spin, Parity, Charge, Baryon or Lepton number, etc.

DOESN'T Decay is an Experimental Issue that backs up the beliefs

Specific Activity: $A=dN/dt = \lambda N$

Activity of 1 mole of material (6.02×10^{23} atoms) with $T_{1/2}=10^9$ y ($\lambda=2.2 \times 10^{-17}$ s) is ~0.4 mCi (1 Ci=3.7×10^{10} dps) (or 13 MBq) .... a blazing source, so it is quite easy to set VERY long limits on stability.

Current limit on proton half-life, based on just counting a tank of water is $T_{1/2} > 1.5 \times 10^{25}$ yr.

Stable Nuclei: Segre's Chart

~ 280 Nuclei have Half-lives $>10^6$ years

So are (quite) stable against

Decay of their constituents (p,n,e)

Weak Decay (β^+ β^- and E.C.)

α,p,n decays

More complex cluster emission

Fission

(Mostly because of energy conservation)

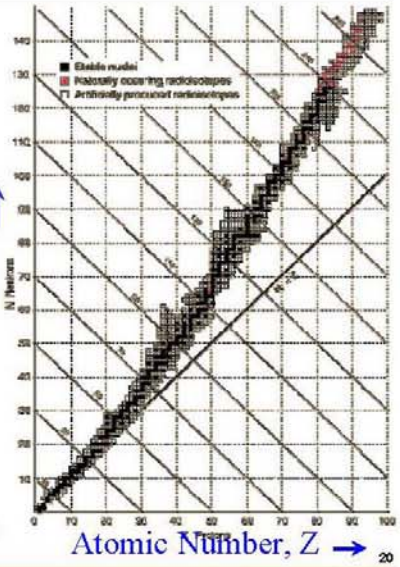

Mean Lifetime

$$f_{decay}(t) = \frac{Ae^{-\lambda t}}{\int_0^\infty Ae^{-\lambda t}\,dt} = \lambda e^{-\lambda t}$$

Probability for decay of a nuclear state (normalized distribution function); **λ** – decay constant

$$P_n(t) = \int_0^t \lambda e^{-\lambda t'} dt'$$

Probability that a nucleus will decay within time *t*

$$1 - P_n(t) = 1 - \int_0^t \lambda e^{-\lambda t'} dt' = e^{-\lambda t}$$

Probability that a nucleus will remain at time *t*

$$< t >= \tau = \int_0^\infty t e^{-\lambda t} dt = \frac{1}{\lambda}$$

The average survival time (mean lifetime - **τ**) is then the mean value of this probability

Half-life & Decay Width

$T_{1/2}$: the time required for half the atoms in a radioactive substance to disintegrate

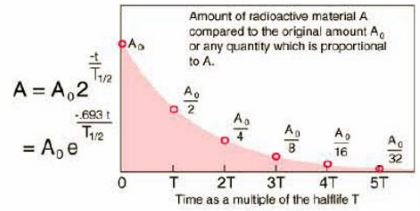

relation between τ, $T_{1/2}$ and **λ** $\tau = \frac{T_{1/2}}{\ln 2} = \frac{1}{\lambda}$

$$\Gamma = \frac{\hbar}{\tau} = \frac{6.58 \times 10^{-16}}{\tau[s]} \quad [\text{eV}]$$

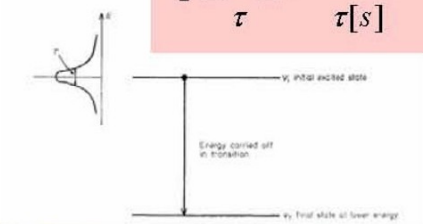

$$\Gamma \propto |< \psi_1 | M | \psi_2 >|^2$$

Determine the matrix element describing the mode of decay between the initial and final state

log ft Values

$$\log ft = \log f + \log t$$

$t \equiv T_{1/2}^{\beta_i} = \dfrac{T_{1/2}}{BR_i}$ partial half-life of a given β^- (β^+, EC) decay branch

$f \equiv f_\beta \equiv f_n, n = 0,1,2\ldots$

statistical rate function (phase-space factor): the energy & nuclear structure dependences of the decay transition

Decay Mode	Type	log *ft*
β–	allowed	$\log f_0^-$
β–	1st-forb	$\log f_0^- + \log(f_1^-/f_0^-)$
EC+β+	allowed	$\log(f_0^{EC} + f_0^+)$

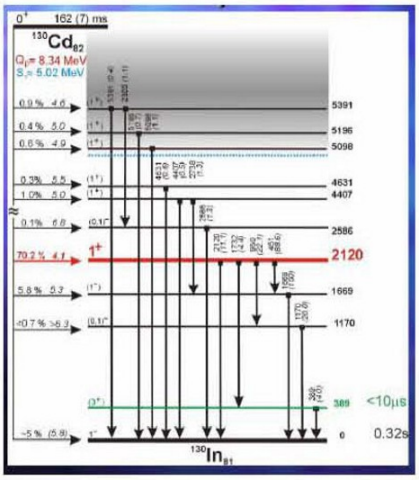

$f_0^-, f_1^-, etc.$ N.B. Gove and M. Martin, Nuclear Data Tables **10** (1971) 205

Hindrance Factor in α–decay

$$|I_i - I_f| \le L \le |I_i + I_f|$$

$$\pi_i \pi_f = (-1)^L$$

Strong dependence on L

L=0 - unhindered decay (fast)

$$HF_i = \frac{T_{1/2}^{Exp}(\alpha_i)}{T_{1/2}^{Theory}} = \frac{T_{1/2}^{Exp}/BR_i}{T_{1/2}^{Theory}}$$

$T_{1/2}^{Theory}$ M.A. Preston, Phys. Rev. **71** (1947) 865

$$t_{1/2}^{\alpha} = \ln 2 \frac{r_c}{2v} \frac{\mu^2(H_i^2 + K_i^2) + \tan^2\alpha_0(C_i^2 + S_i^2) + 2\mu\tan\alpha_0(C_iK_i - S_iH_i)}{\mu^2\tan\alpha_0(H_iC_i + K_iS_i)Q_i}\Bigg|_{\alpha=0}$$

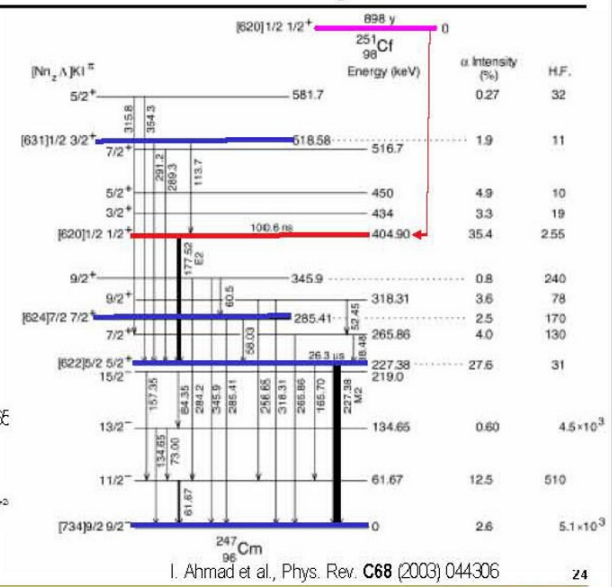

I. Ahmad et al., Phys. Rev. **C68** (2003) 044306

γ–ray Decay

$$|I_i - I_f| \le L \le |I_i + I_f|$$

$\Delta\pi(EL) = (-1)^L$ electric multipole

$\Delta\pi(ML) = (-1)^{L+1}$ magnetic multipole

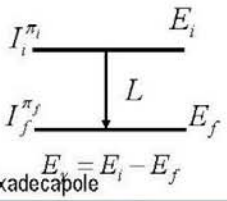

dipole	quadrupole	octupole	hexadecapole	
E1:L=1,yes	E2:L=2,no	E3:L=3,yes	E4:L=4,no	E5:L=5,yes
M1:L=1,no	M2:L=2,yes	M3:L=3,no	M4:L=4,yes	M5:L=5,no

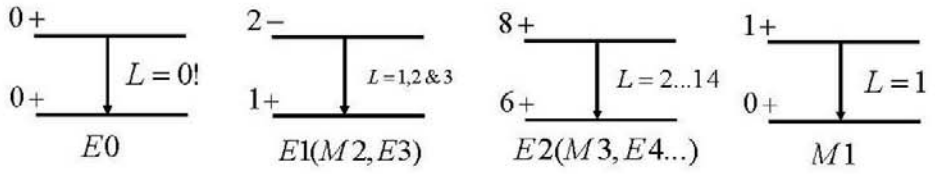

25

Pioneering Science and Technology

Office of Science U.S. Department of Energy

Partial Lifetime & Transition Probability

$$T_{1/2}^{\gamma} = T_{1/2}^{\exp} \times \frac{\sum I_{\gamma_i} \times (1 + \alpha_{\gamma_i})}{I_\gamma}$$

partial half-life

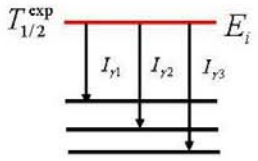

$$P_\gamma(XL: I_i \to I_f) = \frac{\ln 2}{T_{1/2}^{\gamma}} = \frac{8\pi(L+1)}{L[(2L+1)!!]^2}\left(\frac{E_\gamma}{\hbar c}\right)^{2L+1} B(XL: I_i \to I_f)$$

partial γ–ray Transition Probability reduced Transition Probability

$$B(XL: I_i \to I_f) = \frac{\left|\langle I_i \| M(XL) \| I_f \rangle\right|^2}{2I_i + 1}$$

contains the nuclear structure information

26

Pioneering Science and Technology

Office of Science U.S. Department of Energy

Hindrance Factor in γ–ray Decay

$$F_{W(N)} = \frac{B(XL)_{Theory}}{B(XL)_{Exp}} = \frac{T^{\gamma}_{1/2}(XL)_{Exp}}{T^{\gamma}_{1/2}(XL)_{Theory}}$$

... usually an upper limit, but ...

Hindrance Factor: Weisskopf (W): based on spherical shell model potential

Nilsson (N): based on deformed Nilsson model potential

EL	$B(EL)_W, e^2 fm^{2L}$	$T^{\gamma}_{1/2}(EL)_W$, sec	ML	$B(ML)_W, \mu_N^2 fm^{2L-2}$	$T^{\gamma}_{1/2}(ML)_W$, sec
E1	$0.06446A^{2/3}$	$6.762A^{-2/3}E_\gamma^{-3}\times10^{-15}$	M1	1.7905	$2.202E_\gamma^{-3}\times10^{-14}$
E2	$0.0594A^{4/3}$	$9.523A^{-4/3}E_\gamma^{-5}\times10^{-9}$	M2	$1.6501A^{2/3}$	$3.100A^{-2/3}E_\gamma^{-5}\times10^{-8}$
E3	$0.0594A^{2}$	$2.044A^{-2}E_\gamma^{-7}\times10^{-2}$	M3	$1.6501A^{4/3}$	$6.655A^{-4/3}E_\gamma^{-7}\times10^{-2}$
E4	$0.06285A^{8/3}$	$6.499A^{-8/3}E_\gamma^{-9}\times10^{4}$	M4	$1.7458A^{2}$	$2.116A^{-2}E_\gamma^{-9}\times10^{5}$
E5	$0.06929A^{10/3}$	$2.893A^{-10/3}E_\gamma^{-11}\times10^{11}$	M5	$1.9247A^{8/3}$	$9.419A^{-8/3}E_\gamma^{-11}\times10^{11}$

Quadrupole Deformation

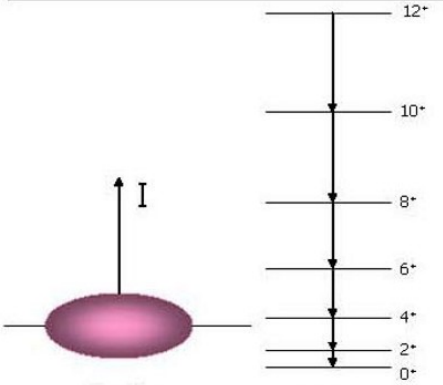

$I = J\omega$

^{156}Dy

$E_I = \hbar^2/2J\ I(I+1)$

B(E2) ~ 200 W.U.

deformed nucleus

$$B(E2) = \frac{8.16\times10^{13}}{E_\gamma^5[keV]\tau_\gamma[ps]}[e^2b^2]$$

$$B(E2; KI_i \rightarrow KI_f) = \frac{5}{16\pi}Q_0^2\left\langle I_i K20 \middle| I_f K\right\rangle^2$$

(from collective models)

$$\beta_2 \approx -7\sqrt{\frac{\pi}{80}} + \sqrt{\frac{49\pi}{80} + \frac{7\pi Q_0}{6eZr_0^2A^{2/3}}}$$

$$\tau_\gamma[ps] = (1.58\pm0.28)\times10^{14}E_{2_1^+}^{-4}[keV]Z^{-2}A^{2/3}$$

$$\beta_2 = \frac{466\pm41}{A\times\sqrt{E_{2_1^+}[keV]}}$$

Octupole Deformation

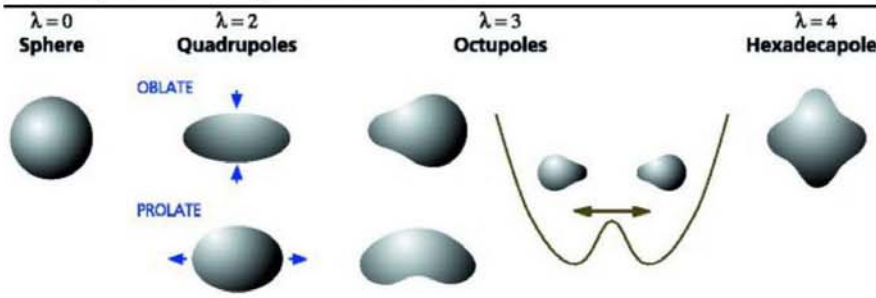

$$\tau_{E3}[s] = 0.012264 \times E_{3_1^-}^{-7} \times [B(E3)\uparrow]^{-1}$$

$$E_{3_1^-}[MeV]; B(E3)\uparrow [e^2 fm^6]$$

$$\beta_3 = \frac{4\pi}{ZR^3}\sqrt{\frac{B(E3)\uparrow}{e^2}}$$

K-forbidden Decay

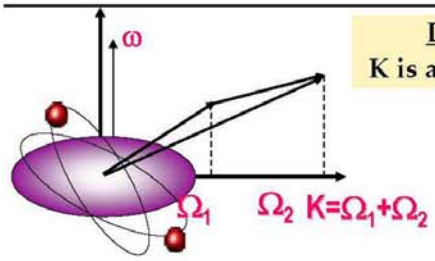

Deformed, axially symmetric nuclei
K is approximately a good quantum number
each state has not only
J^π but also K

- The solid line shows the dependence of F_W on ΔK for some E1 transitions according to an empirical rule: $\log F_W = 2\{|\Delta K| - \lambda\} = 2\nu$
- i.e. F_W values increase approximately by a factor of 100 per degree of K forbiddenness
- $f_\nu = (F_w)^{1/\nu}$ – reduced hindrance per degree of K forbiddenness

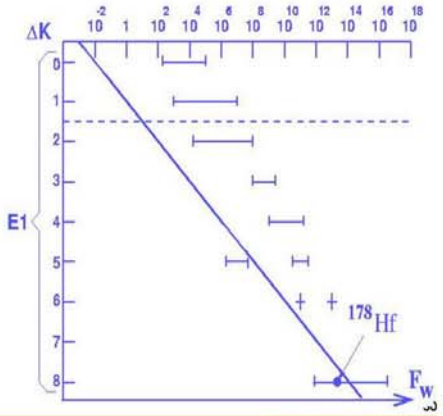

Experimental Techniques

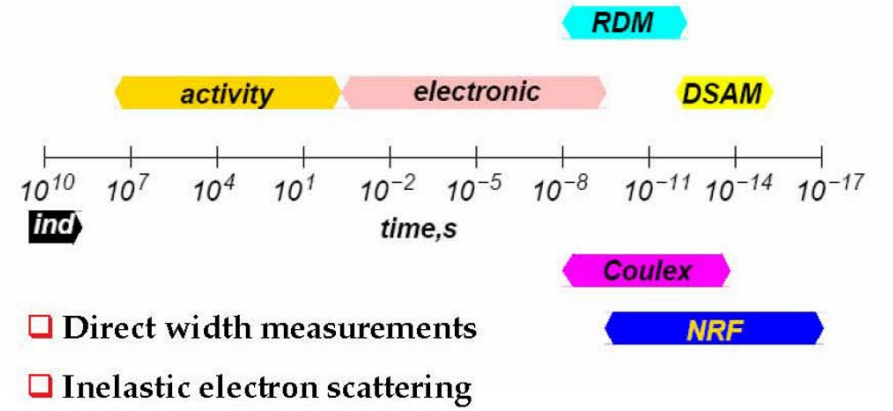

- Direct width measurements
- Inelastic electron scattering
- Blocking technique
- Mossbauer technique

Specific Activity

Time Range: a few seconds up to several years

$$A = \lambda N = \lambda N_0 e^{-t/\tau}$$

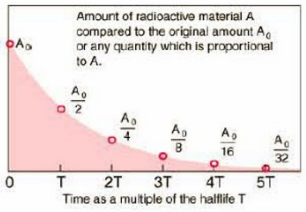

- Statistical uncertainties are usually small
- Systematic uncertainties (dead time, geometry, etc.) dominate

usually want to follow at least 5 x $T_{1/2}$

Tag on specific signature radiations (α, β, ce or γ) in a "singles" mode

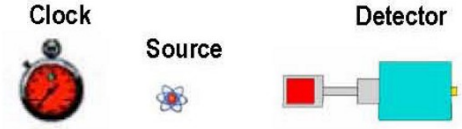

Specific Activity: Example 1

PHYSICAL REVIEW C, VOLUME 63, 047307

Half-lives of Au, Hg, and Pb isotopes from photoactivation

K. Lindenberg, F. Neumann, D. Galaviz, T. Hartmann, P. Mohr, K. Vogt, S. Volz, and A. Zilges
Institut für Kernphysik, Technische Universität Darmstadt, Schlossgartenstraße 9, D-64289 Darmstadt, Germany

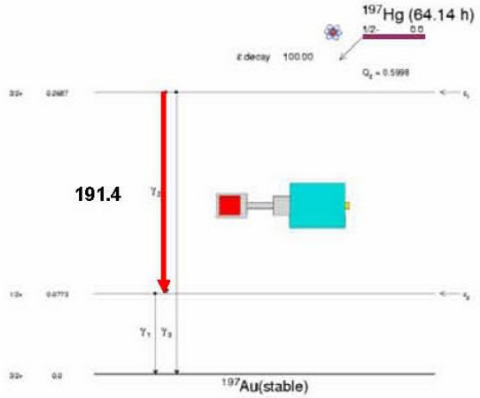

- More than 270 spectra were measured
- Followed 4 x $T_{1/2}$

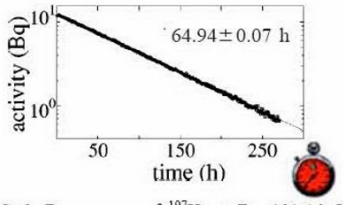

FIG. 3. Decay curve of ^{197}Hg at E_γ=191.4 keV.

Specific Activity: Example 2

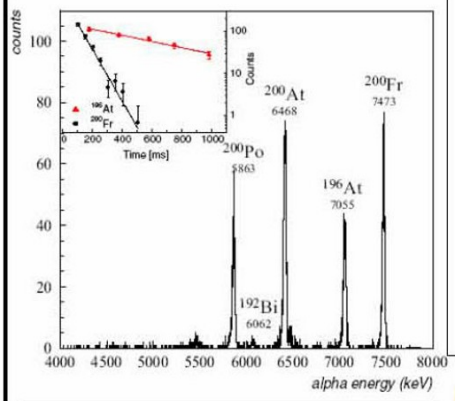

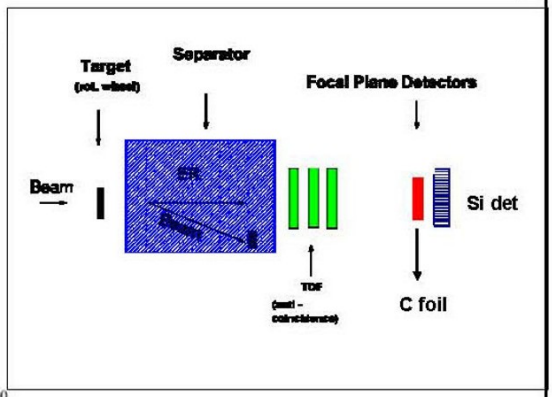

Isotope	Energy (keV)	$T_{1/2}$	Reference
^{200}Fr	7473(12)	49(4) ms	this work
	7500(30)	570^{+270}_{-140} ms	[4]
	7468(9)	19^{+13}_{-6} ms	[5]

1 GeV pulsed proton beam on 51 g/cm2 ThCx target

on-line mass separation (ISOLDE)/CERN

H. De Witte et al., EPJ A23 (2005) 243

Very Long-lived Cases – Example 1

Time Range: longer than 10^2 yr

$$A = \lambda N \qquad T_{1/2} = \ln 2 \frac{N_{182}}{A_{182}}$$

the number of atoms estimated by other means, e.g. mass spectrometry

VOLUME 93, NUMBER 17 PHYSICAL REVIEW LETTERS week ending 22 OCTOBER 2004

New Half-Life Measurement of ^{182}Hf: Improved Chronometer for the Early Solar System

C. Vockenhuber,[1,*] F. Oberli,[2] M. Bichler,[3] I. Ahmad,[4] G. Quitté,[2] M. Meier,[2] A. N. Halliday,[2] D.-C. Lee,[5] W. Kutschera,[1] P. Steier,[1] R. J. Gehrke,[6] and R. G. Helmer[6]

^{180}W	^{181}W	^{182}W	^{183}W	^{184}W	^{185}W	^{186}W
^{179}Ta	^{180}Ta	^{181}Ta	^{182}Ta	^{183}Ta	^{184}Ta	^{185}Ta
^{178}Hf	^{179}Hf	^{180}Hf	^{181}Hf	^{182}Hf	^{183}Hf	^{184}Hf
^{177}Lu	^{178}Lu	^{179}Lu	^{180}Lu	^{181}Lu	^{182}Lu	^{183}Lu

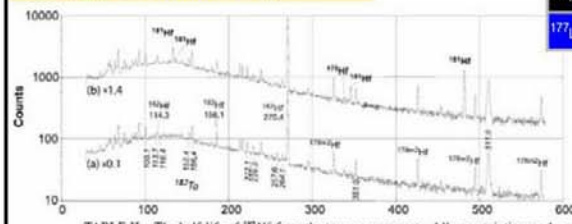

Material	Atomic abundance (%) ^{174}Hf	^{176}Hf	^{177}Hf	^{178}Hf	^{179}Hf	^{180}Hf	^{182}Hf
Helmer 1	≈ 0.0058	4.791	0.605	29.06	25.77	39.64	0.124
Helmer 2	≈ 0.00014	4.377	0.149	17.15	31.30	46.91	0.112
Natural	0.16	5.21	18.60	27.30	13.63	35.10	

TABLE II. The half-life of ^{182}Hf from the two measurements. All uncertainties are 1σ uncertainties.

Material	Method	Half-life ($\times 10^6$ yr)	Uncorrelated uncertainty ($\times 10^6$ yr)	Total uncertainty ($\times 10^6$ yr)
Helmer 1	Neutron activation + activity measurement	9.034	±0.241	±0.251
Helmer 2	Isotope dilution + activity measurement	8.896	±0.057	±0.089
	Weighted mean	8.904	±0.056	±0.088

35

Pioneering Science and Technology

Office of Science U.S. Department of Energy

Very Long-lived Cases – Example 2

$$\frac{A_p(t)}{A_d(t)} = \frac{\lambda_d}{\lambda_d - \lambda_p}\left(1 - e^{-(\lambda_d - \lambda_p)t}\right)$$

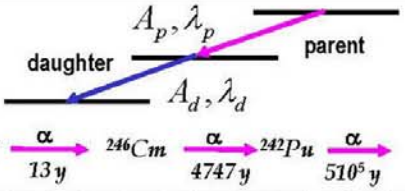

$^{250}Cf \xrightarrow{\alpha,\ 13\ y} {}^{246}Cm \xrightarrow{\alpha,\ 4747\ y} {}^{242}Pu \xrightarrow{\alpha,\ 510^5\ y}$

$T_{1/2}(^{250}Cf)$=13.05 (9) y

- *Mass separated samples (1975!)*
- *Parent/daughter activity*
- *Alpha counting technique*

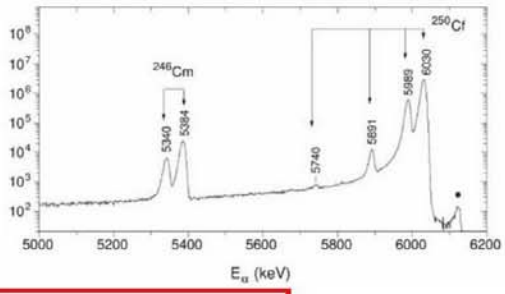

$T_{1/2}$ = 4747 (46) *years / Compared to values ranging from* $T_{1/2}$=2300 *up to 6620 years*

36

Pioneering Science and Technology

Office of Science U.S. Department of Energy

Electronic Techniques

Time Range: tens of ps up to a few seconds

The "Clock" - TAC, TDC (START/STOP); Digital Clock

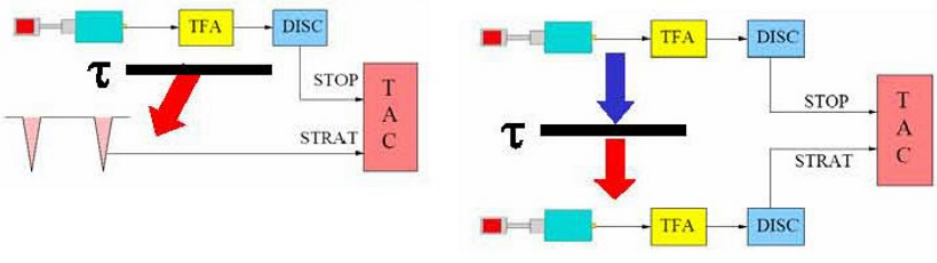

"singles" – E_γ-time, E_α-time

"coincidence" – $E_{\gamma 1}$-$E_{\gamma 2}$-Δt ; $E_{\alpha 1}$-$E_{\gamma 1}$-Δt
$E_{\alpha 1}$-$E_{\alpha 2}$-Δt

Difficulties at the boundary: e.g. for very short– and very long-lived cases!

37

Pioneering Science and Technology

Office of Science U.S. Department of Energy

Prompt Response Function

- **all detectors and auxiliary electronics show statistical fluctuations in the time necessary to develop an appropriate pulse for the "clock"**
  - **depend on the characteristics of the detectors: e.g. light output for scintillators, bias voltage, detector geometry, etc.**
  - **instrumental imperfections in the electronics – e.g. noise in the preamplifiers**

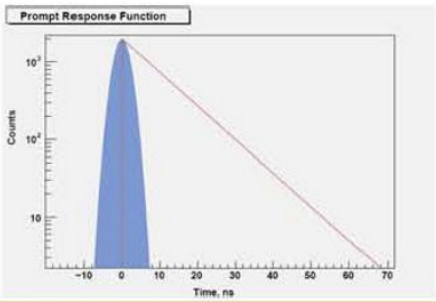

Some typical values

Detector	FWHM, ps
plastic scintillators	~100
BaF_2	~100
Si	~200
Na(I)	~500
Ge	0.6-9 ns

38

Pioneering Science and Technology

Office of Science U.S. Department of Energy

Prompt Response Function Ge Detectors

$$F(x,\lambda) = \int_{-\infty}^{\infty} f(t,\lambda)\,P(x-t)\,dt$$

$f(t,\lambda) = \lambda e^{-\lambda t}\,(t \geq 0) or = 0 (t < 0)$ **decay**

PRF $P(z) = \frac{1}{\sigma\sqrt{2\pi}} e^{-\frac{1}{2}(z/\sigma)^2}$

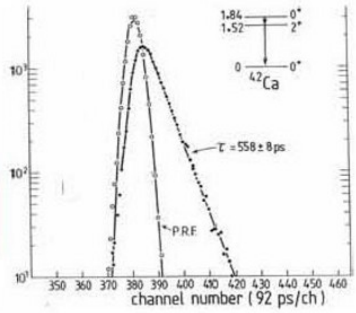

a schematic illustration

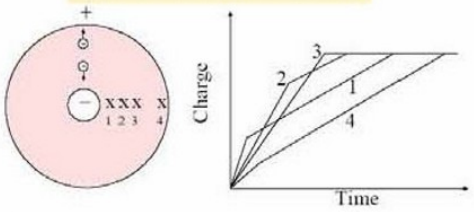

PRF depends on:

- ❑ the size of the detector
- ❑ the energy of the γ–ray

39

Recoil-shadow Technique

the shortest lifetime that can be measured is limited by the TOF

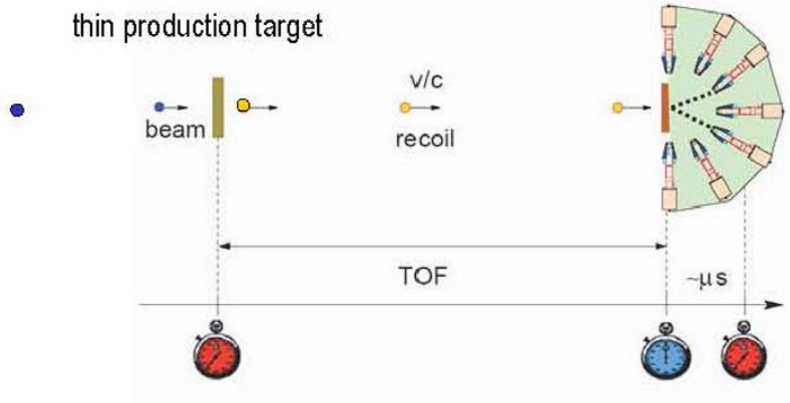

40

One example: ^{140}Dy experiment at ANL

^{54}Fe + ^{92}Mo @ 245 MeV

α2n channel, mass 140 only 5% from the total CS

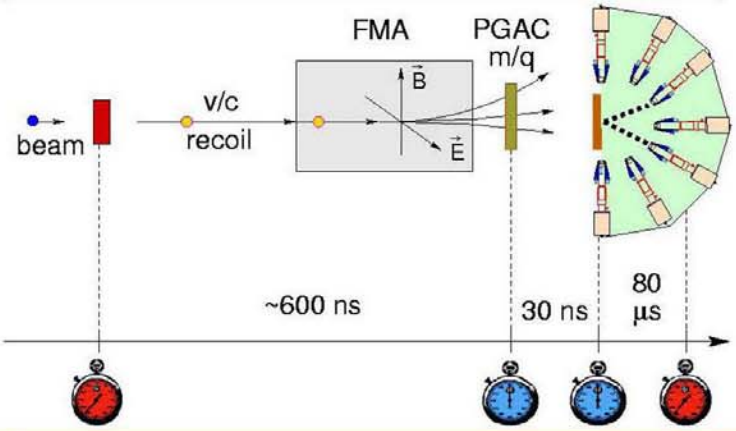

Pioneering Science and Technology

Office of Science U.S. Department of Energy

Some of the equipment used

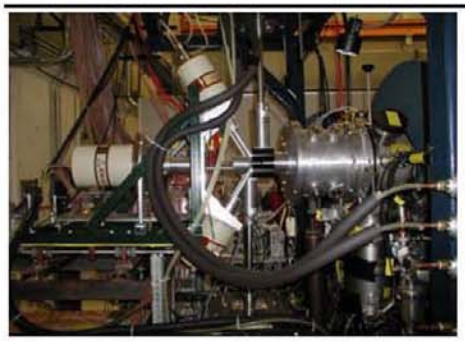

1 70% Gammasphere HpGe detector
4 25% Golf-club style HPGe detectors
2 LEPS detectors
1 2"x2" Large Area Si detector

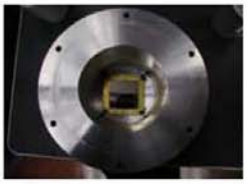

2"x2" Si Detector

Pioneering Science and Technology

Office of Science U.S. Department of Energy

^{140}Dy: Experimental Results

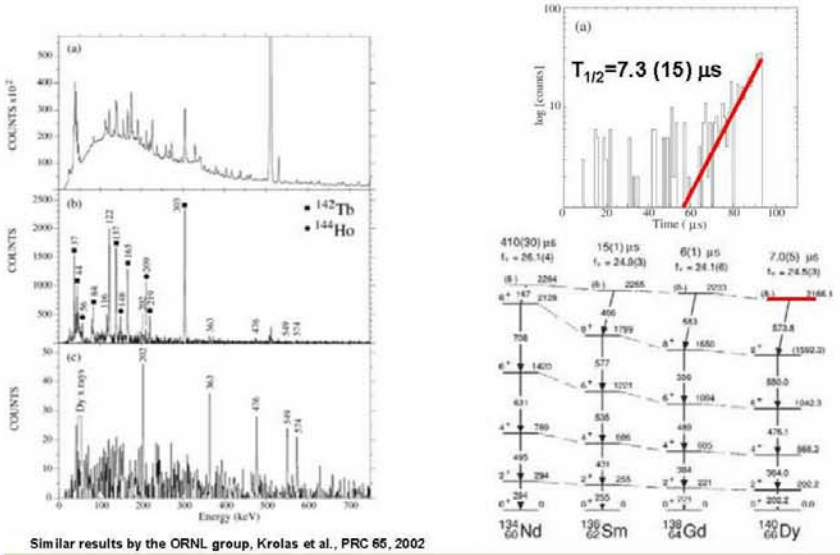

Similar results by the ORNL group, Krolas et al., PRC 65, 2002

43

Pioneering Science and Technology

D.M. Cullen et al., Phys. Lett. B529 (2002)

Office of Science U.S. Department of Energy

Recoil-decay Tagging

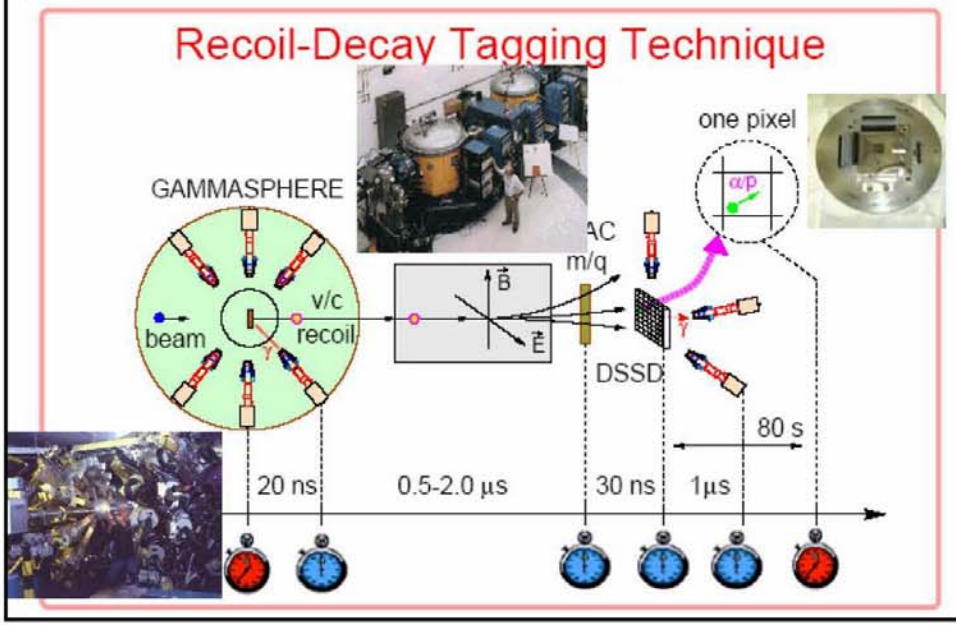

Heart of RDT: DSSD

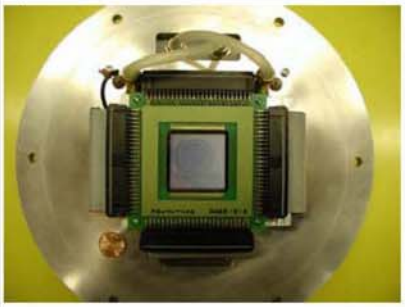

80 x 80 detector 300 μm strips,
Each with high, low, and delay line amplifiers, for implant, decay, and fast-decay recognition.

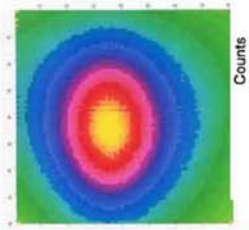

Data from DSSD showing implant pattern 40 cm beyond the focal plane

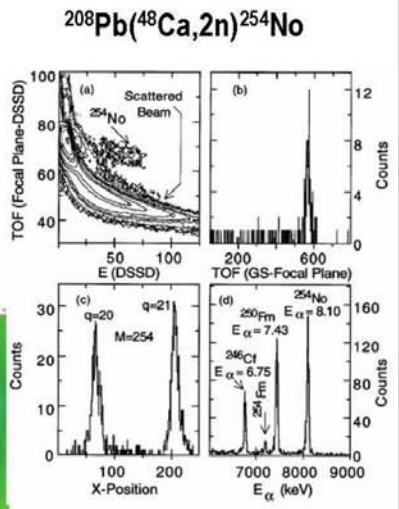

45

Pioneering Science and Technology

Office of Science U.S. Department of Energy

α–α (parent-daughter) Correlations

Implantation->Decay 1->Decay 2 within a single pixel

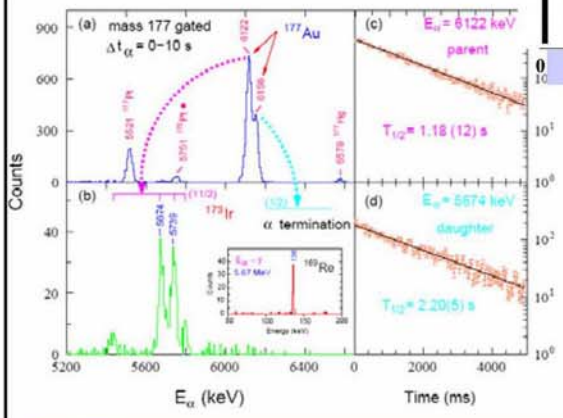

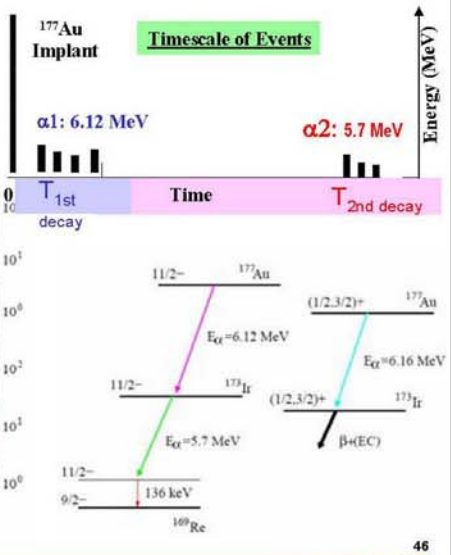

46

Pioneering Science and Technology

F.G. Kondev et al. Phys. Lett. B528 (2002) 221

Office of Science U.S. Department of Energy

Neutron Deficient Nuclei

Severe complications

- Charged particle emission:
  - → The fusion-evaporation cross section is fragmented into many channels.
    - → It limits the absolute production.
- Fission process: *fissibility parameter* ~ Z^2/A
  - → Depletion of the high-l values.
    - → It limits the population of residues at high angular momentum.
  - → Huge, unwanted background.

47

Pioneering Science and Technology

Office of Science U.S. Department of Energy

Odd-Z Au (Z=79) Isotopes

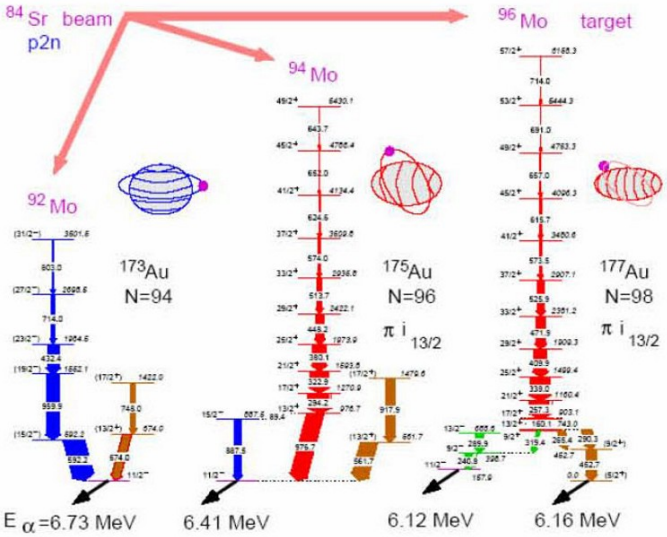

48

Pioneering Science and Technology

F.G. Kondev et al. Phys. Lett. B528 (2002) 221

Office of Science U.S. Department of Energy

Odd-Z Au (Z=79) Isotopes – sample spectra

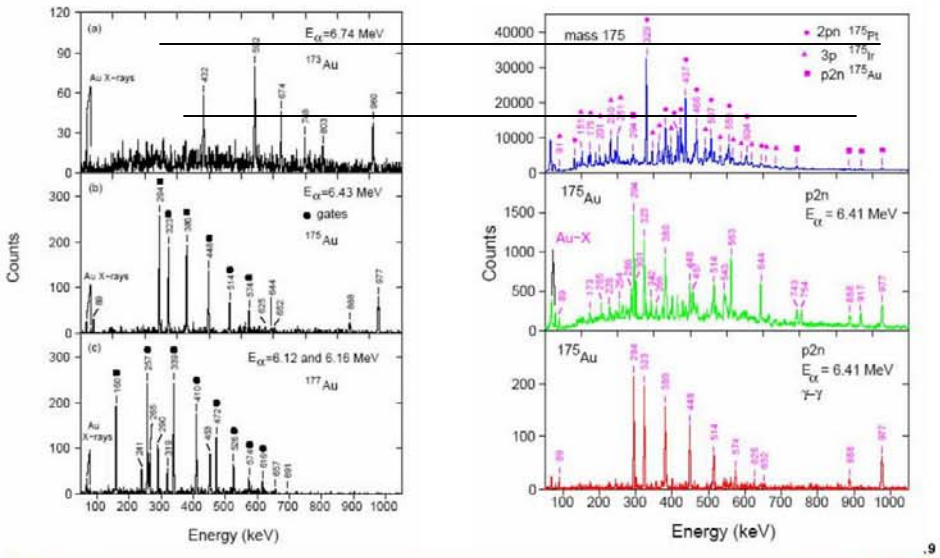

Pioneering Science and Technology

Office of Science U.S. Department of Energy

.9

α–γ Correlations

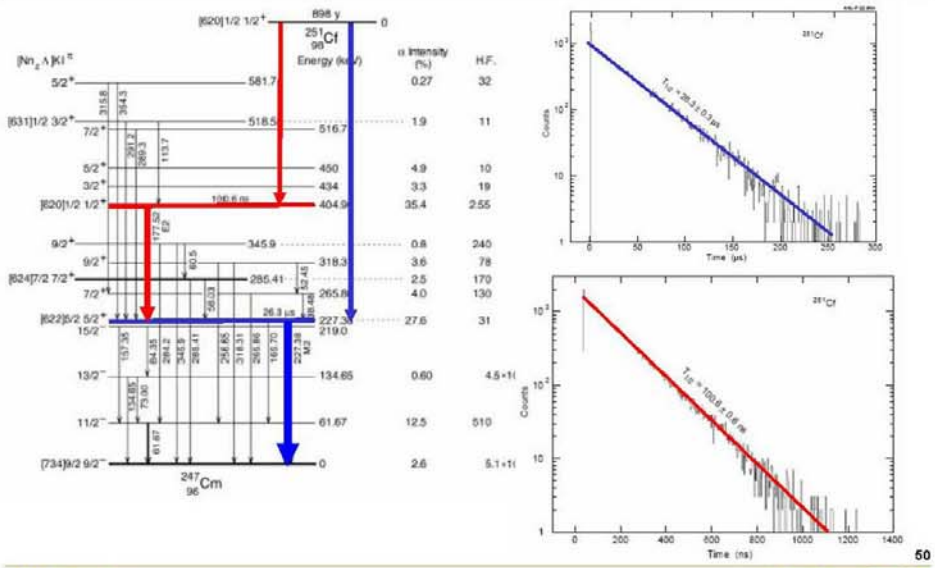

Pioneering Science and Technology

I. Ahmad et al., Phys. Rev. **C68** (2003) 044306

Office of Science U.S. Department of Energy

50

Pulsed Beam Technique

the shortest lifetime that can be measured is limited by the width of the pulsed beam

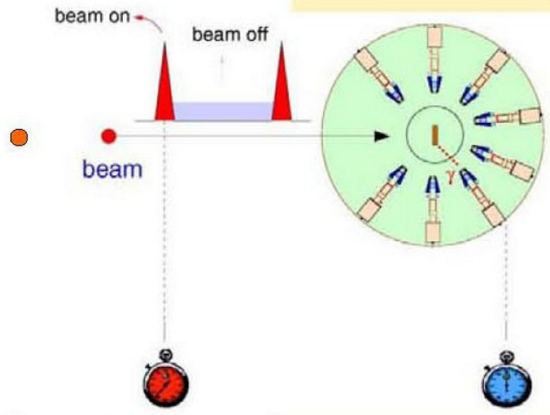

- **Less effective, but …**
  - ✓ **well defined "clock"**
  - ✓ **sensitive to in-beam and decay events**

- **"singles": γ–time**
- **coincidence: γ–γ–time**

the longest lifetime that can be measured is limited by the time interval between the beam pulses

Pulsed Beam γ–time

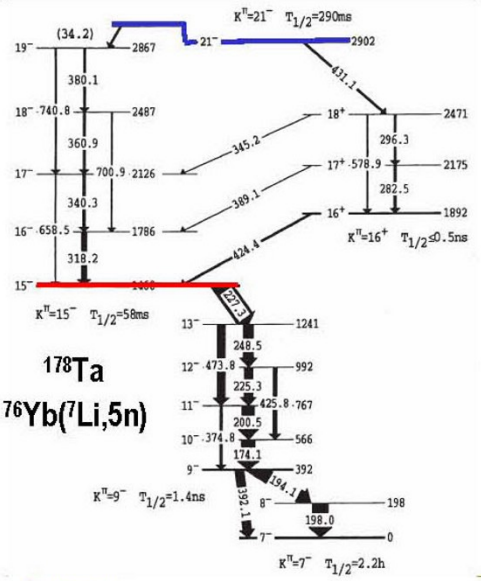

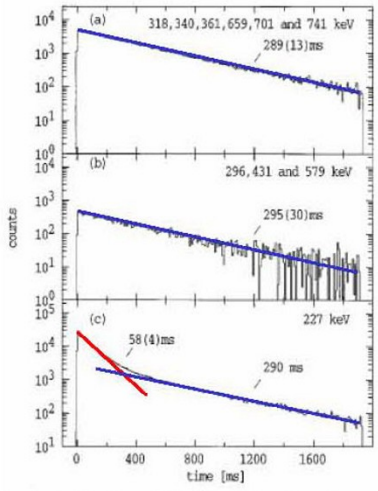

reveals the time history of levels above the 58 ms isomer !

F.G. Kondev et al. Phys. Rev. C54 (1996) R459

Pulsed Beam γ–time (short–lived)

The importance of PRF

In γ–time measurements PRF depends on E_γ for a single transition

^{175}Ta

^{170}Er(^{10}B,5n)

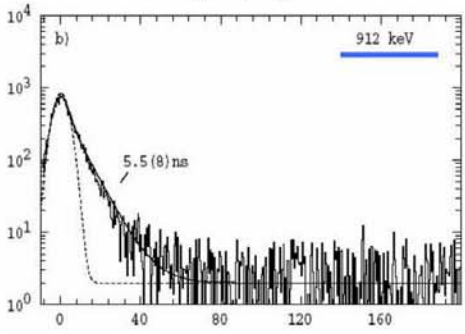

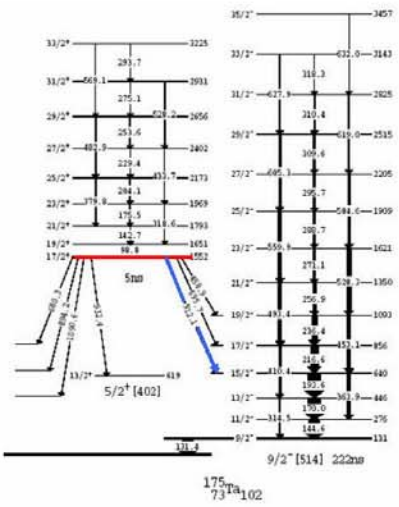

53

Pioneering Science and Technology

F.G. Kondev et al. Nucl. Phys. A601 (1996) 195

Office of Science U.S. Department of Energy

Limitations: Pulsed Beam γ–time

- Complicated when more than one isomer is presented
- Complicated because of contaminations
- Limited time range – e.g. TAC (Ortec 567) – 3 ms
- Rate dependent time distortions

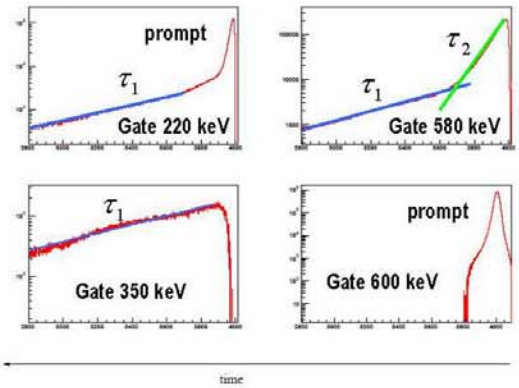

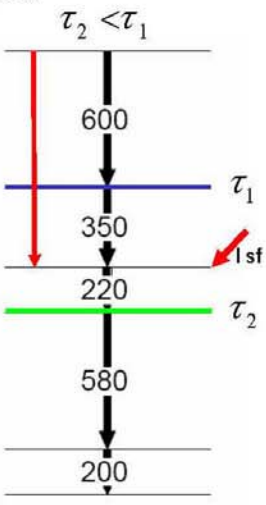

54

Pioneering Science and Technology

Office of Science U.S. Department of Energy

Pulsed Beam γ–γ time Technique

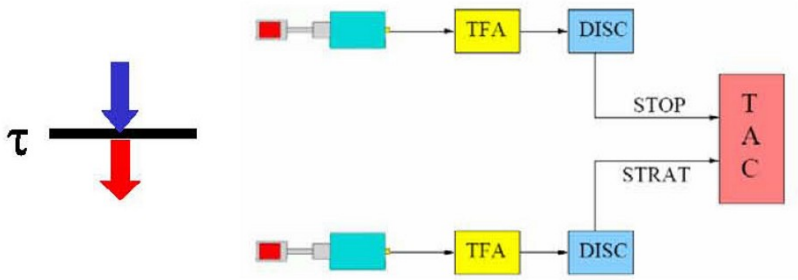

"coincidence" – $E_{\gamma 1}$-$E_{\gamma 2}$-Δt ; $E_{\alpha 1}$-$E_{\gamma 1}$-Δt
$E_{\alpha 1}$-$E_{\alpha 2}$-Δt

55

Pioneering Science and Technology

Office of Science U.S. Department of Energy

γ–γ–time: Decay of the 9/2– Isomer in ^{173}Ta

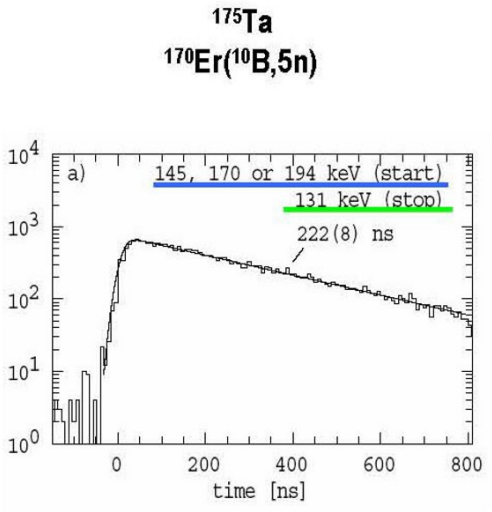

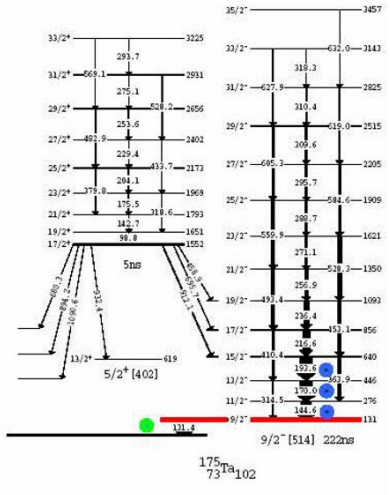

56

Pioneering Science and Technology

F.G. Kondev et al. Nucl. Phys. A601 (1996) 195

Office of Science U.S. Department of Energy

γ–γ–time: Decay of the 21/2– Isomer in ^{173}Ta

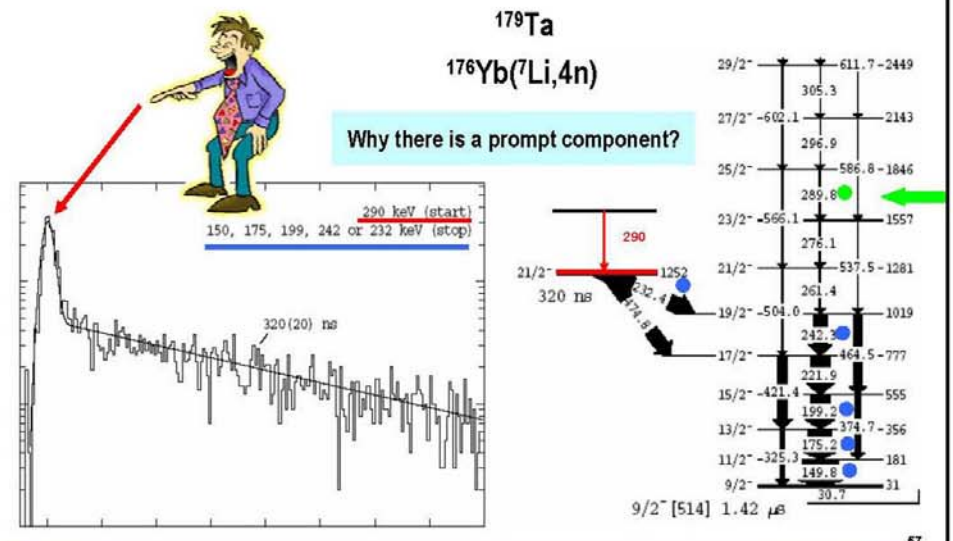

F.G. Kondev et al. Nucl. Phys. A617 (1997) 91

57

Centroid-shift Technique: γ–time

Time Range: near PRF

$$F(x,\lambda)=\int_{-\infty}^{\infty} f(t,\lambda)P(x-t)dt \qquad M_r(F(t))=\int_{-\infty}^{\infty} t^r F(t)dt \qquad \tau = M_1(F(t)) - M_1(P(t))$$

Introduced by Z. Bay, Phys. Rev. 77 (1950) 419

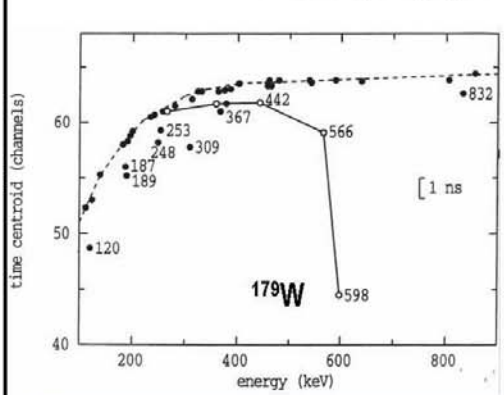

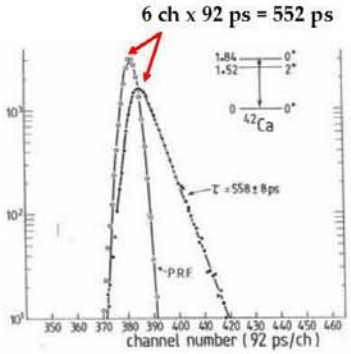

58

Centroid-shift Technique: γ–γ–time

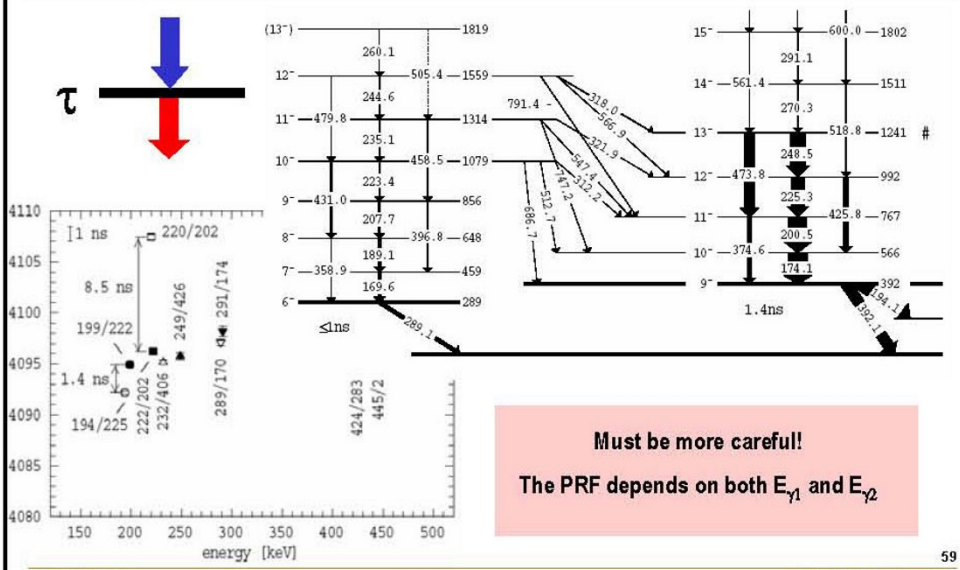

Must be more careful!

The PRF depends on both $E_{\gamma 1}$ and $E_{\gamma 2}$

Pioneering Science and Technology

F.G. Kondev et al. Nucl. Phys. A632 (1998) 473

Office of Science U.S. Department of Energy

Coulomb Excitations

Time Range: up to hundreds of ps

Observables
- Number of gamma rays detected (N_γ)
- Number of beam particles detected (N_{beam})
- Energy of de-excitation gamma ray (E_γ)

$$E < V_{cb}$$

$$\eta = \frac{Z_1 Z_2 e^2}{\hbar v} >> 1$$

^{19}F(1 MeV) on ^{238}U η~1.6

^{40}Ar(152 MeV) on ^{238}U η~130

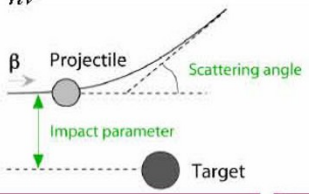

Experimental results
- Coulomb excitation cross section (σ)
- Reduced transition probability B(E2,↑)
- Energy of excited state

$$\sigma = \frac{N_\gamma}{\varepsilon} \frac{1}{N_{\text{target}} N_{\text{beam}}}$$

$$\sigma_{0\to 2} \approx \left(\frac{Z_{\text{target}} e^2}{\hbar c}\right)^2 \frac{\pi}{e^2 b_{\min}^2} \mathrm{B(E\,2,0^+ \to 2^+)}$$

Details in: Winther and Alder, Nucl. Phys. A **319** 518 (1979).

Pioneering Science and Technology

Office of Science U.S. Department of Energy

Intermediate Energy Coulomb Excitations

Primary beam: ^{76}Ge @ 130 MeV/nucl.
Secondary beam: ^{54}Ti @ 88 MeV/nucl.
β=0.406
^{197}Au target thickness: 257.67 mg/cm^2
Θ_{max} = 3.20° (CM)
Number of ^{54}Ti particles detected: 91.665E6

SeGA
(Segmented Germanium Array)—Eighteen 32-fold segmented HP germanium detectors

Measured for ^{54}Ti
- E_γ = 1497(4) keV
- $\sigma(\theta<\Theta_{max})$ = 83(15) mb
- B(E2, ↑) = 357(63) e^{2}fm^4

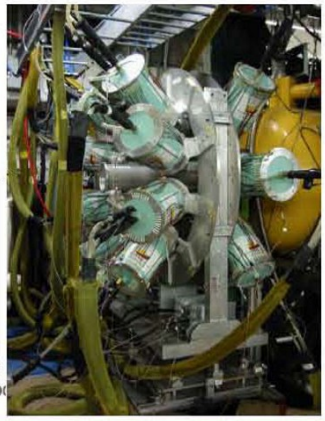

$\tau = 1.5(3)\,ps$

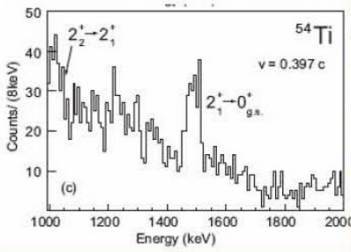

61

Pioneering Science and Technology

Office of Science U.S. Department of Energy

Deduction of Transition Multipolarity

Basic techniques

- Internal conversion electrons
- Angular distributions
- Angular correlations (DCO ratios)
- Gamma-ray polarization

62

Pioneering Science and Technology

Office of Science U.S. Department of Energy

Internal Conversion Electrons

$$\alpha^{tot} = \frac{I_{ce}}{I_\gamma} = \alpha_K + \alpha_L + \alpha_M + \dots$$

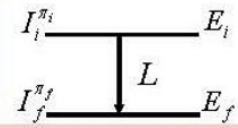

$$E_\gamma = E_i - E_f$$
$$E_i = E_\gamma - B_i, i = K, L, \dots$$

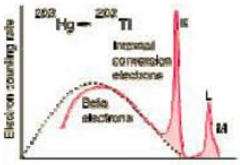

Intensity ratio

∞	E0
1	Low energy isomers
10^{-1} <	50< Z
10^{-2} - 10^{-3}	30<Z < 50
10^{-4} - 10^{-5}	Z < 30

$$\alpha_K(EL) \propto Z^3 \left(\frac{L}{L+1}\right)\left(\frac{2m_e c^2}{E}\right)^{L+5/2}$$

Important for heavy nuclei, where inner electron shells are closer to the nucleus

Important for low-energy transitions

63

Pioneering Science and Technology

Office of Science U.S. Department of Energy

Internal Conversion Electrons

Sensitive to L

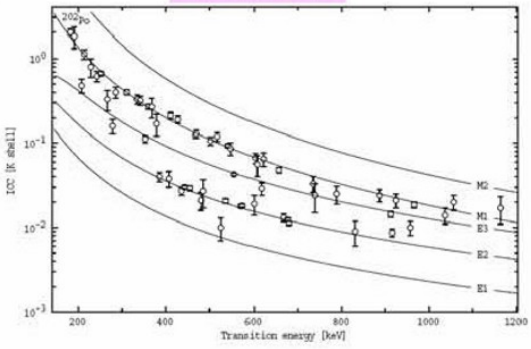

allows deduction of the mixing ratios

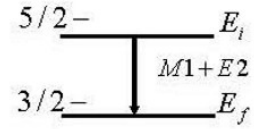

$1 \le L \le 4$ $\quad M1, E2, M3, E4$

$$\delta^2 = \frac{I_\gamma(E2)}{I_\gamma(M1)} \qquad \alpha^{M1/E2} = \frac{\alpha_{M1} + \delta^2 \alpha_{E2}}{1+\delta^2} \qquad \delta^2 = \frac{\alpha_{M1} - \alpha^{exp}}{\alpha^{exp} - \alpha_{E2}}$$

64

Pioneering Science and Technology

Office of Science U.S. Department of Energy

Direct ICC Measurements

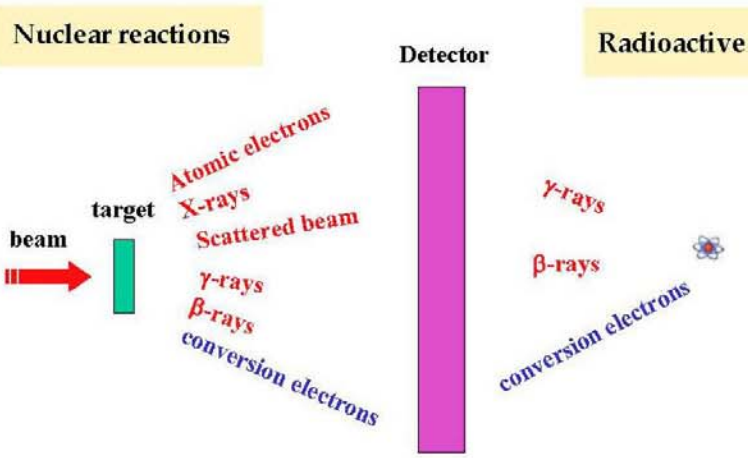

Basic Electron Transporters

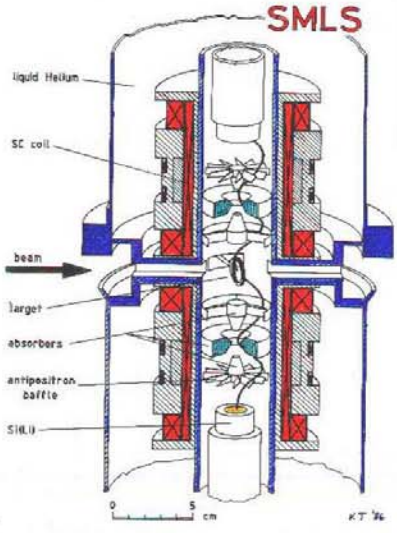

Superconducting solenoid

- Broad-range mode – 100 keV up to a few MeV
- Lens mode – finite transmitted momentum bandwidth ($\Delta p/p$~15-25%) – high peak-to-total ratio

Mini-orange (looks like a peeled orange)

- transmission > 20%
- small size and portability, but poorer quality

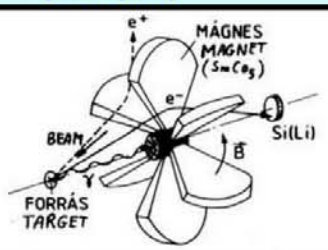

Superconducting Solenoid Spectrometer

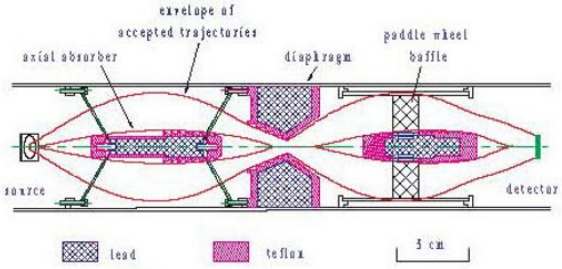

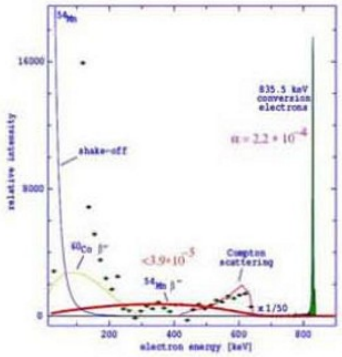

67

Pioneering Science and Technology

Office of Science U.S. Department of Energy

Conversion Electron Measurements

$\alpha_K(431) = 0.056(7)$
$\alpha_L(431) = 0.033(4)$
$\frac{K}{L}(431) = 1.7(2)$

$\alpha_K^{th}(431) = 0.008(E1);0.022(E2);0.058(E3);0.067(M1);0.21(M2)$
$\alpha_L^{th}(431) = 0.001(E1);0.006(E2);0.032(E3);0.010(M1);0.040(M2)$
$\frac{K}{L}(431) = 6.7(E1);3.9(E2);1.9(E3);6.5(M1);5.2(M2)$

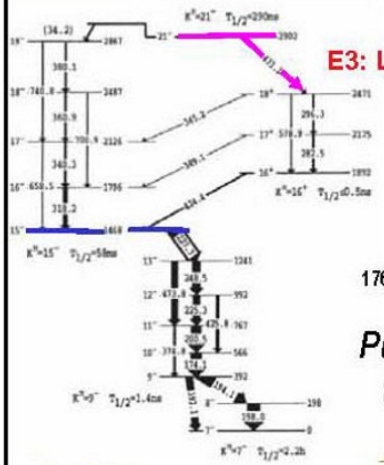

E3: L=3, π=yes

^{178}Ta

^{176}Yb(^{7}Li,5n)

Pulsed-beam technique

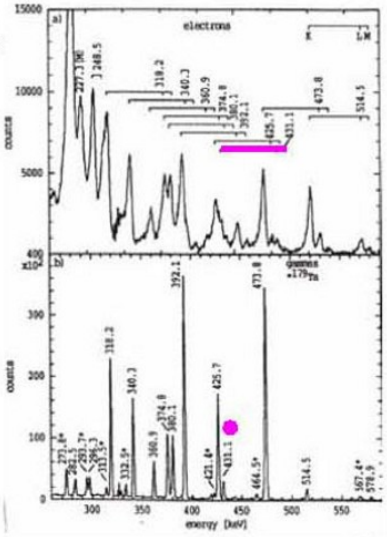

68

F.G. Kondev et al. Nucl. Phys. A632 (1998) 473

SACRED Electron Spectrometer

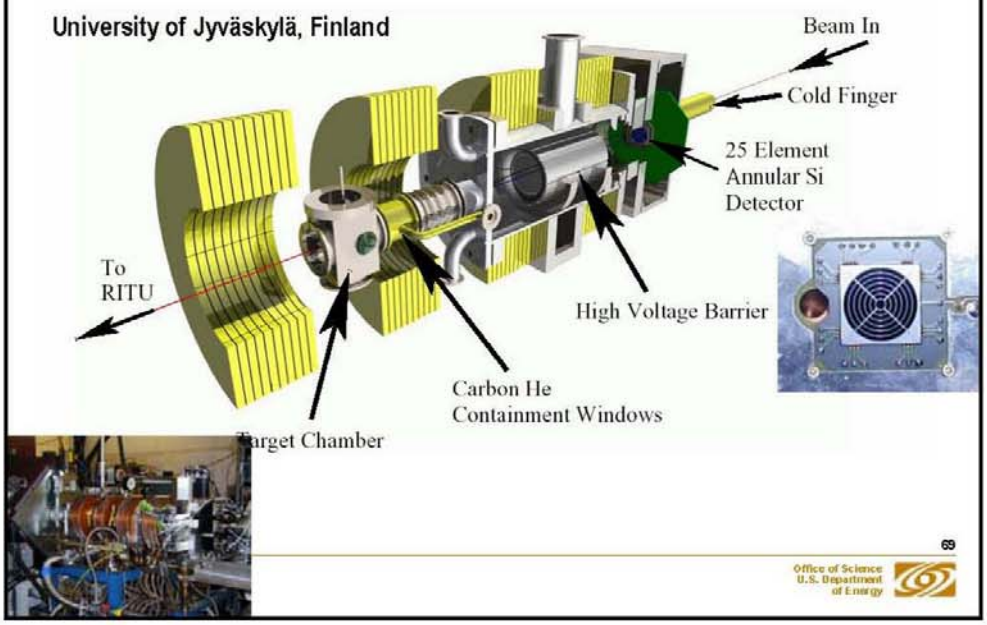

69

Office of Science
U.S. Department
of Energy

Recoil-gated CE Spectrum from $^{208}Pb(^{48}Ca,2n)^{254}No$

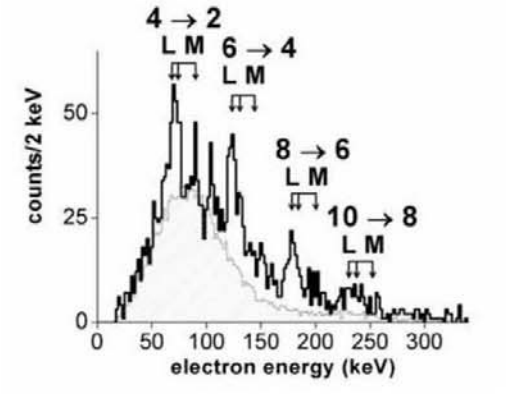

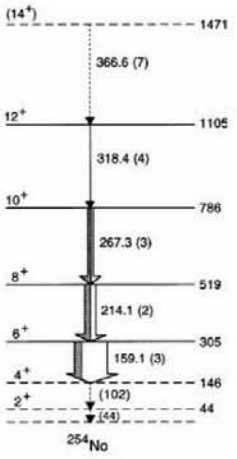

70

Pioneering
Science and
Technology

P.A. Butler et al.,PRL 89 (2002) 202501

Office of Science
U.S. Department
of Energy

ICC from Total Intensity Balances – example 1

Works well for γ rays with energies below about 250 keV

In out-of-beam (or decay) coincidence data

$$I_{\gamma_i}^{tot} = I_{\gamma_i} \times (1+\alpha_i^{tot}) \equiv I_{\gamma_o}^{tot} = I_{\gamma_o} \times (1+\alpha_o^{tot})$$

$$\alpha_o^{tot} \equiv (I_{\gamma_i}\varepsilon_o / I_{\gamma_o}\varepsilon_i) \times (1+\alpha_i^{tot}) - 1$$

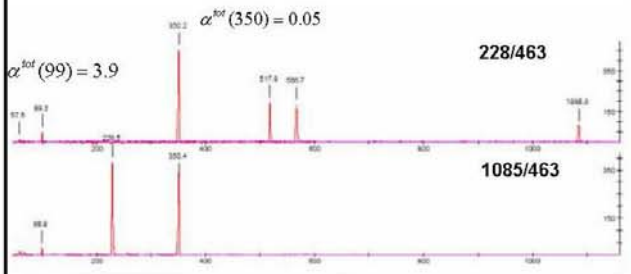

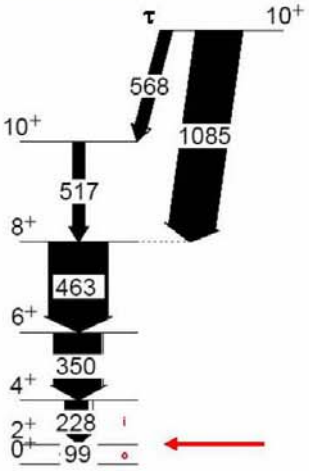

71

Pioneering Science and Technology

Office of Science U.S. Department of Energy

ICC from Total Intensity Balances – example 2

In-beam: only when gating from "above"

$$I_{\gamma_i}^{tot} = I_{\gamma_i} \times (1+\alpha_i^{tot}) \equiv I_{\gamma_o}^{tot} = I_{\gamma_o} \times (1+\alpha_o^{tot})$$

$$I_{\gamma_i}^{tot} = I_{\gamma_o}^{tot} + I_{sf}$$

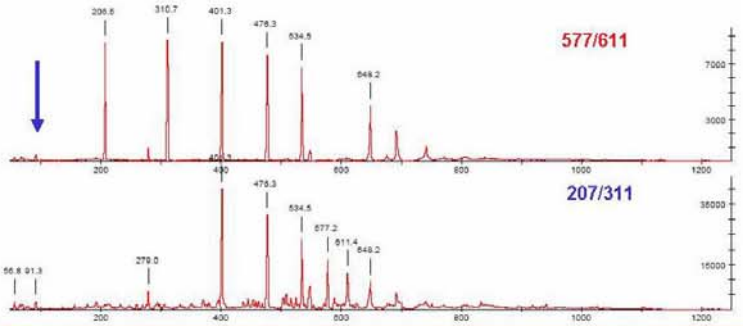

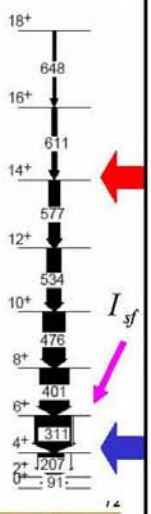

Pioneering Science and Technology

Office of Science U.S. Department of Energy

Angular Distributions

The gamma rays emitted from nuclear reactions exhibit angular distributions:

$$W(\theta) = 1 + A_{22}P_2(\cos\theta) + A_{44}P_4(\cos\theta)$$

$$A_{22} = \alpha_2 A_2^{\max}; A_{44} = \alpha_4 A_4^{\max}$$

$$\alpha_k(J_i) = \rho_k(J_i)/B_k(J_i)$$

$$\rho_k(J) = \sqrt{(2J+1)} \times \sum_m (-1)^{J-m} < J, m, J-m \mid k0 > P_m(J)$$

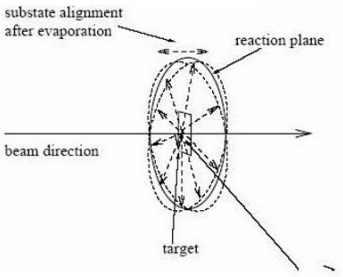

The orientation of the nucleus will be slightly attenuated by the emission of evaporated particles (n,p,α) and γ–rays.

$$P_m(J) = \frac{\exp(-m^2/2\sigma^2)}{\sum_{m=-J}^{J} \exp(-m^2/2\sigma^2)}$$

73

Pioneering Science and Technology

Office of Science U.S. Department of Energy

Angular Distributions: Experiment

Measure: the γ-ray yield as a function of θ

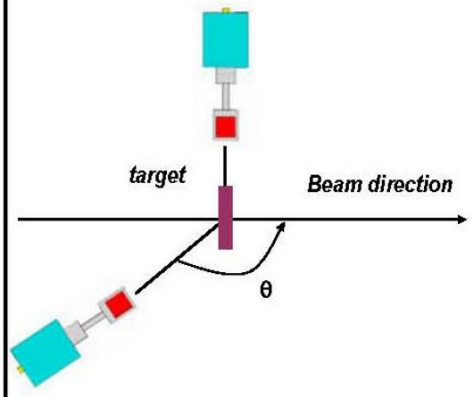

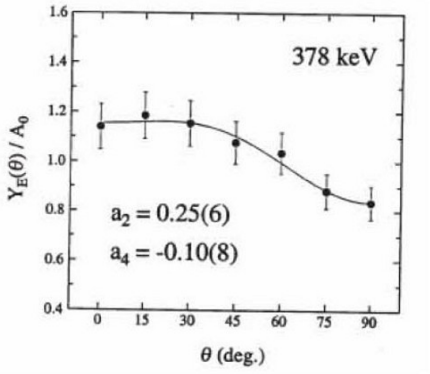

Using a single detector – "singles" mode – contaminants

Using a large gamma-ray array – "coincidence" mode - you must be careful!

74

Pioneering Science and Technology

Office of Science U.S. Department of Energy

How to determine the mixing ratios?

I) <u>If both A2 and A4 have been measured – see</u>
E. Der Mateosian and A.W. Sunyar, ADNDT 13 (1974) 407

II) <u>If only A2 has been measured (A4~0)</u>

1) Determine the attenuation coefficient (α_2) for known E2 transitions depopulating levels of known spin (gs band in even-even nuclei)

$$\alpha_2 = A_2^{\exp} / A_2^{\max}$$

$$A_2^{\max} = B_2 \times F_2$$

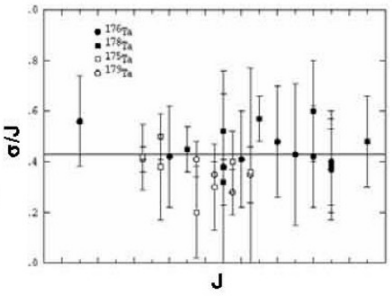

Tabulated in E. Der Mateosian and A.W. Sunyar, ADNDT 13 (1974) 391

2) For a given transition determine:

$$A_2^{\max} = A_2^{\exp} / \alpha_2$$

3) From E. Der Mateosian and A.W. Sunyar, ADNDT 13 (1974) 407 get δ

75

Pioneering Science and Technology

Office of Science U.S. Department of Energy

Angular Distributions: Example 1

^{175}Ta

^{170}Er(^{10}B,5n)@64 MeV

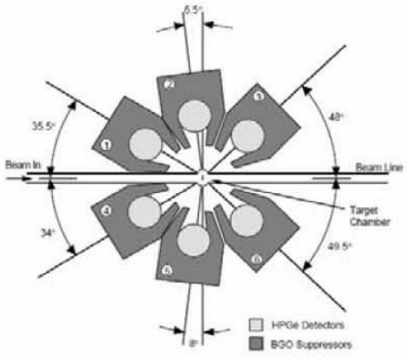

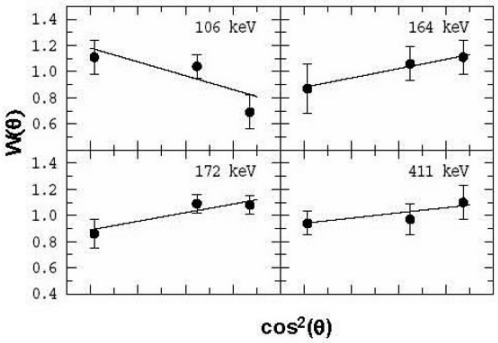

172γ: δ(AD)=0.44 -13+17; δ(RM)=0.54 -/+5

CAESAR array/Canberra (AUS)

76

Pioneering Science and Technology

Office of Science U.S. Department of Energy

Angular Distributions: Example 2

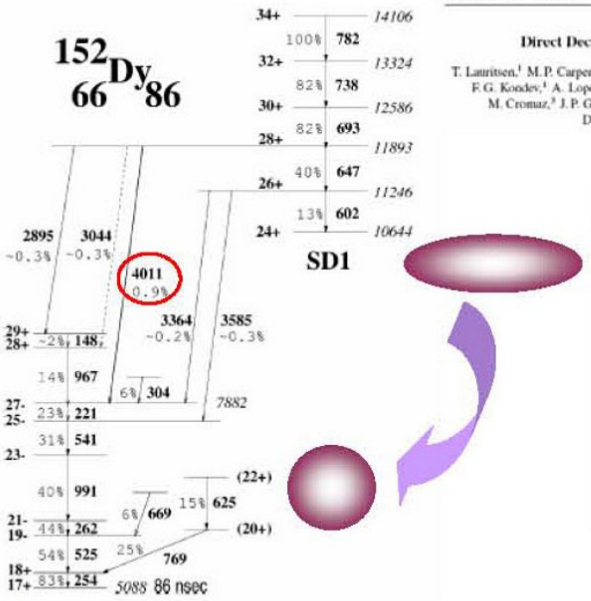

VOLUME 88, NUMBER 4 PHYSICAL REVIEW LETTERS 28 JANUARY 2002

Direct Decay from the Superdeformed Band to the Yrast Line in $^{152}_{66}Dy_{86}$

T. Lauritsen,[1] M.P. Carpenter,[1] T. Døssing,[2] P. Fallon,[3] B. Herskind,[2] R.V.F. Janssens,[1] D.G. Jenkins,[1] T.L. Khoo,[1] F.G. Kondev,[1] A. Lopez-Martens,[4] A.O. Macchiavelli,[3] D. Ward,[3] K.S. Abu Saleem,[1] I. Ahmad,[1] R. Clark,[3] M. Cromaz,[3] J.P. Greene,[1] F. Hannachi,[4] A.M. Heinz,[5] A. Korichi,[4] G. Lane,[5] C.J. Lister,[1] P. Reiter,[1,5] D. Seweryniak,[1] S. Siem,[1] R.C. Vondrasek,[1] and I. Wiedenhöver[1,6]

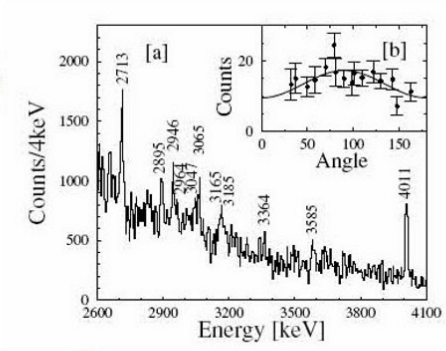

$A_2 = -0.35(12)$ and $A_4 = -0.02(16)$

77

Pioneering Science and Technology

Office of Science U.S. Department of Energy

Experimental nuclear structure:

F. G. Kondev

Argonne National Laboratory, USA

E-mail: kondev@anl.gov

Experimental Nuclear Structure Part II

Filip G. Kondev
kondev@anl.gov

Workshop on "Nuclear Structure and Decay Data: Theory and Evaluation", Trieste, Italy

April 4-15th, 2005

Argonne National Laboratory

A U.S. Department of Energy
Office of Science Laboratory
Operated by The University of Chicago

Outline

I) Lecture I: Experimental nuclear structure techniques

- reactions used to populate excited nuclear states
- techniques used to measure the lifetime of a nuclear state
  - *Coulomb excitation, electronic, specific activity, indirect*
- Techniques used to deduce J^{π}
  - *ICC, angular distributions, DCO ratios, etc.*

II) Lecture II: Contemporary Nuclear Structure Physics at the Extreme

- spectroscopy of nuclear K-Isomers
- physics with large γ–ray arrays
- gamma-ray tracking – the future of the nuclear γ–ray spectroscopy

Generation of Angular Momentum in Nuclei

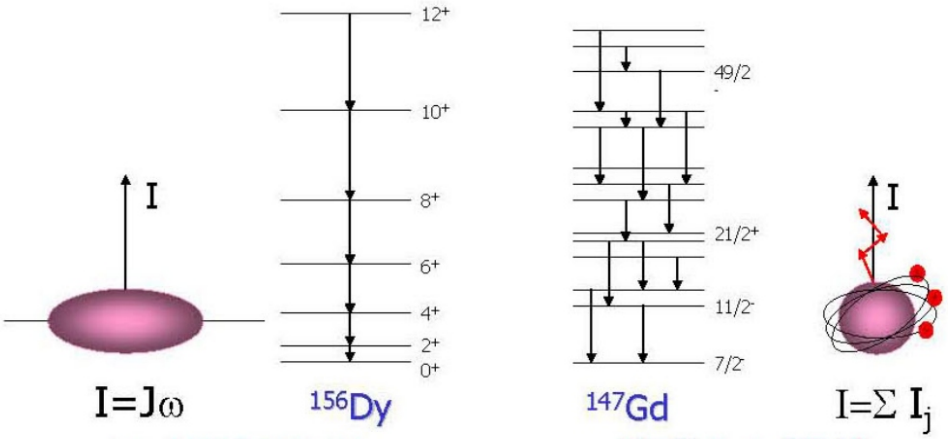

$I=J\omega$ ^{156}Dy ^{147}Gd $I=\Sigma I_j$

$E_I=\hbar^2/2J\ I(I+1)$

$B(E2) \sim 200$ W.U.

$E_I=\Sigma e_j + \Sigma\Sigma V_{jk}$

deformed nucleus spherical nucleus

3

Pioneering Science and Technology

Office of Science U.S. Department of Energy

What is a Nuclear Isomer?

Nuclear Isomer – a *long-lived excited nuclear state* ($T_{1/2} > 1$ *ns*) *decays by emission of* α, β, γ, p, *fission, cluster*

The first one discovered by O. Hahn in Berlin in 1921 – decay of ^{234}Pa *(70 s)*
von Weizsacker, A. Bohr & B. Mottelson

$$1/\tau \sim E_\gamma^{2\lambda+1} |< \psi_f | T | \psi_i >|$$

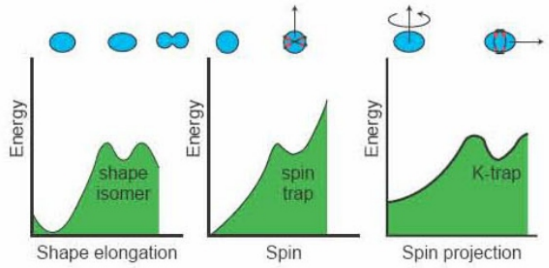

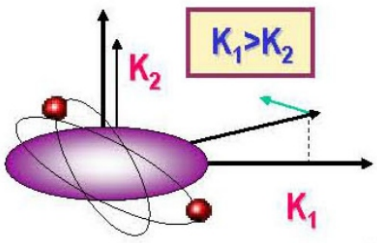

4

Pioneering Science and Technology

Office of Science U.S. Department of Energy

K-Isomers – the Building Blocks

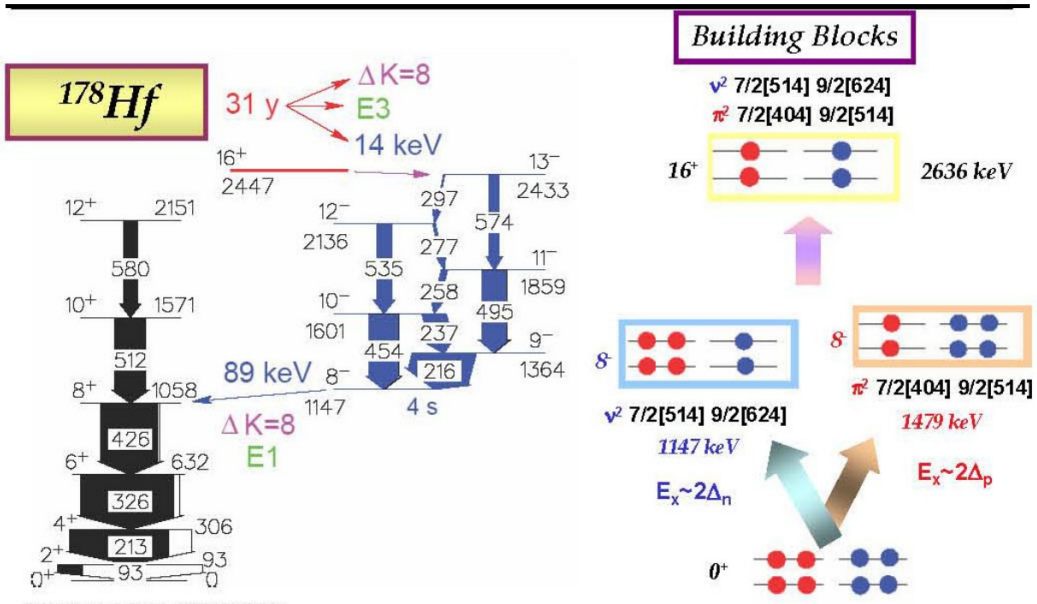

K-Selection Rule and Reduced Hindrance

K-Isomer decay usually proceeds by minimizing ΔK

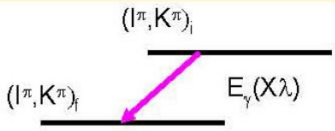

Usually not this way!

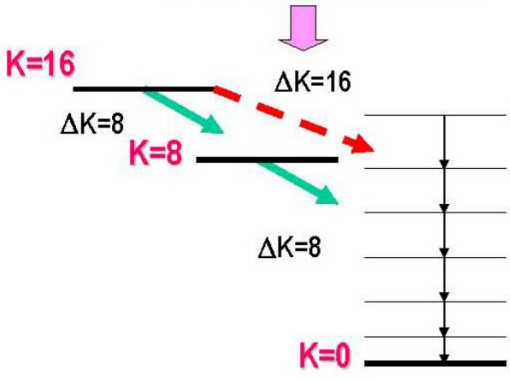

$\nu=\Delta K-\lambda$ – degree of K-forbiddenness

$F=\tau^{\gamma}(X\lambda)/\tau^{w}(X\lambda)$ – hindrance factor

$f_\nu=(F)^{1/\nu}$ – reduced hindrance per degree of K-forbiddenness – gives yardstick for "goodness" of K-quantum number

$f_\nu>20$ – K-hindered decay

$f_\nu<10$ - anomalous decay

Why Study Isomers ?

- Powerful spectroscopy tool - highly selective "devices"
- Advanced physics
  - ✓ The mapping of intrinsic orbitals close to and remote from the Fermi surface providing an indirect probe of deformation and potentials used in mean-field descriptions.
  - ✓ The limits to the existence of high-K states, both at high excitation energy and as a function of proton and neutron number and the competition between collective and intrinsic excitation.
  - ✓ The question of the dilution of the K-quantum number due to both random interactions in regions of high-level density, and to chance degeneracies in regions of low level density.
  - ✓ As a seniority- and configuration-dependent probe of the major residual interactions in deformed nuclei, specifically pairing and spin-spin interactions.

Why Study Isomers? – cont.

- Interesting astrophysical applications: stellar thermometers and chronometers
  - ✓ There is considerable interest in the role of nuclear structure effects (the precise disposition of excited states) and the possible role of the K-quantum number in the formation and possible photo-destruction of isomeric nuclei such as ^{176}Lu, ^{180}Ta and ^{186}Re in hot stellar processes.

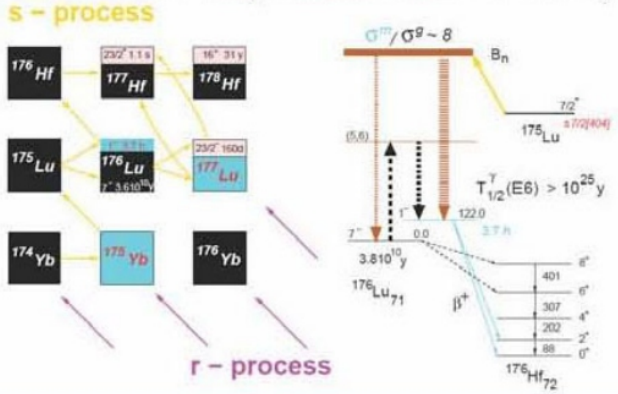

Why Study Isomers? – cont.

Applications

- Activation analysis
- Medicine
- Gamma-ray lasers/batteries?
- Transmutation of nuclear waste?

Exotic Studies

- Radioactive targets – high-spin/seniority, e.g. ^{178m2}Hf, ^{177m}Lu
- Radioactive beams – the future of nuclear knowledge

9

Pioneering Science and Technology

Office of Science U.S. Department of Energy

K Isomers: Where to find them?

- Deformed nuclei with axially-symmetric shape

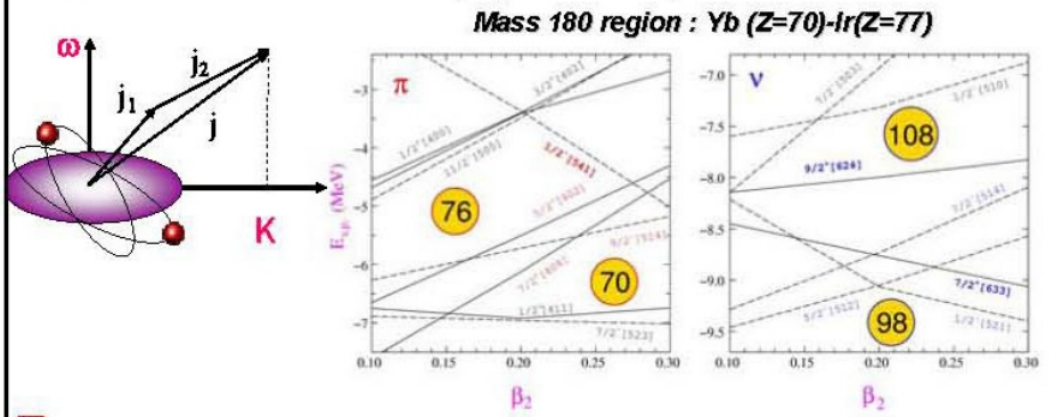

- High-K orbitals near the Fermi surface

π 5/2[402], 7/2[404], 9/2[514]

ν 5/2[512], 7/2[514], 7/2[633], 9/2[624]

→ 7-qp, K=49/2

10

Pioneering Science and Technology

Office of Science U.S. Department of Energy

K-Isomers in the A~180 Region

- *Seniority 2 and higher*
- $T_{1/2} < 1$ *s (small) /* $T_{1/2} > 1$ *s (large)*

HI,xn – fusion evaporation
Deep-inelastic collisions
Incomplete fusion

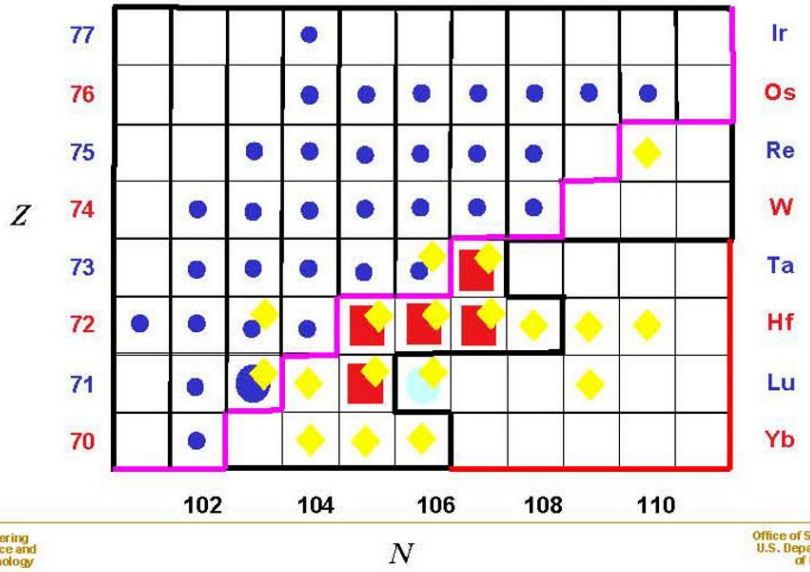

11

Pioneering Science and Technology

Office of Science U.S. Department of Energy

Pairing Destruction in Nuclei

In general there are two anti-pairing mechanisms :

(a) Coriolis anti-pairing – induced by the fast rotation

(b) Blocking – occupation of level(s) by unpaired nucleon(s)

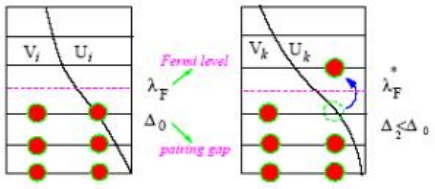

$V^2_{i(k)}$ $U^2_{i(k)}$ the probability that a given state is or is not occupied

uniform levels distribution

$\Delta_\nu = [\Delta_0 (\Delta_0 - \nu/\rho)]^{1/2}$

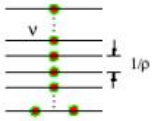

ν – the number of blocked particles (seniority)

ρ – level density near the Fermi surface

$1/\rho \sim 300$ keV and $\Delta_0 \sim 900$ keV
$\nu = 3$ $\Delta = 0$!

Pioneering Science and Technology

Office of Science U.S. Department of Energy

Pairing Gap & Seniority

illustrative example: blocked multi–quasiparticle calculations – protons $^{177}_{73}Ta_{104}$

mean field – Nilsson potential *pairing* – BCS model, LN model

LN: *W. Nazarewicz et al. NP A512 (1990)*
W. Satula et al. NP A578 (1994)

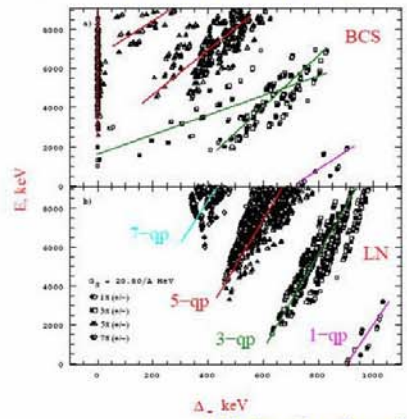

(i) the number of blocked levels
seniority dependence

(ii) their location

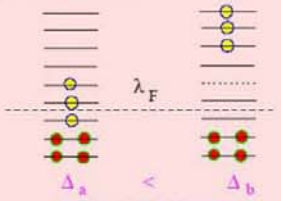

configuration dependence

(iii) the single–particle density

$\Delta \sim exp\,[-1/G\,\rho]$

shell structure dependence

(a) Has the pairing really gone ? (b) How to prove it?

rotation of the MQP state comes to the rescue

Pairing & Moment of Inertia

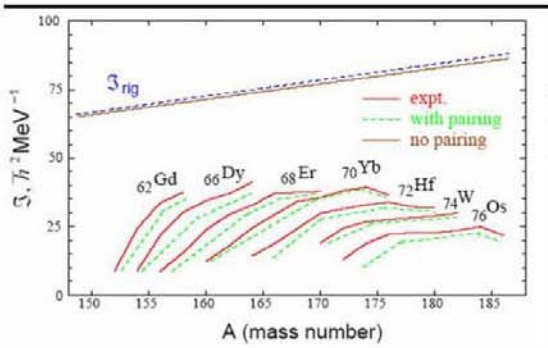

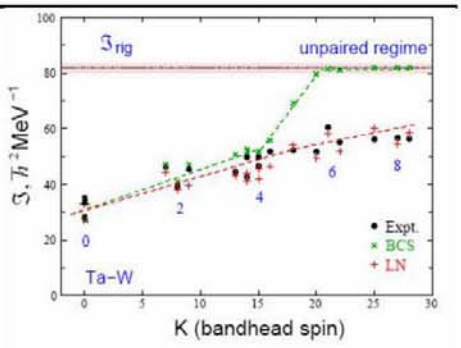

- *Implication:* yet higher seniority states would not show marked decrease in pairing
  G.D. Dracoulis et al., Phys. Lett. B419 (1998)
- *Is the rigid rotation a signature of quenched pairing?*
  $\Im$ is smaller than $\Im_{rig}$ due to shell effects
  S. Frauendorf et al., Phys. Rev. C61 (2000)
- *Needs an experimental confirmation !*

… at Extreme of Seniority – the case of ^{175}Hf

- Tentative quantum properties, e.g. J^{π} and $T_{1/2}$
- Exotic structure - must involve at least 9 qp, a case where the pairing may be completely gone!
- Unprecedented decay pattern – $\Delta K=11$! (662 keV)

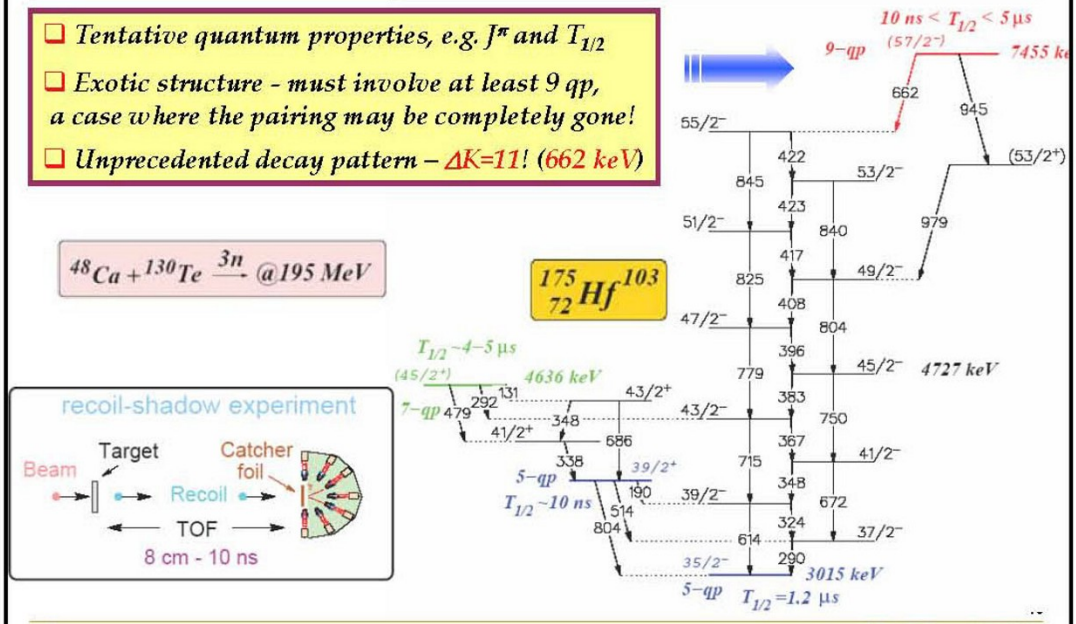

Pioneering Science and Technology

N.L. Gjorup et al., Z. Phys. A337 (1990)

Office of Science U.S. Department of Energy

^{175}Hf Experiments at ANL and ANU/Canberra

Pulsed Beam Technique

- Well defined "clock"
- Sensitive to in-beam and decay events

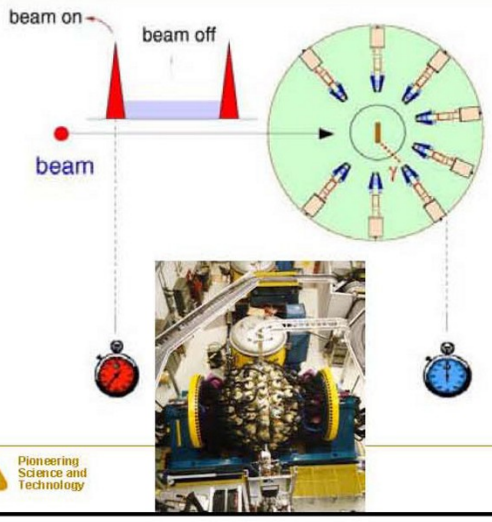

ANL Experiment

$^{48}Ca(^{130}Te,3n)$@194 MeV

- Pulsed beam & Gammasphere
  1 ns on / 825 ns off
- Thin target
  1 ns on / 82.5 ns off

Complementary Experiment at ANU

$^{9}Be(^{170}Er,4n)$@50 MeV

- Pulsed beam & CAESAR array
  (8 CS Ge detectors)
  4 μs on/60 μs off

16

Pioneering Science and Technology

Office of Science U.S. Department of Energy

Decay of the 57/2- Isomer

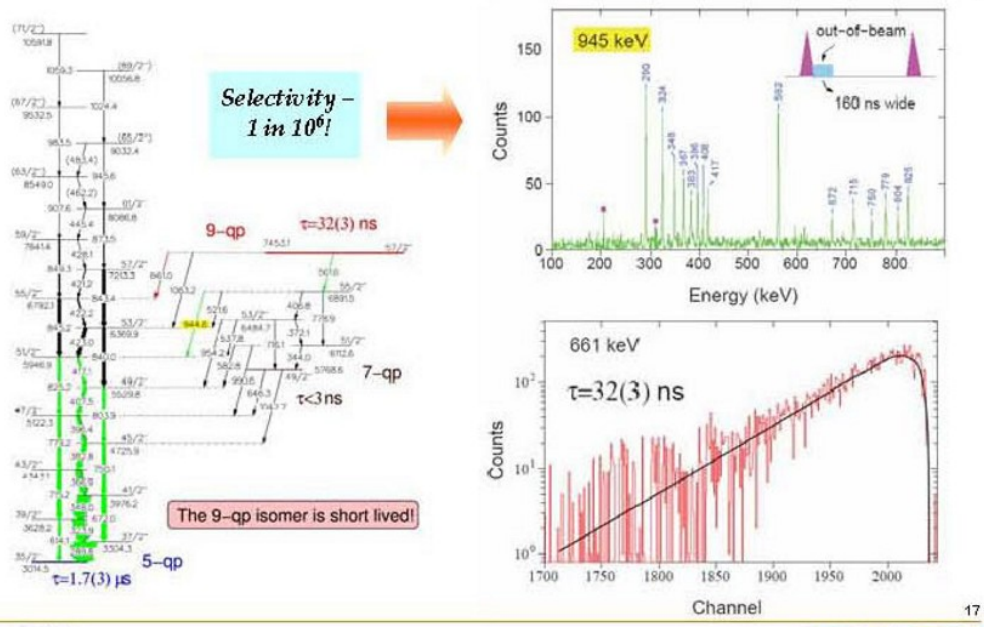

Structures Above the 45/2+ Isomer

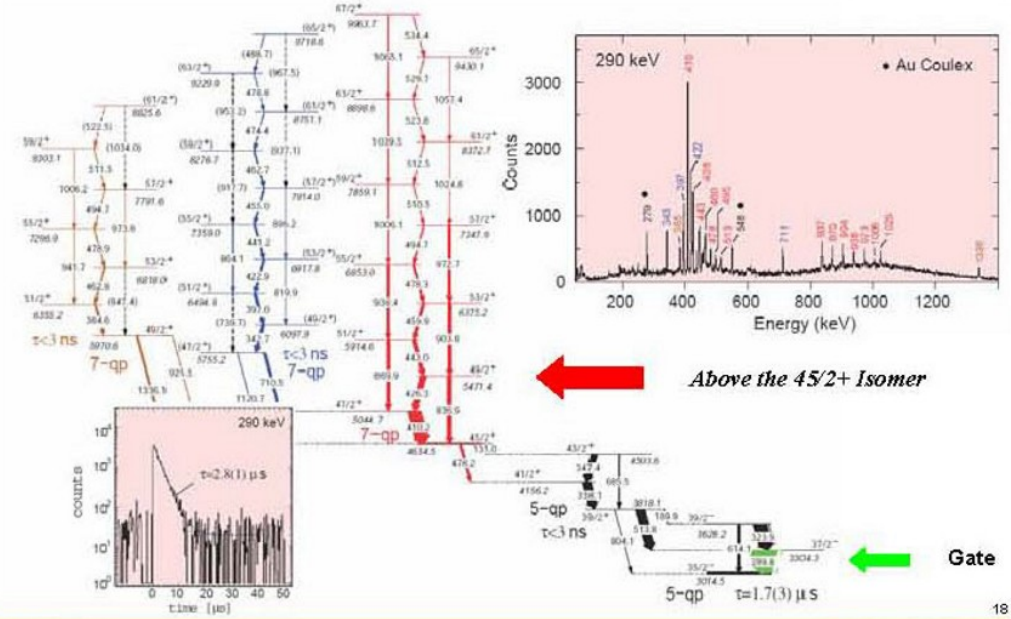

"Normal" Decay Branches

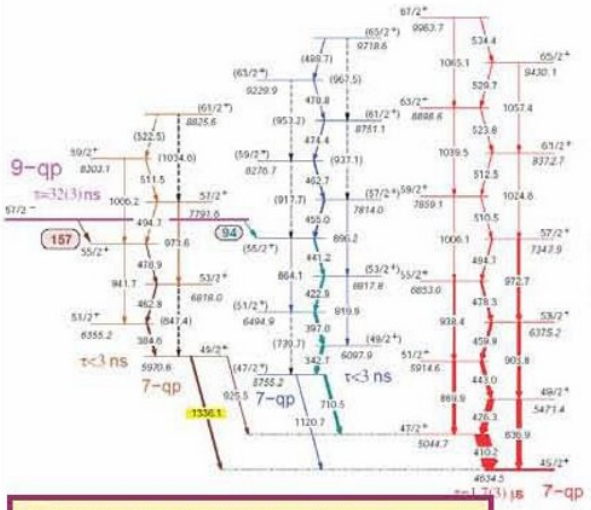

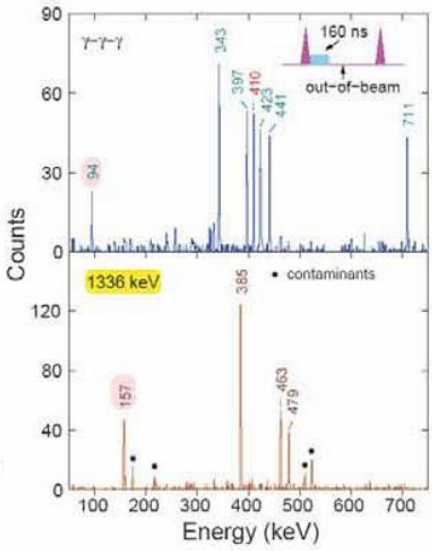

- 94 keV Mult: E1 - 18% branch
- 157 keV Mult: E1 – 17% branch

K-hinderances in the Decay of the 57/2- Isomer

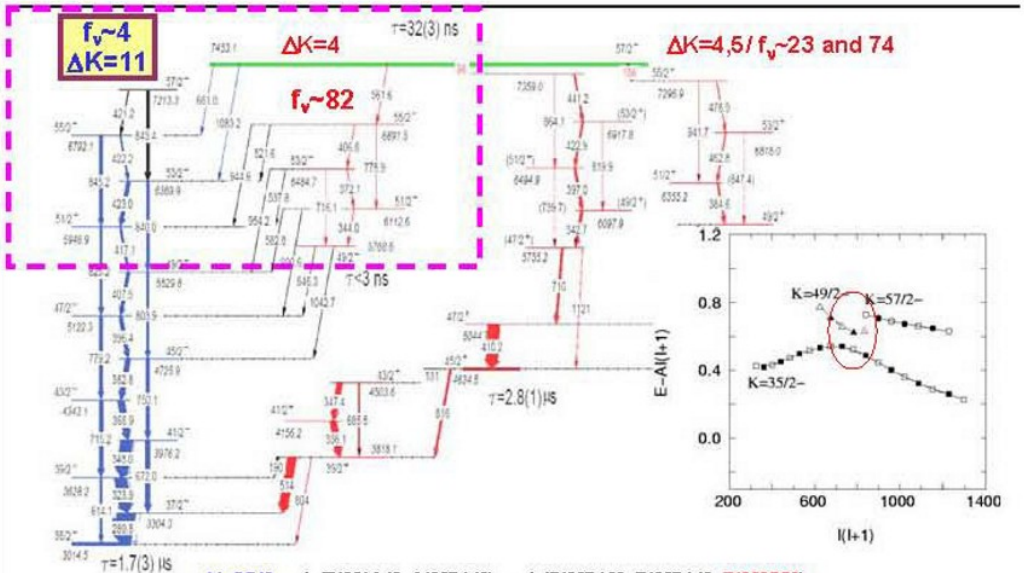

K=35/2-: π^2 (7/2[404], 9/2[514]) x ν^3 (5/2[512], 7/2[514], 7/2[633])
K=49/2-: 35/2- x ν^2 (5/2[642], 9/2[624])

Rotation of the 57/2- Isomer

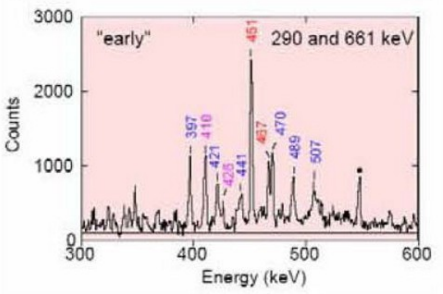

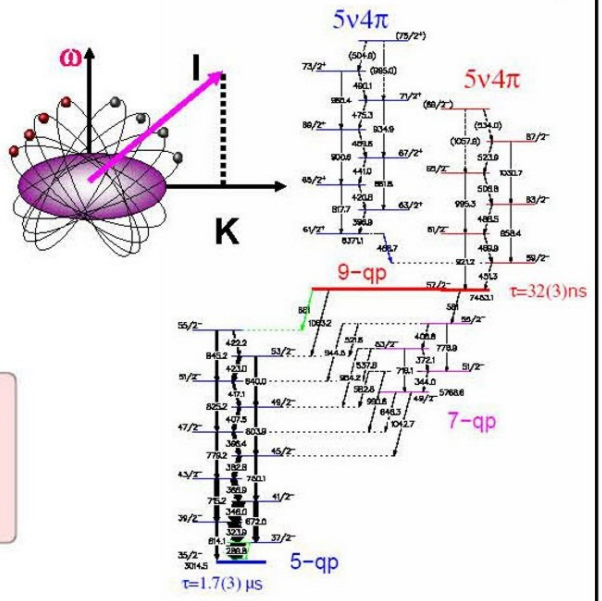

- two new 9−qp structures
- collectivity still persists
- $g_K - g_R$ – configurations

Pioneering Science and Technology

Office of Science U.S. Department of Energy

Has the Pairing Really Gone?

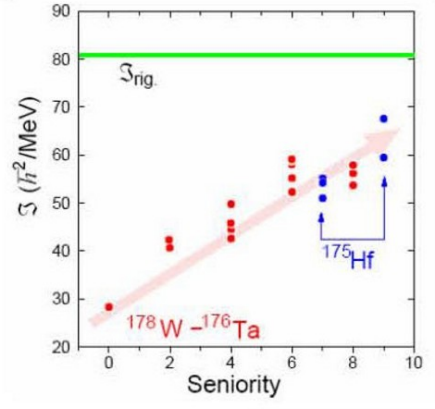

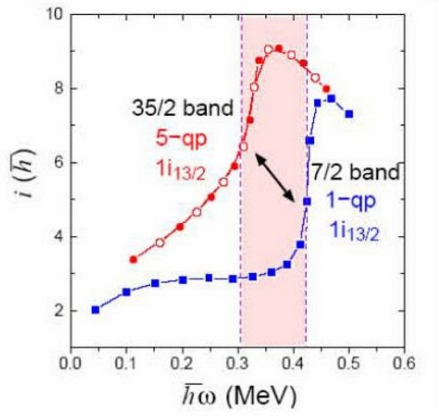

- even at 9−qp $\Im < \Im_{rig.}$
- pairing is still important
- "dynamic" vs. "static"

22

Pioneering Science and Technology

Office of Science U.S. Department of Energy

… at Extreme of Neutron number – the case of ^{177}Lu

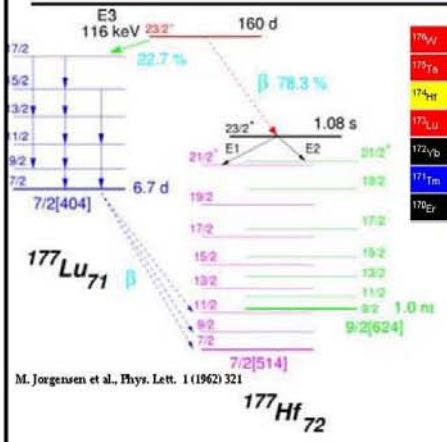

M. Jorgensen et al., Phys. Lett. 1 (1962) 321

Deformed shell-model
- Nilsson s.p. levels
- Pairing - LN prescription

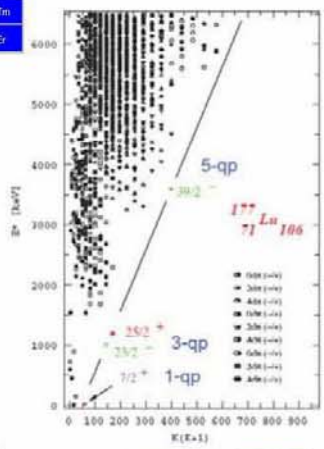

J.J. Carroll *et al.*, *Hyp. Int.* 135 (2001) 3

Isomer	Prod. factor $\sigma_{(n,\gamma)}$ [b]	Storage factor E_γ [keV]	Storage factor $T_{1/2}$ [y]	Triggering factor* ICS$_{trig}$ [eV b]	Triggering factor* E_{trig} [keV]	Output factor (E_γ) [keV]	Overall figure of merit
$^{177}Lu^m$	2.8	970	0.44	427	$\sim 10^4$	<100	100	230	0.056
$^{178}Hf^{m2}$	$\sim 10^{-6}$	2,446	31	75,826	$< 3 \times 10^4$	~10	3,000	300	0.00014

Pioneering Science and Technology

Office of Science U.S. Department of Energy

Structures Above the K^π=23/2 - Isomer

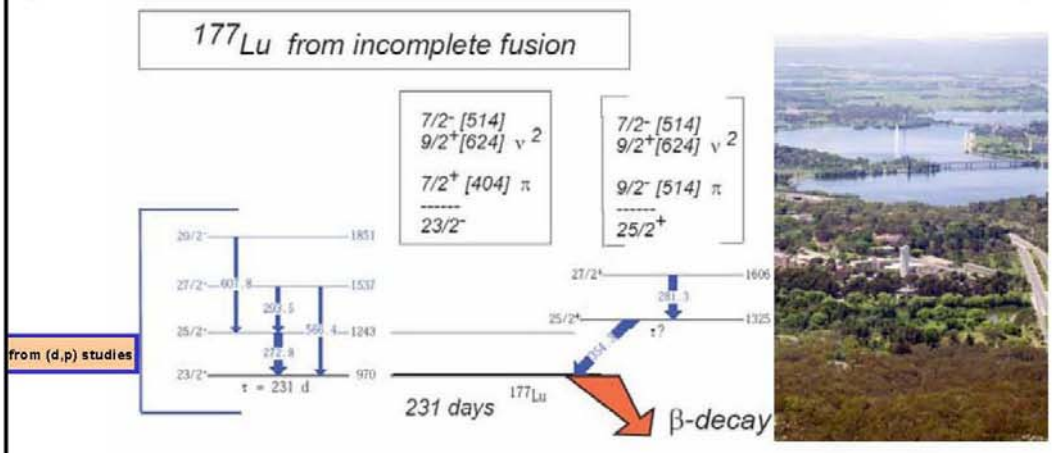

α–γ–γ–time coincidences 4p particle-detector array;
37 MeV 7Li ; angular momentum in 6-13 h - breakup-compound

$^{176}Yb(^7Li,\alpha 2n)$ McGoram ANU PhD; to be published

24

Pioneering Science and Technology

Office of Science U.S. Department of Energy

Evidence for a β– decaying Isomer?

PHYSICAL REVIEW C **69**, 024320 (2004)

Evidence for a high-spin β-decaying isomer in ^{177}Lu

Sareh D. Al-Garni,[1,*] P. H. Regan,[1,†] P. M. Walker,[1] E. Roeckl,[2] R. Kirchner,[2] F. R. Xu,[3] L. Batist,[2,4] A. Blazhev,[2,5] R. Borcea,[2] D. M. Cullen,[6,7] J. Döring,[2] H. M. El-Masri,[1] J. Garces Narro,[1] H. Grawe,[2] M. La Commara,[2,8] C. Mazzocchi,[2,9] I. Mukha,[2,10] C. J. Pearson,[1] C. Plettner,[2] K. Schmidt,[2] W.-D. Schmidt-Ott,[11] Y. Shimbara,[12] C. Wheldon,[1,2,6] R. Wood,[1] and S. C. Wooding[1,2]

11.4 MeV/nucleon ^{136}Xe beam on ^{186}W target; thermal ion source; mass separation

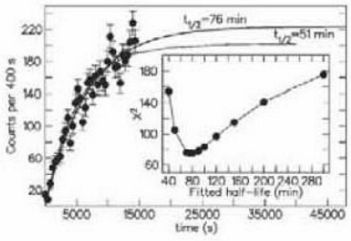

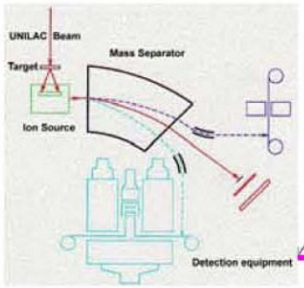

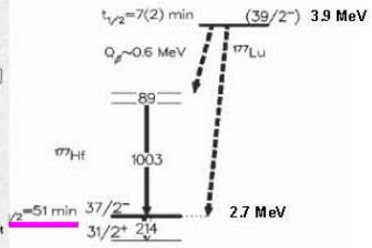

^{177}Hf

Deep Inelastic Experiment at ANL

Pulsed beam & Gammasphere at ANL

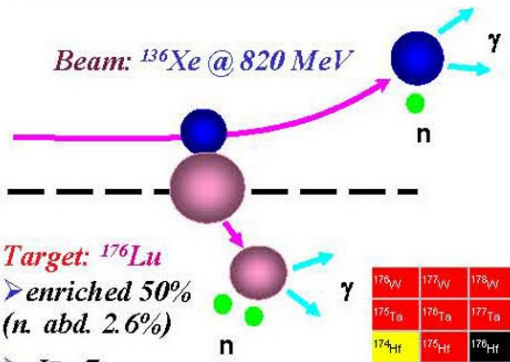

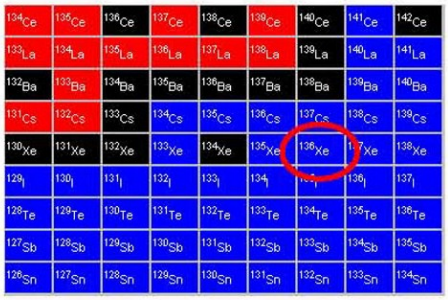

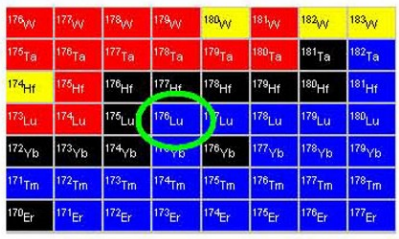

Projectile-like Nuclei

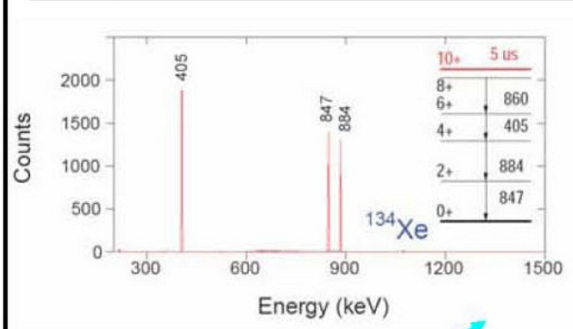

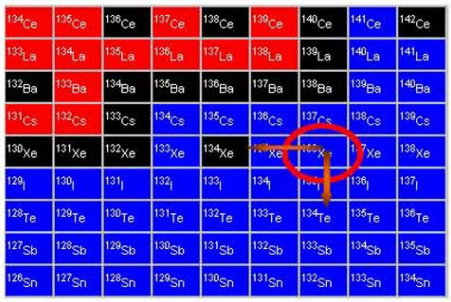

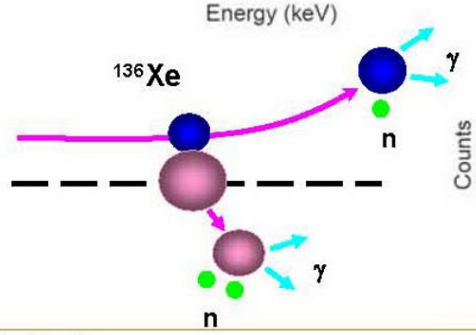

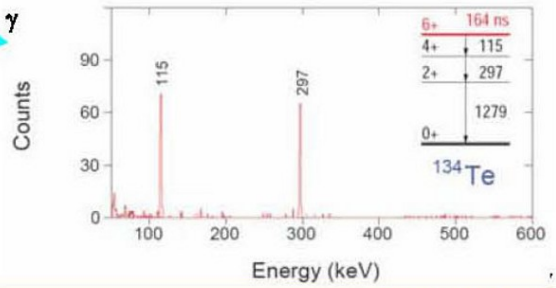

Pioneering Science and Technology

Office of Science U.S. Department of Energy

Target-like Nuclei

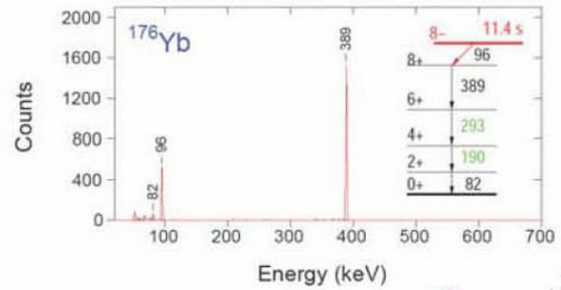

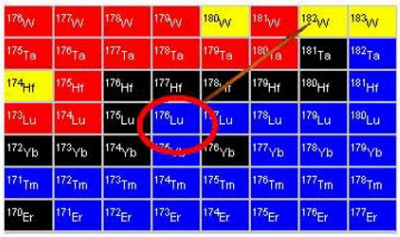

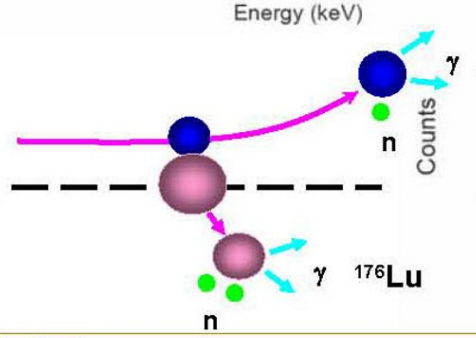

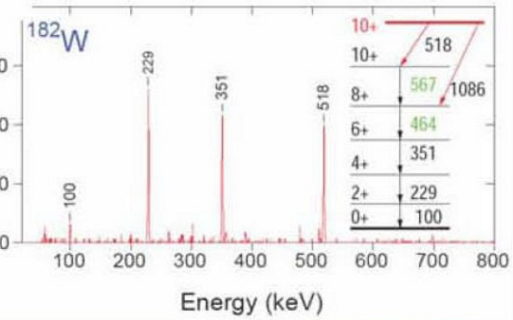

Pioneering Science and Technology

Office of Science U.S. Department of Energy

K^{π}=39/2- Isomer in ^{177}Lu

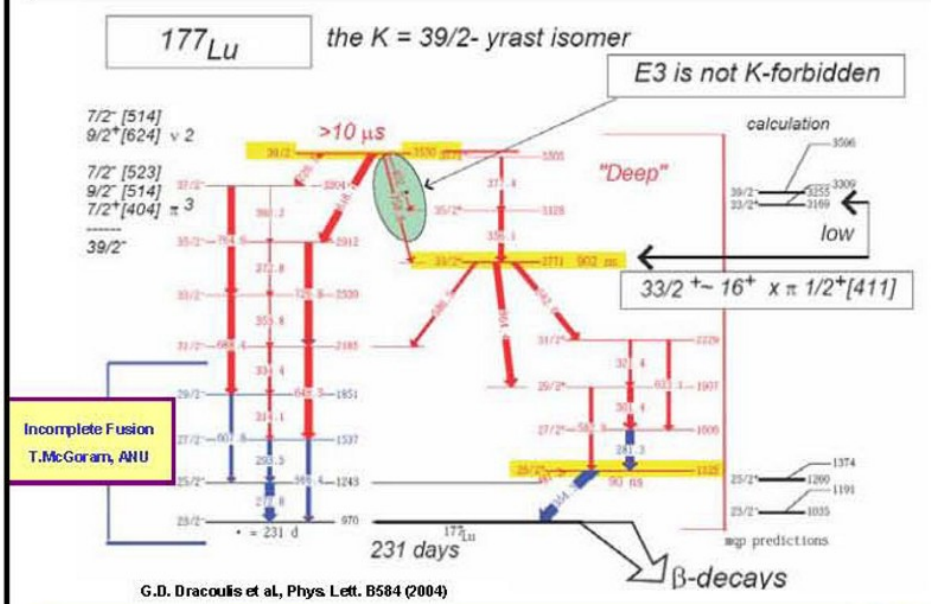

29

Is this the claimed β^--decaying isomer?

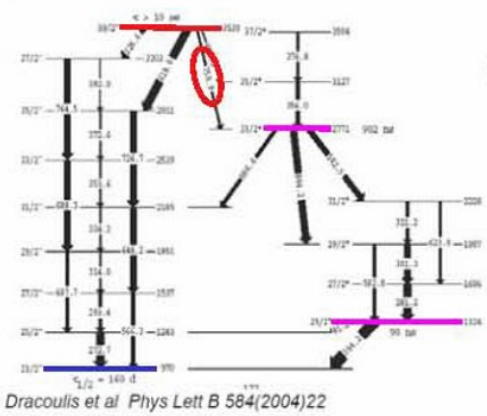

Q_β - logft & strength of internal γ-ray branches

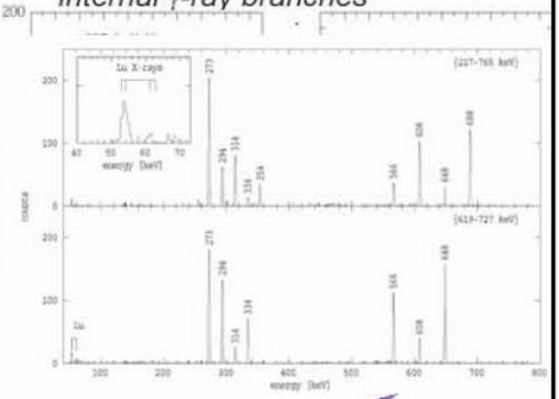

- *Ex=3.5 MeV (3.9 MeV)*
- *unambiguous γ-ray decay signature (no such gammas in the spectrum)*
- *unprecedented transition strength for the 759 keV, non K-forbidden, E3 transition (10^9! times retarded compared to W.u. if $T_{1/2}$=7 min)*

30

In-Flight Technique Using Projectile Fragmentation

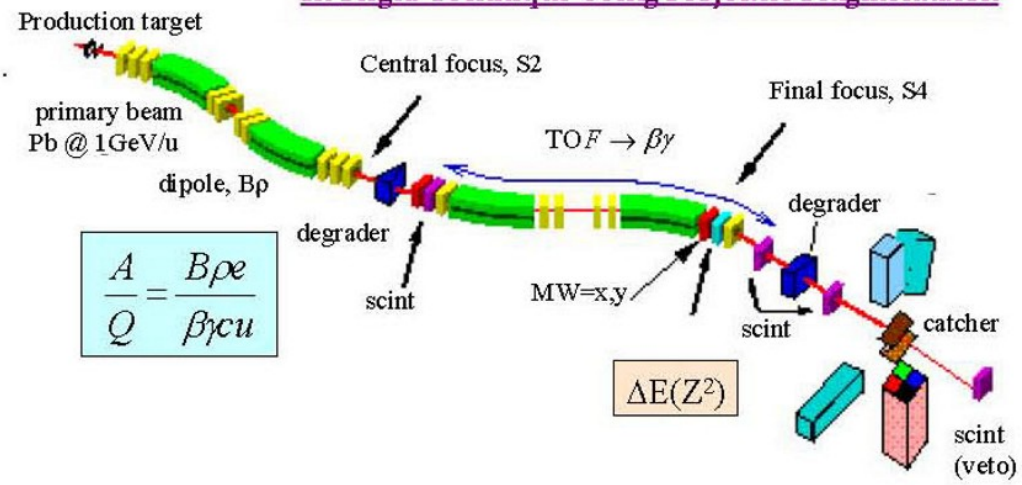

$$\frac{A}{Q} = \frac{B\rho e}{\beta\gamma cu}$$

Use FRS@GSI or LISE3@GANIL to ID nuclei.
Transport some in isomeric states (TOF~ 300 ns).
Stop and correlate isomeric decays with nuclei id.

31

Pioneering Science and Technology

Office of Science U.S. Department of Energy

^{92}Mo Fragmentation on ^{nat}Ni Target

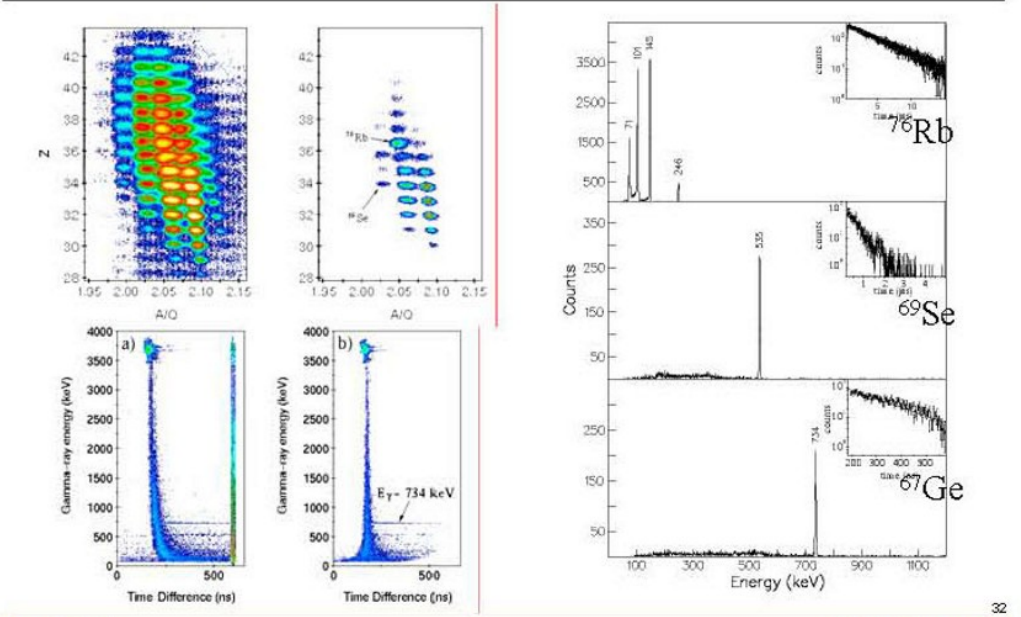

32

Pioneering Science and Technology

C. Chandler et al. Phys. Rev. C61 (2000) 044309

Office of Science U.S. Department of Energy

Future of γ–ray Spectroscopy

- Historical perspective
- Principle of gamma ray tracking
- Physics opportunities
- Technical challenges
- Status of project

Gamma-ray Detector Development

Crucial to Nuclear Physics Research

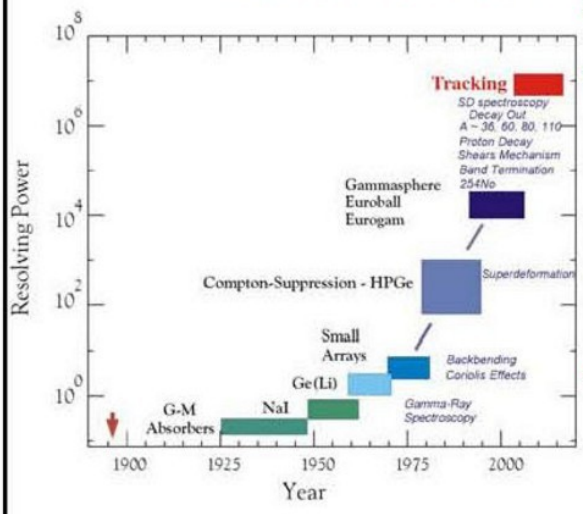

- Advances in detector technology have resulted in new discoveries.
- Innovations have improved detector performance.
  - **Energy resolution**
  - **Efficiency**
  - **Peak-to-total ratio**
  - **Position resolution**
  - **Directional information**
  - **Polarization**
  - **Auxiliary detectors**
- Tracking is feasible, will provide new opportunities and meet the challenges of new facilities.

$$R \sim \left[\frac{P}{T} \times \varepsilon \times \frac{E_{spacing}}{\Delta E}\right]^n$$

Why Gamma-ray Arrays?

❑ High energy resolution	ΔE_γ=2.5 keV @ 1.3 Mev
❑ Large P/T ratio	~60%
❑ Large photopeak efficiency	10% @ 1.3 MeV
❑ Good timing resolution	<10 ns
❑ Wide energy range	~30 keV – 20 MeV
❑ Large solid angle	~ 4π
❑ High granularity	high fold coincidences
❑ High resolving power	ability to isolate a given sequence of γ rays

35

Pioneering Science and Technology

Office of Science U.S. Department of Energy

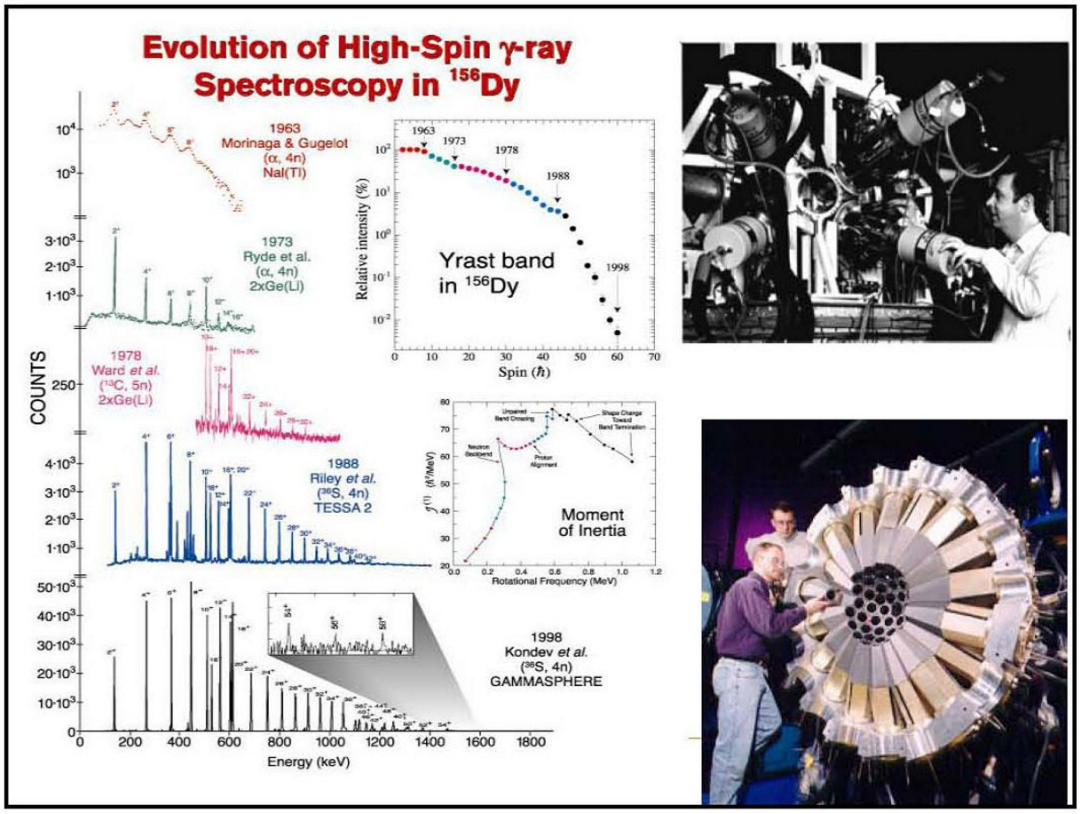

Historical Perspective

~1980 states to spin ~30
naked Ge arrays

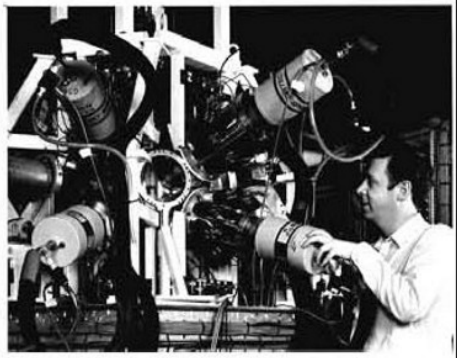

~1980-1982 TESSA
Escape suppressed array at NBI

1983 TESSA to Daresbury
Heavier Ion beams
6 ESS using NaI(Tl)
Channel selection included, 50 element inner BGO ball

I ~ 1% sensitivity

37

Pioneering Science and Technology

Office of Science U.S. Department of Energy

Historical Perspective – Era of Large Arrays

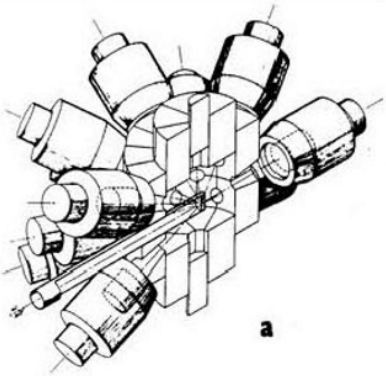

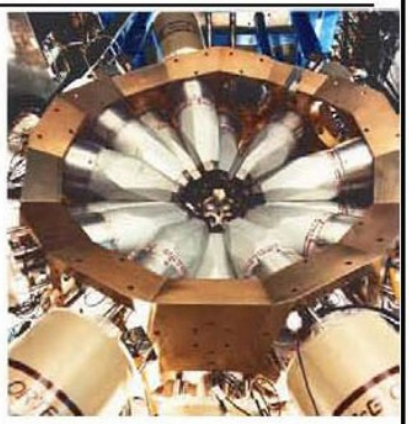

~1987
BGO replaces NaI(Tl)
HERA, TESSA3

I ~ 0.1% sensitivity

~1995
Large γ-ray arrays
Eurogam, Gasp, Gammasphere, Euroball's

I ~ 0.001% sensitivity

38

Pioneering Science and Technology

Office of Science U.S. Department of Energy

Interaction of Gamma Rays with Matter

~ 100 keV ~1 MeV ~ 10 MeV γ-ray energy

Photoelectric	Compton Scattering	Pair Production
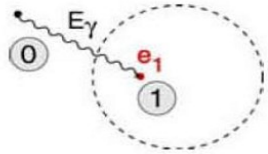	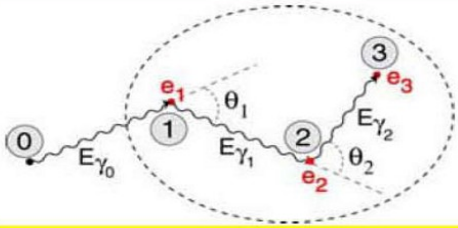	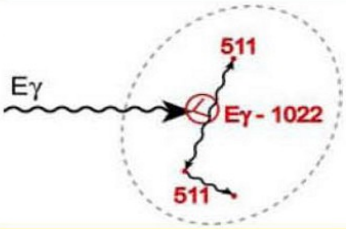
Isolated hits	Angle/Energy	Pattern of hits
Probability of interaction depth	$E_{\gamma'} = \frac{E_\gamma}{1+\frac{E_\gamma}{m_0c^2}(1-\cos\theta)}$	$E_{1st} = E_\gamma - 2\,mc^2$

39

Compton Suppression – Improving the Peak to Background Ratio

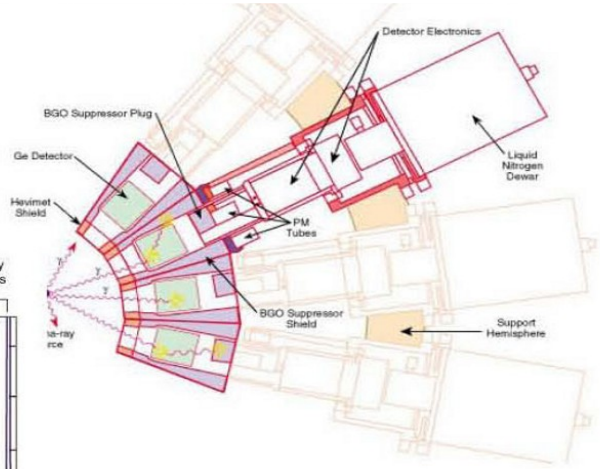

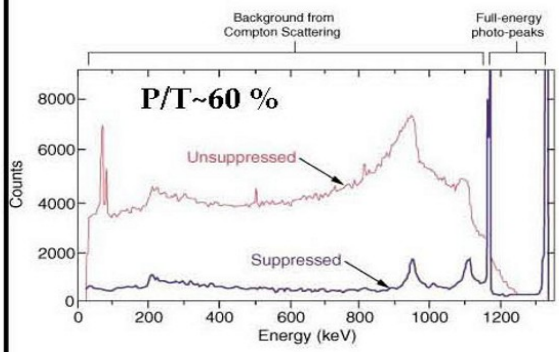

40

Gammasphere Spectrometer

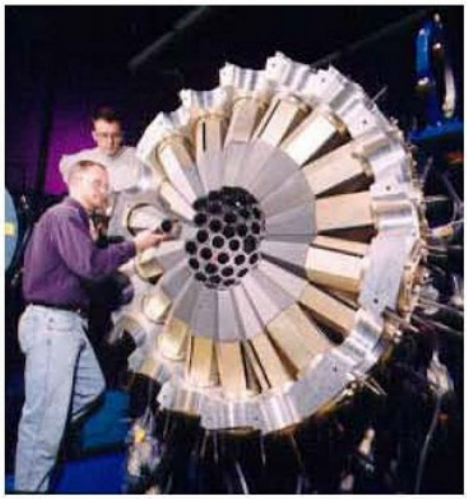

- A spectrometer with high detection sensitivity to nuclear electromagnetic radiation due to its high resolution, granularity and efficiency
- Consists of a spherical shell of 110 large volume HpGe detectors each enclosed in a BGO shield
- Funded by DOE, US

41

Pioneering Science and Technology

Office of Science U.S. Department of Energy

Gammasphere Operation

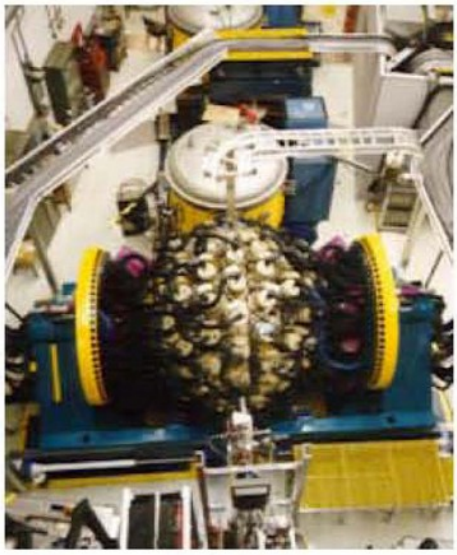

- From 1993 to 1997 GS was constructed and sited at the 88-Inch Cyclotron, LBNL
  - 130 experiments
  - super deformation
- From 1998 to 2000 GS operated at ATLAS, ANL
  - 101 experiments
  - nuclei far from stability
- From March 2000 till January 2002 at LBNL
- Since March 2002 till now GS is back at ANL

42

Pioneering Science and Technology

Office of Science U.S. Department of Energy

Euroball

European collaboration
France, Denmark, Germany, Italy, Sweden and the UK

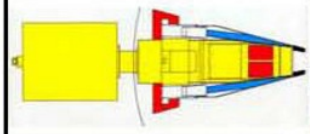

30 Large single crystal Ge detectors

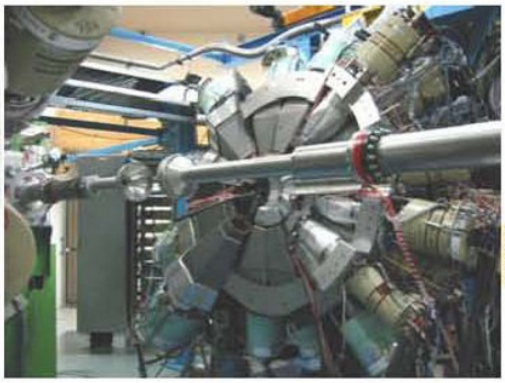

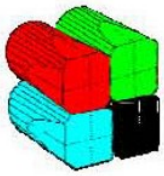

26 Clover Ge detectors
4 crystals per cryostat

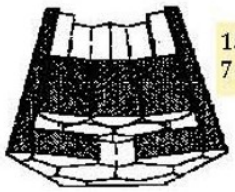

15 Cluster Ge detectors
7 encapsulated Ge crystals per cluster

239 Ge crystals
Suppression shields
Total peak efficiency ~9.4%
Intensity limit ~ 10^{-5}

43

Pioneering Science and Technology

Office of Science U.S. Department of Energy

Gamma-ray Arrays in USA & Canada

FSU Array, USA

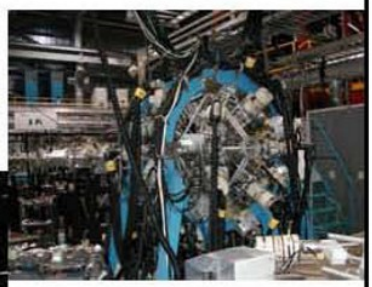

Yrast Ball, Yale University
10 Clover
17 Ge

CLARION, ORNL

8π, TRIUMF
~100 Ge detectors

44

Pioneering Science and Technology

Office of Science U.S. Department of Energy

Gamma-ray Arrays in Europe

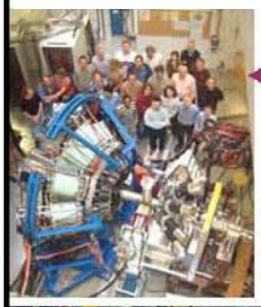

RISING, GSI

JUROGAM, JYFL

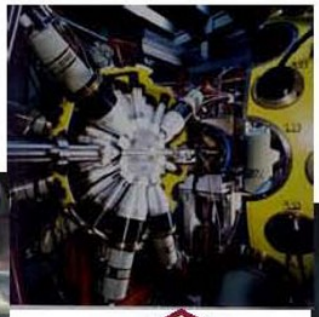

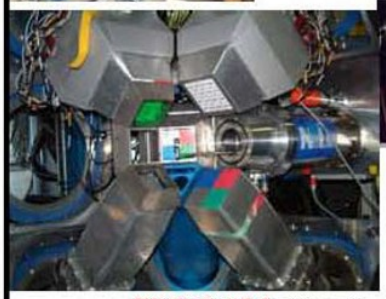

GASP, INFN

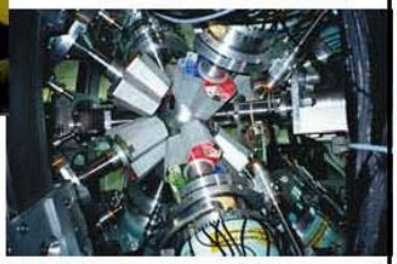

EXOGAM, Ganil

MINIBALL, RexIsolde

45

Pioneering Science and Technology

Office of Science U.S. Department of Energy

Australia, Asia & Africa

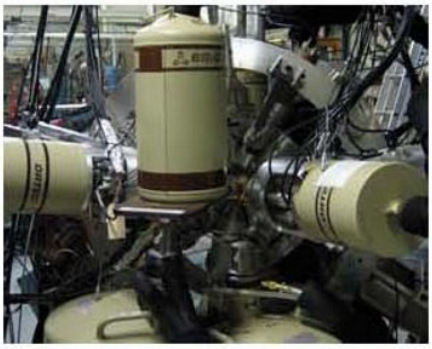

CAESAR, Australia

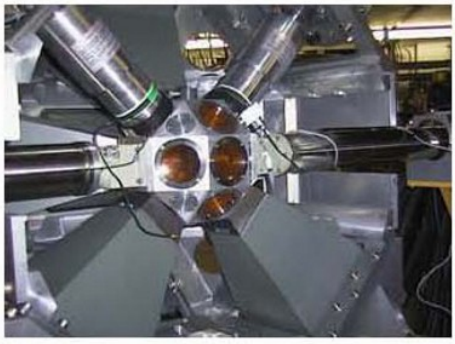

Afrodite, South Africa

Smaller arrays operate in India, China and Japan

46

Pioneering Science and Technology

Office of Science U.S. Department of Energy

Gamma-ray Tracking Concepts

- Compton Suppressed Ge

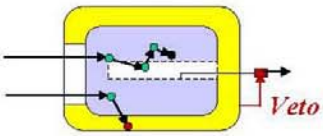

$N_{det} = 100$
Peak efficiency = 0.1
Efficiency limited

- Ge Sphere

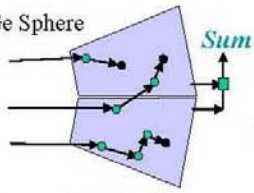

$N_{det} = 1000$ (summing)
Peak efficiency = 0.6
Too many detectors

- Gamma Ray Tracking

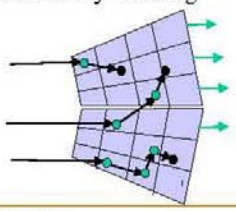

$N_{det} = 100$
Peak efficiency = 0.6
Segmentation

Pulse shape analysis in segments ➔ 3D position

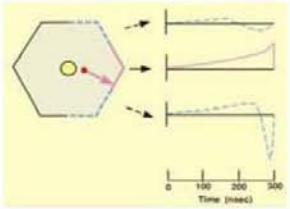

Tracking of photon interaction points ➔ energy, position

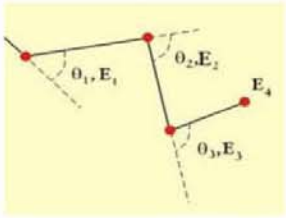

47

Pioneering Science and Technology

Office of Science U.S. Department of Energy

1970s 1980s 1990s 2000s

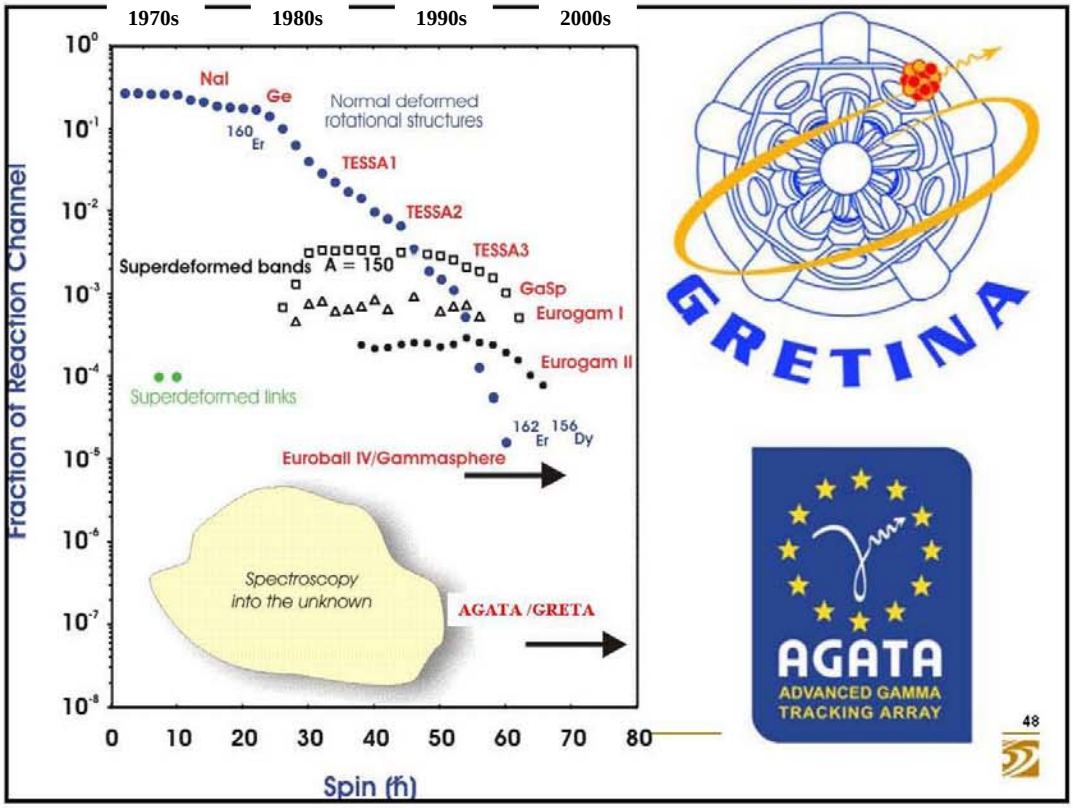

48

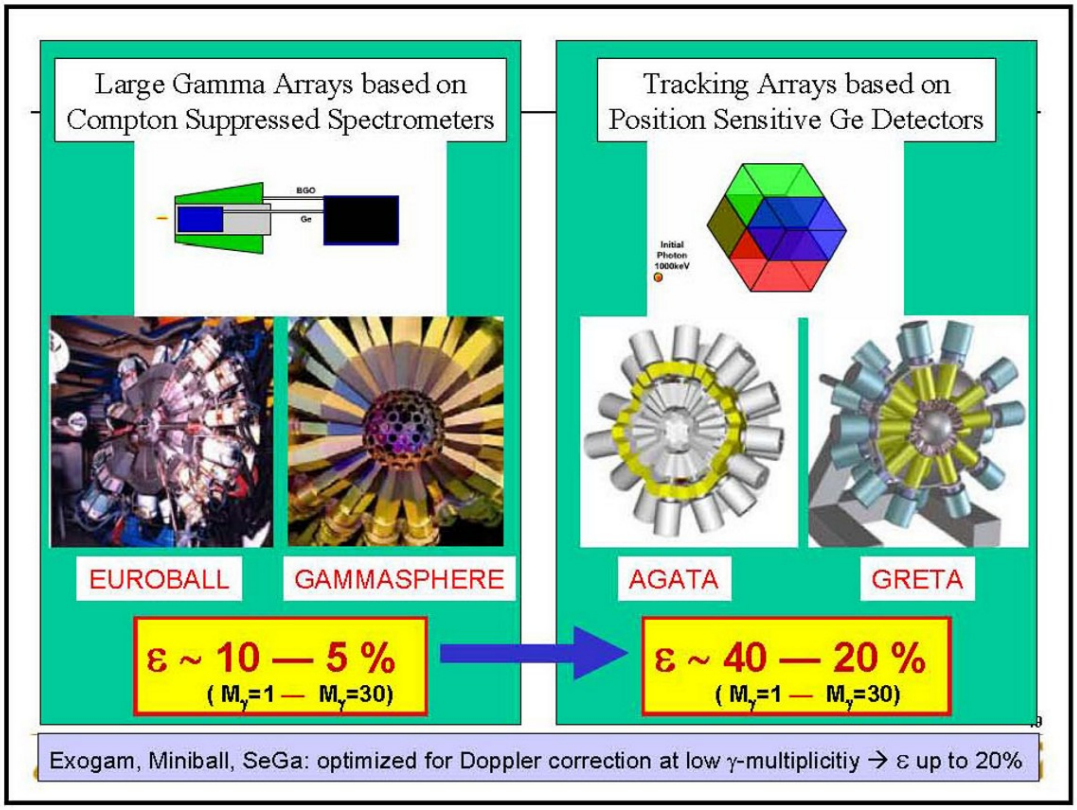

GRETA/GRETINA

- **Resolving power: 10^7 vs. 10^4**
  - Cross sections down to ~1 nb
    - *Most exotic nuclei*
    - *Heavy elements (e.g. ^{253,254}No)*
    - *Drip-line physics*
    - *High level densities (e.g. chaos)*
- **Efficiency (high energy) (23% vs. 0.5% at E_γ=15 MeV)**
  - Shape of GDR
  - Studies of hypernuclei
- **Efficiency (slow beams) (50% vs. 8% at E_γ=1.3 MeV)**
  - Fusion evaporation reactions
- **Efficiency (fast beams) (50% vs. 0.5% at E_γ=1.3 MeV)**
  - Fast-beam spectroscopy with low rates -> RIA
- **Angular resolution (0.2° vs. 8°)**
  - N-rich exotic beams
    - *Coulomb excitation*
  - Fragmentation-beam spectroscopy
    - *Halos*
    - *Evolution of shell structure*
    - *Transfer reactions*
- **Count rate per crystal (100 kHz vs. 10 kHz)**
  - More efficient use of available beam intensity
- **Linear polarization**
- **Background rejection by direction**

50

Pioneering Science and Technology

Office of Science U.S. Department of Energy

AGATA
(Advanced GAmma Tracking Array)

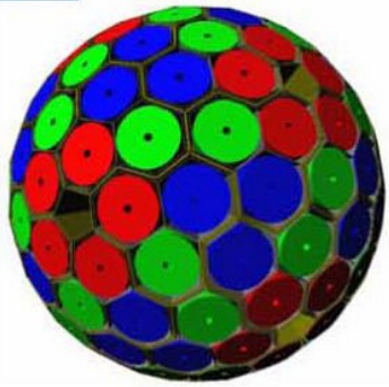

Main features of AGATA

Efficiency: 40% (M_γ=1) 25% (M_γ=30)
today's arrays ~10% (gain ~4) 5% (gain ~1000)

Peak/Total: 55% (M_γ=1) 45% (M_γ=30)
today ~55% 40%

Angular Resolution: ~1° →
FWHM (1 MeV, v/c=50%) ~ 6 keV !!!
today ~40 keV

Rates: 3 MHz (M_γ=1) 300 kHz (M_γ=30)
today 1 MHz 20 kHz

- 180 large volume 36-fold segmented Ge crystals in 60 triple-clusters
- Digital electronics and sophisticated Pulse Shape Analysis algorithms allow
- Operation of Ge detectors in position sensitive mode → γ-ray tracking

51

Pioneering Science and Technology

Office of Science U.S. Department of Energy

Highly-segmented Ge Detectors

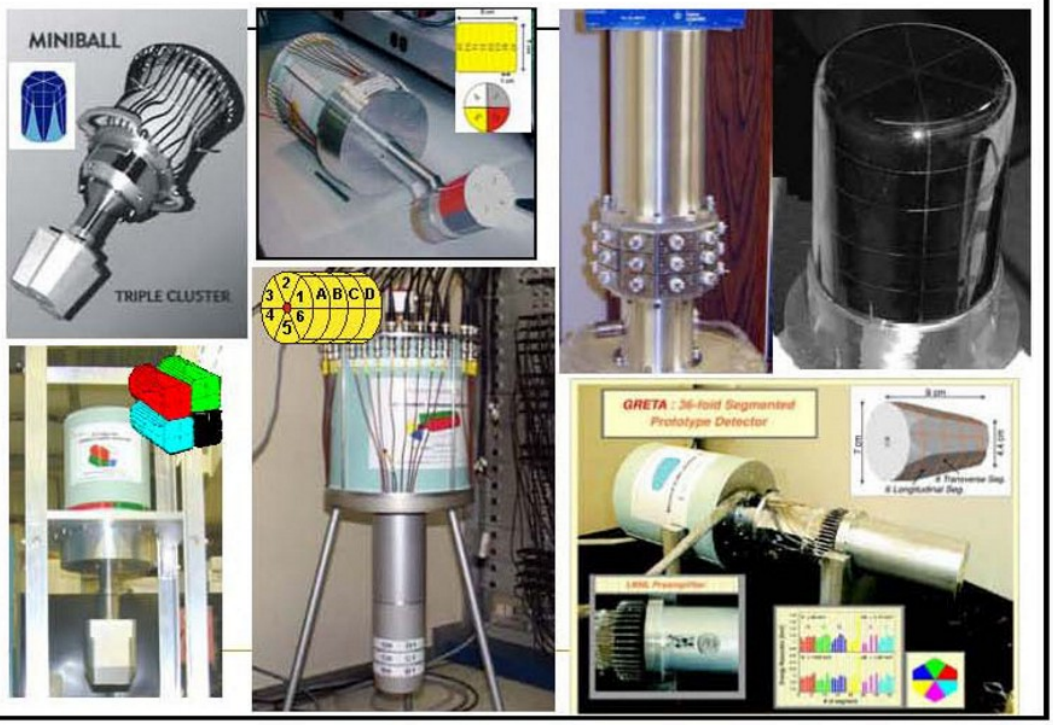

Canisters AGATA and EUROBALL

AGATA EUROBALL

GRETINA Detectors

- Tapered hexagon shape
- Highly segmented 6 × 6 = 36
- Close packing of 3 crystals
- 111 channels of signal

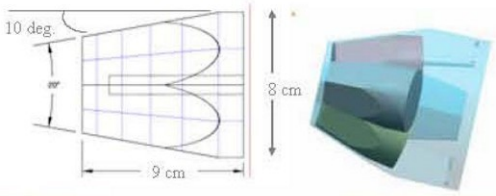

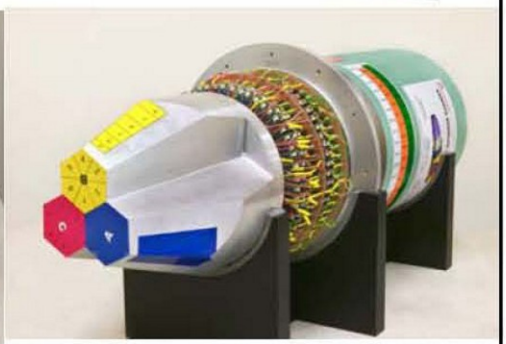

Received June 4, 2004

AGATA Detectors

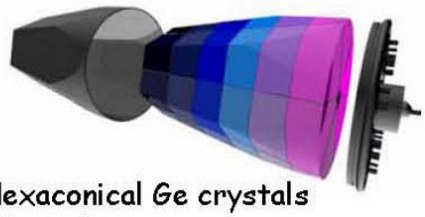

Hexaconical Ge crystals
90 mm long
80 mm max diameter
36 segments
Al encapsulation
0.6 mm spacing
0.8 mm thickness
37 vacuum feedthroughs

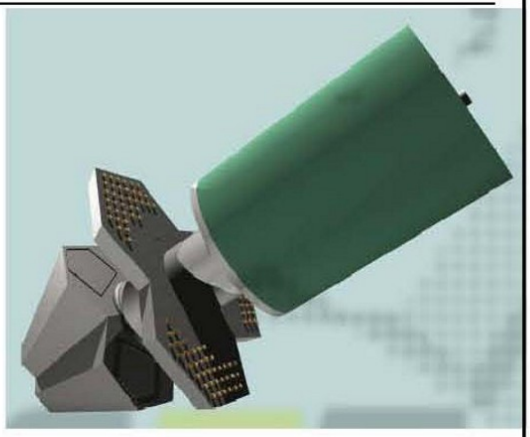

3 encapsulated crystals
111 preamplifiers with cold FET
~230 vacuum feedthroughs
LN_2 dewar, 3 litre, cooling power ~8 watts

55

Pioneering Science and Technology

Office of Science U.S. Department of Energy

Ingredients of γ–ray Tracking

1
Highly segmented HPGe detectors

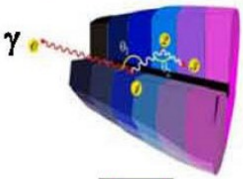

2
Digital electronics to record and process segment signals

3
Pulse Shape Analysis to decompose recorded waves

4
Identified interaction
$(x,y,z,E,t)_i$

Reconstruction of tracks e.g. by evaluation of permutations of interaction points

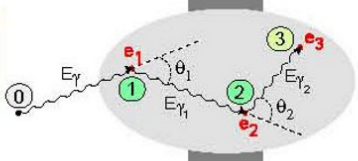

reconstructed γ-rays

In-beam Test

Experiment

- LBNL 88" Cyclotron
- Prototype II detector
- $^{82}Se + {}^{12}C$ @ 385 MeV
- ^{90}Zr nuclei ($\beta \sim 8.9\%$)
- 2055 keV ($10^+ \rightarrow 8^+$) in ^{90}Zr
- Detector at 4 cm and 90°
- Three 8-channels LBNL signal Digitizer modules (24 ch.)

Analysis

- Event building
- Calibration : cross talk
- Signal decomposition
- Doppler correction

In-beam Test Results

Doppler Corrected using first hit position determined by signal decomposition

Corrected using center of segment only

No correction

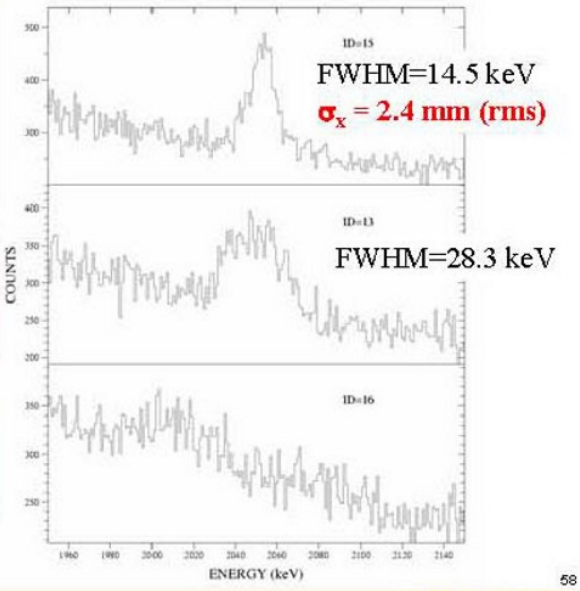

TIGRESS, TRIUMF, CANADA

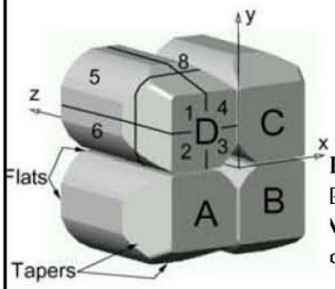

ISAC II

Nuclear Structure:

Evolution of Nuclear Shell Structure
Pairing Correlation far from Stability
Mirror Nuclei and Isospin Symmetry
oulomb Excitation with Bragg/PPAC
Fusion Evaporation reactions with CsI(Tl) and neutron detector arrays

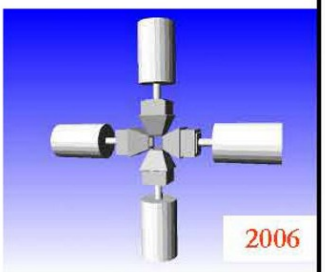

Nuclear Astrophysics:

Structure studies of astrophysically important states
Transfer reactions with EMMA/Si Array

Pioneering Science and Technology

Office of Science U.S. Department of Energy

Gamma Ray Lines of the Cosmos

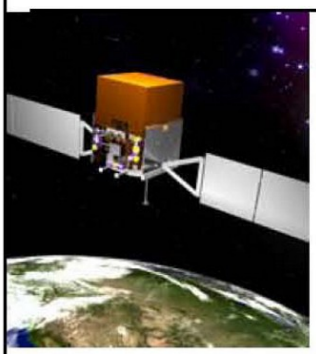

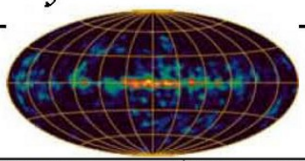

Science Objective	Isotopes and Lines (MeV)
Understand Type Ia SN explosion mechanism and dynamics	^{56}Ni (0.158, ***0.812***, …) ^{56}Co (***0.847***, ***1.238***, …) ^{57}Co (0.122)
Understand Core Collapse SN explosion mechanism and dynamics	^{56}Ni (0.158, ***0.812***, …) ^{56}Co (***0.847***, ***1.238***, …) ^{57}Co (0.122), ^{26}Al (***1.809***, ***0.511***)
Map the Galaxy in nucleosynthetic radioactivity	^{26}Al (***1.809***, ***0.511***) ^{60}Fe, ^{60}Co (***1.173***, ***1.332***) ^{44}Ti (0.068, 0.078, ***1.16***)
Map Galactic positron annihilation radiation	e^+–e^- annihilation (***0.511***, 3 photon continuum) SN Ia ^{56}Co positrons (***0.511***) ^{26}Al and ^{44}Ti positrons (***0.511***)
Understand the dynamics of Galactic Novae	^{13}N, ^{14,15}O, ^{18}F positrons (***0.511***) ^{7}Be (***0.478***), ^{22}Na (***1.275***, ***0.511***)
Cosmic Ray Interactions with the ISM	^{12}C (4.4), ^{16}O (6.1), ^{20}Ne(***1.634***), ^{24}Mg(***1.369***,2.754), ^{28}Si(***1.779***), ^{56}Fe(***0.847***,***1.238***)
Neutron Star Mass-Radius	p-n (***2.223***)

60

Office of Science U.S. Department of Energy

The Concept

Position sensitive gamma ray detectors have been under development for many years

- In Space Science
- In Medical Imaging
- In Basic Nuclear Research
- In Homeland Security and Verification.

Scintillator: NaI, CsI, LSO

Semi-conductor: Si, CdZnTe, CdTe

High Purity Germanium: offers the best energy resolution and timing for intermediate (40-2500 keV) radiation. Very large and efficient detectors can now be fabricated.

Key Question:

Can reliable, efficient, high resolution *position sensitive* germanium detectors be produced and incorporated into practical devices?

61

Pioneering Science and Technology

Office of Science U.S. Department of Energy

Ge Strips Detectors – an excellent choice!

- based on the HpGe planar detector technology
- have orthogonal electrodes (strips) that provide position localization of the interactions
- operates like a conventional p-i-n diode
- pulse-shape analysis – the depth of the interactions

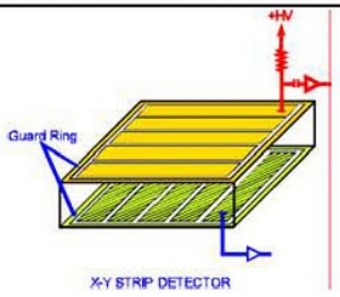

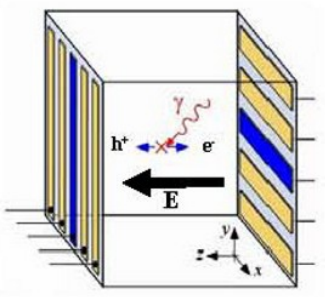

62

Pioneering Science and Technology

Office of Science U.S. Department of Energy

Technology: Wafer Selection

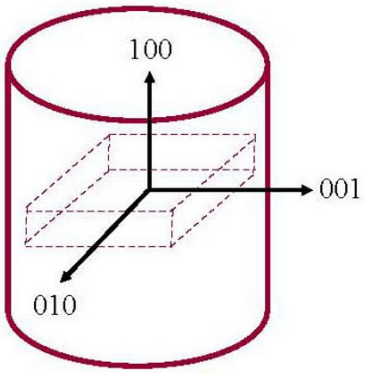

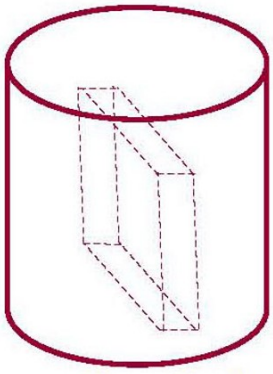

Across Boule

Uniform Impurities

LIMITED SIZE

Along Boule

LARGEST SIZE

Impurity Gradients

REAL NEED FOR FINANCING OF FACILITY TO GROW BIGGER BOULES.....(15cms)

63

Pioneering Science and Technology

Office of Science U.S. Department of Energy

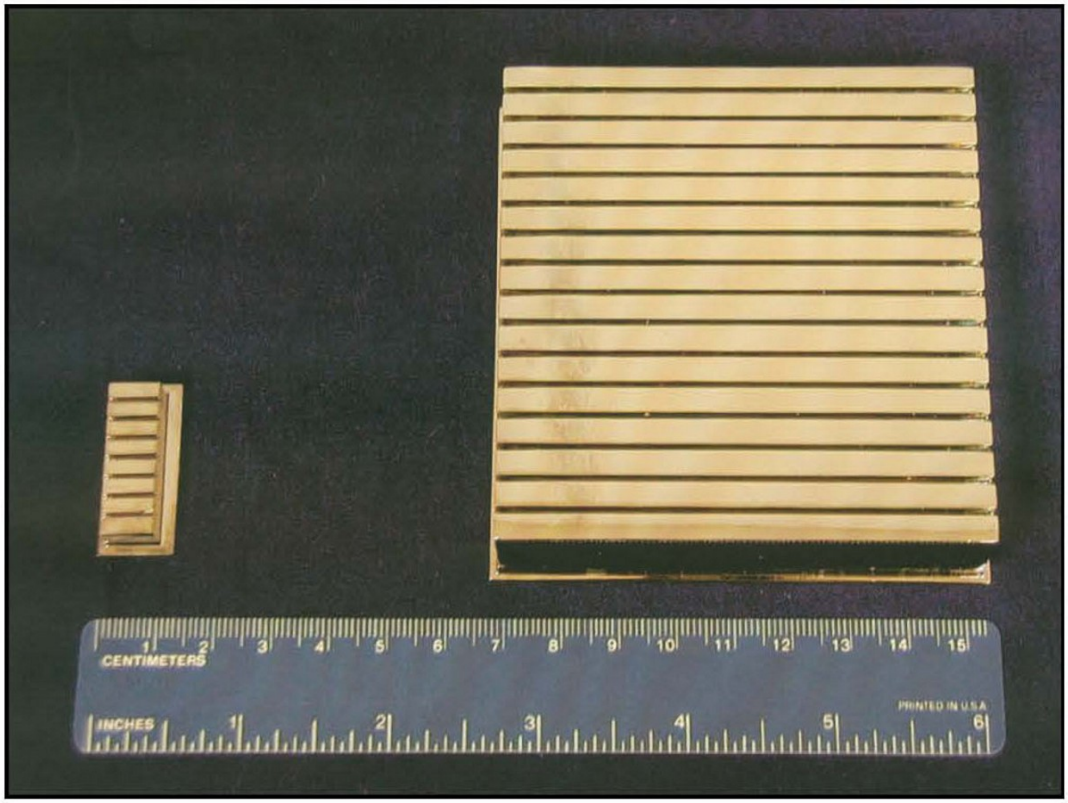

ANL HPGe Strips Detector

With the premier US germanium detector manufacturer, Ortec, we have built

- ***the biggest*** (~90 mm x 90 mm x 20 mm)
- ***the best*** (~1.0 keV at 122 keV, ~2.0 keV at 1.3 MeV)

Ge strips detector in the world!

Pioneering Science and Technology

Office of Science U.S. Department of Energy

2D Imaging Capabilities

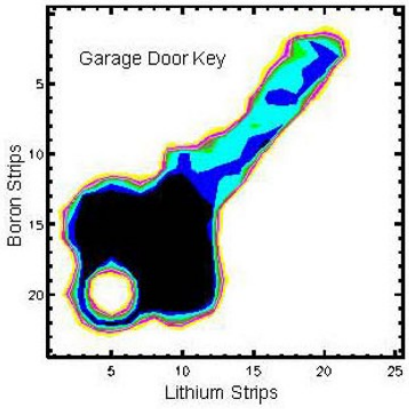

25 x 25 strip HpGeDSSD
60 keV γ-rays from ^{241}Am source

S.E. Inderhees et al., IEEE 43 (1996) 1467

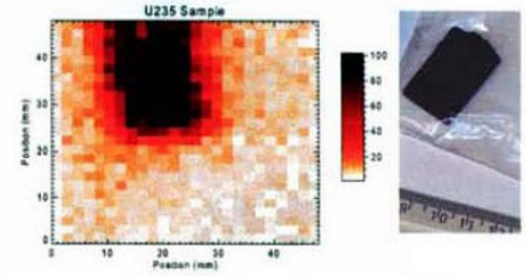

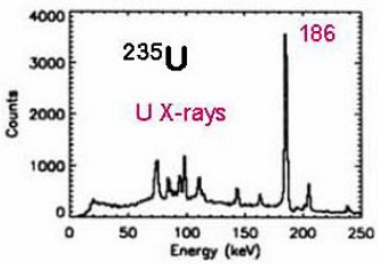

Imaging and characterization

66

Pioneering Science and Technology

Office of Science U.S. Department of Energy

Compton Camera

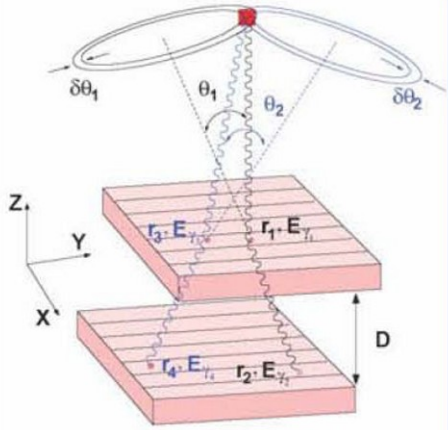

Concept

- Gamma ray Compton scatters in the first detector
- Positions and energies of individual interactions enables to determine pathway of gamma ray in the detector – *gamma-ray tracking*!
- Energies and positions define cone of incident angles (electron path is not measured)
- Cones are projected on a plane or a sphere (one circle per event) for 2D or into a cube (one cone per event) for 3D imaging

$$\cos\theta_1 = [1 - m_e c^2 ((E_\gamma - E_{\gamma 1}) / E_\gamma E_{\gamma 1})]$$

$$E_\gamma = E_{\gamma 1} + E_{\gamma 2}$$

67

Pioneering Science and Technology

Office of Science U.S. Department of Energy

Compton Camera

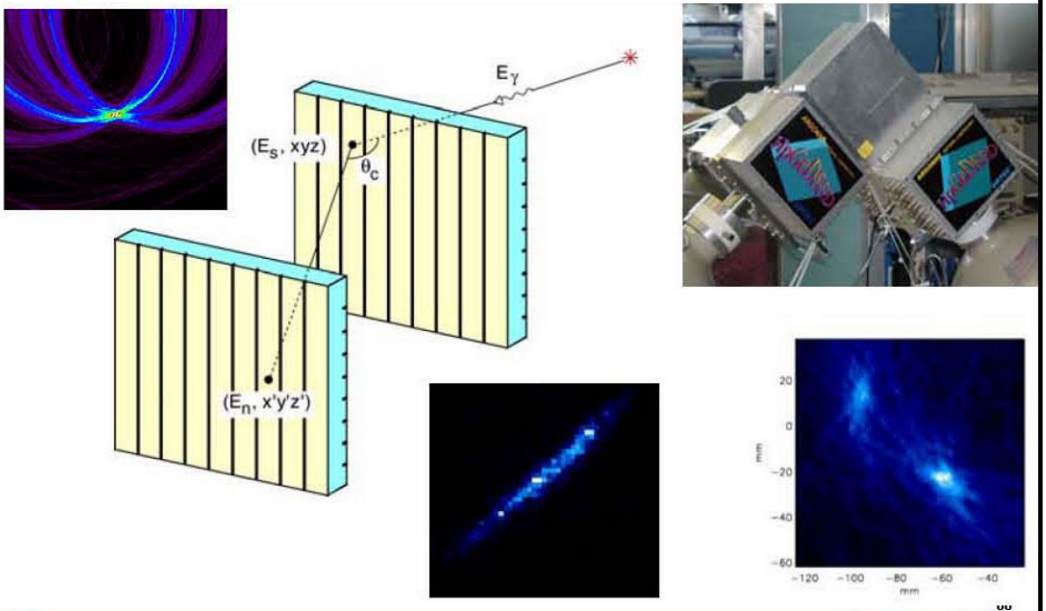

Pioneering Science and Technology

Office of Science U.S. Department of Energy

Döppler Correction

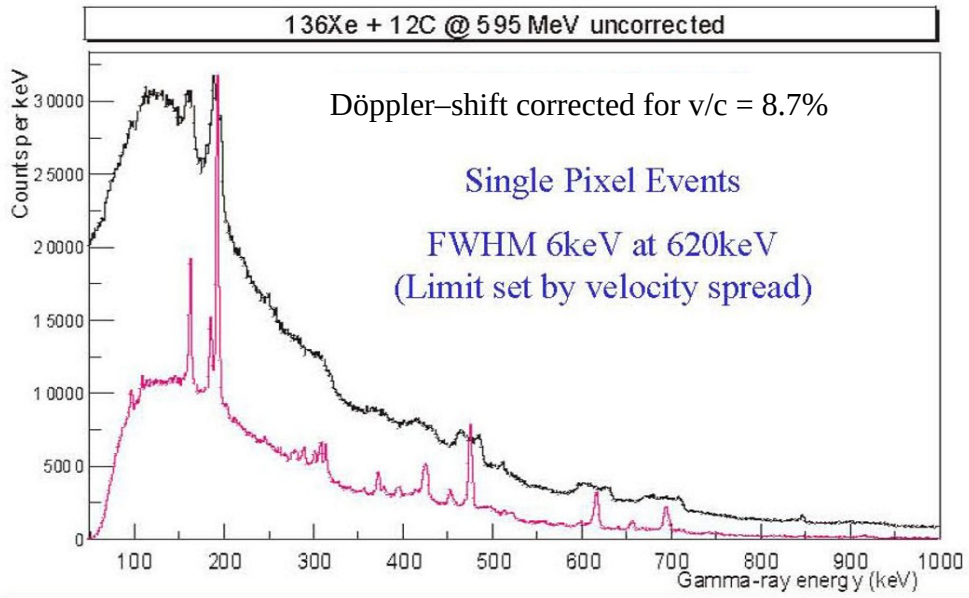

Pioneering Science and Technology

Office of Science U.S. Department of Energy

Polarization in α–γ Coincidences

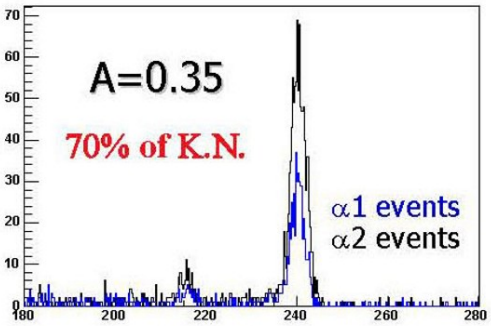

"Second Neighbor" analysis has even bigger asymmetry, and almost as much data.

16 pixels vs. 4.

"Worlds Best" figure of merit

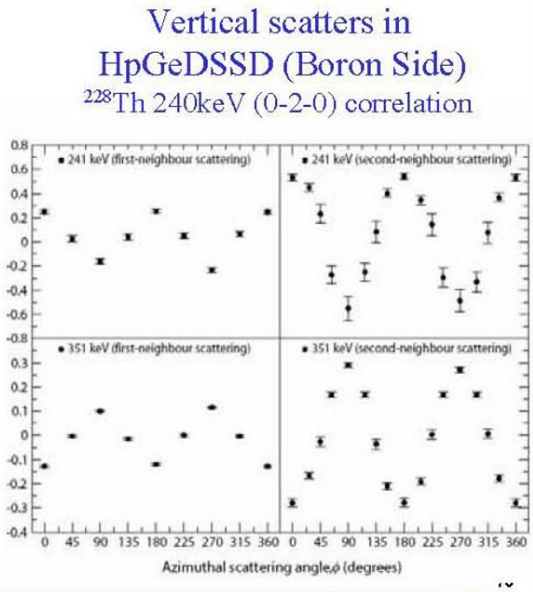

Pioneering Science and Technology

Office of Science U.S. Department of Energy

Imaging

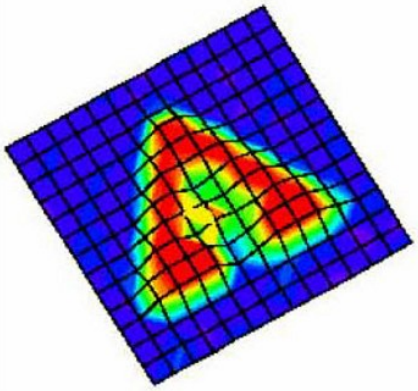

Direct Determination of materials by differential absorption

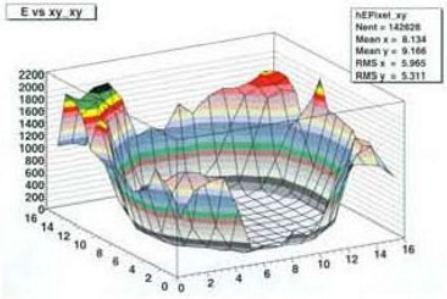

Varying source-object-detector baseline can give large magnification
This image 5mm steel ball bearing

71

Pioneering Science and Technology

Office of Science U.S. Department of Energy

Digital Signal Processing

Here lies the most exciting prospect. The drifting charge created by the gamma rays induces images that allows the interaction points to be accurately located.

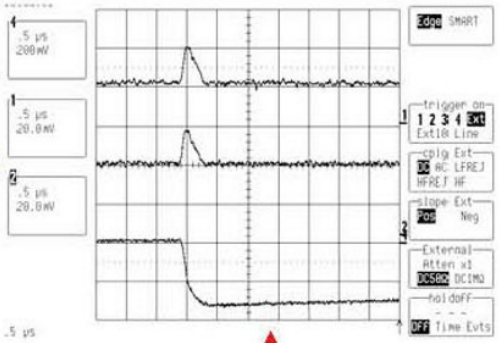

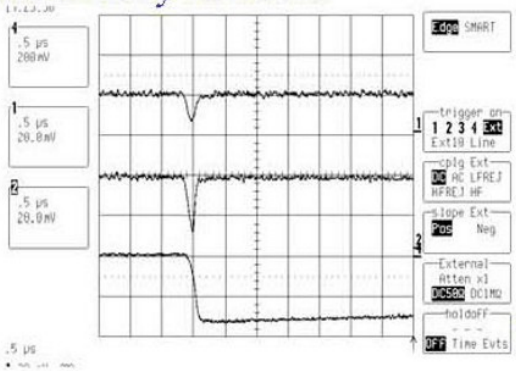

Shallow (Close to Electrode)
Central

Deep (Far from Electrode)
Right Side

72

Office of Science U.S. Department of Energy

Digital Pulse Processing

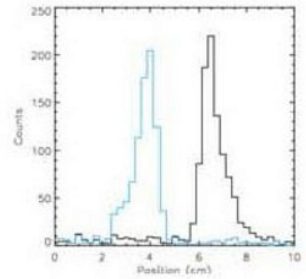

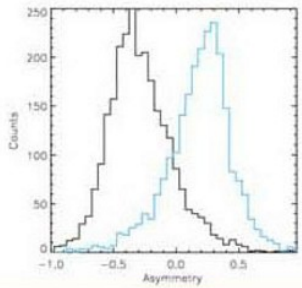

DEPTH
From front-back time difference of charge pulse arrival

1-2 mm
but depends on position

LATERAL
From asymmetry of induced transient signals

Nuclear Data Section
International Atomic Energy Agency
P.O. Box 100
A-1400 Vienna
Austria

e-mail: services@iaeand.iaea.org
fax: (43-1) 26007
cable: INATOM VIENNA
telex: 1-12645
telephone: (43-1) 2600-21710
Web: http://www-nds.iaea.org